PIEZOMAGNETISM AND MAGNETOSTRICTION IN MAGNETIC MATERIALS

by

Reginald Anthony Michael SCOTT, B.Sc., A.R.C.S.

A thesis submitted for the
Degree of Doctor of Philosophy
in the University of London.

Department of Electrical Engineering,
Imperial College of Science and Technology.

October, 1965.

ABSTRACT

Magnetostrictive strain is usually an even function of magnetic field, but certain antiferromagnetic materials exhibit a strain which depends linearly on the applied magnetic field.

A resistance strain gauge apparatus capable of detecting strains of 10^{-8} has been constructed to investigate this hitherto unreported effect in various crystals of hematite (αFe_2O_3). A well-known magnetic transition occurs in antiferromagnetic hematite at about -15° C, above which the material has canted spins. At low temperatures, two types of antiferromagnetic domains related by time inversion can exist in this material, with the linear magnetostriction coefficient reversing sign from one to the other. Magnetic annealing to eliminate one of these domains was effected by freezing in a single domain state from the high temperature phase.

In this condition the strain E_{ij} produced by a field H is given, in usual tensor notation, by $E_{ij} = Q_{ijk}H_k$ and in hematite only Q_{222} and Q_{321} are independent non-zero. These coefficients were measured in synthetic and natural crystals and had the values in the most pure material of $\pm$ 23 x 10^{-11} Oe^{-1} and $\mp$ 5 x 10^{-11} Oe^{-1} respectively, and to be virtually temperature independent in the range 77° K - 220° K. Magnetostriction also revealed a field induced reduction of the magnetic transition temperature, this being related to the relative thermodynamic potentials of the two phases.

Above a certain field strength applied at low temperatures in the opposite direction to the annealing field, the applied field caused antiferromagnetic domain switching so that the energetically favourable domain state, and hence the measured strain, reversed with the magnetic field. Domain switching was produced by wall movement which was found to occur over a limited range of magnetic fields, and hysteresis loops of domain sign versus applied field have been obtained.

ACKNOWLEDGEMENTS

I wish to express my deep gratitude to my supervisor, Professor J. C. Anderson, for guidance and advice throughout the course of this research and also for provision of the necessary laboratory facilities. I am also greatly indebted to Dr. R. R. Birss for his assistance with the initial theoretical work and for valuable comments on the implications of the experimental results.

This research project has only been possible through the generosity of Professor M. Blackman from whom were borrowed all the single crystal specimens that were investigated. Associated with this I would like to thank Mr. T. E. Gallon of his department for performing magnetic remanence measurements on the crystals.

Thanks are also extended to Miss P. J. Carter for typing this thesis. Finally, the financial support provided by the Science Research Council, in the form of a Research Studentship, is gratefully acknowledged.

C O N T E N T S

	Page
ABSTRACT	2.
ACKNOWLEDGEMENTS	4.
CHAPTER I INTRODUCTION	
1.1. INTRODUCTION	11.
1.2. CRYSTAL SYMMETRY	
1.2.1. Classical Symmetry	12.
1.2.2. Time Inversion Operator	15.
1.2.3. Magnetic Symmetry	16.
1.3. FORBIDDEN EFFECTS	18.
1.3.1. Expansion of Thermodynamic Potential Energy	19.
1.3.2. Pyromagnetism	22.
1.3.3. Magnetoelectric Effect	24.
1.3.4. Piezomagnetism	26.
1.3.5. Linear Magnetostriction	28.
1.3.6. Non-linear Susceptibility	29.
1.4. PIEZOMAGNETISM	
1.4.1. Historical Basis	31.
1.4.2. Experimental Verification	32.
1.4.3. Piezomagnetism and Antiferromagnetic Domains	35.
1.5. HEMATITE	
1.5.1. Crystal Structure	37.
1.5.2. Spin Structure	41.

	Page
1.5.3. Morin Transition	42.
1.5.4. Antiferromagnetic Domains	43.
1.5.5. Antiferromagnetic Domain Annealing	46.
1.5.6. Remanence	48.
1.6. THE PRESENT INVESTIGATION	51.
CHAPTER II APPARATUS	
2.1. APPARATUS REQUIREMENTS	
2.1.1. Strain Sensitivity Requirements	53.
2.1.2. Strain Measurement Devices	54.
2.1.3. Temperature Requirements	57.
2.2. RESISTANCE STRAIN GAUGES	58.
2.3. METHOD OF MEASUREMENT	
2.3.1. Bridge	60.
2.3.2. Bridge Current	66.
2.3.3. Null Detection System	67.
2.3.4. Photocell Amplifier	68.
2.3.5. Galvanometer Attenuator	70.
2.4. CRYSTAL HOLDER	
2.4.1. Design Requirements	72.
2.4.2. Comparitor Gauge	73.
2.4.3. Description of the Specimen Holder	75.
2.5. THE MAGNET	78.
2.5.1. Magnet Power Supply	80.
2.5.2. Demagnetisation	82.

		Page
2.6.	TEMPERATURE BATHS	82.
2.7.	CHECKING AND CALIBRATION MEASUREMENTS	
	2.7.1. Magnetoresistance of the Strain Gauges	84.
	2.7.2. Effect of Magnet on Measurement Apparatus	86.
	2.7.3. Resistance Calibration of Measurement Circuit	89.
	2.7.4. Strain Calibration of Gauges	90.
	2.7.5. Alignment of Specimen in Field	93.
2.8.	MEASUREMENT PROCEDURE	95.
2.9.	DISCUSSION OF APPARATUS	
	2.9.1. Accuracy of Results	97.
	2.9.2. Apparatus Limitations	99.
CHAPTER III	EXPERIMENTAL SPECIMENS AND ASSOCIATED CALCULATIONS	
3.1.	EXPERIMENTAL SPECIMENS	
	3.1.1. Crystal Orientation	101.
	3.1.2. Synthetic Crystal	104.
	3.1.3. Annealed Synthetic Crystal	104.
	3.1.4. Elba Crystal	107.
	3.1.5. Arizona Crystal	107.
	3.1.6. St. Gothard Crystal	110.
	3.1.7. Effect of Impurities on the Transition Temperature	112.
	3.1.8. Polycrystalline Specimens	112.
3.2.	MAGNETOSTRICTION THEORY	
	3.2.1. Derivation of Form of 3rd Rank Axial c-tensor in Group $\bar{3}$m	114.

Page

3.2.2. Derivation of Form of 4th Rank Polar i-tensor in Group $\bar{3}$m 119.

3.2.3. Derivation of Form of 3rd Rank Axial c-tensor in Group 2/m 124.

3.2.4. Linear Magnetostriction in Hematite through the Magnetic Transition 127.

3.2.5. Magnetostriction Data from Elastic Constants 128.

3.2.6. Spin-lattice Interaction Theory 131.

3.3. THEORY APPLIED TO SPECIMENS USED

3.3.1. Form of Linear Magnetostriction on (110) Plane in Hematite 133.

3.3.2. Optimum Position for Strain Measurement on (110) Plane 137.

3.3.3. Form of Linear Magnetostriction on (111) Plane in Hematite 139.

3.3.4. Optimum Position for Strain Measurement on (111) Plane 141.

3.3.5. Form of 'Square Law' Magnetostriction on (110) Plane 142.

3.3.6. Form of 'Square Law' Susceptibility on (110) Plane 144.

CHAPTER IV DISCUSSION OF RESULTS

4.1. MAGNETOSTRICTION AT HIGH TEMPERATURES

4.1.1. Synthetic Crystal 146.

4.1.2. Annealed Synthetic Crystal 148.

4.1.3. Elba Crystal 152.

4.1.4. Arizona Crystal 155.

4.1.5. St. Gothard Crystal 158.

		Page
4.1.6.	Polycrystalline Specimens	160.
4.2.	MAGNETOSTRICTION AT HIGH TEMPERATURES	
4.2.1.	Synthetic Crystal	162.
4.2.2.	Annealed Synthetic Crystal	165.
4.2.3.	Elba Crystal	166.
4.2.4.	Arizona Crystal	168.
4.2.5.	St. Gothard Crystal	169.
4.2.6.	Polycrystalline Specimens	170.
4.3.	ANTIFERROMAGNETIC DOMAIN ANNEALING	171.
4.3.1.	Angular Dependence	172.
4.3.2.	Demagnetisation	175.
4.3.3.	Rate of Cooling	176.
4.3.4.	Field Dependence	176.
4.3.5.	Memory of Annealing	178.
4.4.	LINEAR MAGNETOSTRICTION COEFFICIENTS	180.
4.4.1.	Synthetic Crystal	180.
4.4.2.	Annealed Synthetic Crystal	184.
4.4.3.	Elba Crystal	187.
4.4.4.	Arizona Crystal	191.
4.5.	ANTIFERROMAGNETIC DOMAIN SWITCHING	195.
4.5.1.	Angular Dependence of the Switching Field	196.
4.5.2.	Hysteresis of Domain Switching	199.
4.5.3.	Rate of Domain Switching	203.
4.5.4.	Possible Mechanism for Antiferromagnetic Domain Switching	206.

		Page
4.6.	TEMPERATURE DEPENDENCE OF MAGNETOSTRICTION	209.
4.6.1.	High Temperature Phase	209.
4.6.2.	Low Temperature Phase	210.
4.6.3.	Field Dependence of Transition Temperature	215.
4.6.4.	Anomalous Strains at the Transition Temperature	221.
CHAPTER V	FINAL CONCLUSIONS	223.
APPENDIX I.	Classification of antiferromagnetics showing forbidden effects	227.
APPENDIX II.	Relationship between tensor components of a 3rd rank axial tensor in group $\bar{3}m$	229.
APPENDIX III.	Relationship between tensor components of a 4th rank polar tensor in group $\bar{3}m$	231.
APPENDIX IV.	Derivation of the linear magnetostriction coefficients from elastic and magneto-elastic constants in group $\bar{3}m$	236.
BIBLIOGRAPHY		241.

CHAPTER I

INTRODUCTION

1.1. INTRODUCTION

Magnetostriction is the name given to the phenomenon of ~~compression or extension~~ deformation of a material in a magnetic field. The change in dimensions can be considered either as a change in length or a change in volume, and the former, which is known as longitudinal magnetostriction, is of interest in this present work.

The ~~change in length~~ deformation is most suitably represented mathematically as a strain, which is a second rank tensor. The general expansion of this strain tensor E_{ij} as a power series of the first rank magnetic field tensor H_k can be written

$$E_{ij} = a_{ijk}H_k + b_{ijkl}H_kH_l + \ldots\ldots\ldots \qquad (1.1)$$

where i, j, k, l have the values 1, 2 or 3, corresponding to three Cartesian axes. The series converges rapidly, but for reasons which will be discussed later, the coefficient of the first term is zero in some magnetic materials and in all non-magnetic materials. In this case the second term predominates and the strain produced is independent of the sense of the applied magnetic field. However, in certain antiferromagnetics the first term is non-zero and predominates in the strain equation. In this case the magnetostrictive strain reverses as the sense of the magnetic field is reversed, and this effect is known by the appropriate name of Linear Magneto-

striction. A suitable material for observation of this effect is ferric oxide or hematite, and this work investigates linear magnetostriction in hematite under various conditions of temperature and field.

1.2. CRYSTAL SYMMETRY

1.2.1. Classical Symmetry

A crystalline lattice is conventionally considered to be formed in space by an infinite repetition of a basic pattern or unit cell. Crystal symmetry is then characterised by the allowable operations which transform this array into itself. One such operation is the rotation of the lattice through an angle of $2\pi/n$ until it transforms the ~~unit cell~~ lattice back into itself, and the crystal is then said to have an n-fold axis of rotation and symmetry operator $\pm$ n. Examples of symmetry operators are 1, 2, $\pm$ 3, $\pm$ 4, and $\pm$ 6. There may be many n-fold axes in a particular unit cell and so they are subscripted x, y, z, xy, ... etc., where z in the main axis and y is the two-fold axis, to indicate the crystallographic direction of the rotation axis. Similarly the subscript $\perp$ on the operator 2, indicates that the two-fold axis is perpendicular to the main crystal axis.

Another set of operators which are denoted by $\bar{1}$, $\bar{2}$, $\pm \bar{3}$, $\pm \bar{4}$, and $\pm \bar{6}$, correspond to the normal rotation followed by inversion of the ~~unit cell~~ lattice through a fixed point. There is another symmetry operation for uniaxial crystals designated by /m such as 2/m, 4/m and 6/m.

This describes a reflection or mirror plane perpendicular to the symmetry axis. A crystalline lattice also has in general, translation operators, but crystal symmetry does not concern itself with these as they do not govern the macroscopic properties of the crystal. Whilst in one crystalline lattice all rotation and rotation-inversion operators may be permissible, in another, only a selected few such as 1, $\bar{1}$, 2_z, $\bar{2}_z$, $\pm 4_z$, $\pm \bar{4}_z$ may be permissible and so it is convenient to classify crystal lattices as belonging to one or other symmetry group. A table listing the symmetry operators in each of 32 symmetry groups has been published by Birss[1], thus for example, group 4/m has the operators 1, $\bar{1}$, 2_z, $\bar{2}_z$, $\pm 4_z$, $\pm \bar{4}_z$ and group 6mm has the operators 1, 2_z, $6(\bar{2}_\perp)$, $\pm 3_z$, $\pm 6_z$.

The symmetry of a crystal and the symmetry of the physical properties exhibited by the crystal is related by Neumann's Principle which states that the elements of the symmetry group possessed by the crystal are also possessed by every physical property of the crystal. For this to be valid it is necessary that the property tensor be invariant under all permissible symmetry operations allowed by the crystal. If $d_{ijk...n}$ is a property tensor, then for it to be invariant under certain symmetry operations it must transform according to the relations

$$d_{ijk...n} = \pm \sigma_{ip}\sigma_{jq}\sigma_{kr}\cdots\cdots\cdots\cdots\sigma_{nu}\, d_{pqr...u} \qquad (1.2)$$

where σ is the matrix corresponding to a particular permissible symmetry operation. The negative sign must be used when the trans-

formation of an axial tensor changes right handed co-ordinates to left handed co-ordinates and vice-versa. Although there are as many similar equations as there are different symmetry operators in a group, it is not necessary to use them all as some symmetry matrices may be obtained from what are known as generating matrices, viz.

$$\left[\bar{2}_z\right] = \left[\bar{1}\right]\left[2_z\right] \quad \text{and} \quad \left[-3_z\right] = \left[+3_z\right]\left[+3_z\right] \qquad (1.3)$$

and no further simplification is obtained by using products of these generating matrices.

The generating matrices which are of interest to this present work are listed below.

$$\left[\bar{1}\right] = \begin{bmatrix} -1 & 0 & 0 \\ 0 & -1 & 0 \\ 0 & 0 & -1 \end{bmatrix} \qquad \left[2_y\right] = \begin{bmatrix} -1 & 0 & 0 \\ 0 & 1 & 0 \\ 0 & 0 & -1 \end{bmatrix}$$

$$\left[2_z\right] = \begin{bmatrix} -1 & 0 & 0 \\ 0 & -1 & 0 \\ 0 & 0 & 1 \end{bmatrix} \qquad \left[+3_z\right] = \begin{bmatrix} -\frac{1}{2} & \frac{\sqrt{3}}{2} & 0 \\ -\frac{\sqrt{3}}{2} & -\frac{1}{2} & 0 \\ 0 & 0 & 1 \end{bmatrix} \qquad (1.4)$$

Substitution of the first three matrices into equation (1.2) leads to a number of tensor components being equated to zero, whilst substitution of the matrix $\left[+3_z\right]$ gives linear relationships between the non-vanishing components. The considerable simplification of macroscopic property tensors arising from equations of this type utilising crystal symmetry, underline the importance of this subject as a tool in solid state physics.

1.2.2. Time Inversion Operator

The symmetry of the spatial distribution of the crystalline lattice has already been discussed, but in addition to periodic geometry, the lattice can have a periodic magnetic structure. This is possessed by all materials with an ordered spin arrangement, i.e. ferromagnetics, ferrimagnetics and antiferromagnetics. A possible additional symmetry operation for these materials is the operation representing a reversal or inversion of time[2], the spatial co-ordinates being unaltered. Electron spin is associated with angular momentum, and thus electron spin and magnetic moment both being reversed by the operation of time inversion are time anti-symmetric. This produces the possibility of the additional operator of time inversion being present in any magnetic crystal.

It is also possible, by considering the effects of time inversion, to divide all property tensors into two types; tensors whose components are invariant under time inversion (called i-tensors), and those whose components all change sign under time inversion (called c-tensors). Immediately it can be seen that since magnetic moment is time antisymmetric, all properties involving only odd powers of magnetisation or magnetic field are characterised by c-tensors, and from Neumann's Principle it follows that these properties can only be exhibited by crystals which are time antisymmetric. It is now necessary to investigate the actual restrictions imposed by the crystal symmetry of magnetic crystals on c-tensor properties.

1.2.3. Magnetic Symmetry

The description of the crystalline point symmetry has been modified by Tavger and Zaitsev[2] to accommodate the possibility of time inversion. Suppose the time inversion operation, which reverses all the spins of the lattice, is designated by a ~~symmetry~~ operator R. Then R is just an additional operator for non-magnetic crystals, but for many magnetic crystals, although R is not an operator by itself, it can quite possibly occur in combination with classical ~~symmetry~~ operators. Magnetic symmetry operators are defined as the combination of classical symmetry operators with the time inversion operator R required to transform the crystal back into itself.

It must be noted at this point that spin magnetic moment is not a true vector, because it transforms as a vector only in simple rotation, and in rotation-reflection it does not behave like one. Rotation-reflection may be considered as consisting of a rotation followed by an inversion of space co-ordinates. In the latter operation the components of a vector change sign, but the components of the pseudovector of spin are unchanged. The combination of an n-fold rotation axis and the operation of time inversion is written as an $\underline{n}$ operator, i.e. $\underline{1}$, $\underline{2}$, $\pm\underline{3}$, $\pm\underline{4}$, and $\pm\underline{6}$. Similarly a combination of an $\bar{n}$-fold rotation inversion axis and the operation of time inversion is written as an $\underline{\bar{n}}$ operator, i.e. $\underline{\bar{1}}$, $\underline{\bar{2}}$, $\pm\underline{\bar{3}}$, $\pm\underline{\bar{4}}$ and $\pm\underline{\bar{6}}$.

In similarity to classical operators, a crystalline lattice may

allow all classical operations, or all magnetic operations, or a restricted number of ~~either or~~ both, and so it is convenient to extend the concept of classical symmetry groups to cover the inclusion of magnetic operators. A table listing the 58 magnetic symmetry groups in addition to the 32 classical symmetry groups has been published by Birss[1][4], thus for example, group $\underline{4}/m$ has the operators 1, $\bar{1}$, 2_z, $\bar{2}_z$, $\pm \underline{4}_z$, $\pm \bar{\underline{4}}_z$ and group $\underline{6}mm$ has the operators 1, $\underline{2}_z$, $3(\bar{2}_\perp)$, $3(\bar{\underline{2}}_\perp)$, $\pm 3_z$, $\pm \underline{6}_z$.

The relation between the symmetry of the crystal in space-time and the symmetry of static physical properties exhibited by the crystal, is the same as considered previously for classical symmetry. This is Neumann's Principle which states that any symmetry operation permissible within the crystal is exhibited in the static physical properties of the crystal. As a result of the inclusion of the time inversion operation, Neumann's Principle is incorrect for dynamic properties, such as transport phenomena.

The classification of physical tensors as time symmetric or time antisymmetric is often obvious. Less obvious, but of fundamental interest is the classification of the electric and magnetic field vectors, $\underline{E}$ and $\underline{H}$. Time inversion reverses spin which in turn reverses any macroscopic magnetisation which the crystal may possess. The time antisymmetry of magnetic moment suggests that the magnetic field vector $\underline{H}$ is a c-tensor. Conversely, electric charge is time symmetric and this suggests that the electric field vector $\underline{E}$ is an i-tensor.

For Neumann's Principle to be valid in space-time it is necessary for the property tensor to be invariant under all permissible space-time symmetry operations allowed by the crystal. For the 58 magnetic symmetry groups it is essential to distinguish not only between polar and axial tensors as previously, but also between tensors which are invariant (i-tensors) and which change sign (c-tensors) under time-inversion. The i-tensor properties transform in an identical manner to property tensors in non-magnetic groups (i.e. according to equation (1.2)). The time antisymmetric property tensor $d_{ijk...n}$ transforms according to the relation

$$d_{ijk...n} = (-1) \pm \sigma_{ip}\, \sigma_{jq}\, \sigma_{kr} \ldots\ldots \sigma_{nu}\, d_{pqr...u} \qquad (1.5)$$

the (-1) being used when σ involves $\mathcal{R}$

and arising from the reversal of c-tensors under time inversion. The addition of (-1) makes it possible to use the matrices σ corresponding to space-only symmetry operations. The sign ambiguity is resolved as before, by using the negative sign when the transformation of an axial c-tensor changes right handed co-ordinates to left handed co-ordinates and vice versa. The generating matrices used for σ are identical to those of classical symmetry discussed in section 1.2.1.

1.3. FORBIDDEN EFFECTS

Magnetic symmetry does not forbid any tensor in all crystal classes, but however, certain types of tensors are zero in certain crystal classes. For example, all c-tensors are zero in non-magnetic symmetry groups. Magnetic symmetry is only a very recent develop-

ment[2], and previously it was thought[3] that the structure of all crystals was time symmetric so that static properties characterised by c-tensors were forbidden. For this reason various magnetic interaction effects are called Forbidden Effects even though space-time symmetry has now shown that some crystals have a time anti-symmetric structure which permits the existence of these effects. The time anti-symmetric crystals may be ferromagnetic, ferrimagnetic or antiferromagnetic, but only the latter will be considered here, for in ferromagnetic and ferrimagnetic materials the spin direction, and hence the magnetic symmetry, is strongly dependent on the magnetic field applied to the crystal.

1.3.1. Expansion of Thermodynamic Potential Energy

A thermodynamic potential ~~or Helmholtz free energy~~ Φ is the energy (apart from the thermal energy) which a body contains on account of its environment, and is exactly analogous to the kinetic and potential energies of mechanical systems. The environment may be expressed in general terms as a series expansion of the various effects which contribute energy to the body in question, and in the case considered here these are the magnetic field H_i, electric field E_i and stress σ_{ij}. Using the usual tensor notation the thermodynamic potential can be expanded as

$$-\bar{\Phi} = a_i H_i + b_i E_i + c_{ij}\sigma_{ij} + d_{ij} H_i H_j + e_{ij} E_i E_j + f_{ijkl}\sigma_{ij}\sigma_{kl}$$
$$+ g_{ij} H_i E_j + h_{ijk} E_i \sigma_{jk} + p_{ijk} H_i \sigma_{jk} + q_{ijk} H_i H_j E_k$$
$$+ r_{ijkl} E_i H_j \sigma_{kl} + s_{ijkl} H_i H_j \sigma_{kl} + t_{ijk} H_i E_j E_k + u_{ijkl} E_i E_j \sigma_{kl}$$
$$+ v_{ijklm} E_i \sigma_{jk}\sigma_{lm} + w_{ijklm} H_i \sigma_{jk}\sigma_{lm} + x_{ijk} H_i H_j H_k$$
$$+ y_{ijk} E_i E_j E_k + z_{ijklmn}\sigma_{ij}\sigma_{kl}\sigma_{mn} + \cdots\cdots\cdots \qquad (1.6)$$

Experimentally, the first terms are the largest, so that the series converges and the expansion is valid for all practical values of the variables.

The differential of the potential $\bar{\Phi}$ with respect to the magnetic field H_i gives the magnetic ~~induction~~ polarization I_i, thus

$$I_i = \frac{-\partial \bar{\Phi}}{\partial H_i} = a_i + d_{ij} H_j + g_{ij} E_j + p_{ijk}\sigma_{jk} + q_{ijk} H_j E_k$$
$$+ r_{ijkl} E_i \sigma_{kl} + s_{ijkl} H_j \sigma_{kl} + t_{ijk} E_j E_k$$
$$+ w_{ijklm}\sigma_{jk}\sigma_{lm} + x_{ijk} H_j H_k + \cdots\cdots\cdots \qquad (1.7)$$

Most of the coefficients can be named; a_i is the pyromagnetic constant, d_{ij} is the usual magnetic susceptibility, and x_{ijk} is the second order susceptibility constant. Considering the electric cross-effects, g_{ij} is the magnetoelectric coefficient, t_{ijk} is the second order magnetoelectric coefficient; and considering the stress cross-effects, p_{ijk} is the piezomagnetic coefficient, and w_{ijklm} is the second order piezomagnetic coefficient.

Differentiation of the potential $\bar{\Phi}$ with respect to electric field E_i gives the electric ~~induction~~ polarization P_i, thus

$$P_i = \frac{-\partial \bar{\Phi}}{\partial E_i} = b_i + e_{ij}E_j + g_{ij}H_j + h_{ijk}\sigma_{jk} + q_{ijk}H_jH_i$$
$$+ r_{ijkl}H_j\sigma_{kl} + t_{ijk}H_iE_k + u_{ijkl}E_j\sigma_{kl}$$
$$+ v_{ijklm}\sigma_{jk}\sigma_{lm} + y_{ijk}E_jE_k + \ldots\ldots \qquad (1.8)$$

Most of these coefficients can be named; b_i is the pyroelectric constant, e_{ij} is the usual electric susceptibility, and y_{ijk} is the second order susceptibility constant. Considering the individual magnetic and stress cross-effects, g_{ij} is the magnetoelectric coefficient, q_{ijk} is the second order magnetoelectric coefficient, h_{ijk} is the piezoelectric coefficient and v_{ijklm} is its second order term.

Finally, differentiating the potential $\bar{\Phi}$ with respect to stress σ_{ij} gives the strain ξ_{ij}, thus

$$\xi_{ij} = \frac{-\partial \bar{\Phi}}{\partial \sigma_{ij}} = c_{ij} + f_{ijkl}\sigma_{kl} + h_{ijk}E_i + p_{ijk}H_i + r_{ijkl}E_iH_j$$
$$+ s_{ijkl}H_iH_j + u_{ijkl}E_iE_j + v_{ijklm}E_i\sigma_{lm}$$
$$+ w_{ijklm}H_i\sigma_{lm} + z_{ijklmn}\sigma_{kl}\sigma_{mn} + \ldots\ldots \qquad (1.9)$$

Most of these coefficients can also be named; c_{ij} is the thermal expansion strain, f_{ijkl} is the elastic constant and z_{ijklmn} is the second order elastic constant of the medium. Considering the individual magnetic and electric cross-effects, h_{ijk} is the linear electrostriction coefficient, but u_{ijkl} is the usually measured 'square law' electrostriction coefficient, p_{ijk} is the linear magnetostriction coefficient, but s_{ijkl} is the usually measured 'square law' magnetostriction coefficient.

Remembering that H_i is a c-tensor and E_i and σ_{ij} are i-tensors, it follows that a_i, g_{ij}, p_{ijk}, r_{ijkl}, t_{ijk}, w_{ijklm}, x_{ijk} are coefficients of forbidden effects. Some common forbidden effects are discussed in more detail in the following sections.

1.3.2. Pyromagnetism

This is the most simple forbidden effect and is characterised by a first rank axial c-tensor Q_i defined by the equation

$$I_i = Q_i \theta \qquad (1.10)$$

where I_i is the intensity of magnetisation in the crystal caused by a temperature change of θ. Obviously, non-magnetic crystals cannot exhibit pyromagnetism, and in addition odd rank axial and even rank polar tensors are zero in the 21 magnetic crystal classes for which $\bar{1}$ is a symmetry operator. First rank axial c-tensors vanish identically in a further 38 groups, so that the number of classes for which pyromagnetism is possible is 31. These are 1, $\underline{1}$, 2, $\underline{2}$, m, $\underline{m}$, 2/m, $\underline{2}/\underline{m}$, $\underline{222}$, $\underline{mm2}$, $\underline{mm2}$, $\underline{mmm}$, 4, $\bar{4}$, 4/m, $\underline{422}$, $4\underline{mm}$, $\bar{4}\underline{2m}$, $4/\underline{mmm}$, 3, $\bar{3}$, $\underline{32}$, $3\underline{m}$, $\bar{3}\underline{m}$, 6, $\bar{6}$, 6/m, $\underline{622}$, $6\underline{mm}$, $\bar{6}\underline{m2}$, $6/\underline{mmm}$. In these 31 groups there are only three possible forms of the tensor Q_i, viz. the matrix $\begin{bmatrix} Q_1 & Q_2 & Q_3 \end{bmatrix}$ or $\begin{bmatrix} Q_1 & Q_2 & 0 \end{bmatrix}$ or $\begin{bmatrix} 0 & 0 & Q_3 \end{bmatrix}$.

Pyromagnetism is the property of a crystal to exhibit a spontaneous moment which will, in general, be temperature dependent. In antiferromagnetics the small magnetisation in the absence of an applied magnetic field is attributable to a slight tilting or

canting of the normally antiparallel spins so that their compensation is no longer perfect. The canting angle is very small, for in αFe_2O_3 the canted magnetic moment has been measured[5] as 10^{-4} of the total sublattice moment. Physically, it can be considered that spin canting is a possibility only in a crystallographic system where canting can exist without any loss of symmetry from the purely antiparallel state[6], and so the permissible spin directions for a crystal to exhibit pyromagnetism are severely restricted[7].

Hematite, αFe_2O_3, has a rhombohedral corundum type structure. In its high temperature magnetic phase, the four metallic ions which are situated along the principal body diagonal of the rhombohedral unit cell have their spins lying in the plane perpendicular to this axis, and the crystal belongs to the magnetic symmetry group 2/m which permits pyromagnetism. The antiparallel spin pairs are trigonally disposed perpendicular to the principal axis in successive unit cells, and because there is no 3-fold rotation operator along this axis, the spin pairs can incline slightly to give a moment perpendicular to the symmetry axis. This remanent magnetisation has been thoroughly investigated by many workers including Nagata et al[8] and Tasaki and Iida[9].

An identical crystallographic structure is exhibited by the low temperature phase of αFe_2O_3, although this has the spins directed along the principal axis. Because this is a 3-fold symmetry axis no spin canting from this axis is permissible without lowering the

symmetry, and hence the symmetry group $\bar{3}m$ is not pyromagnetic. Rather similar crystallographic and magnetic structures are exhibited by Cr_2O_3 and by $FeCO_3$, and because in each case the spins are directed along the principal axis[10], pyromagnetism is forbidden. Conversely $MnCO_3$ and $CoCO_3$ do not have the ionic spins directed along the principal axis[10], and in similar circumstances to hematite, spontaneous magnetisation can exist and has been measured by Borovik-Romanov and Orlova[11].

Manganese fluoride, ferrous fluoride, cobalt fluoride and nickel fluoride are all isomorphic antiferromagnetic difluorides having the rutile type of structure. In MnF_2, FeF_2 and CoF_2 the spins are directed along the tetragonal axis[12] and the crystal structure is in group $4/mmm$ which means pyromagnetism is forbidden. In NiF_2 the spins lie at an angle to the tetragonal axis[13] and so the magnetic symmetry is reduced to group mmm which permits spin canting without further reduction of the symmetry. A comprehensive investigation of pyromagnetism in nickel fluoride has recently been conducted by Bozorth and Joenk[14].

1.3.3. Magnetoelectric Effect

The magnetoelectric effect which involves electric and magnetic field interactions in the thermodynamic potential is characterised by a second rank c-tensor. If I_i is the magnetic polarisation induced by an electric field E_j, then a defining equation of the magnetoelectric tensor Q_{ij} can be of the form

$$I_i = Q_{ij} E_j \qquad (1.11)$$

Since I_i are components of an axial c-tensor of first rank and E_j are components of a first rank polar i-tensor, then Q_{ij} is a second rank axial c-tensor.

It is impossible for any crystal in a non-magnetic symmetry group to exhibit the magnetoelectric effect, and in addition, being an even rank axial tensor, it is zero in the 21 magnetic classes for which $\bar{1}$ is a symmetry operator. This leaves 69 magnetic classes, but second rank axial c-tensors vanish identically in a further 11 groups, so that the number of classes in which the magnetoelectric effect is possible is 58. These are 1, $\underline{\bar{1}}$, 2, $\underline{m}$, $\underline{2/m}$, $\underline{2}$, m, $\underline{2/m}$, 222, $\underline{mm2}$, $\underline{mmm}$, $\underline{mm2}$, $\underline{222}$, mm2, $\underline{mmm}$, 3, $\underline{\bar{3}}$, 32, $\underline{3m}$, $\underline{\bar{3}m}$, $\underline{32}$, 3m, $\underline{\bar{3}m}$, 23, $\underline{m3}$, $\underline{m3m}$, 4, $\underline{\bar{4}}$, $\underline{4/m}$, $\underline{4}$, $\underline{\bar{4}}$, $\underline{4/m}$, 422, $\underline{4mm}$, $\underline{\bar{4}2m}$, $\underline{4/mmm}$, $\underline{422}$, $\underline{4mm}$, $\underline{\bar{4}2m}$, $\underline{\bar{4}2m}$, $\underline{4/mmm}$, $\underline{422}$, 4mm, $\underline{\bar{4}2m}$, $\underline{4/mmm}$, 432, $\underline{\bar{4}3m}$, 6, $\underline{\bar{6}}$, $\underline{6/m}$, 622, $\underline{6mm}$, $\underline{\bar{6}m2}$, $\underline{6/mmm}$, $\underline{622}$, 6mm, $\underline{\bar{6}m2}$, $\underline{6/mmm}$, and in these 58 groups there are 11 different forms of the magnetoelectric tensor Q_{ij}.

The magnetoelectric effect was predicted by Dzyaloshinskii[15] in 1959 and first observed experimentally by Astrov[16] in 1960 by subjecting an unoriented crystal of Cr_2O_3 to an alternating electric voltage and detecting the induced magnetisation by means of a coil and amplifier. The magnetic symmetry group to which chromium oxide belongs is $\underline{3m}$, for although it has the same crystallographic structure as hematite (which is in group $\bar{3}m$), its spin structure is vastly different. Measurements on an oriented crystal of Cr_2O_3 were first performed by Folen et al[17] using a 1 kc/s electric field and

detecting the magnetisation as a few microvolts signal induced into a search coil of 10,000 turns. As expected, the magnetoelectric magnetisation dropped rapidly to zero at the Neel temperature of 307° K when the structure became magnetically disordered. The converse effect of applying a magnetic field and observing an electrical polarisation was first performed on Cr_2O_3 by Rado and Folen[18], who reported an exactly similar temperature dependence to that of the converse effect measured by Folen et al.

Two other entirely different materials have been investigated, the first being Ti_2O_3 in which the electric polarisation produced by a magnetic field was measured by Al'shin and Astrov[19]. The second material is gallium ferrite (Ga_2FeO_3), which is pyromagnetic and probably belongs to the symmetry class 2mm. Rado[20] found that in gallium ferrite the magnetoelectric coefficients exceeded those of Cr_2O_3 by an order of magnitude, and it is possible that the magnetoelectric effect in selected ferrites may, in the future, have some commercial use if its magnitude can be further increased.

1.3.4. Piezomagnetism

The piezomagnetic effect which involves interaction between stress and magnetic field in the crystalline lattice is characterised by a third rank c-tensor. If I_i is the magnetic polarisation induced by a stress component T_{jk} then a defining equation of the piezomagnetic tensor P_{ijk} can be of the form

$$I_i = P_{ijk}T_{jk} \quad . \tag{1.12}$$

Since I_i are first rank axial tensor components and T_{ij} are second rank polar i-tensor components, the P_{ijk} is a third rank axial c-tensor.

It is impossible for any crystal in a non-magnetic symmetry group to exhibit the piezomagnetic effect, and in addition being an odd rank axial tensor it is zero in the 21 magnetic classes for which $\bar{1}$ is a symmetry operator. This leaves 69 magnetic classes, but because P_{ijk} is symmetrical in the last two indices (i.e. $T_{jk} = T_{kj}$) this causes the piezomagnetic tensor in the three classes 432, $\bar{4}3m$ and $m3m$ to be zero. This is a small example of the simplification that can be afforded by utilising the intrinsic symmetry of the property tensor. There remain 66 magnetic classes which are 1, $\bar{1}$, 2, m, 2/m, $\underline{2}$, $\underline{m}$, $\underline{2/m}$, 222, mm2, mmm, $\underline{222}$, $\underline{mm2}$, $\underline{mm2}$, $\underline{mmm}$, 23, m3, $\underline{m3m}$, 3, $\bar{3}$, 32, 3m, $\bar{3}m$, $\underline{32}$, $\underline{3m}$, $\underline{\bar{3}m}$, 4, $\bar{4}$, 4/m, $\underline{4}$, $\underline{\bar{4}}$, $\underline{4/m}$, 422, 4mm, $\bar{4}2m$, 4/mmm, $\underline{422}$, $\underline{4mm}$, $\underline{\bar{4}2m}$, $\underline{\bar{4}2m}$, $\underline{4/mmm}$, $\underline{422}$, $\underline{4mm}$, $\underline{\bar{4}2m}$, $\underline{4/mmm}$, $\underline{432}$, $\underline{\bar{4}3m}$, 6, $\bar{6}$, $\underline{6}$, $\underline{\bar{6}}$, 6/m, $\underline{6/m}$, 622, 6mm, $\bar{6}m2$, 6/mmm, $\underline{622}$, $\underline{6mm}$, $\underline{\bar{6}m2}$, 6/mmm, $\underline{622}$, $\underline{6mm}$, $\underline{\bar{6}m2}$, $\underline{\bar{6}m2}$, $\underline{6/mmm}$, and in these groups there are 16 different forms of the piezomagnetic tensor P_{ijk}.

The piezo magnetic effect was first observed experimentally by Borovik-Romanov[21] in 1959. Using single crystals of cobalt and manganese fluorides he observed a shift in the magnetisation curve parallel to the magnetisation axis when pressure was applied to the crystal. Both these antiferromagnetic difluorides belong to the magnetic symmetry group $\underline{4/mmm}$ which has only two different components in the three terms of the matrix characterising the

effect. These piezomagnetic coefficients were later measured[22] as a function of temperature using an ultrasonically applied pressure. The coefficients were found to follow a type of Brillouin magnetisation curve up to the Neel temperature of the material. The only other material that has been experimentally investigated[22] is $FeCO_3$ which belongs to the symmetry group $\bar{3}m$. The experimental evidence for the piezomagnetic effect will be discussed more fully in section 1.4.2.

1.3.5. Linear Magnetostriction

This effect involves interaction between magnetic field and strain in the crystalline lattice and can be considered as the converse of piezomagnetism. If E_{ij} is the strain induced by a magnetic field H_k then the defining equation of the linear magnetostriction coefficient is

$$E_{ij} = Q_{ijk} H_k \qquad (1.13)$$

Since E_{ij} are second rank polar i-tensor components and H_k are first rank axial c-tensor components, then Q_{ijk} is a third rank axial c-tensor.

The restrictions for crystal classes having a non-zero Q_{ijk} are the same as for the piezomagnetic tensor P_{ijk} with the additional provision, suggested by Birss and Anderson[23], that pyromagnetism must not be present. This reduces the 66 piezomagnetic classes to 35 classes exhibiting linear magnetostriction and 31 classes exhibiting pyromagnetism. Their reason for excluding the pyromagnetic

classes is that in them the linear magnetostriction will probably be much smaller than the magnetostriction associated with ferromagnetic domain reorientation in the material. This argument, however, does not preclude the possibility of true linear magnetostriction in high fields after the domain magnetisation has aligned itself with the field. The 35 magnetic symmetry groups permitted to exhibit linear magnetostriction are 222, mm2, mmm, 32, 3m, $\bar{3}$m, 23, m3, m3m, 4, $\bar{4}$, 4/m, 422, 4mm, $\bar{4}$2m, 4/mmm, 422, 4mm, $\bar{4}$2m, $\bar{4}$2m, 4/mmm, 432, $\bar{4}$3m, 6, $\bar{6}$, 6/m, 622, 6mm, $\bar{6}$m2, 6/mmm, 622, 6mm, $\bar{6}$m2, $\bar{6}$m2, 6/mmm, and in these groups there are eight different forms of the tensor Q_{ijk}.

Linear magnetostriction in hematite (αFe_2O_3), which exists in the magnetic group $\bar{3}$m at low temperatures, is the subject of the present work. Apart from this, no experimental investigation of linear magnetostriction has been published although it is an effect which should be exhibited by the piezomagnetic fluorides of cobalt and manganese, (group 4/mmm), and ferrous carbonate ($\bar{3}$m).

1.3.6. Non-linear Susceptibility

The fifth and final forbidden effect that has been measured is non-linearity in susceptibility of antiferromagnetics. The intensity of magnetisation can be described by a series expansion of magnetic field, thus

$$I_i = \chi_{ij}H_i + C_{ijk}H_iH_j + \ldots\ldots \qquad (1.14)$$

Since I_i are components of a first rank axial c-tensor and H_i and H_j are each components of a first rank axial c-tensor also, then the usual antiferromagnetic susceptibility χ_{ij} is a polar i-tensor and C_{ijk} is a third rank axial c-tensor.

The restrictions on the magnetic symmetry classes which can exhibit a non-linearity in susceptibility are the same as for piezomagnetism but with the additional restriction of the reversibility of the order in which the free energy may be successively differentiated with respect to the two components of $\underline{H}$. This causes the tensors in the eight magnetic classes 422, 4mm, $\bar{4}$2m, 4/mmm, 622, 6mm, $\bar{6}$m2 and 6/mmm to be zero[23]. This subject has been investigated theoretically by Shtrikman and Treves[24] and they concluded that there were only two possible forms of the non-linear susceptibility tensor. The only experimental investigation of C_{ijk} was made by Gorodetzky and Treves[25] in the orthoferrites $RFeO_3$ (where R is a rare earth ion), which are also pyromagnetic. Their results indicated a value of C_{ijk} of the order of 10^{-8} e.m.u./mole at room temperature.

Both linear magnetostriction and non-linear susceptibility are recently formulated forbidden effects and consequently any experimental evidence not associated with the present work is scanty and mainly non-existent. The lack of evidence on this branch of the forbidden effects may be considered as the reason why this line of research was adopted.

1.4. PIEZOMAGNETISM

1.4.1. Historical Basis

The first mention of piezomagnetism in the literature was by Voigt[26] in 1928. He derived the reasons for the existence of the effect from the thermodynamic potential by using comparisons with piezoelectricity which was a well-known phenomenon at that time. The atomic explanation which he gave was that the electron orbits are deformed by pressure to give a non-compensation of moments within the atom which results in an external magnetic moment being produced. This basic reasoning is certainly incorrect, as he did not appreciate the essential differences between magnetic and non-magnetic materials (i.e. the effect of spin ordering). Voigt also produced a list of allowed piezomagnetic tensors from the symmetry of the tensor in each of the classical crystallographic groups.

It was not until 1953 that the piezomagnetic effect was again considered theoretically. Zocher and Török[3] concluded that since the pyromagnetic and piezomagnetic coefficients are time anti-symmetric and a crystalline lattice is always time symmetric, these were truly forbidden effects. The suggestion that a crystal with ordered spin arrangement could be time antisymmetric, made by Tavger and Zaitsev[2] in 1956, opened up the possibility of the existence of all the hitherto forbidden effects. In a review of 'the problem of piezomagnetism' in 1958, Dzyaloshinskii[27] suggested suitable materials for investigation as - low temperature αFe_2O_3, $FeCO_3$, MnF_2, CoF_2 and FeF_2, and calculated the form of the piezo-

magnetic tensor in each case from the magnetic symmetry elements of the appropriate spin structure which give terms of similar symmetry in the thermodynamic potential. This work was followed by a review of magnetic crystallographic groups and their properties by Le Corre[28]. Many materials for which neutron diffraction data was available were classified into their magnetic symmetry groups, and in these, the possibility of piezomagnetism was examined. In addition to the previously mentioned materials, Le Corre also suggested CrSb and the similar isomorphic intermetallic compounds CrS, FeS, MnTe, FeTe, MnAs, MnBi, as likely to exhibit a piezomagnetic moment.

In early 1959, just before the first observations of piezomagnetic moments were reported, Moriya[29] published a theoretical evaluation of the magnetisation that could be produced in cobalt fluoride by the application of pressure. CoF_2 has a crystal structure of the rutile type with the magnetic ions lying on two planes with spin directions in opposition. A linear compression applied in the plane distorts the crystalline fields within the two planes and this distortion has a different effect on the two kinds of spin. This produces resultant magnetic moments on each plane and hence an external magnetisation which is rather like ferrimagnetism.

1.4.2. Experimental Verification

Later in 1959 Borovik-Romanov[21] reported the first experimental observation of the piezomagnetic effect. To detect the

magnetic moment they used a specially constructed torsion balance in which a press containing the specimen was suspended on a vertical wire. The press was controlled by helium gas pressure in the surrounding space acting upon an evacuated sealed bellows, so that as the gas pressure was reduced the compressed bellows tried to expand, and by way of a lever, applied a magnified pressure to the specimen. In this way a maximum pressure of 500 kg/cm^2 was applied to a 1 mm^2 cross-section of the crystal at liquid hydrogen temperature of either material. Their results indicated that the maximum pressure on a specimen of CoF_2 produced a magnetisation of 10 gauss/mole, being independent of the magnitude of the field used to measure it. The effect in MnF_2 was approximately 100 times smaller than in CoF_2.

These experimental details were amplified in a later paper[30]. This also included curves showing that both the tensor components of piezomagnetism in cobalt fluoride were constant under stress, thus implying that the second order coefficient, w_{ijklm}, from equation (1.7), was negligibly small. A magnetic moment was obtained in CoF_2 when the pressure was directed along a crystal axis and also when the pressure was applied at 45° to the crystal axis (i.e. a shear stress). In MnF_2 the effect was almost exactly 100 times smaller and their sensitivity was such that the magnetisation produced by the maximum stress was almost the minimum detectable. The paper also derived from the thermodynamic potential energy, the permissible directions of pressure induced magnetisation, the

results agreeing completely with experiment and also with the predictions of magnetic symmetry. It was suggested that the application of stress caused the sublattice magnetisations to be no longer exactly antiparallel, which is rather similar to the spontaneous rotation of spins in pyromagnetics, thus causing an external magnetisation to appear. From the experimental results, the rotational angle was calculated to be 10^{-3} radians, which is about ten times larger than the pyromagnetic rotation in hematite[5].

The third and final experimental report was presented by Borovik-Romanov et al[22] in 1962 at the Kyoto Magnetism Conference. The piezomagnetic effect in $FeCO_3$ was discovered, and in addition it was found that magnetic annealing (i.e. cooling in a magnetic field) gave a greatly enhanced effect. This observation was ascribed to the production of a single antiferromagnetic domain state throughout the crystal. The report also revealed that work on CoF_2 was still proceeding using an entirely different apparatus. Pressure was applied ultrasonically to the crystal and the induced moment picked up by coils placed round the specimen. In this way, a temperature dependence of the effect was obtained, showing the moment dropped rapidly to zero as the Neel temperature is approached, in a similar manner to the temperature dependence of the sublattice magnetisation. A serious disadvantage to the previous static pressure apparatus was the inability to measure at any other temperature than 20.4° K, due probably to the unknown thermal expansion of the rod transmitting the pressure from room temperature to

liquid hydrogen temperature. The use of ultrasonically applied pressure overcame this difficulty. There is no further reported work on piezomagnetism in the literature.

1.4.3. Piezomagnetism and Antiferromagnetic Domains

Although it is not a necessary condition of antiferromagnetism, the spin structure of these materials is generally uniaxial and these conditions allow the possibility of the existence of 180° domain walls. These walls may be defined as occurring where there is a 180° phase shift in the repetition pattern of spin direction. 180° domains are linked to each other by the time inversion operator R, and if R is not an operator of the crystal as a whole - which is certainly correct if the crystal exhibits the forbidden effects - then the domains must be distinguishable by any property of the crystal that does not have R as operator. The forbidden effects, characterised by c-tensors, will therefore show reversal of sign with reversal of domain type.

This was noted by Le Corre[28] who considered what happens to the domains when an antiferromagnetic crystal is cooled through the Neel point. If no energy is applied to give one domain type preference over the other, then the material, when cooled, would have a statistically equal distribution of the two domain types. If a preferential energy is given to one domain when cooling, then this favourable domain type will grow throughout the crystal and the material will cool as a single antiferromagnetic domain. The

preferential energy was suggested by Le Corre to be available from the simultaneous impression of magnetic field and stress in a piezomagnetic material when cooling through the Neel point.

The existence of 180° antiferromagnetic domains was experimentally verified[30] in 1960 by the piezomagnetic effect. It was found that cooling crystals of cobalt and manganese fluoride in a magnetic field with a mechanical stress applied, gave an increase in the piezomagnetic moment in both materials. The increase was so considerable in MnF_2 that the moment only became detectable when the magnetic annealing procedure was followed. At low measurement fields the piezomagnetic moment had a direction which was identical to the direction of the annealing field, but however, in measurement fields in the opposite direction to the piezomagnetic moment, and above about 600 oersteds, the magnetisation of the specimen reversed. This is obviously due to the extra piezomagnetic energy given to the domain type which was of unfavourable orientation during annealing, arising from the measurement field and the stress together applied to the crystal. It is probable that during annealing very small regions of unfavourably oriented domain type still exist, being pinned to lattice imperfections and the like. It is these small regions of opposite domain type which can grow and spread throughout the crystal when given sufficient energy.

According to Borovik-Romanov, the reversal of magnetisation occurred slowly, so that almost complete reversal took seven minutes in a field of 1000 oersteds. It is important to mention here

that it was observed that the results on domain reversal were not readily reproducible. This is probably accountable if it is assumed that the domain mobility is very low at the low temperature used. At 20.4° K the thermal vibration energy of the magnetic ions is very small, so that if a magnetic energy of just less than a critical value is applied to an ion, the probability of the total energy exceeding the critical value is also small. Since this is a statistical energy process, the potential barrier may be surmounted in milliseconds at room temperature, but it would take very considerably longer at liquid hydrogen temperature. With this as a basis, it would seem possible that the observed speed of domain reversal could be explained, as also could the unreproducibility in the reversal results.

This section illustrates the use of results obtained from the measurement of forbidden effects to give a good indication of the antiferromagnetic domain state of a material. The present work utilizes linear magnetostriction to investigate antiferromagnetic domains in hematite.

1.5. HEMATITE

1.5.1. Crystal Structure

Investigation of linear magnetostriction was performed on ferric oxide (αFe_2O_3). This oxide, which is more commonly known by its mineralogical name, hematite, has a corundum type crystal structure

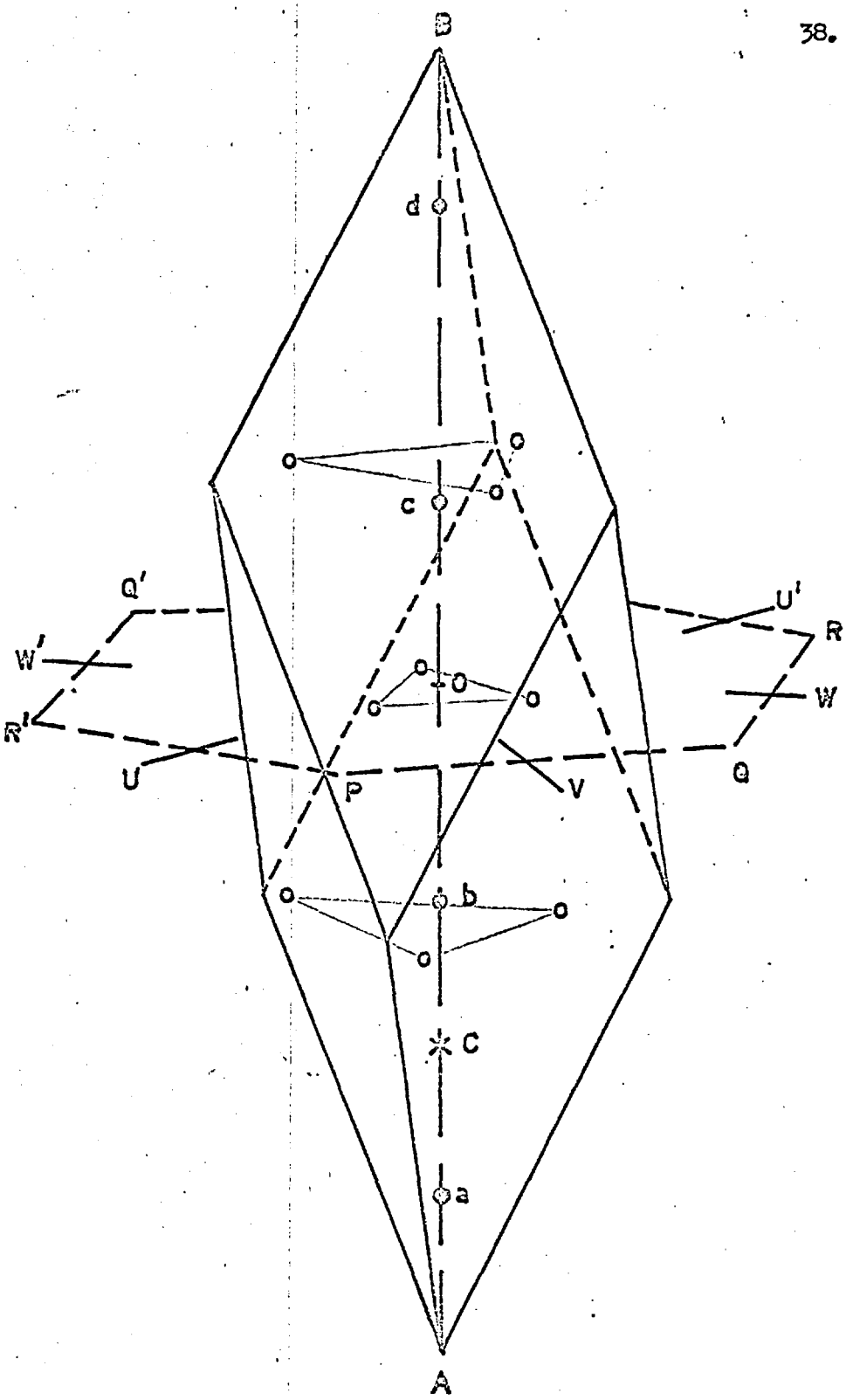


Figure 1. The unit cell of hematite, oxygen ions shown as open circles, iron ions shown as solid circles.

as established by Pauling and Hendricks[31] and shown in Figure 1. The unit cell is rhombohedral with its centre at O, and having four metallic ions situated along the [111] axis AB, at the points a, b, c, d, so that Aa = Ob = Oc = Bd. The oxygen ions, which are shown as open circles in Figure 1, are arrayed in trigonal layers perpendicular to the [111] axis. Each iron atom is surrounded by six oxygen atoms which are not at the corners of a regular octahedron although they appear to be so, for three of these atoms are closer to the iron atom than the other three. Each oxygen atom is surrounded by four iron atoms, two of which are nearer than the other two. The structure can be represented as being composed of planes containing iron atoms only, separated by planes containing oxygen atoms only. Figure 2 shows the position of the oxygen atoms relative to a succession of equally spaced (111) planes, the number indicating the perpendicular distance of the planes from A (towards B) in units of one-sixth the distance AB.

Considering this classical structure of the crystal it can be seen that AB is a 3-fold rotation axis, and OU, OV, and OW are 2-fold rotation axes. There is a centre of symmetry which can be seen from Figure 2 to be at C, where AC = CO, since C lies on the line AB at a distance of $1\frac{1}{2}$ of the units used from A. Hence plane 1 is an inversion through C of plane 2, and plane 0 is an inversion through C of plane 3, etc. The classical symmetry elements are 1, $\bar{1}$, $3(2_\perp)$, $3(\bar{2}_\perp)$, $\pm 3_z$, $\pm \bar{3}_z$, so that the structure belongs to the point group $\bar{3}m$.

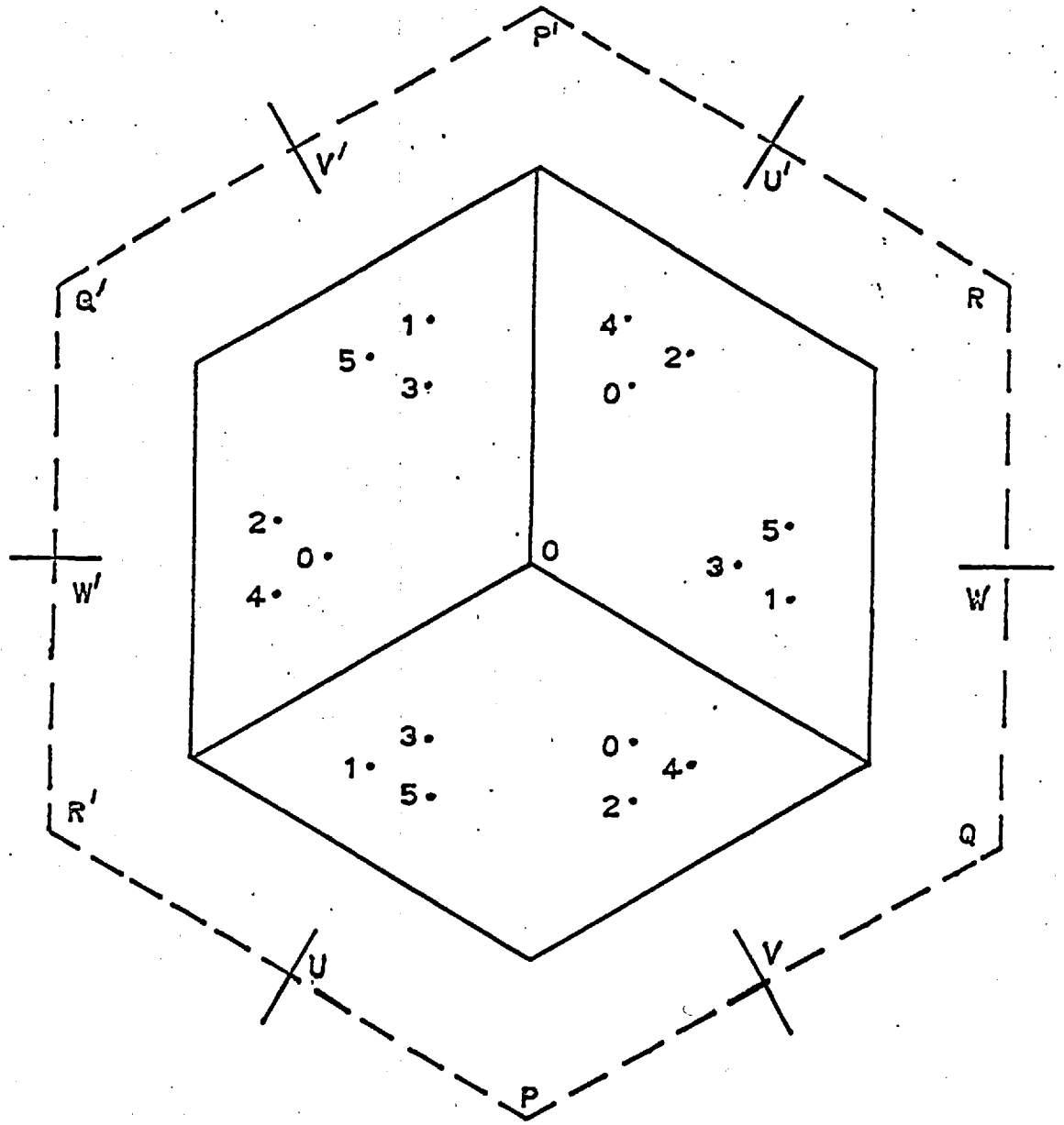


Figure 2. The positions of the oxygen ions relative to a succession of equally spaced (111) planes, the numbers indicating the perpendicular distance of the planes from A (towards B) in units of one sixth the distance AB.

1.5.2. Spin Structure

Determination of the spin structure of hematite was reported by Shull, Strauser and Wollan[32] in 1951. Spins on adjacent Fe^{3+} ions are parallel and antiparallel and conform to the signature + + - - for a, b, c, d, so that each ion has a ferromagnetic coupling in one direction and an antiferromagnetic coupling in the opposite direction. The actual direction of the spin moment is also of importance, and it was found that between 250° K and the Neel point of 950° K, the spins lay in any one of the symmetry planes BOR, BOQ or BOP, making a small angle with the [111] axis. In the low temperature spin arrangement, the point C in Figure 1 is still the centre of symmetry, and because the spin moments lie along the 3-fold axis, one 3-fold and three 2-fold rotation axes are still permitted. This gives symmetry elements 1, $\bar{1}$, $3(\bar{2}_{\perp})$, $3(2_{\perp})$, $\pm 3_z$, $\pm \bar{3}_z$ which correspond to the magnetic symmetry group $\bar{3}m$. A material in this group is permitted from symmetry consideration to exhibit piezomagnetism, linear magnetostriction, and a non-linear susceptibility term, but the pyromagnetic tensor is zero.

In the high temperature spin arrangement the spins at a and b may point, for example, nearly parallel to OR whilst those at c and d point parallel to OR'. At these temperatures the only magnetic rotation axis of the unit cell is the one 2-fold axis perpendicular to the spin direction (i.e. OV in this case). The point C is still the centre of symmetry so that the appropriate symmetry elements are 1, $\bar{1}$, 2, $\bar{2}$, and the material belongs to the magnetic group 2/m.

This group permits pyromagnetism, piezomagnetism and a non-linear susceptibility term, but does not permit linear magnetostriction as defined by Birss and Anderson[23], because of the pyromagnetism.

Physically the pyromagnetism is permissible because it is possible to rotate the spins about AB away from OR and OR' towards the direction OV without altering any of the magnetic symmetry elements. It is possible to rotate the two sets of spins through 90° so that their directions coincide, whilst still preserving 2/m symmetry, and then the crystal would exhibit pure ferromagnetism. In hematite, however, internal forces prevent the spins rotating far from the antiparallel position, so that with the experimental[5] ratio of canted moment to the total sublattice moment as 2×10^{-4}, the spins are only 2.5 minutes of arc from the antiparallel position.

1.5.3. Morin Transition

There are many properties of hematite, both magnetic and non-magnetic which show discontinuities at about 250° K where the spin structure transition occurs. The transition was first reported from magnetic measurements by F. J. Morin[33] in 1950 and now generally bears his name, for although the susceptibility of hematite had been measured many times previously[34] and no transition detected, measurements had not been taken below 0° C. At the transition the parallel magnetic susceptibility changes rapidly from a value of 17×10^{-6} per gram below the transition to 130×10^{-6} per gram above. Morin also found that 1% titanium impurity was sufficient

to completely suppress the transition.

Magnetostriction is an effect closely linked with magnetisation and would thus be expected to show a sharp discontinuity at the Morin transition. The assumption was shown to be correct by Urquhart and Goldman[35] who observed a strain increase of approximately eight times as the temperature was raised through the transition, in a fixed field of 6500 oersteds. These authors also reported a linear decrease in the transition temperature (as defined by the strain discontinuity) with applied field, which amounted to six degrees C. in 8000 oersteds.

Other crystal properties which are not closely linked with magnetisation would be expected to show a very reduced dependence on the Morin transition. Recently the magnetic transformation has been detected[36] as a slight change of slope in the thermal expansion vs. temperature curve indicating a peak in the expansion coefficient. In 1951 Morin[37] performed conductivity and Hall coefficient measurements on hematite and his results do not appear to exhibit any peculiarity within the transition temperature range.

1.5.4. Antiferromagnetic Domains

Two quite different types of antiferromagnetic domains can exist in hematite. Let us consider first those existing from 250° K to 950° K and which have a resultant magnetisation due to the canted moments. It was mentioned in section 1.5.2. that the spins could lie in any one of the symmetry planes BOR, BOQ, or BOP of Figure 1,

giving the overall canted spin magnetisation along OV, OU, or OW respectively. In the extended lattice of any real crystal of hematite there is the possibility of 120° magnetic domains existing as none of the directions OV, OU, or OW is energetically more favourable to the canted moment. There is a further possibility that each 120° domain can support two domains, one with the canted moment directed 180° away from the other, because OV is no more favourable to magnetisation than OV', etc.

Polarized neutron experiments at room temperature have shown[38] that each of the trigonal domains becomes nearly a single 180° domain type in fields of the order of 100 Oersteds, and that the remanent magnetisation is caused by hysteresis of reversal of these canted spin 180° domains. Up to 100 Oersteds the distribution of trigonal domains is isotropic, but above this value the canted moment rotates to become parallel to the applied field causing the spins to be situated perpendicular to the field direction.

Room temperature domain effects in hematite were first found by utilising the stray fields of the domains to deflect an electron beam reflected at grazing incidence from the crystal[39]. A little later, domains were actually observed[40] using the Faraday effect in very thin synthetic crystals. Blackman and Gustard[41] have observed the domain walls microscopically using an acetone based magnetic colloid, and noted that the wall magnetisation disappears below the transition temperature. After repeatedly cooling and warming the crystal through the transition temperature range, the

domain pattern regularly returned to its original configuration, which would indicate that the crystal retains some kind of memory of its high temperature domain state when cooled below the Morin transition temperature.

Let us now consider antiferromagnetic domains existing below 250° K, which is an entirely different situation. Neutron diffraction cannot distinguish between a spin system in a certain unit cell with c-axis vertical, being up, up, down, down, or down, down, up, up, because it can only distinguish spin dense planes and directions and not the sense of individual spins. Adjacent regions of these two possible spin distributions can be described as 180° domains, although neither domain has a nett magnetisation. These domains can be distinguished by use of polarized neutrons[38,42] and it has been found by this method that when hematite is cooled through the Morin transition in the absence of a magnetic field, the crystal contains a roughly equal distribution of the two 180° domains. It was necessary to cool the crystal in a field of several hundred oersteds to obtain a high polarisation ratio below the transition.

The effect of the antiferromagnetic domain pattern in a material exhibits itself in the magnitude and sign of the forbidden properties, for the domains are related to each other by the time inversion operator R, and since magnetic symmetry shows that R is not an operator of the crystal as a whole, the domains must be distinguishable by any c-tensor property. Examples of these properties that do not have R as operator are piezomagnetism, linear magneto-

striction, and non-linear susceptibility in αFe_2O_3, and the magneto-electric effect in Cr_2O_3.

1.5.5. Antiferromagnetic Domain Annealing

It has been established experimentally, both by this work and by the polarized neutron experiments, that antiferromagnetic domain annealing in hematite can be effected by cooling the crystal from a largely single domain condition above the transition. In a canted spin antiferromagnetic there are two types of 180° domain walls, those in which the ferromagnetic component reverses sign (FW) and those in which the antiferromagnetic component reverses sign (AFW). The situation is shown diagramatically in Figure 3 where (a) represents a single domain, and (b) FW alone, (c) AFW alone, and (d) FW and AFW in coincidence, and the ferromagnetic component is shown as straight out of or into the page by the usual convention. It is of importance to note that (b) and (c) are not walls between domains related by time inversion, since this operator reverses all the spins including the canted moment. From the canted moment coupling energy[42] it is probable that all the 180° domains are related by time inversion, and so only FW and AFW in coincidence are permissible. Application of a sufficiently large magnetic field at room temperature acting on the canted moment, removes all FW and because of their association also removes all AFW. The crystal is then in the single domain state (a) and can be cooled through the Morin transition into a single domain state at low temperatures. The field

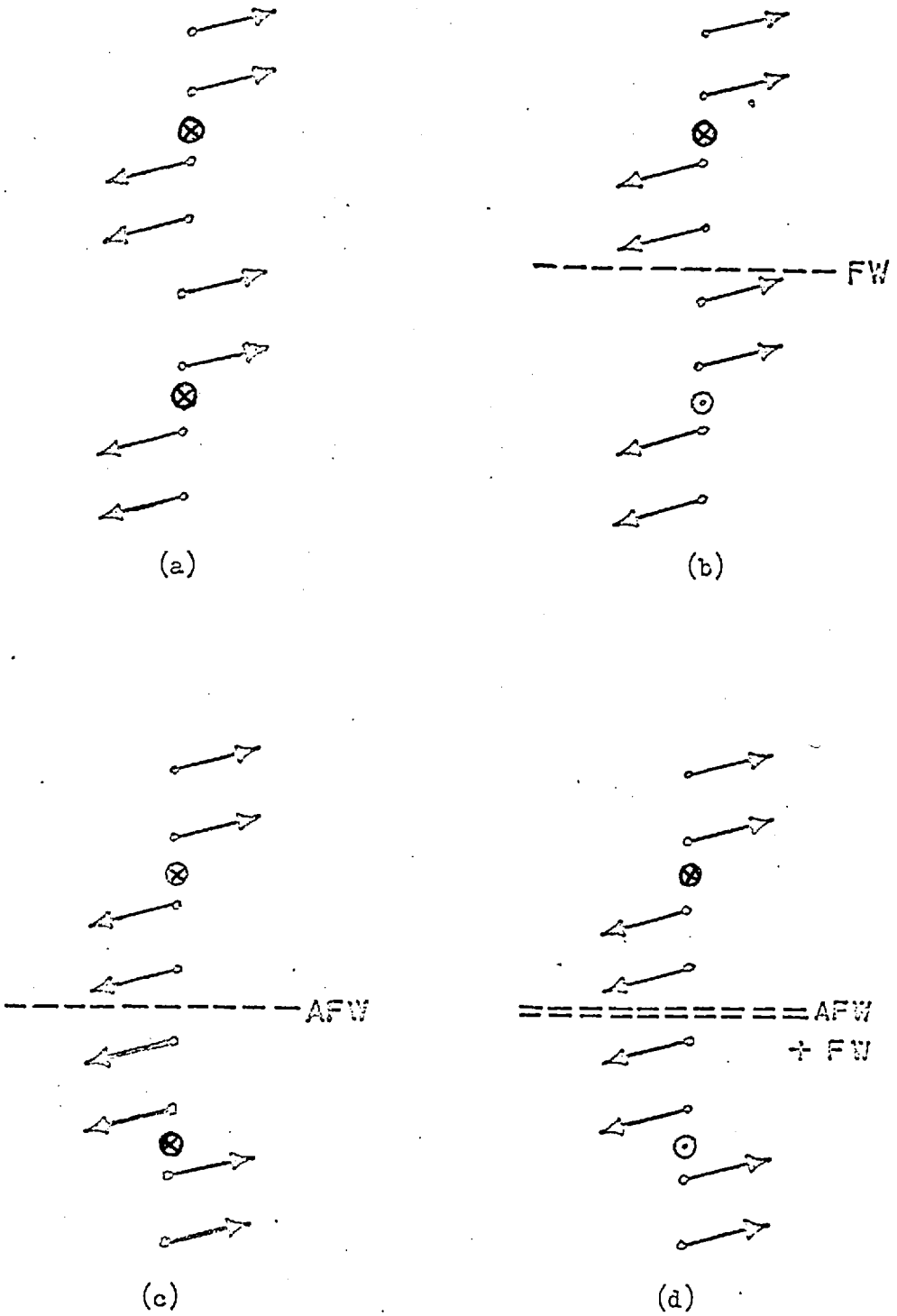


Figure 3. High temperature domain pattern and walls in hematite (a) represents a single domain (b) FW alone (c) AFW alone and (d) FW and AFW in coincidence.

needed to anneal a single domain into the low temperature phase is that required to produce a single domain at room temperature.

1.5.6. Remanence

Room temperature hematite has a considerable remanent magnetisation in the (111) plane due to hysteresis of reversal of the canted spin 180° domains. Only relatively recently has it been noticed that remanence is still present to a very small extent below the Morin transition. It has been found by Lin[43] that upon cooling a natural crystal under field free conditions, the magnetic remanence, whilst decreasing in value through the transition, also rotated from being in the (111) plane to being along the $[\bar{1}\bar{1}\bar{1}]$ axis. The rotation of the magnetisation vector is shown clearly in Figure 4 which is reproduced from Lin's paper.

At the same time it was found independently by Iwata et al[44] that the remanent magnetisation acquired at room temperature, and the magnetisation memorized by the specimen when cooled once to - 200° C and then brought back to room temperature, are independent of the field producing the remanence and are always in the ratio 1:0.52. A reverse magnetic field applied at - 200° C could reduce the room temperature moment only if it exceeded a threshold value of about 40 kilo-oersteds, and similarly a specimen could be given a room temperature remanence by the application of a field in excess of 50 kilo-oersteds at - 200° C. The cooling and warming memory of remanence was also found by Nagata[8] to be constant when performed

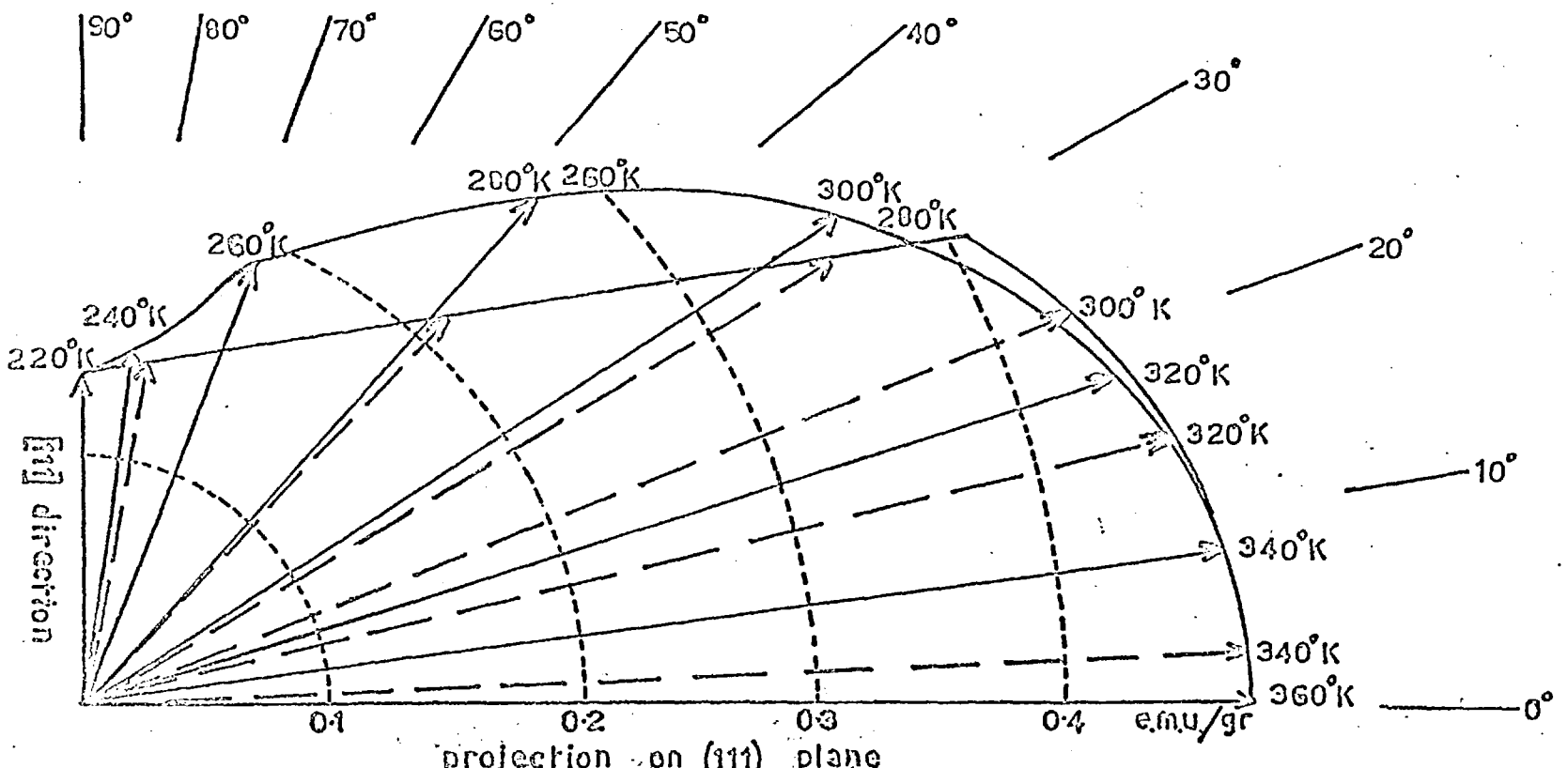


Figure 4. Polar plot of magnitude and direction of the remanence vector in an Elba hematite crystal.

Ascending temperature - full arrow. Descending temperature - broken arrow.

From: LIN, S. T. J. Phys. Soc. Japan, 17-B-I, 229 (1962).

under field free conditions. Tasaki and Iida[45] report that the direction of the low temperature moment follows closely that of the applied field through the transition, so it would appear that at the Morin temperature the anisotropy preference for remanence along the [111] axis is only slight, but well below this temperature the anisotropy energy has increased radically.

The explanations for the low temperature remanent magnetisation are many and varied. It has been suggested by Iwata et al[44] that this remanence may be due to the magnetisation of antiferromagnetic domain boundaries. Although the boundaries could have a small magnetisation; cooling the crystal in a high magnetic field would remove boundaries and so reduce the low temperature remanence, which is in complete opposition to the experimental results of these authors. An alternative suggestion by Iwata et al was that the remanence was the result of some kind of crystal distortion, and this is supported by Tasaki and Iida[46] who noted that the memory of room temperature remanence through a cooling-warming cycle increased as small single crystals were crushed even smaller. This could be due to internal stresses produced by grinding and crushing, but the relation between stress and magnetic moment is a little more dubious, for the piezomagnetic moment cannot exist along the 3-fold z-axis in group $\bar{3}$m.

A third different suggestion of the origin of the low temperature remanent moment is to assume the existence of slightly unequal sublattice moments. This idea of Lin's[43] is probably the most promising for it can account for the increase of remanence when the

crystal is cooled from a single domain state (i.e. cooled in a magnetic field). In this state the residual unbalance of the sublattice moments are aligned with each other so that the direction of remanence will depend on the cooling field direction, in agreement with experiment. The inequality of sublattice moments may not necessarily be a fundamental property of hematite, for ferrous impurity ions could preferentially occupy a ferric site in one of the sublattices. This would agree with the experimental observations that the single crystal remanence decreases after prolonged heating in oxygen.

1.6. THE PRESENT INVESTIGATION

The converse method of measuring the magnetoelectric effect was reported only two years after the experimental discovery of the property, but although the piezomagnetic effect was measured in 1958, the converse of it has not been studied. The present investigation completes the task by examining linear magnetostriction, which is in effect the converse of piezomagnetism.

Linear magnetostriction and other forbidden effects can be predicted by crystal symmetry to exist in many materials whose magnetic structure has been investigated. A large list of these may be found in Appendix I. Hematite was chosen to be the material in which linear magnetostriction was to be examined, because not only does a magnetic transition occur at a convenient temperature of - 15° C, but any forbidden effect identifies an overall antiferromagnetic

domain direction which is of specific interest in hematite. Antiferromagnetic domain behaviour in αFe_2O_3 has already been studied by polarised neutron diffraction, and it was intended that the results of the present work should provide information about domains in the same material so that comparisons could be made. Finally it was hoped that this work could shed new light on the magnetic transition and on the origin of the low temperature remanence.

CHAPTER II

APPARATUS

2.1. APPARATUS REQUIREMENTS

2.1.1. Strain Sensitivity Requirements

Magnetostriction is a perturbation effect and always results in very small changes in dimensions for any applied field. Ferromagnetic metals have saturation magnetostrictive changes in dimensions of the order of 2×10^{-5} of the total length[47]. Very few magnetostriction measurements on antiferromagnetics have been published, and although saturation does not occur, no strains greater than 5×10^{-6} have been reported in fields up to 10 kilo-oersteds.

An early measurement on polycrystalline nickel oxide by Belov and Levitin[48] implied that their apparatus had a strain sensitivity of at least one part in 10^8. Later a small range of single crystal measurements were reported, the first being by Alberts and Lee[49] who stated that the sensitivity and stability of their arrangement was such that a strain of 10^{-7} could be measured. In other measurements on nickel oxide and cobalt oxide crystals, Nakamichi and Yamamoto[50] whilst not explicitly stating the sensitivity of their apparatus, implied from their results, a strain sensitivity of 5×10^{-7}. McGuire and Crapo[51] who measured the magnetostriction of manganese oxide in addition to the two

previously mentioned materials, also appear to have a measurement sensitivity of 5×10^{-7}.

The earliest reported measurement of magnetostriction in antiferromagnetics was by Urquhart and Goldman[35] who measured single crystals of the material under consideration, (i.e. hematite). Their measurements were made mainly at room temperature and just below, so that points could be obtained above and below the Morin transition temperature of -15° C. The implied sensitivity of their apparatus was such that a strain of 10^{-7} could be measured. At room temperature these authors encountered a magnetostrictive strain of 10^{-5} at 6.5 kilo-oersteds in the most favourable crystallographic direction, which reduced to a value of 5×10^{-7} in the same field just below the Morin transition.

From these published apparatus specifications it was concluded that a strain measurement sensitivity of at least 5×10^{-8} was necessary accurately to measure magnetostriction in hematite at low temperatures. It was however later found desirable from the measurements, (section 4.2.), that linear magnetostriction in low fields should be investigated, and a strain measuring sensitivity of one part in 10^{8} was necessary to attain reasonable accuracy of measurement under these conditions. The final apparatus was accordingly modified to comply with this requirement.

2.1.2. Strain Measurement Devices

The problems of remote measurement of small changes in dimensions

at various temperatures have produced a number of different techniques. Belov and Levitin[48] attained a sensitivity of one part in 10^8 by using a wire probe and 'photo-electro-optical amplifier', but this method was rejected through lack of any published description.

Two suitable methods remain. A capacitance method[52], and a resistance strain gauge method[53,54,55]. The former utilises the change in dimensions of the specimen to alter the capacitance of a parallel plate condenser connected in a resonant electrical circuit and the capacitive change is recorded by measuring the change in resonant frequency. An objection to adopting this method of measurement for single crystal hematite is the obvious difficulty of mounting an irregularly shaped single crystal so as to form a parallel plate condenser. In the other method the magnetostrictive strain is communicated to a resistance strain gauge which undergoes a fractional change in resistance, this change being determined with the aid of a very sensitive Wheatstone bridge. In principle, the sensitivity limitation of this method is the sensitivity of the null-detector used in balancing the resistance bridge.

The use of a strain guage method gives numerous advantages arising from its particular suitability when dealing with small specimens and single crystals. It is perhaps significant that all the antiferromagnetic single crystal measurements previously mentioned utilised a strain gauge technique. Table I summarises various methods of measurement and the resultant strain sensitivities.

TABLE I Comparison of Magnetostriction Methods and Strain Sensitivity of Various Workers.

Authors	Material	Method	Strain Sensitivity
Belov and Levitin[48]	p/c NiO	P.E.O.A.	10^{-8}
Alberts and Lee[49]	s/c NiO	S.G.	10^{-7}
Nakamichi and Yamamoto[50]	s/c NiO,CoO	S.G.	5×10^{-7}
McGuire and Crapo[51]	s/c NiO,MnO,CoO	S.G.	5×10^{-7}
Urquhart and Goldman[35]	s/c αFe_2O_3	S.G.	10^{-7}
Callen et al[52]	s/c Y.I.G.	C.C.	10^{-7}
Birss and Lee[55]	s/c and p/c Ni	S.G.	2×10^{-7}
Scott (this work)	s/c αFe_2O_3	S.G.	10^{-8}

P.E.O.A. - Photo-electro-optical-amplifier
S.G. - Strain Gauge
C.C. - Capacitance Change

Because this method measures strain directly and not extension, no particular advantage is obtained by the use of specimens which exceed considerably the length of the gauge. When dealing with single crystals the use of small specimens is essential, and for all materials it is desirable to have the specimen as small as possible so that both it and the low temperature enclosure may be accommodated within the poles of an electromagnet. Since the strain gauges are stuck to the specimen, the measurement is not seriously affected by small

movements of the specimen as a whole, caused for example by vibrations or the magnetic forces acting upon it.

2.1.3. Temperature Requirements

The thermal expansion of hematite[56,36] just below the Morin transition is 7×10^{-6} per degree C. so that the strain that accompanies 1° C. change in temperature is about one hundred times the initially desired measurement sensitivity. Hence, although the temperature variation of magnetostriction is probably small except near the Morin transition, the strains introduced by thermal expansion can completely dominate those caused by magnetostriction. These considerations led to a requirement that the temperature stability of the specimen be better than 1/100 of a degree Centigrade, and since from magnetic symmetry considerations it has been shown that linear magnetostriction in hematite will be of primary interest below the Morin transition temperature of about -15° C., measurements must be performed both above and below this temperature.

Birss and Lee[55] have described a low temperature apparatus for keeping strain gauges at a constant temperature, but they report that it is difficult to preserve the temperature of the specimen within such limits that the balance of the bridge is not disturbed by changes in the resistance of the active gauge arising from the thermal expansion of the specimen. Their method was to use a melting solid-liquid constant temperature bath for their lowest temperature and then to allow the apparatus to warm up slowly to

room temperature whilst contained in a Dewar flask. Their strain sensitivity was 2×10^{-7}, and since it was intended that this apparatus should be at least ten times more sensitive, measurements were only taken whilst the specimen holder was within a liquid bath. It was found that boiling gas baths were far superior in temperature stability than melting liquids and thus most measurements were performed at liquid nitrogen boiling point. Even so, boiling liquid baths have small rapid fluctuations in temperature due to the formation of bubbles and to overcome this the specimen was mounted on a heavy metal holder within the bath.

2.2. RESISTANCE STRAIN GAUGES

The measurement technique is based upon the fact that most metals have a linear relationship between applied strain and electrical resistance, so that if wires of these materials are affixed to a test surface, the change in resistance of the wires when a strain is applied to the surface is an accurate measure of the strain in the surface. Further required conditions are that the wire must be free from strain hysteresis and have a comparitively low temperature coefficient of resistance, and these conditions are met together with a high strain sensitivity in certain metal alloys.

The resistance strain gauge used consisted of a rectangular grid of fine nickel-chromium wire of about 0.0027 cm. diameter, cemented to a paper backing. The ends of the fine wire were spot

welded to metal strips for terminal connections. The gauge, which was type 6J supplied by H. Tinsley and Co. Ltd. had a nominal resistance of 98 ohms and an 'active' area of 0.8 x 0.15 cm. Each gauge was stuck onto a cleaned surface of the specimen using a double layer of nitrocellulose adhesive (Durofix), and then allowed to dry at room temperature under a standard pressure of 8 oz. for at least 24 hours. Final drying was achieved by passing a current of 10 milli-amps through each gauge for another 24 hours prior to making measurements.

If δR is the change in resistance of a strain gauge of resistance R when strained by an amount $\delta l/l$ then the proportionality factor G is given by

$$G = \frac{\delta R/R}{\delta l/l} \qquad (2.1)$$

and this is known as the gauge factor. It may be derived approximately as follows:-

Assume the gauge wire has a total length l, diameter d, cross-sectional area A and specific resistivity ρ, then the total resistance is given by

$$R = \frac{\rho l}{A} \qquad (2.2)$$

To a fair approximation, the specific resistivity of nichrome is independent of strain for small strains. Assuming this, the change in resistance due to strain is found by differentiation to be

$$\delta R = \frac{\rho \delta l}{A} - \frac{\rho l \delta A}{A} \qquad (2.3)$$

Poisson's Ratio for the wire is defined as

$$\sigma = -\frac{\delta d/d}{\delta l/l} \qquad (2.4)$$

so that

$$\sigma = -\frac{2l}{\pi d^2}\,\frac{\delta A}{\delta l} \qquad (2.5)$$

since $A = \pi(\frac{d}{2})^2$

so that, replacing in equation (2.3)

$$\delta R = \frac{\rho\delta l}{A} + \frac{\rho l}{A}\,\frac{2\sigma\delta l}{l} \qquad (2.6)$$

$$= \frac{\rho\delta l}{A}\,(1 + 2\sigma) \qquad (2.7)$$

so that $\frac{\delta R}{R} = \frac{\delta l}{l}\,(1 + 2\sigma)$ (2.8)

Thus $G = (1 + 2\sigma)$ (2.9)

The commercial strain gauges used had a room temperature gauge factor of 2.08 and the value at various other temperatures is discussed in section 2.7.4.

2.3. METHOD OF MEASUREMENT

2.3.1. Bridge

Measurements of the change in resistance of the gauge were made by incorporating it as one arm of a basically conventional D.C. Wheatstone bridge, which could measure resistance changes down to 10^{-5} ohms. The resistor in series with the active gauge was also a strain gauge which was stuck to a dummy specimen situated adjacent to the hematite specimen and experiencing the same temperature and field. The two other arms of the circuit shown in Figure 5(a) were resistance boxes placed outside the low temperature enclosure. The

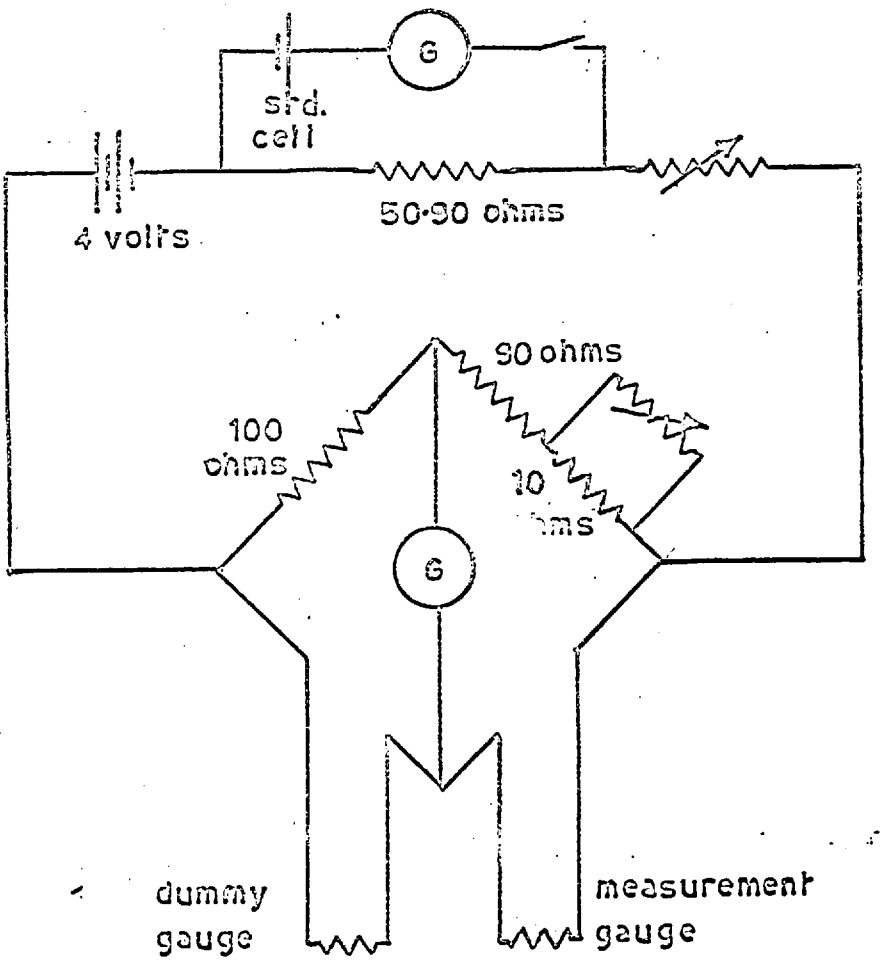


Figure 5(a). The bridge and associated circuits.

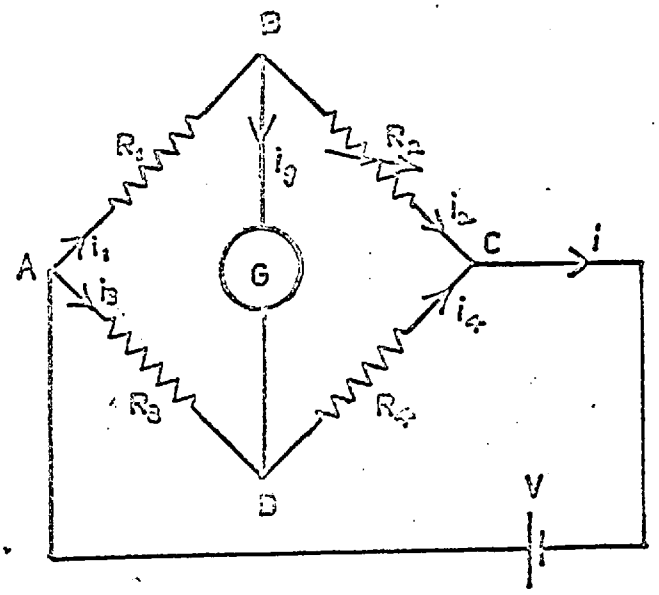


Figure 5(b). A diagrammatic form of Wheatstone bridge.

third arm was a 100 ohms resistance box, but the fourth arm consisted of a 90 ohms resistance in series with a parallel combination of 10 ohms and a four-decade 10,000 ohms resistance box. This latter combination allowed very small changes to be made in the resistance of one arm to balance the bridge exactly or for calibration purposes.

A diagrammatic form of a simplified Wheatstone bridge is shown in Figure 5(b). Suppose initially that the respective arms have resistances R_1, R_2, R_3 and R_4 and the bridge is close to balance. In this condition the bridge has an off-balance current i_g. Suppose the galvanometer resistance is R_g, the voltage applied to the bridge is V, and currents i_1, i_2, i_3 and i_4 are as shown in Figure 5(b). Applying Kirchoff's Law that the total current at any point in a network is zero, we have

at point A $$i - i_1 - i_3 = 0 \qquad (2.10)$$

at point D $$i_3 + i_g - i_4 = 0 \qquad (2.11)$$

at point C $$i_2 + i_4 - i = 0 \qquad (2.12)$$

Similarly, applying Kirchoff's Law that the total voltage around any circuit is zero, we have

around ABD $$R_1 i_1 + R_g i_g - R_3 i_3 = 0 \qquad (2.13)$$

around BCD $$R_2 i_2 - R_4 i_4 - R_g i_g = 0 \qquad (2.14)$$

Eliminating i_1 by replacing equation (2.10) into equation (2.13)

$$R_1(i - i_3) + R_g i_g - R_3 i_3 = 0$$

Hence $$R_1 i + R_g i_g - (R_3 + R_1)\, i_3 = 0 \qquad (2.15)$$

Eliminating i_2 by replacing equation (2.12) into equation (2.14)

$$R_2(i - i_4) - R_4 i_4 - R_g i_g = 0$$

Hence $$R_2 i - R_g i_g - (R_4 + R_2)\, i_4 = 0 \qquad (2.16)$$

Replacing for i_4 from equation (2.11)

$$R_2 i - R_g i_g - (R_4 + R_2)\, i_3 - (R_4 + R_2)\, i_g = 0 \qquad (2.17)$$

Multiply equation (2.15) by $-(R_4 + R_2)$ and equation (2.17) by $(R_3 + R_1)$ and adding to eliminate i_3 we get

$$- R_1(R_4 + R_2)i - R_g(R_4 + R_2)i_g + R_2(R_3 + R_1)i - R_g(R_3 + R_1)i_g - (R_4 + R_2)(R_3 + R_1)i_g = 0$$

$$\left[- (R_4 + R_2)(R_3 + R_1) - R_g \left\{ (R_4 + R_2) + (R_3 + R_1) \right\} \right] i_g = \left[R_1(R_4 + R_2) - R_2(R_3 + R_1) \right] i$$

$$= \left[R_1 R_4 - R_2 R_3 \right] i \qquad (2.18)$$

Looking at the whole parallel circuit

$$V = i \left[\frac{1}{\frac{1}{R_1 + R_2} + \frac{1}{R_3 + R_4}} \right]$$

$$= i \left[\frac{(R_1 + R_2)(R_3 + R_4)}{R_1 + R_2 + R_3 + R_4} \right]$$

Hence $$i = \frac{V(R_1 + R_2 + R_3 + R_4)}{(R_1 + R_2)(R_3 + R_4)} \qquad (2.19)$$

Replacing equation (2.19) into equation (2.18) we get

$$\left[(R_4 + R_2)(R_1 + R_3) + R_g(R_1 + R_2 + R_3 + R_4) \right] i_g = (R_2 R_3 - R_1 R_4) V \frac{(R_1 + R_2 + R_3 + R_4)}{(R_1 + R_2)(R_3 + R_4)}$$

Thus $$\left[\frac{(R_4 + R_2)(R_1 + R_3)}{R_1 + R_2 + R_3 + R_4} + R_g \right] i_g = \left[\frac{(R_2 R_3 - R_1 R_4)}{(R_1 + R_2)(R_3 + R_4)} \right] V \qquad (2.20)$$

and so $$i_g = \frac{(R_2R_3 - R_1R_4)\,V}{R_g(R_1 + R_2)(R_3 + R_4) + \Delta} \qquad (2.21)$$

where $$\Delta = \frac{(R_4 + R_2)(R_1 + R_3)(R_1 + R_2)(R_3 + R_4)}{R_1 + R_2 + R_3 + R_4} \qquad (2.22)$$

$$\Delta(R_1 + R_2 + R_3 + R_4) = (R_4R_1 + R_3R_4 + R_1R_2 + R_2R_3)(R_1R_3 + R_2R_3 + R_1R_4 + R_2R_4) \qquad (2.23)$$

$$= R_1^2R_3R_4 + R_1R_3^2R_4 + R_1^2R_2R_3 + R_1R_2R_3^2 + R_1R_2R_3R_4 + R_2R_3^2R_4 + R_1R_2^2R_3 + R_2^2R_3^2 + R_1^2R_4^2 + R_1R_3R_4^2 + R_1^2R_2R_4 + R_1R_2R_3R_4 + R_1R_2R_4^2 + R_2R_3R_4^2 + R_1R_2^2R_4 + R_2^2R_3\,R_4 \qquad (2.24)$$

$$= (R_1R_3R_4 + R_1R_2R_3 + R_2R_3R_4 + R_1R_2R_4)(R_1 + R_2 + R_3 + R_4) + R_2^2R_3^2 + R_1^2R_4^2 - 2R_1R_2R_3R_4 \qquad (2.25)$$

The bridge is sufficiently close to balance that the usual equality may be used,

i.e. $$R_2R_3 = R_1R_4$$

Thus $$\Delta = R_1R_3R_4 + R_1R_2R_3 + R_2R_3R_4 + R_1R_2R_4 \qquad (2.26)$$

and so $$\Delta = \sum_4 R_1R_2R_3 \qquad (2.27)$$

replacing in equation (2.21)

$$i_g = \frac{(R_2R_3 - R_1R_4)\,V}{\sum_4 R_1R_2R_3 + R_g(R_1 + R_2)(R_3 + R_4)} \qquad (2.28)$$

At balance $R_2R_3 = R_1R_4$ and so $i_g = 0$. Suppose now that R_1, R_2, R_3 and R_4 are the resistance values for balance; when R_2 is changed to $R_2 + \delta R_2$ the off-balance current is given by

$$\delta i_g = \frac{\left[(R_2 + \delta R_2)\, R_3 - R_1 R_4\right] V}{\sum_4 R_1(R_2 + \delta R_2)R_3 + R_g(R_1 + R_2 + \delta R_2)(R_3 + R_4)}$$

$$= \frac{V\,(R_2 R_3 - R_1 R_4) + V\,\delta R_2 R_3}{\sum_4 R_1(R_2 + \delta R_2)R_3 + R_g(R_1 + R_2 + \delta R_2)(R_3 + R_4)} \qquad (2.29)$$

Since R_1, R_2, R_3 and R_4 are values for balance, the first term is zero, and so

$$\delta i_g = \frac{V\, R_3\, \delta R_2}{\sum_4 R_1 R_2 R_3 + R_g(R_1 + R_2)(R_3 + R_4)} \qquad (2.30)$$

Thus the off-balance current is directly proportional to the small change in resistance from balance, and this provides a useful method of measuring small changes in resistance of one arm. The procedure for measurement was to balance the bridge to an accuracy of at least 10^{-4} ohms in the absence of a magnetic field on the specimen and then to observe the change in the small off-balance current through the sensitive detector when the magnetic field was applied to the specimen. In this way the circuit could remain untouched whilst measurements were in progress.

The stability of the bridge circuit was of considerable importance and it was essential to ensure that it was unaffected by changes in room temperature. The connections from the specimen holder to the bridge were made of heavy gauge flexible wires twisted together and lagged to reduce the effect of local ambient temperature changes. All components of the bridge with the exception of the galvanometer were contained within a well lagged box

having a close fitting lid, and in addition, all connections within the box consisted of brass strips of cross-section 0.5 by 0.25 in.

2.3.2. Bridge Current

Equation (2.18) shows that for fixed resistance values, the off-balance bridge current is proportional to the total current flowing through the bridge; so that stability and reproducibility of the bridge current were essential. This was achieved by comparing the potential drop caused by the total bridge current passing through a fixed resistor, to the output voltage of a Weston standard cell. The comparison being made by connecting the two in opposition via a Pye Scalamp galvanometer of internal resistance 24 ohms. This circuit, which is shown in Figure 5(a) stabilised the bridge current to $\pm$ 0.03% over long periods of time.

From equation (2.18) it would appear obvious that the highest bridge current possible should be used. The maximum current was governed by its heating effect in the gauges, and was found experimentally to be a maximum of 10 milliamps per gauge, since above this value the scatter on the final output results increased above the normal 'background' scatter. For this reason, a nominal 20 milliamps was chosen for bridge current. The power for the bridge was provided by two 2 volt 60 amp-hour accumulators which were left connected continuously for stability reasons.

2.3.3. Null Detection System

A system was needed to measure the off-balance current from a D.C. Wheatstone bridge unbalanced by less than 10^{-5} ohm and to accept this voltage from a source of output impedence of approximately 100 ohms. A very sensitive Cambridge galvanometer, having a sensitivity of~250 mm. per microamp with scale at one metre and input impedence of 25 ohms, was chosen after many tests had shown that available D.C. amplifiers (both direct and vibrating system type) had excessive drift or incompatible input impedence. Using a lamp and transparent scale two metres from the galvanometer, the sensitivity was found to be 3.7×10^{-4} ohms per cm. of scale, which corresponded to a strain of 1.85×10^{-6} per cm. of scale.

The bridge off-balance current is given by equation (2.30)

$$i_g = \frac{V R_3 \delta R_2}{\sum_4 R_1 R_2 R_3 + R_g(R_1 + R_2)(R_3 + R_4)}$$

$$\lim_{i_g \to 0} \left(\frac{\delta i_g}{\delta R_2}\right) = \frac{di_g}{dR_2} = \frac{V R_3}{\sum_4 R_1 R_2 R_3 + R_g(R_1 + R_2)(R_3 + R_4)} \qquad (2.31)$$

If $\delta\theta$ is the change in galvanometer deflection angle caused by a bridge resistance change δR_2 then the overall ~~current~~ sensitivity S is given by

$$S = \frac{\delta\theta}{\delta R_2 / R_2} = \frac{\delta\theta}{di_g} \frac{di_g}{\delta R_2} R_2 \qquad (2.32)$$

and $\frac{d\theta}{di_g}$ is the galvanometer sensitivity S_g, so that

$$S = \frac{S_g V R_3 R_2}{\sum_4 R_1 R_2 R_3 + R_g(R_1 + R_2)(R_3 + R_4)} \qquad (2.33)$$

Equation (2.33) gives the terms that must be kept constant in order to produce a constant overall measurement sensitivity. The experimentally determined overall sensitivity of 3.7×10^{-3} ohms per cm. of scale was about forty times less sensitive than the desired value, and from equation (2.33) a possible way to improve it was to increase the effective galvanometer sensitivity. This was achieved by the use of a split photocell amplifier.

2.3.4. Photocell Amplifier

This consisted of two photo-voltaic cells each about 2.5 cms. square which are encapsulated side-by-side with only a very thin insulation (i.e. less than 1 mm.) between them, see Figure 6(a). The difference between the output voltages of the two cells was measured using a Pye Scalamp galvanometer having an input impedence of 1400 ohms. The voltage difference was adjusted to zero when both the cells were equally illuminated, by using a shunt resistor across one of the cells. Then, a difference in illumination of the two cells caused by the primary galvanometer light spot moving to cover more of one cell and less of the other, showed itself as a deflection of the secondary galvanometer. The overall photocell amplifier gain, measured in cms. deflection on final scale per cm. deflection of primary galvanometer light spot, was 37:1 so that the

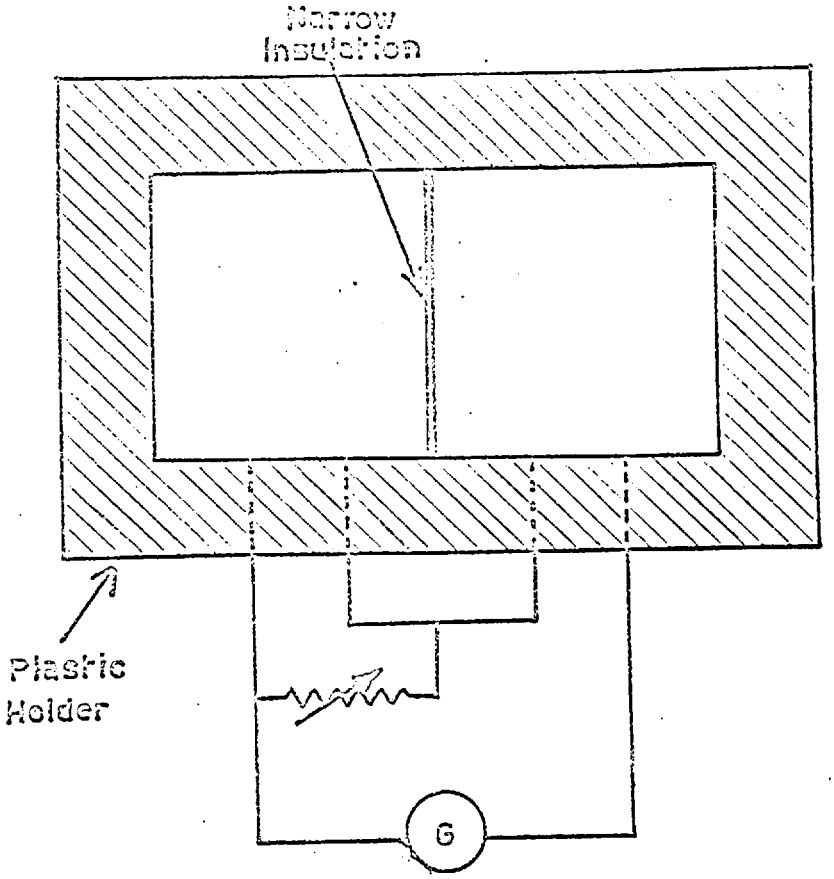


Figure 6(a). A schematic split-photocell and its measurement circuit.

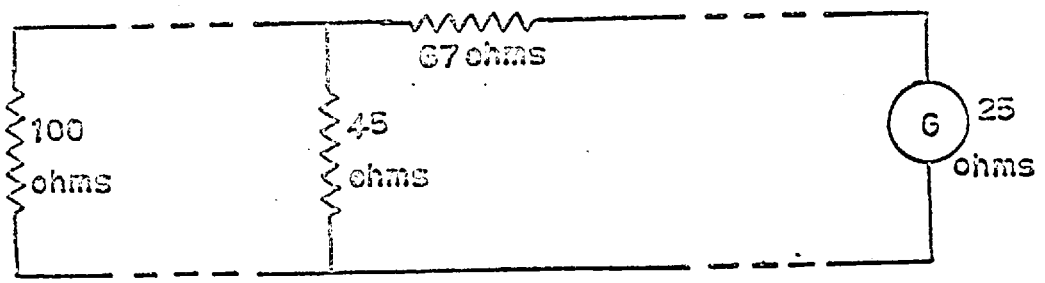


Figure 6(b). The galvanometer 3:1 attenuator circuit.
Input impedence 25 ohms, output impedence 100 ohms.

overall sensitivity was found to be 10^{-5} ohms per cm. of final scale, which corresponded to a strain measurement of 5×10^{-8} per cm. of final scale.

Using the usual circular light spot from the primary galvanometer lamp it was found that the photocell response was rather non-linear. When the light spot was made rectangular the response was completely linear within the working range. The range was conveniently limited by the scale of the secondary galvanometer which resulted in the use of a range of only $\pm$ 4 mm. about the centre of the photocell. Although the path of the light beam from the primary galvanometer to the split photocell must necessarily be within a darkened cover it was also desirable to be able accurately to move the light spot across the photocell. This was achieved by mounting the split photocell on a slider which could be moved perpendicularly to the light beam by means of a screw arrangement. Operation of the screw was effected by means of a handle projecting from the light tight enclosure, as shown in Figure 7. This slider was used frequently to move the split photocell a small amount so that in its shorted position the primary galvanometer light spot lay symmetrically between the two halves of the photocell.

2.3.5. Galvanometer Attenuator

The maximum strain that could be measured within the linear region of the split photocell response was approximately 7.5×10^{-7} cm. per cm. However, as noted in section 2.3.3., the strain sens-

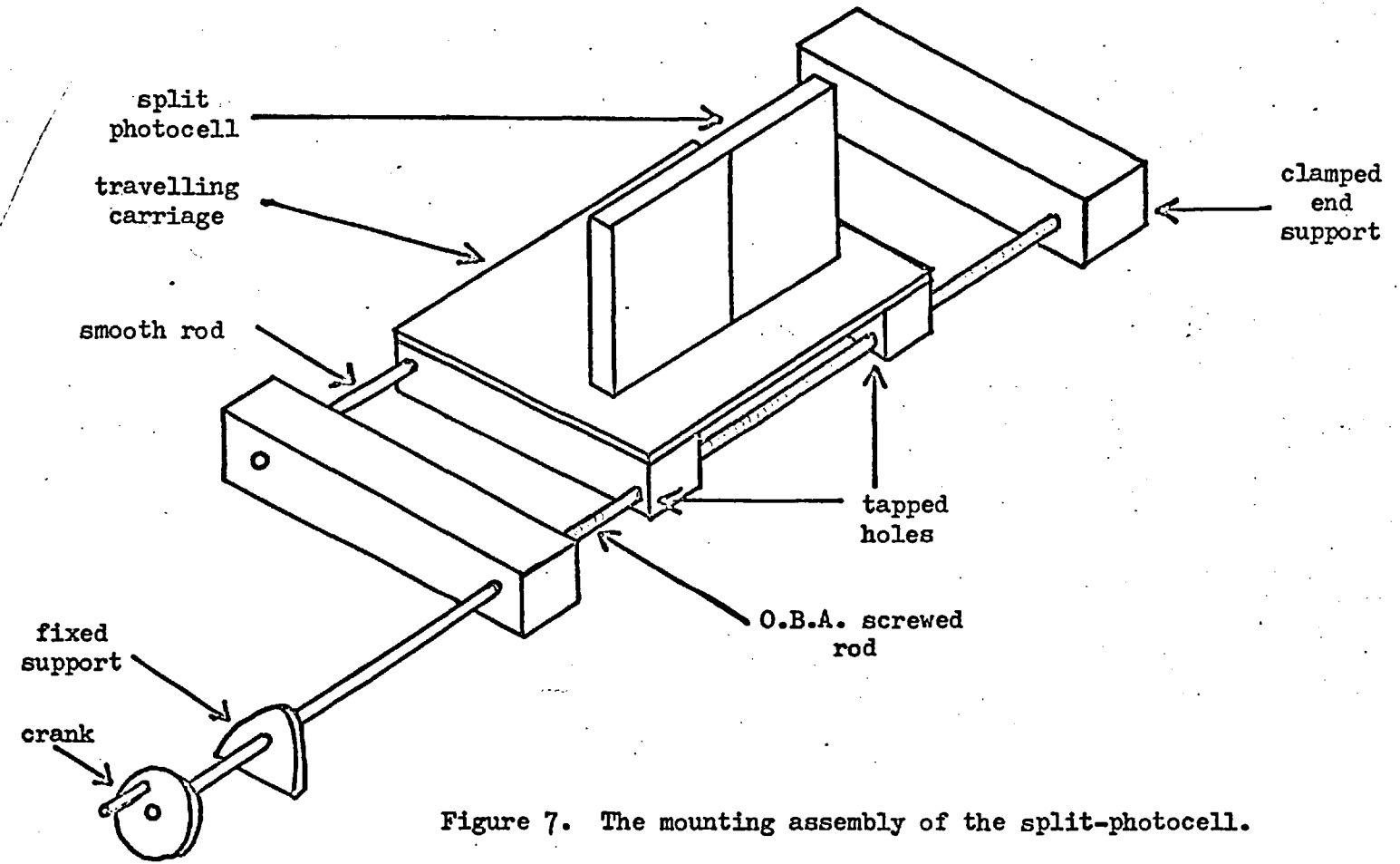


Figure 7. The mounting assembly of the split-photocell.

itivity of the basic galvanometer at this distance was 1.85×10^{-6} cm./cm. per cm. of scale. This meant that strains of 1.0×10^{-6} could only be read on the scale to $\pm$ 0.5 mm. in 5 mm., and so an intermediate measurement range became desirable, and in order to achieve this, an attenuator was constructed for the primary galvanometer. Under normal conditions the galvanometer had an input resistance of 25 ohms, and the circuit an output resistance of 100 ohms. A 3:1 attenuator was designed to have the same input resistance as the galvanometer and the same output resistance as the circuit. This was achieved by means of the circuit shown in Figure 6(b), in which one third of the total current passes through the galvanometer, and two thirds through the 45 ohms resistance. With the attenuator in circuit as indicated, a maximum strain of about 2.2×10^{-6} could be measured using the galvanometer-photocell combination.

2.4. CRYSTAL HOLDER

2.4.1. Design Requirements

The dummy comparison gauge and the experimental specimen with the strain gauge attached were required to be mounted with the plane containing each gauge horizontal, so that when the electromagnet was turned about a vertical axis the magnetic field also rotated in this plane. All connecting wires must be securely clamped as any movement of these (due either to the magnetic forces or to vibration) would

cause spurious changes in resistance. It was also essential that the crystal holder performing these purposes should be non-magnetic, as heavy as possible to improve temperature stability, and should be rigidly mounted in the low temperature bath at the centre of the pole gap.

2.4.2. Comparitor Gauge

The arm of the Wheatstone bridge carrying the current in series with the measurement strain gauge also contained a comparison strain gauge, see Figure 5(a). To reduce the temperature stability requirements this gauge was stuck onto a similar sized piece of soda-glass which had a coefficient of linear expansion roughly similar to that of hematite, i.e. 8×10^{-6} per degree Centigrade at room temperature[56,36]. It was found by initial measurements that the resistance of the gauge wire changed by 2% over the range of 200 deg C. between room and liquid nitrogen temperature, as shown in Figure 8. A comparison between the thermal expansion of the specimen, temperature change in resistance of the gauge, and the desired magnetostriction measurement accuracy are shown in Table II, and the need to compensate for these effects by the use of a comparator gauge is quite evident. The soda-glass dummy and gauge were located adjacent to the active gauge and oriented identically to it, so that both experienced the same temperature and magnetic field.

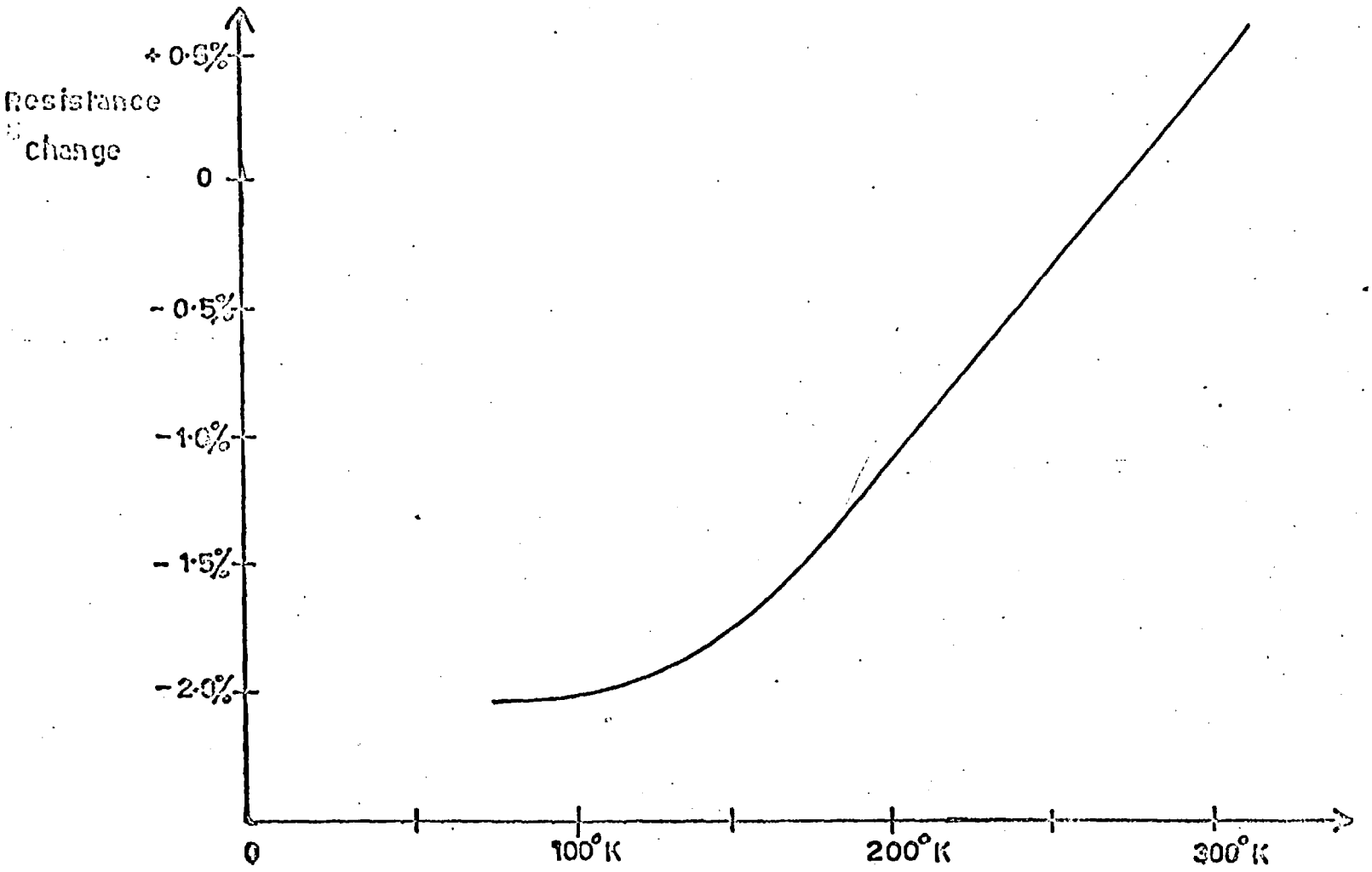


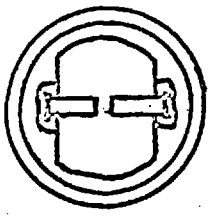
Figure 8. Dependence of resistance of gauge wire on temperature.

TABLE II Comparison of Strains Caused by Various Effects.

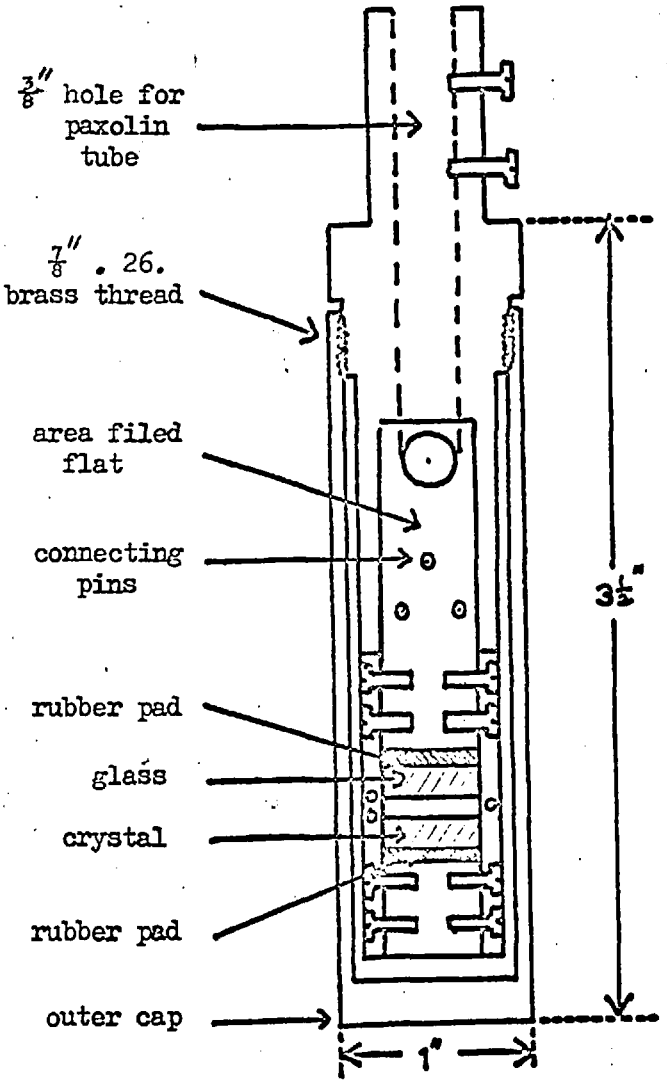
Strain equivalent to gauge temperature increasing by 1 deg C.	10^{-4}
Specimen expansion strain caused by temperature increase of 1 deg C.	8×10^{-6}
Desired magnetostrictive strain measurement accuracy	10^{-8}

2.4.3. Description of the Specimen Holder

The crystal holder was constructed mainly of brass, and was essentially a jig, holding both the specimen under investigation and the glass dummy, so that their strain gauge faces lay parallel to each other and also parallel to the plane of rotation of the field. The specimen holder, which is shown in Figure 9, had the specimen stuck to the lower end of the large brass block and the dummy specimen stuck to the upper face of the lower small brass block. To avoid magnetostrictive and thermal distortion of the crystal and dummy it was necessary to interpose rubber pads, 1/16 inch thick, between each specimen and the brass block, so that a small degree of flexibility was achieved in the horizontal plane. The very short strain gauge leads were soldered to pins mounted in the brass holder but insulated from it. The insulation was achieved by drilling small blind holes in the brass and then filling them completely with 'Araldite' epoxy resin. After hardening, a short



(a)



(b)

Figure 9. The brass crystal holder (a) end view (b) side view.

hole slightly larger than the tinned copper pin was drilled in the Araldite and the pin was affixed with more resin. A high insulation resistance was essential. Suppose, for example, 100 ohm gauges are used and it is required to measure strain to one part in 10^8. This change is equivalent to shunting the gauge with a 10,000 Meg-ohm resistance, so that the leakage resistance must be stable to more than 10,000 Meg-ohms although not necessarily greater than this value.

Enamelled copper wires stuck to the brass, carried the connections to a connector block area (as shown in Figure 9), where contact was made, via insulated pins, to copper wires taking the connections up the inside of the support tube. The specimen holder was enclosed with a screw fitting brass cap which also contained the thermocouple. At liquid nitrogen temperatures the air in the enclosure liquefied and the vacuum so produced drew in more liquid nitrogen through the threads from the surrounding constant temperature bath, and the bubbling of the liquid in the confined space had a detrimental effect on the adhesion of the strain gauges. An electrical insulant liquid was required to fill the space, and following other authors[55,57], a silicone fluid (M.S. 550) was used. Very low temperatures have prohibited its use as a circulatory liquid, but as a static fluid the gradual solidification below -70° C was no serious bar to its use at temperatures well below this. Experimentally it was found that the presence of the silicone fluid even at -196° C did not affect the magnetostrictive

strain by any measurable amount, but measurement stability was greatly improved. The only material that would seriously affect the magnetostrictive strain is one that has an appreciable compressibility modulus at the particular temperature compared with that of hematite at the same temperature.

It was chosen to rotate the magnetic field about the specimen holder rather than the converse, so that the specimen holder needed to be rigidly supported between the poles of the electromagnet. The support consisted of a short length of 3/8 inch diameter paxolin tube connecting at room temperature to a 2 ft. long brass tube of the same diameter, through both of which the bridge wires passed. The brass tube was firmly clamped to a brass levelling device which was supported on the bench, as indicated in Figure 10. The screw adjusters also served to position the crystal holder exactly in the centre of the electromagnet pole gap.

2.5. THE MAGNET

A Newport electromagnet, type E, having flat 7" diameter pole faces and a gap of 2" was used. Rotation of the magnetic field was facilitated by mounting the magnet on a turntable graduated in degrees. This was in turn bolted to a 1" thick steel plate supported by three large levelling screws which ensured that the axis of rotation of the magnet was vertical. Finally, as is shown in Figure 10, this was mounted on a carriage which could run along a short railway track. This enabled the magnet to be conveniently

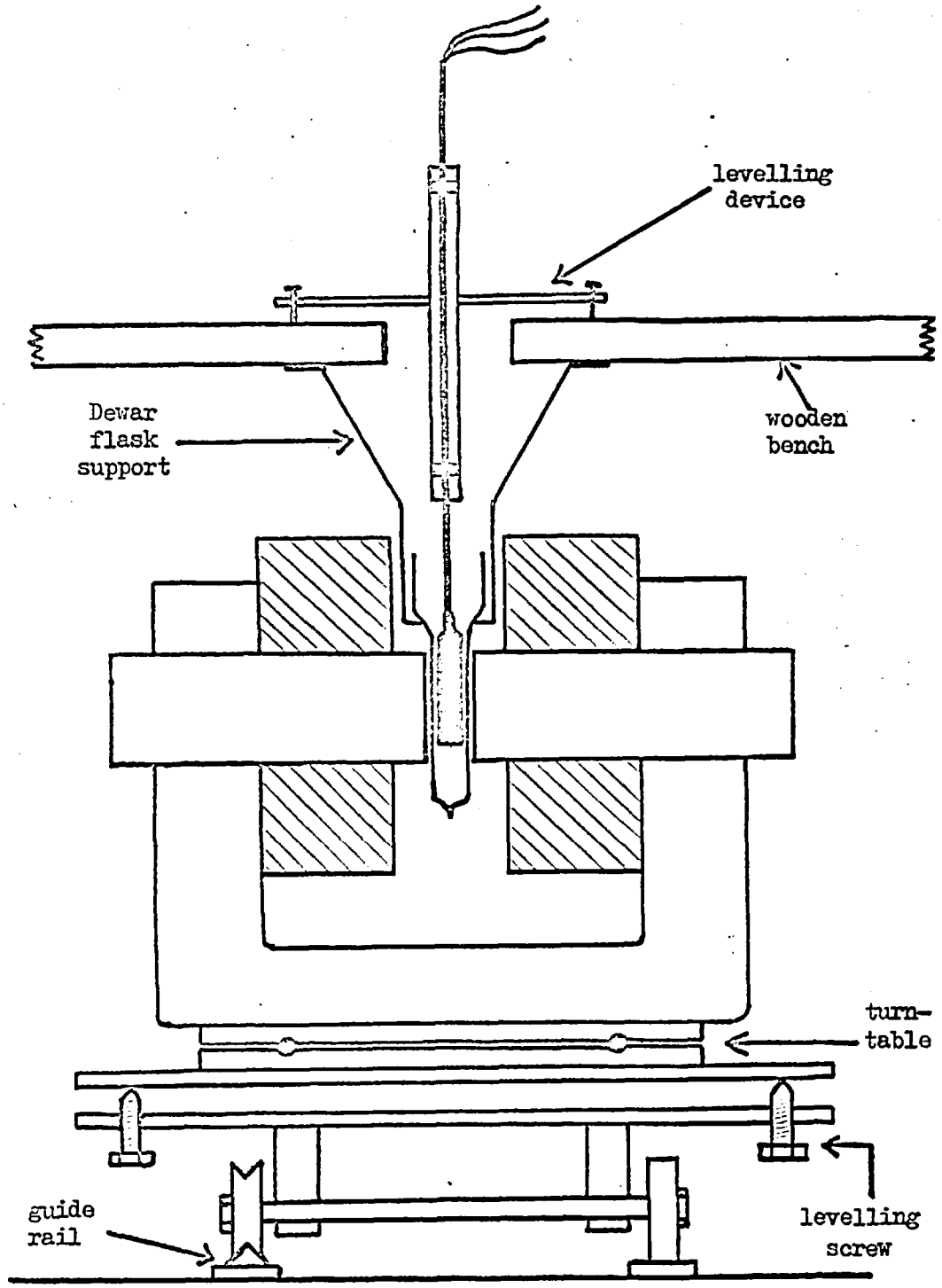


Figure 10. The general design of magnet, Dewar flask and crystal holder.

removed to obtain access to the Dewar flask and specimen holder. Although the magnet and associated supporting apparatus weighed approximately 13 cwt., repositioning it to better than ± 0.5 mm. was a simple matter.

A field of 10 kilo-oersteds was attainable and measurements were, on occasions, performed in fields up to this value. The magnitude of the fields used was determined by use of a 'Norma' fluxmeter and search coil to an accuracy of ± 15 oersteds. The field calibration of the magnet is shown in Figure 11. The sense of the fields (i.e. position of the North) for a fixed current direction, was determined using a magnetic compass.

2.5.1. Magnet Power Supply

Current for the magnet was provided by a stabilised D.C. power supply, giving separate outputs for each coil and a maximum total current of 40 amps with a stability of ± 10 milliamps. The interior circuitry of this apparatus compared the potential drop caused by the output current passing through a standard resistance to the manually pre-set value and utilised the difference to control the output via silicon controlled rectifiers. Short term stability was very necessary as small changes in the magnetic field were picked up by the gauge wires as an induced voltage in the measuring circuit. Provision was made for reversing the current flowing through each of the magnet coils after first reducing it to zero.

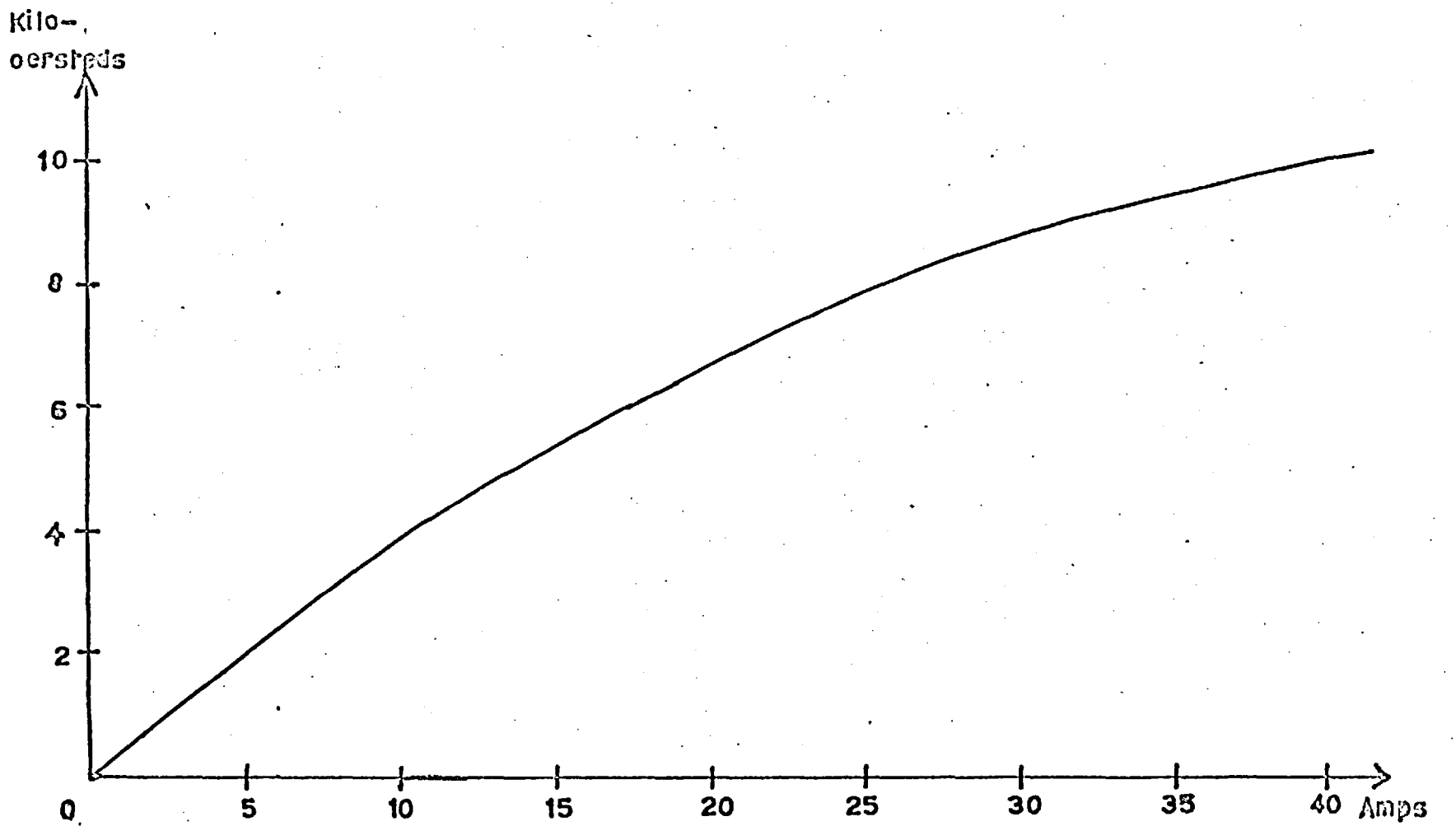


Figure 11. Field calibration of the electromagnet.

2.5.2. Demagnetisation

Demagnetisation of the magnet and specimen was accomplished by repeatedly reversing the current whilst reducing it by small decrements from the maximum value. This procedure reduced the remanent field of the magnet to about 40 oersteds, due to the inability of the power supply to produce a lower current than 0.1 amp. Further demagnetisation was effected by connecting the magnet coils in series across the a.c. mains via a variable transformer. At 50 c.p.s. the coils had an impedence of 120 ohms, so that the current could be reduced to 0.005 amp and consequently the remanent field was reduced to about two oersteds or less. This condition was considered to be completely demagnetised for this work.

2.6. TEMPERATURE BATHS

It was shown in Section 2.1.3. that the temperature stability of the whole apparatus was of utmost importance. The specimen holder was maintained at a fixed low temperature to better than 1/100 deg. C. by immersion in a liquid bath contained within a double walled glass Dewar flask of 2" external diameter.

At low temperatures it is common to utilise the melting points of various organic liquids, but however, one is greatly restricted in this particular application due to the slight solubility of silicone fluid in many organic liquids. The converse solubility is of greater importance as there is then a possibility of the solute attacking the strain gauge adhesive. Members of the paraffin series

were found to be inert for this purpose. The lowest temperature attained, and also incidentally, the bath most frequently used, contained boiling liquid nitrogen at -196° C. The next lowest temperature was that of melting isopentane. In common with Birss and Lee[55], it was found that the solidification point of isopentane depended on its purity. Redistilled isopentane was used, and by the regular addition of suitable amounts of liquid nitrogen, the temperature of the bath was kept tolerably steady at -160° C. Another convenient steady temperature is the subliming point of solid carbon dioxide at -78.5° C., and for good thermal contact it is usually contained within a liquid. Although an alcohol is often used, isopentane performed this function perfectly.

The remaining constant temperatures up to room temperature utilised the melting of pure ice and of aqueous solutions. A saturated aqueous solution of calcium chloride melts at -44° C., and a saturated aqueous solution of sodium chloride melts at -23° C. Both solutions were kept in the melting condition by regular addition of small amounts of liquid nitrogen which reformed the ice on the surface of the solutions in the Dewar flask. The temperatures were measured and checked frequently using a copper-constantan thermocouple mounted on the specimen holder. A list of the temperatures and baths used is shown in Table III.

TABLE III List of Temperature Baths Used.

Temperature		Temperature Bath
-196° C	77° K	Boiling liquid nitrogen
-160° C	113° K	Melting isopentane
-77° C	196° K	Subliming carbon dioxide in isopentane
-44° C	229° K	Melting of saturated aqueous CaCl solution
-23° C	250° K	Melting of saturated aqueous NaCl solution
0° C	273° K	Melting of pure ice
+23° C	296° K	Room temperature

2.7. CHECKING AND CALIBRATION MEASUREMENTS

2.7.1. Magnetoresistance of the Strain Gauges

When placed in a magnetic field, most materials change their resistance to some extent, due to the conduction electron paths being modified by the field. This is an obvious source of error when using a resistance strain gauge under such conditions, although by making a comparison between two gauges, both within the magnetic field, the measured effect must be almost completely eliminated. One of each batch of gauges used was stuck on the dummy specimen and the active gauge removed from the circuit and replaced by a resistance box situated some distance from the magnet. The measured magnetoresistance was found to be very small and roughly

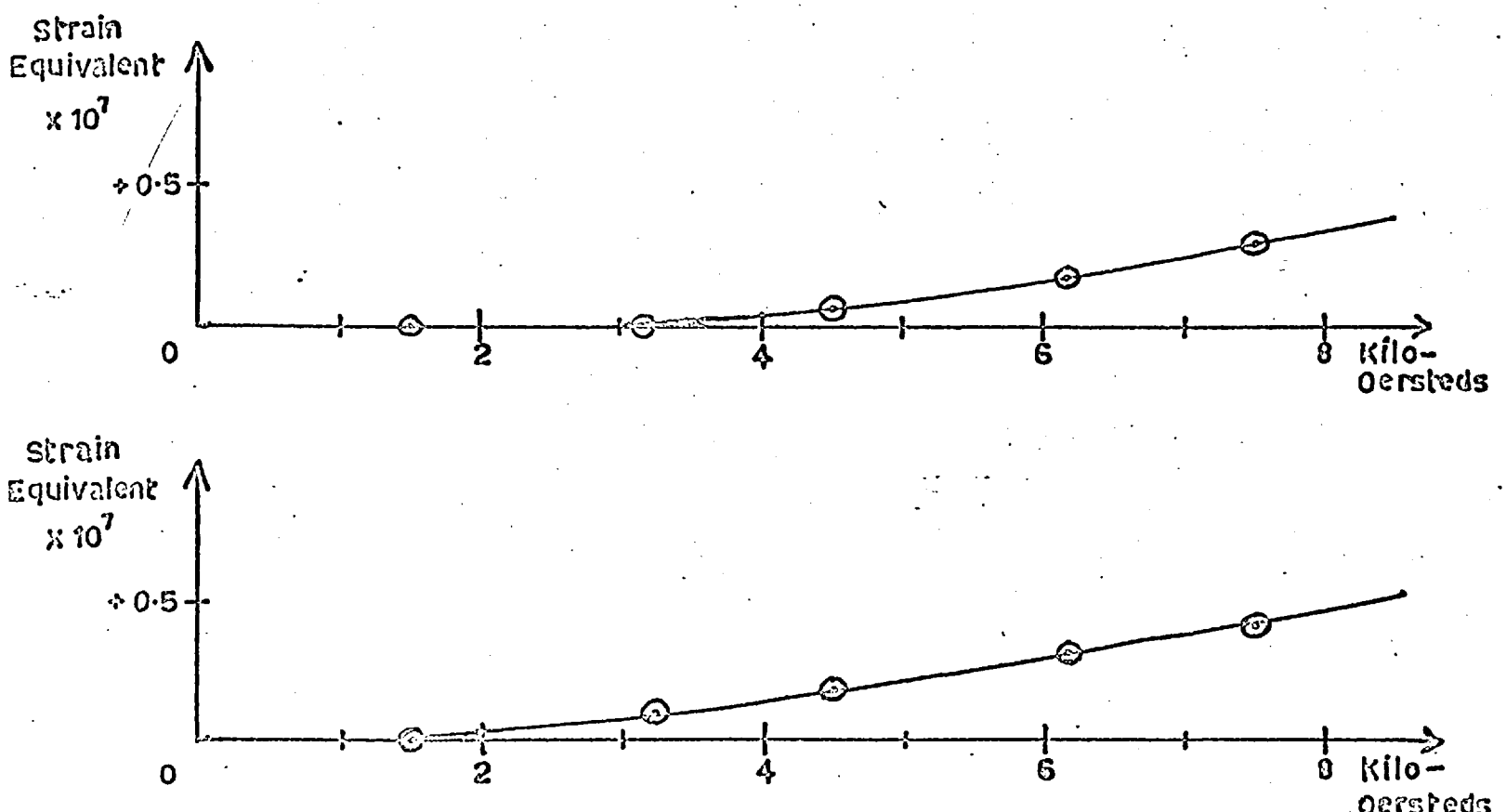


Figure 12. Magnetoresistance of the strain gauge wire in two mutually perpendicular directions in the plane of the gauge.

isotropic. Its field variation is shown in Figure 12, and is of course independent of the sense of the field. Although the magnetoresistance was completely undetected below 4 kilo-oersteds, its value rose to 8×10^{-6} ohms in a field of 9 kilo-oersteds and this corresponded to a pseudostrain of 4×10^{-8} cm. per cm.

However, in the normal measurement arrangement, two strain gauges were connected either side of the Wheatstone bridge, so that the magnetoresistance of one should balance out the magnetoresistance of the other. Even if the balancing process were imperfect to the extent of 10% of the total magnetoresistance being measured, this corresponds to a pseudostrain of 4×10^{-9} which is completely undetectable to the measurement apparatus.

2.7.2. Effect of Magnet on Measurement Apparatus

A very large stray field existed anisotropically outside the pole pieces of the electromagnet. This field was probably considerably increased by mounting the magnet on thick steel levelling plates on a steel carriage on steel rails, but at the time no other suitable material was available. The variation of the field outside the magnet with distance from the centre of the magnet pole-gap is shown in Figure 13.

When the apparatus was first constructed it was found that both the direction and the sense of the field had its effect on the measurement part of the circuit. It was partly caused by the

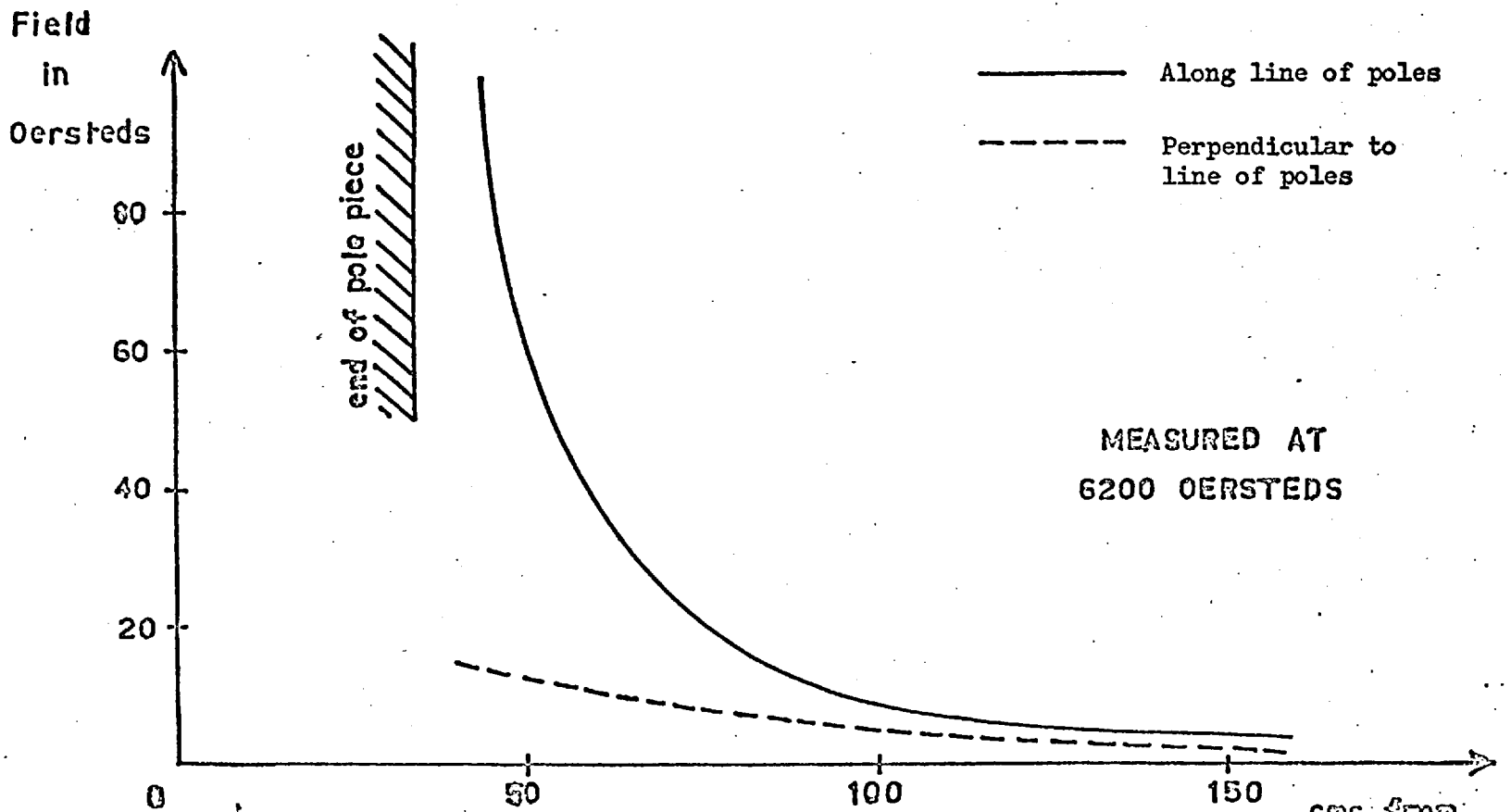


Figure 13. Magnetic field plot outside of the magnet.

primary galvanometer coil being slightly affected by the field, which is of course a directional effect. This was overcome by moving the galvanometer further away from the magnet, and eventually a distance of three metres was found to be sufficient. However, it was found that the output of the split photocell, although constructed of semi-conducting materials, was unaffected by the magnetic field. This was probably due to them both being polycrystalline and connected together in opposition.

The primary source of field interference with the measurement circuit was the connection from the bridge to the galvanometer. This was mainly due to the induced voltage caused by a change in field, which being very large compared with the off-balance current, imposed a severe strain on the sensitive primary galvanometer. The impulse caused a slight permanent twist in the galvanometer suspension which altered the zero current reading appreciably when measured using the photocell amplifier. Various magnetic and electrical shielding of the wires was tried and the connections finally consisted of shielded twin-cored co-axial copper cable passing through its own earthed soft iron conduit. The induced voltage was considerably increased when the strain gauges were connected into the bridge in the normal measurement process. This problem was finally overcome by shorting the primary galvanometer each time the field was changed; the most suitable means was a small electric relay situated very close to the galvanometer but

operated from a distance. Eventually all extraneous field effects on the measurement circuit were reduced to less than the short term stability level which was set by the thermal stability of the strain gauges.

2.7.3. Resistance Calibration of Measurement Circuit

The calibration of the off-balance current through the detecting device in terms of the off-balance resistance was effected by varying the resistance of the four decade 10,000 ohms resistance box in parallel with the 10 ohms resistor in one arm of the bridge, (see Figure 5(a)). If R_1' is the value of the variable resistance, then the resistance of the parallel combination is given by

$$R_1 = \frac{10\ R_1'}{10 + R_1'} \tag{2.34}$$

So that if the variable resistance is changed from R_1' to R_2', the change in resistance of the bridge arm is given by

$$\delta R = 10 \left[\frac{R_1'}{10 + R_1'} - \frac{R_2'}{10 + R_2'} \right] \tag{2.35}$$

$$= \frac{100\ (R_1' - R_2')}{(10 + R_1')(10 + R_2')} \tag{2.36}$$

As may be seen from Figure 5(a), if the resistance of this bridge arm is increased, the off-balance current is in the opposite direction to the current caused by an increase in active gauge resistance. The small resistance change δR of equation (2.36) if ex-

pressed as resistance per unit length of output scale, may be directly replaced into equation (2.1) to give the strain per unit length of output scale. It is important to note that whilst an increase in gauge resistance indicates an expansion of the specimen, the same galvanometer current corresponds to a decrease of resistance of the variable arm of the bridge.

The procedure for calibration was to alter the parallel resistance value and to observe the difference in final scale reading. This was repeated twice more and from this the off-balance resistance per centimetre of scale was calculated using equation (2.36). In a similar manner the linearity of the split photocell output with light spot position was frequently checked (see Section 2.3.4.), by moving the photocell a known amount perpendicularly to the light beam, whilst observing measurements on the final scale. By both of these methods the linearity of the whole measurement system was checked at least once in every set of results.

2.7.4. Strain Calibration of Gauges

It was shown in Section 2.2. that the gauge factor of a resistance strain gauge depends on Poisson's Ratio of the material which forms the wire of the gauge. It was stressed that equation (2.9) was only approximate, because resistivity also changes when a material is strained. Both Poisson's Ratio and resistivity are temperature dependent, and so it follows that the gauge factor will

also be a function of temperature. The gauge factor must be measured by applying a known strain to the gauge and measuring the resultant change in resistance.

The investigations of Day and Sevand[58] indicated that the temperature variation is small, with the gauge factor deviating from its room temperature value by less than 3% down to -125° C. and by about 6% at liquid nitrogen temperatures. A very suitable test apparatus for this purpose has been described by McClintock[59]. It consisted of a cantilever of uniform thickness clamped at one end and with its width tapering uniformly to zero at the free end. This was the shape of cantilever calculated to experience a uniform stress, and hence to exhibit a uniform strain along the whole of its length, so that under these conditions, measurement of strain over a finite length of material did not introduce errors. Strain gauges were stuck on both sides of the cantilever which was bent at its free end by means of a block of fixed dimensions. The use of materials with the same coefficient of thermal expansion for all parts permitted the calibration of the strain gauges to extend over a wide range of temperatures.

The gauges used in the work reported here were type 6J produced by H. Tinsley and Co. Ltd. and a complete temperature calibration of this particular type of gauge had previously been performed by Birss and Lee[55]. They used an electromagnetically operated thin phosphor-bronze cantilever in an apparatus almost identical to that described by McClintock[59], to determine the

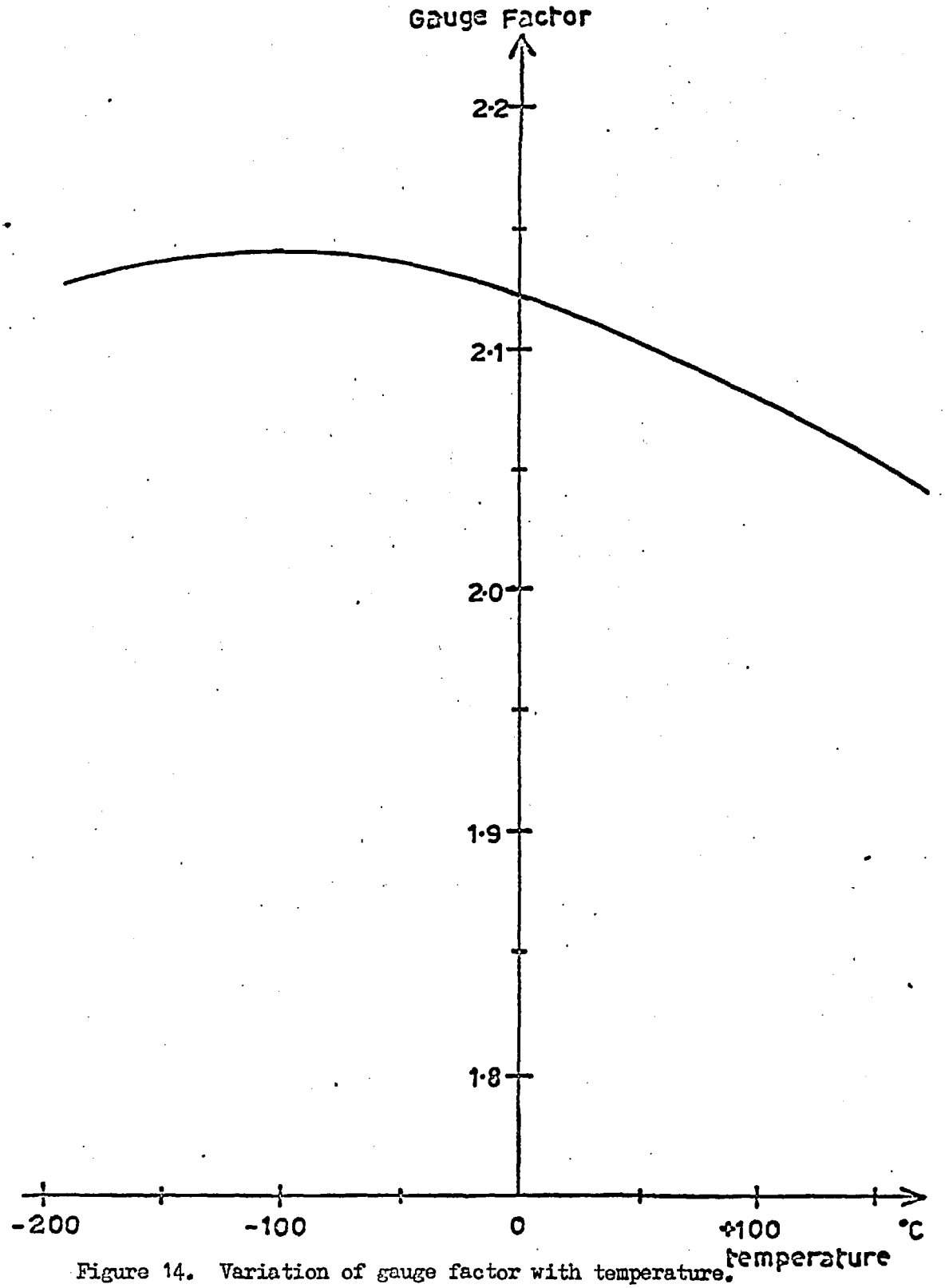


Figure 14. Variation of gauge factor with temperature.

From - BIRSS. R.R. & LEE. E.W. J. Sci. Instr. 37, 225 (1960).

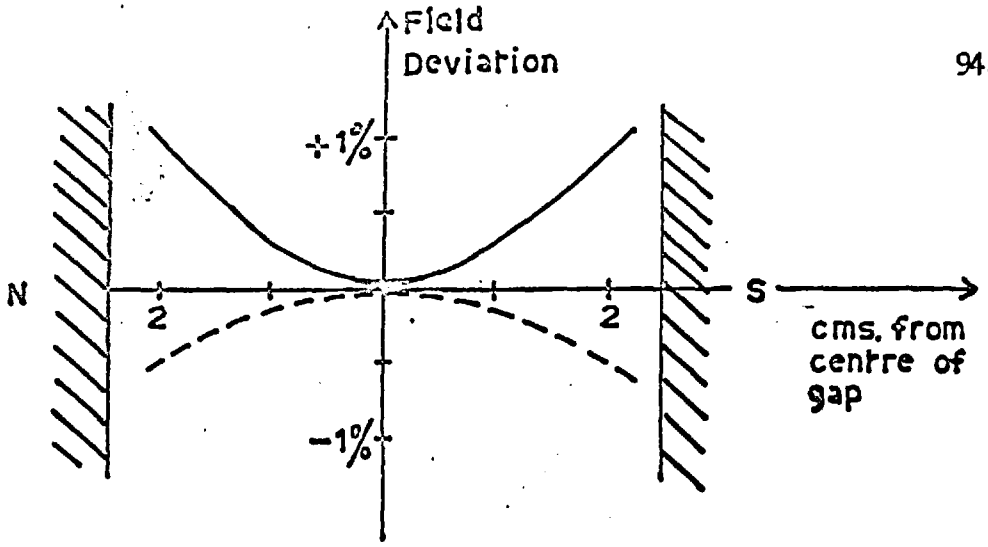
gauge factor of type 6J strain gauges from -200° C to +170° C. Their variation of gauge factor with temperature is reproduced in Figure 14. Below room temperature the gauge factor was constant to about 1% of the room temperature value. Since the overall accuracy of the magnetostriction measurements was certainly no better than this, (as discussed in Section 2.8), no allowance for the change in gauge factor was made when calculating strain sensitivity from equation (2.1)

$$\frac{\delta l}{l} = \frac{\delta R}{GR} \qquad (2.1)$$

However variations of resistance R with temperature (see Figure 8) were allowed for in equation (2.1).

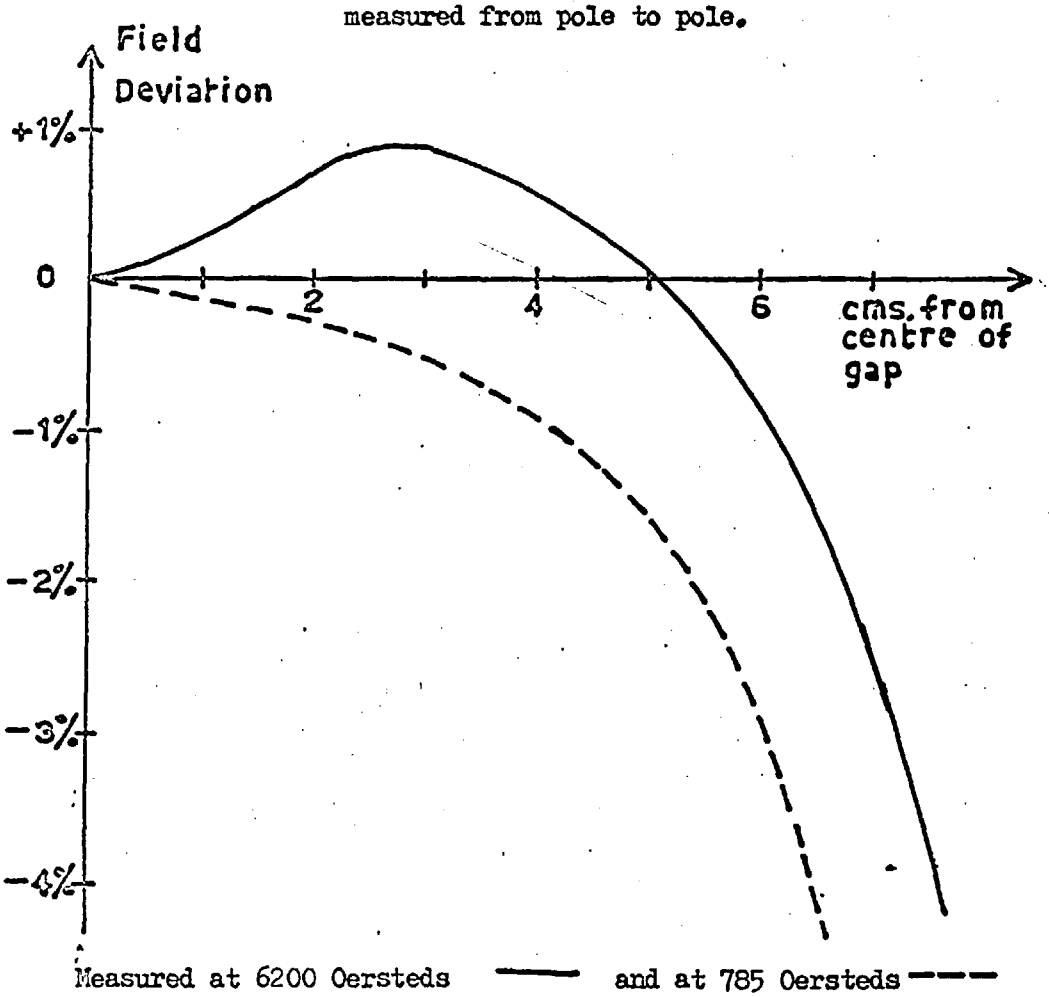
2.7.5. Alignment of Specimen in Field

The specimen was supported at its upper end by a short paxolin tube passing from the constant temperature bath to room temperature, and then by a long brass tube clamped to a position adjustment and levelling device, as in Figure 10. This was used to position the specimen under investigation, as accurately as possible with the aid of a spacer, in the centre of the pole gap. It was considered useful to measure the field variation across the pole gap to determine what accuracy in repositioning the specimen holder was necessary. The variation across the pole gap is shown in Figure 15(a), and perpendicular to the gap is shown in Figure 15(b). The results show that over a distance of at least $\pm$ 2 cms. at the centre of the



Measured at 6200 Oersteds —— and at 785 Oersteds - - -

Figure 15(a). Magnetic field variation between the poles, measured from pole to pole.



Measured at 6200 Oersteds —— and at 785 Oersteds - - -

Figure 15(b). Magnetic field variation between the poles, measured along the line of symmetry, perpendicular to (a).

pole gap, the field is constant to better than 1%, and considering that it was easily possible to reposition the specimen holder to better than $\pm$ 2 mm., no appreciable error was introduced by removing the specimen holder.

2.8. MEASUREMENT PROCEDURE

A general block diagram of the measurement apparatus is shown in Figure 16. Before any measurements were made, the bridge current was always standardized,by comparing the e.m.f. across the standard resistor with that of the standard cell. The bridge current changed slightly as the gauges were cooled, so that the standardization process was repeated when the specimen holder reached the measurement temperature. Whenever measurements were performed below the Morin transition temperature, the usual method was to apply the annealing field at room temperature and then add small amounts of the coolant liquid to the Dewar flask. The annealing field was not removed until the specimen was well below the transition temperature. The apparatus was then left for at least half an hour for the specimen holder to attain the temperature of the liquid bath, during which time the magnet was rotated to the desired orientation with respect to the specimen.

After initially balancing the bridge, the galvanometer reading was taken at zero field between each field measurement so that, in order to minimise errors due to thermal drift, a mean zero value could be used for each reading. An invariant order of procedure

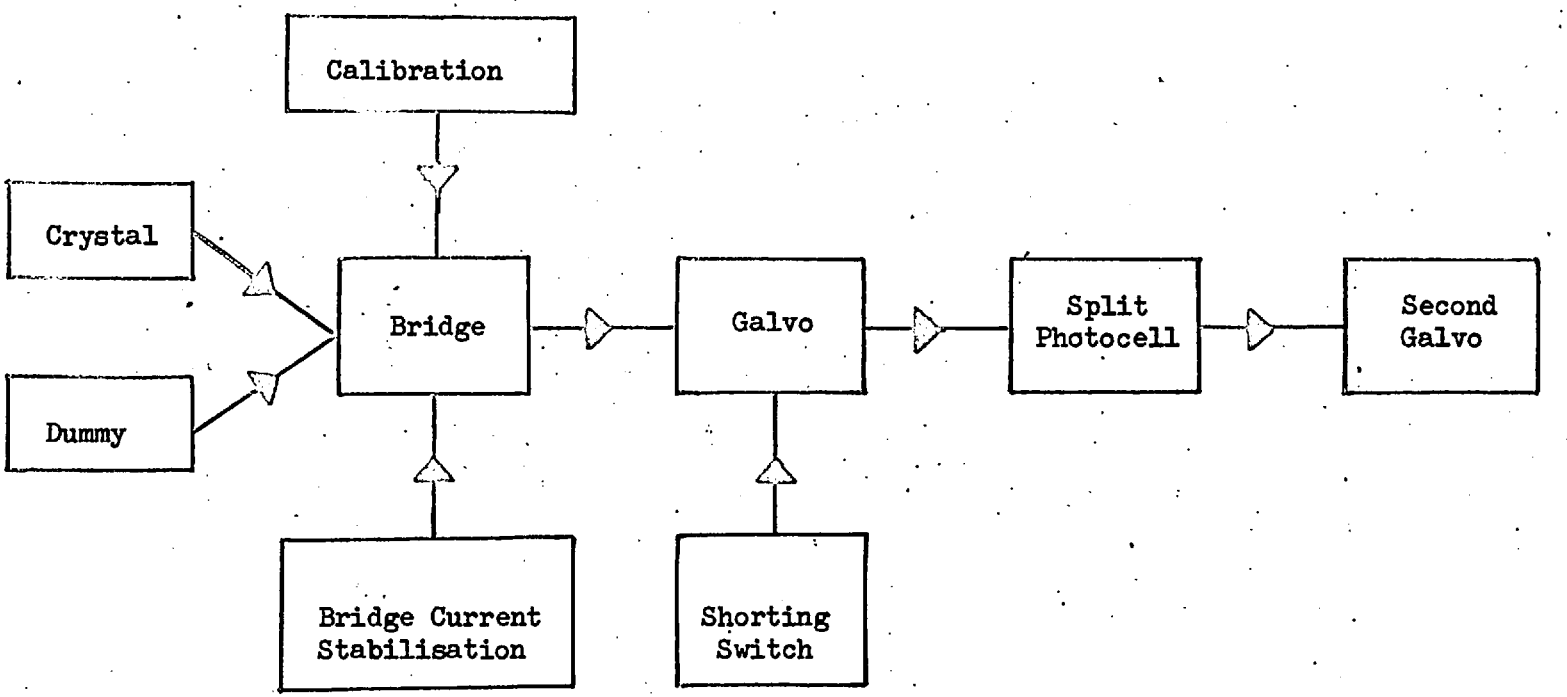


Figure 16. A block diagram of the measurement apparatus.

was to apply a field in the positive direction first, and then one in the negative direction, in each case shorting the primary galvanometer before changing the field. This process was usually repeated twice more for each field value and a mean value of scale reading calculated for each direction of applied field. Normally the field was then increased and the measurement process repeated. Finally the resistance sensitivity of the bridge was measured as described in Section 2.7.3., by varying the parallel resistance of the bridge arm and noting the corresponding secondary galvanometer deflection.

2.9. DISCUSSION OF APPARATUS

2.9.1. Accuracy of Results

In accuracies in any set of measurements may be split into two types, random errors and systematic errors. The random errors are due mainly to the thermal instability of the specimen, which caused a flutter of about $\pm$ 1 or 2 mm. on the final scale. At low temperature and in low fields the magnetostriction was very small, and so an error of $\pm$ 10% when measuring strains in a field of less than 1,000 oersteds was quite possible. This random error could be considerably reduced by repeating each measurement a number of times, and by this means, thrice repetition was used to reduce the error in low fields to less than $\pm$ 4%. At medium and high fields the averaging process reduced the random error of the mean to less than 2%, at which point it was comparable to the systematic error.

Plotting strain against field caused the purely observational errors to become negligibly small.

A second source of random error arose not from the measurement itself, but rather from the material measured, since the magnetostriction depended on the domain state of the crystal, as discussed in Section 4.3. This was a day-to-day error and was only removed by the use of a controlled annealing and measurement procedure.

Systematic errors arising from errors in the resistive arms of the bridge were eliminated by the use of high quality components, so that the ultimate accuracy was set by the accuracy to which the gauge factor and field were known. The field could be measured to better than 1% and as Figure 15 shows, its uniformity over the crystal was $\pm$ 0.5%. The accuracy and repeatability of the gauge factor was the only remaining unknown. Birss and Lee[55] have estimated by measurements of magnetostriction with different gauges having different gauge factors that gauges agree among themselves to better than 3%. This conclusion has been found to be completely justified within the present work using a number of gauges of the same type.

A further error was introduced when taking an angular dependence of strain, for it was assumed that the gauge measured the component of strain only along its length, which was incorrect because of the finite width of the gauge wire 'grid'. The principal sensitivity of a strain gauge which is usually quoted, refers to strain along its length; measured strain perpendicular to the main axis results

from the cross sensitivity. This term is given by

$$\text{Cross sensitivity} = \frac{\text{Width of gauge grid} \times \text{Principal sensitivity}}{\text{Length of gauge grid} \times \text{Number of wires}} \qquad (2.37)$$

and using dimensions given in Section 2.2, the cross sensitivity was calculated to be 0.065. This was about 3% of the principal sensitivity value, and was an unusual systematic error, being angular dependent, so that it was zero when strain and gauge coincided in direction and rose to a maximum of $\pm$ 3% when strain and gauge were perpendicular. In conclusion it may be said that although random errors were reduced by various averaging processes, to below $\pm$ 1% there still remained two possible sources of error, due to insufficient knowledge of the strain gauge sensitivity factor of the actual gauge used, and due to the domain structure of the material. The former probably limits the absolute accuracy of the measurements to $\pm$ 5% and appears to be a fundamental limitation caused by the method of measurement. The latter was only made repeatable by suitable magnetic annealing processes.

2.9.2. Apparatus Limitations

The lower limit of strain detection of this apparatus was one part in 10^8 and this sensitivity was the cause of the only serious practical limitation. Since the strain detection limit was a thousandth of the strain resulting from a temperature change in the specimen of 1 deg C., the impossibility of measuring strain over a

range of temperatures is immediately evident. It would also have been very desirable to have been able slowly to increase the measurement field and to use an X-Y recorder to automatically plot the strain against magnetic field. This was also impossible because of the relatively large e.m.f. induced into the strain gauges by any field variation. Although this could theoretically have been reduced by coils wound in the opposite direction, it is completely impractical as the coils would have to be connected into the part of the circuit which was delicately balanced and which would cause many more spurious voltages.

The limit of strain detection depends on the lower limit to $\frac{\delta R}{R}$ which is difficult to estimate since it depends on the amount of amplification that can, in practice, be applied to the off-balance signal from the Wheatstone bridge. The fundamental limit was far from approached since 10^{-9} amps corresponds to 10^{10} electrons passing per second. However, electrostatic and electromagnetic pick-up and electrical noise arising from electrical contacts, temperature instabilities, thermal e.m.f. and mechanical vibrations limit the maximum sensitivity. The limit could be extended only by ensuring an even greater temperature stability of the measurement apparatus and by developing suitable amplifying equipment.

CHAPTER III

EXPERIMENTAL SPECIMENS AND ASSOCIATED CALCULATIONS

3.1. EXPERIMENTAL SPECIMENS

3.1.1. Crystal Orientation

In the main, single crystals of hematite were used in this investigation, and all of these were oriented by X-ray diffraction using the Laue back reflection technique. Although the unit cell of hematite is rhombohedral with angles of 55° 17' and side of 5.42 Å, this can be considered to be contained within an approximately face centred cubic structure with lattice constant 7.8 Å, as shown in Figure 17. If the structure were exactly face centred cubic, the smaller rhombohedron would have angles of 60°, so that actually the outer structure is face centred rhombohedral with angles of 87°.

Normally the natural cleavage or growth plane for a crystal of hematite is the (110) face in the 55° 17' rhombohedral system or the (100) face in the near cubic system. One type of natural crystal which was examined had a growth plane coincident with the (111) face, which is common to both co-ordinate systems. These cleavage and growth faces were utilised as convenient surfaces for strain measurement, and their orientation was easily determined by X-ray diffraction. Figures 18(a) and 18(b) show typical Laue photographs for (110) planes and (111) planes respectively, and it can be seen that the spot patterns are easily distinguishable. Once oriented, each

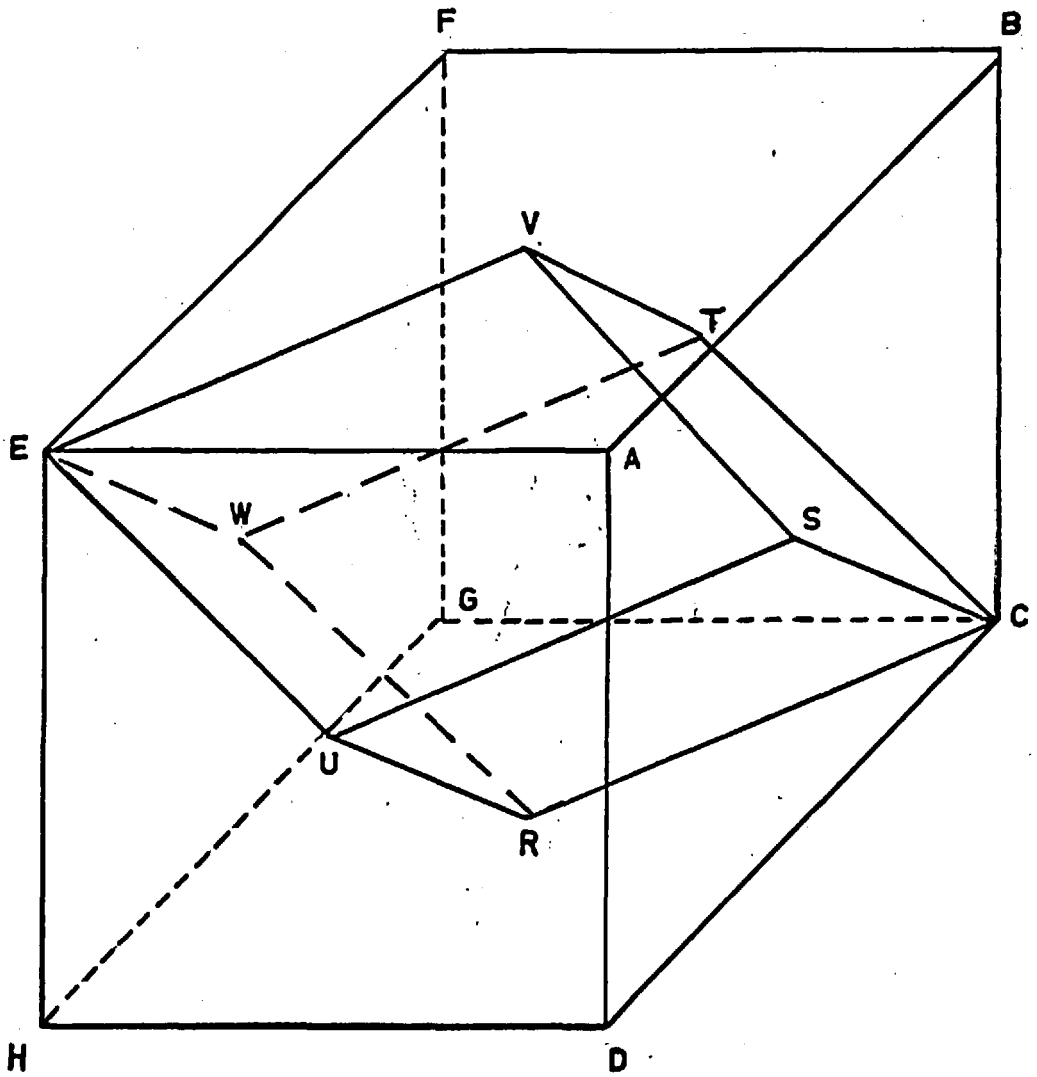


Figure 17. A 60° rhombohedron inside a cube.

(111) plane in rhombohedral system RST is parallel to plane DBG.

(110) plane in rhombohedral system VTRU is parallel to plane ABCD.

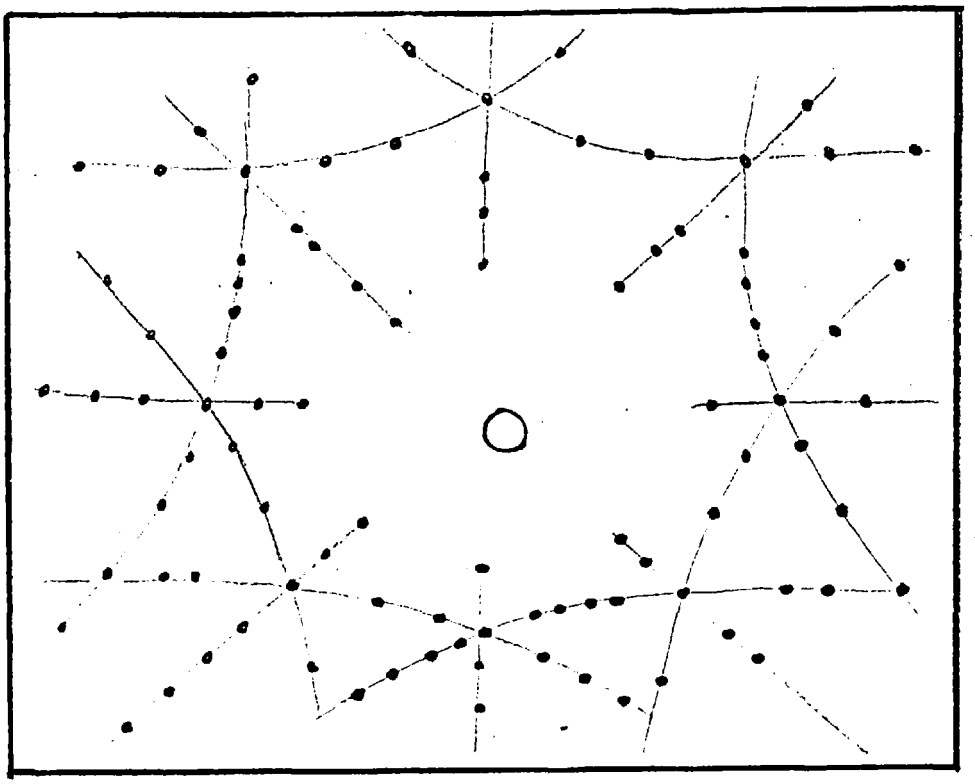


Figure 18(a). Atypical x-ray Laue spot pattern for a beam normal to a (110) face of hematite.

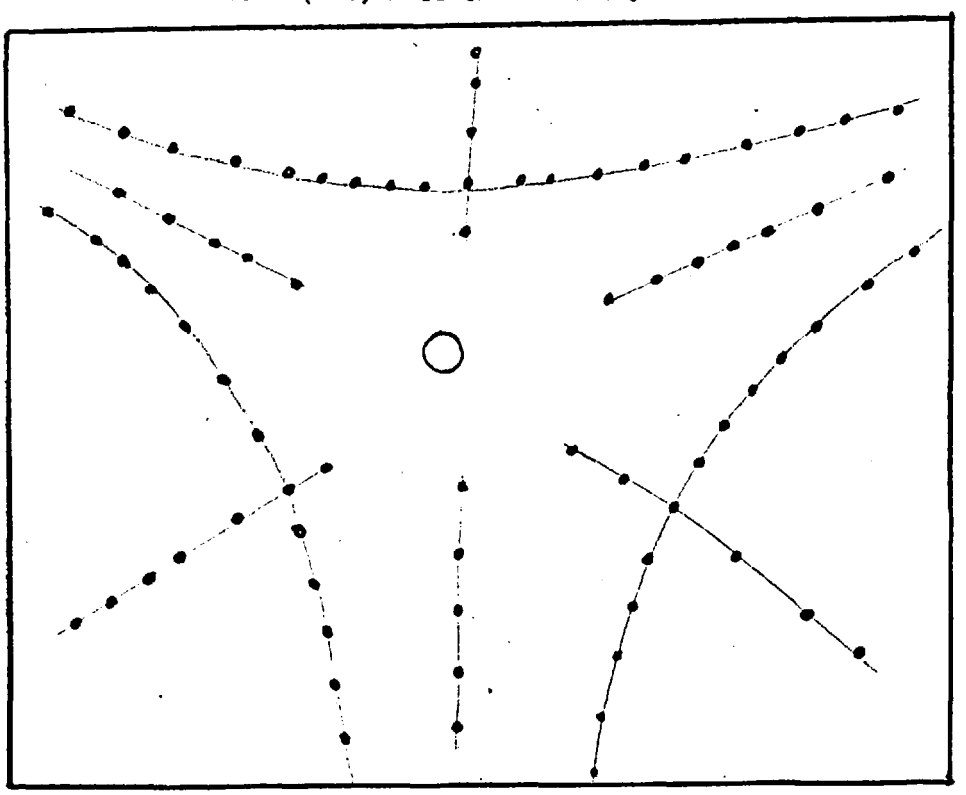


Figure 18(b). A typical x-ray Laue spot pattern for a beam normal to a (111) face of hematite.

crystal was cut to size to fit within the specimen holder using a diamond impregnated wheel, after which the resistance strain gauge was stuck on, as described in section 2.2.

3.1.2. Synthetic Crystal

The synthetic crystal used in the experimental work was prepared by Dr. Remeika of Bell Telephone Laboratories, and used here by kind permission of Prof. M. Blackman. The crystal, which weighed 0.900 grams, had a smooth (110) type growth face and the strain gauge was stuck on this face at an angle of 10° to the $[001]$ rhombohedral direction. This particular angle was convenient from the geometry of the crystal, and not entirely unreasonable from theoretical aspects, as will be seen in section 3.3.2. Figure 19 shows this crystal with the strain gauge attached.

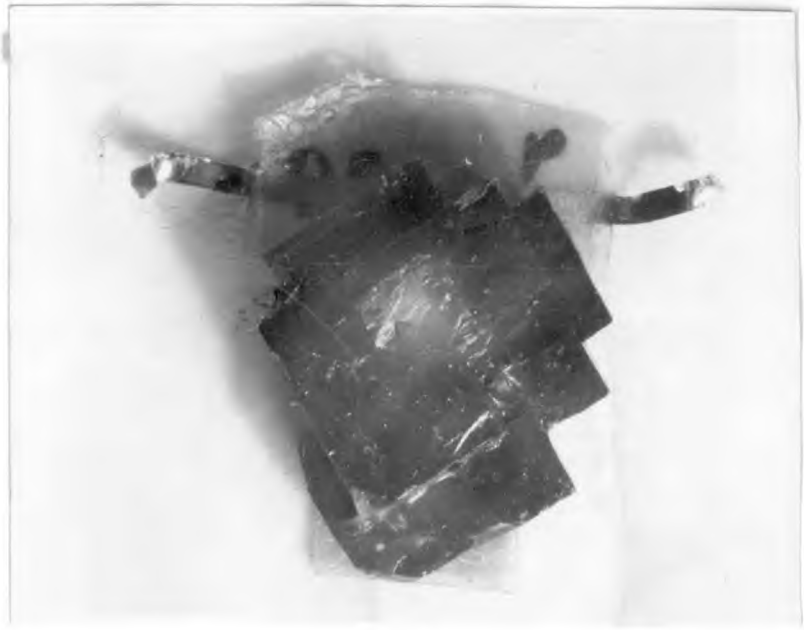
Before any strong magnetic field was applied to the specimen the magnetic remanence was measured as a function of temperature. The resultant curve, of which the warming part is shown in Figure 20, shows a large increase in remanence through the Morin transition but with a constant value at both low and high temperatures. The apparent decrease in remanence upon warming at about -10° C. is probably caused by the onset of a canted spin domain structure, which would temporarily reduce the remanent magnetisation.

3.1.3. Annealed Synthetic Crystal

After measurements were performed on the synthetic crystal, it



(a)



(b)

Figure 19. Synthetic hematite crystal.

(a) strain gauge face. (b) reverse face.

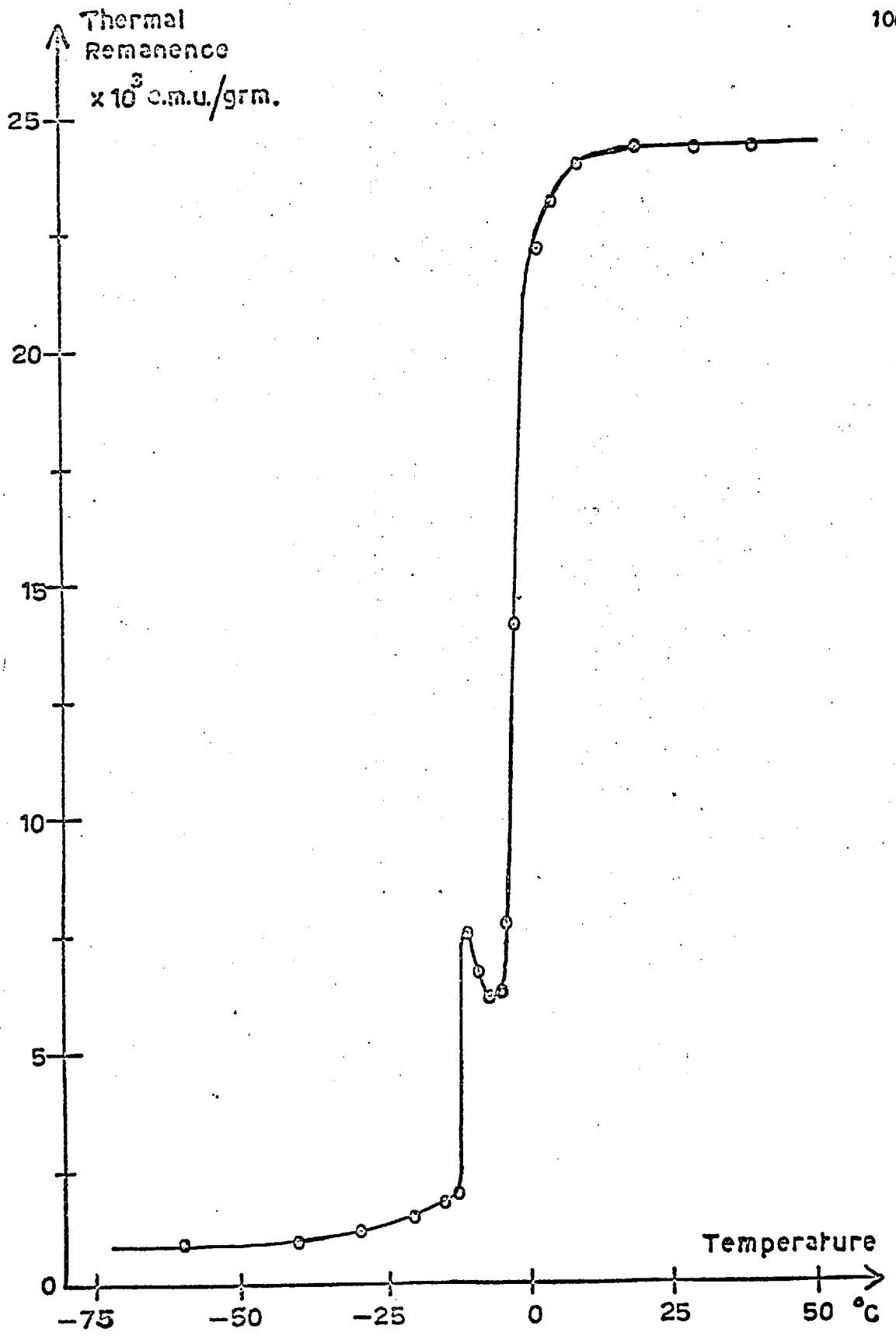


Figure 20. Total magnetic remanence of the unannealed synthetic crystal as a function of temperature.
(provided by T.E. Gallon)

was removed from the apparatus and thermally annealed. This consisted of maintaining the crystal at 1200° C. for ten days in a platinum boat in an atmosphere of pure oxygen. Cooling was achieved at a rate of 5 deg C. per hour, at the end of which it was hoped that the crystal would be free from internal dislocations and strains. The prolonged time at high temperature in oxygen probably caused some oxidation of any remaining ferrous ions. Both the high and low temperature magnetic remanence were considerably reduced by this treatment, as shown by Figure 21. There is no evidence of domain formation upon warming as found previously, and this is probably associated with the reduction of canted spin domain nucleating centres.

3.1.4. Elba Crystal

A number of natural crystals of various properties were used in this work. The most pure was a large single crystal from Elba weighing 2.8 grams and having a particularly fine (110) growth face. The strain gauge was stuck on this face, as shown in Figure 22, along a direction set at 45° to the [001] and [1$\bar{1}$0] axes, both of which lie within the plane. Although the chemical purity of an Elba crystal is far less than that of a good synthetic crystal, Kaye[60] has determined the non-ferrous impurities to be less than 0.01%.

3.1.5. Arizona Crystal

The second natural crystal used was obtained from Arizona and

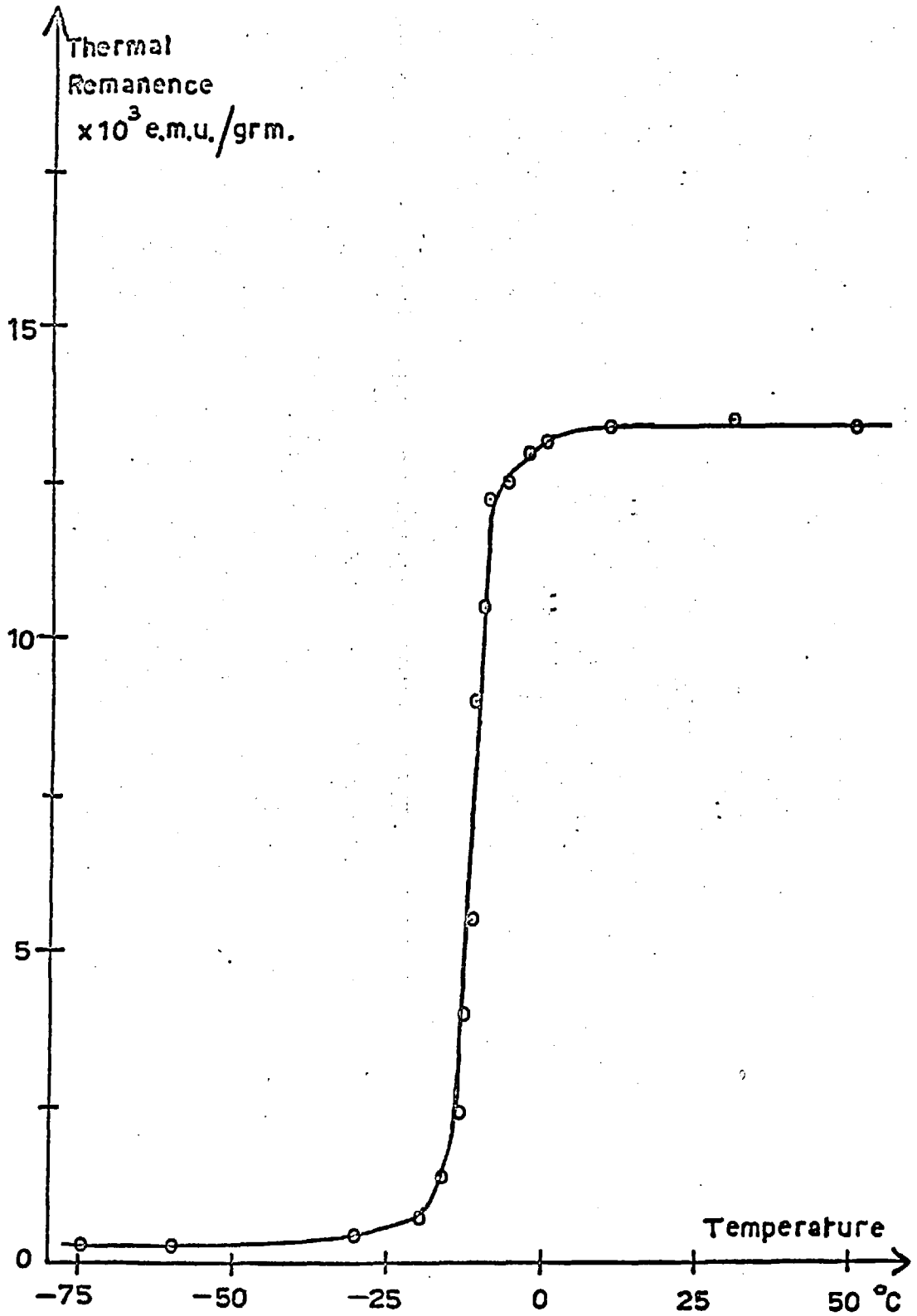


Figure 21. Total magnetic remanence of the annealed synthetic crystal as a function of temperature.
(provided by T.E. Gallon)

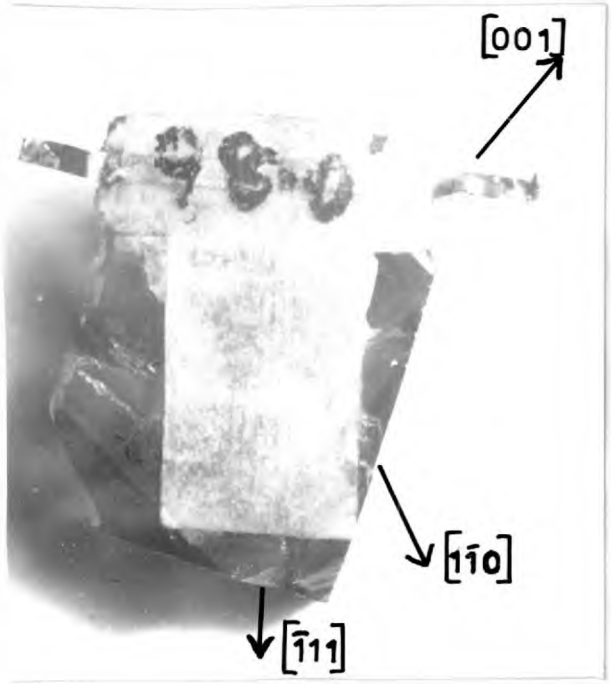


Figure 22. Hematite crystal from Elba.

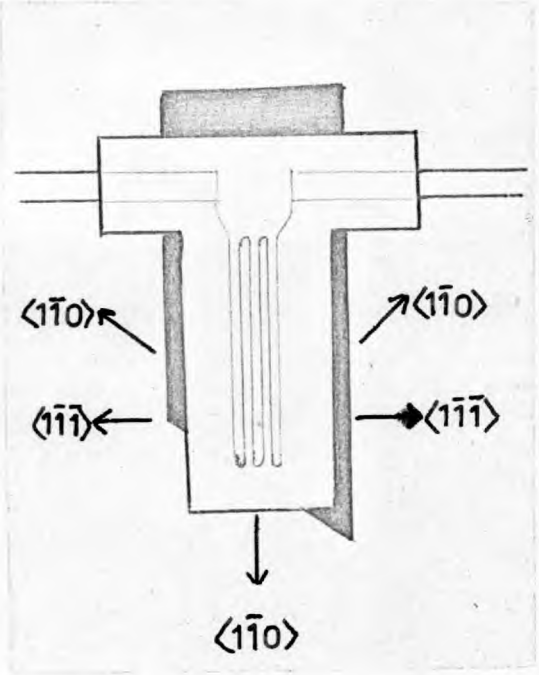


Figure 23. Hematite crystal from Arizona.

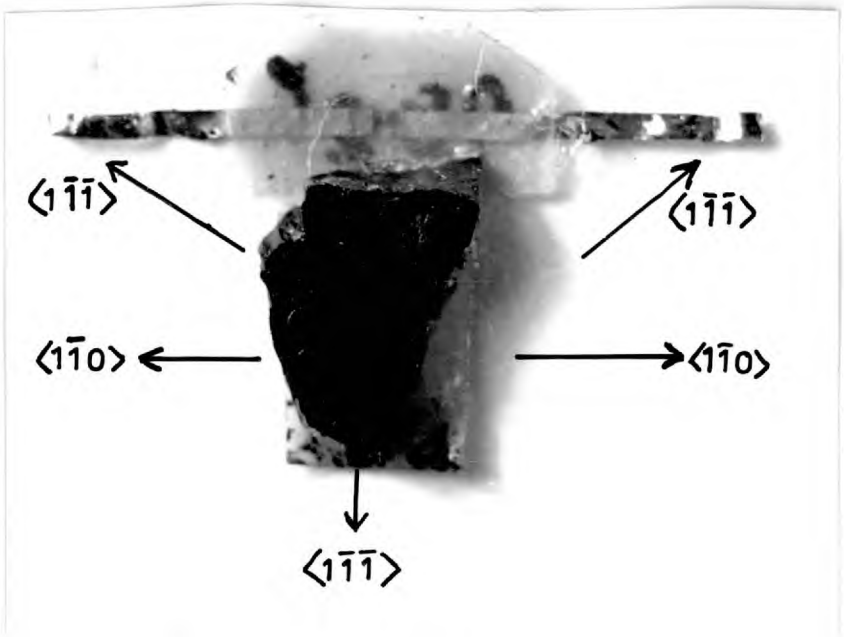
weighed 0.10 grams. This was one of two crystals investigated that had (111) cleavage faces. The gauge was stuck on this face along one of the $\langle 1\bar{1}0 \rangle$ axes as shown in Figure 23. The $\langle 1\bar{1}0 \rangle$ axes are the lines where the planes containing $\langle 100 \rangle$ and $[\bar{1}11]$ axes cut the (111) plane, (see Figure 26 later). The Morin transition in crystals from Arizona was found to be at - 80° C and considerably below the temperature of the pure material, but this is probably completely accountable by the relatively high concentration of foreign ion impurities in Arizona crystals. These concentrations have been determined by Kaye to be approximately 0.3% titanium and 0.3% aluminium.

3.1.6. St. Gothard Crystal

The third natural crystal investigated originated from St. Gothard, Switzerland, and possessed a (111) growth face. The crystal, which weighed 0.80 grams, had the strain gauge stuck along one of the $\langle \bar{1}\bar{1}\bar{1} \rangle$ axes, as shown in Figure 24. These axes are perpendicular to the $\langle 1\bar{1}0 \rangle$ type along which the gauge was stuck to the Arizona crystal in the preceding section. Crystals from St. Gothard have an uncommonly high impurity concentration; measurements by Kaye have shown that the titanium impurity lies between 1% and 3%, aluminium 0.1% and vanadium 0.1% - 0.5%. As a result of this, St. Gothard crystals were found to lack a Morin transition completely, even down to - 200° C, so that measurements in the magnetic symmetry group $\bar{3}m$ were impossible.



(a)



(b)

Figure 24. Hematite crystal from St. Gothard, Switzerland. (a) strain gauge face. (b) reverse face.

3.1.7. Effect of Impurities on the Transition Temperature

The reduction of the Morin transition temperature as the impurities, particularly titanium are increased is well-known. Morin[33] found that 1% of titanium completely supressed the transition. Kaye[60] put this investigation on a more precise foundation and derived an approximately linear relationship between titanium impurity concentration (0.0 - 0.1%) and reduction of the transition temperature (0 - 70° C.) from - 15° C., for single crystals. Titanium appears to have a far greater importance in determining the transition temperature than any other impurity, and this has been suggested as being due to small regions where equal volumes of $FeTiO_3$ and Fe_2O_3 have reacted to form a ferrimagnetic precipitate[61]. These regions may then disturb the magnetocrystalline anisotropy energy of the crystal to such an extent that spin rotation to the $[\bar{1}11]$ axis upon cooling is prevented.

3.1.8. Polycrystalline Specimens

It is quite common to measure magnetostriction on polycrystalline ingots of material, but it is virtually impossible to produce ingots of hematite due to appreciable loss of oxygen from the lattice above 1200° C, even in one atmosphere of the gas. Sintering at a lower temperature is a possibility but it has been found experimentally that specimens made in this manner lack sufficient mechanical strength for magnetostriction measurements. Polycrystalline specimens of hematite can be made by compressing the powder in the presence of a

suitable binding medium. Quantitative magnetostriction measurements on this are only possible if 100% packing density is achieved. Qualitative results can still be obtained with far less packing density provided that compression and extension of the binding material does not mask the strain effects.

To this end a number of pills of hematite powder bound with Araldite M.Y.750 epoxy resin were produced. Two types of powders were used; one was known as B.P.C.1949 grade precipitated ferric oxide prepared by Hopkin and Williams Ltd., and the other was 99.995% pure hematite prepared by Koch-Light Laboratories Ltd. The former of these materials showed no magnetic transition at all, which is probably accountable by at least 0.5% titanium impurity in the material.

The method of preparation of the experimental pills was to mix a small amount of the epoxy resin with about five times its volume of benzene and then compound an equal volume of hematite powder in with this. This dampened powder was evacuated to evaporate the benzene completely and then pressed at 20 tons/sq. inch ($\sim$ 3000 atmospheres) in air until excess resin was extruded, to produce a half inch diameter pill. The pill, when removed from the press was completely submerged in a mould containing more epoxy resin and evacuated for approximately ten minutes to removed any trapped air. When atmospheric pressure was restored very slowly at the natural leakage rate of the system, resin was forced into any microscopic holes in the pill. The thermosetting resin was set in the usual way

by heating at 90° C. in air for half an hour. Magnetostriction specimens were prepared by cutting the required part from the cast block with a diamond impregnated cutting wheel and grinding with alumina powder. Gauges were affixed in the usual manner.

3.2. MAGNETOSTRICTION THEORY

3.2.1. Derivation of Form of 3rd Rank Axial c-tensor in Group $\bar{3}m$

It has been shown in section 1.5.2. that the low temperature phase of hematite has magnetic symmetry operators 1, $\bar{1}$, $3(2_\perp)$, $3(\bar{2}_\perp)$, $\mp 3_z$, $\overline{\mp 3}_z$, so that it exhibits the symmetry of the magnetic group $\bar{3}m$. The generating matrices for derivation of the form of property tensors in this group are, according to Birss[1], $\left[\bar{1}\right]$, $\left[2_y\right]$, $\left[+3_z\right]$, where y is the 2-fold rotation axis and z is the 3-fold rotation axis. If $d_{ijk....n}$ is an axial property tensor, then the requirement that it is invariant under all permissible symmetry operations for a particular symmetry class is the same as saying

$$d_{ijk....n} = |\sigma| \; \sigma_{ip}\sigma_{jq}\sigma_{kr} \cdots\cdots\cdots \sigma_{nu} \, d_{pqr....u} \qquad (3.1)$$

where σ_{ip}, σ_{jq} and σ_{kr} are matrix elements all corresponding to the particular permissible symmetry operation, and then the equation for a third rank axial tensor simplifies to

$$d_{ijk} = |\sigma| \; \sigma_{ip}\sigma_{jq}\sigma_{kr} \, d_{pqr} \, . \qquad (3.2)$$

When i, j and k can each have the values 1, 2 or 3, corresponding to the Cartesian co-ordinates x, y and z respectively, the tensor d_{ijk} has 27 components which are

$$\begin{array}{ccc|ccc|ccc} d_{111} & d_{121} & d_{131} & d_{112} & d_{122} & d_{132} & d_{113} & d_{123} & d_{133} \\ d_{211} & d_{221} & d_{231} & d_{212} & d_{222} & d_{232} & d_{213} & d_{223} & d_{233} \\ d_{311} & d_{321} & d_{331} & d_{312} & d_{322} & d_{332} & d_{313} & d_{323} & d_{333} \end{array}$$

The matrix $[\bar{1}]$ has been listed in equation (1.4) as

$$[\bar{1}] = \begin{bmatrix} -1 & 0 & 0 \\ 0 & -1 & 0 \\ 0 & 0 & -1 \end{bmatrix}$$

so that the determinant $|\sigma|$ in equation (3.2) is equal to -1. The only non-zero matrix elements are σ_{11}, σ_{22} and σ_{33} so that the set of equations that can be derived from equation (3.2) is

$$\begin{aligned} d_{111} &= -\sigma_{11}\,\sigma_{11}\,\sigma_{11}\,d_{111} \\ d_{222} &= -\sigma_{22}\,\sigma_{22}\,\sigma_{22}\,d_{222} \\ d_{333} &= -\sigma_{33}\,\sigma_{33}\,\sigma_{33}\,d_{333} \\ d_{112} &= -\sigma_{11}\,\sigma_{11}\,\sigma_{22}\,d_{112} \end{aligned} \qquad (3.3)$$

etc.

which give the solutions

$$d_{111} = +d_{111}, \qquad d_{222} = +d_{222} \qquad \text{etc.} \qquad (3.4)$$

This generating matrix, $[\bar{1}]$, imposes no restrictions at all on the individual tensor components, so that if a third rank axial tensor had only this matrix, all 27 of its components would be non-zero.

The second matrix $[2_y]$ has also been listed previously in equation (1.4) as

$$[2_y] = \begin{bmatrix} -1 & 0 & 0 \\ 0 & 1 & 0 \\ 0 & 0 & -1 \end{bmatrix}$$

so that the determinant $|\sigma|$ is +1. As in the previous matrix, only the terms σ_{11}, σ_{22} and σ_{33} are non-zero, so that the set of equations relating the components of the property tensor are

$$\begin{aligned} d_{111} &= \sigma_{11}\,\sigma_{11}\,\sigma_{11}\,d_{111} \\ d_{222} &= \sigma_{22}\,\sigma_{22}\,\sigma_{22}\,d_{222} \\ d_{333} &= \sigma_{33}\,\sigma_{33}\,\sigma_{33}\,d_{333} \\ d_{112} &= \sigma_{11}\,\sigma_{11}\,\sigma_{22}\,d_{112} \qquad (3.5) \\ &\text{etc.} \end{aligned}$$

The solutions of the equations listed are

$$\begin{aligned} d_{111} &= -d_{111} \qquad \therefore\ d_{111} = 0 \\ d_{222} &= +d_{222} \\ d_{333} &= -d_{333} \qquad \therefore\ d_{333} = 0 \\ d_{112} &= +d_{112} \qquad (3.6) \end{aligned}$$

In general the combinations $\sigma_{11}\,\sigma_{22}\,\sigma_{22}$ or $\sigma_{33}\,\sigma_{22}\,\sigma_{22}$ or $\sigma_{11}\,\sigma_{33}\,\sigma_{33}$ or $\sigma_{33}\,\sigma_{11}\,\sigma_{11}$ will all give solutions which cause the respective components of d_{ijk} to be zero. The remaining combinations of matrix elements, which are $\sigma_{11}\,\sigma_{11}\,\sigma_{22}$, $\sigma_{33}\,\sigma_{33}\,\sigma_{22}$ and $\sigma_{11}\,\sigma_{22}\,\sigma_{33}$ all give real, non-zero tensor components when equations similar to equation (3.5) are constructed and solved. The 13 non-zero tensor components are d_{121}, d_{211}, d_{231}, d_{321}, d_{112}, d_{132}, d_{312}, d_{332}, d_{123}, d_{213}, d_{233}, d_{323} and also d_{222} derived from equation (3.6).

The third generating matrix $\left[+3_z\right]$ can now be used to provide equations relating the 13 remaining components. From equation (1.4), this matrix has been listed as

$$\left[+3_z\right] = \begin{bmatrix} -\frac{1}{2} & \frac{\sqrt{3}}{2} & 0 \\ -\frac{\sqrt{3}}{2} & -\frac{1}{2} & 0 \\ 0 & 0 & +1 \end{bmatrix}$$

so that the determinant $|\sigma|$ which decides the initial sign in equation (3.2), has the value

$$|\sigma| = -\frac{1}{2}\begin{bmatrix} -\frac{1}{2} & 0 \\ 0 & 1 \end{bmatrix} - \frac{\sqrt{3}}{2}\begin{bmatrix} -\frac{\sqrt{3}}{2} & 0 \\ 0 & 1 \end{bmatrix} = +\tfrac{1}{4} + \tfrac{3}{4} = +1 \qquad (3.7)$$

It can be seen that the $\left[+3_z\right]$ matrix has the elements σ_{13}, σ_{23}, σ_{31} and σ_{32} all equal to zero, so that the only non-zero elements are σ_{11}, σ_{12}, σ_{21}, σ_{22} and σ_{33}. These can be used to provide relationships between the remaining tensor components. One such is

$$d_{121} = \sigma_{11}\,\sigma_{22}\,\sigma_{11}\,d_{121} + \sigma_{12}\,\sigma_{21}\,\sigma_{11}\,d_{211} + \sigma_{11}\,\sigma_{21}\,\sigma_{12}\,d_{112} + \sigma_{12}\,\sigma_{22}\,\sigma_{12}\,d_{222} \qquad (3.8)$$

$$\therefore\ d_{121} = -\tfrac{1}{8}\,d_{121} + \tfrac{3}{8}\,d_{211} + \tfrac{3}{8}\,d_{112} - \tfrac{3}{8}\,d_{222} \qquad (3.9)$$

The complete set of equations are constructed and solved in appendix II. The solutions are

$$d_{231} = -d_{132};\quad d_{312} = -d_{321},\quad d_{123} = -d_{213} \qquad (3.10)$$

and $$d_{121} = d_{211} = d_{112} = -d_{222}. \qquad (3.11)$$

Considering the intrinsic symmetry of the property tensor of linear magnetostriction Q_{ijk}, it can be seen from its defining equation (in section 1.3.5.) that since the str tensor is symmetrical in its first two suffices, i.e.

$$d_{ijk} = d_{jik} \qquad (3.12)$$

a slightly simplified method of writing the tensor which utilises

a double suffix can be employed, viz.

$$d_{11k} = Q_{1k}, \qquad d_{22k} = Q_{2k}, \qquad d_{33k} = Q_{3k},$$
$$d_{23k} = d_{32k} = Q_{4k}, \qquad d_{31k} = d_{13k} = Q_{5k},$$
$$d_{12k} = d_{21k} = Q_{6k}. \tag{3.13}$$

In this notation, equation (3.10) becomes

$$Q_{41} = -Q_{52},\ Q_{52} = -Q_{41},\ Q_{63} = -Q_{63},\ \therefore\ Q_{63} = 0 \tag{3.14}$$

also equation (3.11) becomes

$$Q_{61} = Q_{61} = Q_{12} = -Q_{22} \tag{3.15}$$

so that the only non-zero components are

$$Q_{41} = -Q_{52} \tag{3.16}$$

and $$Q_{12} = Q_{61} = -Q_{22}. \tag{3.17}$$

It is convenient to write the linear magnetostriction tensor in group $\bar{3}m$ which has just been derived, in a suitable 6 x 3 matrix form

$$Q_{Ak} = \begin{bmatrix} 0 & -Q_{22} & 0 \\ 0 & Q_{22} & 0 \\ 0 & 0 & 0 \\ Q_{41} & 0 & 0 \\ 0 & -Q_{41} & 0 \\ -Q_{22} & 0 & 0 \end{bmatrix} \tag{3.18}$$

Then the defining equation for this effect

$$E_{ij} = Q_{ijk} H_k \tag{1.13}$$

or $$E_A = Q_{Ak} H_k, \tag{3.19}$$

gives as component equations

$$E_{11} = -Q_{22} H_2, \quad E_{22} = Q_{22} H_2, \quad E_{33} = 0, \quad E_{23} = E_{32} = Q_{41} H_1$$
$$E_{13} = E_{31} = -Q_{41} H_2, \quad E_{12} = E_{21} = -Q_{22} H_1 \qquad (3.20)$$

From these equations one would expect to observe a longitudinal strain resulting from linear magnetostriction along the x and y axes in a crystal of hematite when a field is applied along the 2-fold axis or y-axis. However, regardless of the direction of any applied magnetic field, linear longitudinal strain resulting from it should never be exhibited along the z-axis or 3-fold rotation axis of the crystal. All of the three possible shear strains are produced by applying the magnetic field in any general direction in the x-y plane of the crystal, and a component of the shear strains will exist along the z-axis which could give the appearance of a longitudinal strain. Components of the shear strains will also be present along the two other axes and these must be combined with the longitudinal strains existing there. Finally, it is evident from the equations (3.20), that if a magnetic field is applied parallel to the z-axis of a hematite crystal, there should be no strains at all resulting from linear magnetostriction.

3.2.2. Derivation of Form of 4th Rank Polar i-tensor in Group $\bar{3}m$

It has been previously mentioned in section 1.3.1. that the strain resulting from a magnetic field $\underline{H}$ does not, in general, consist solely of a term linear in $\underline{H}$ although this is the principal term. There is the possibility of progressively smaller terms in H^2, H^3, etc. being evident, according to the strain tensor expansion

$$E_{ij} = Q_{ijk} H_k + S_{ijkl} H_k H_l + T_{ijklm} H_k H_l H_m + \ldots\ldots \quad (3.21)$$

It is useful to find the form of the tensor S_{ijkl} representing the 'square law' magnetostriction in hematite. Since a tensor in the same magnetic symmetry group as the previous section is being considered, the same generating matrices can be used. These are $\left[\bar{1}\right]$, $\left[2_y\right]$, $\left[+3_z\right]$.

If d_{ijkl} is a 4th rank polar tensor, then the requirement that it is invariant under all permissible symmetry operations for the particular symmetry class is the same as saying

$$d_{ijkl} = \sigma_{ip}\, \sigma_{jq}\, \sigma_{kr}\, \sigma_{ls}\, d_{pqrs}. \quad (3.22)$$

σ_{ip}, σ_{jq}, σ_{kr}, σ_{ls} are matrix elements all corresponding to the particular symmetry operations which are permissible, and these are very similar to those used in the preceding section. The tensor d_{ijkl} needs to be represented by a 3 x 3 x 3 x 3 matrix, but the 3 x 3 matrix

$$\begin{bmatrix} d_{xx11} & d_{xx12} & d_{xx13} \\ d_{xx21} & d_{xx22} & d_{xx23} \\ d_{xx31} & d_{xx32} & d_{xx33} \end{bmatrix}$$

where xx represents in turn

11	12	13
21	22	23
31	32	33

lists all the 81 components.

It has been seen in section 3.2.1. that the matrix $\left[\bar{1}\right]$ affords

no simplification at all of the form of the property tensor. The second matrix $[2_y]$ has been listed in equation (1.4) as

$$[2_y] = \begin{bmatrix} -1 & 0 & 0 \\ 0 & 1 & 0 \\ 0 & 0 & -1 \end{bmatrix}$$

This matrix causes all components containing the following suffices in any order to be zero: 2221, 1112, 3332, 2223, 1123, 1233. Similarly all the components of the tensor d_{ijkl} which are non-zero contain the following suffices in any order: 1111, 2222, 3333, 3331, 1113, 2213, 1122, 2233, 1133. The non-zero elements of d_{ijkl} are therefore d_{1111}, d_{1113}, d_{1122}, d_{1131}, d_{1133}, d_{1212}, d_{1221}, d_{1223}, d_{1232}, d_{1311}, d_{1313}, d_{1331}, d_{1333}, d_{1322}, d_{2112}, d_{2121}, d_{2123}, d_{2132}, d_{2211}, d_{2213}, d_{2222}, d_{2231}, d_{2233}, d_{2312}, d_{2321}, d_{2332}, d_{2323}, d_{3111}, d_{3113}, d_{3122}, d_{3131}, d_{3133}, d_{3212}, d_{3221}, d_{3223}, d_{3232}, d_{3311}, d_{3313}, d_{3322}, d_{3331}, d_{3333}.

The third generating matrix can now be used to give equations relating these 41 remaining components. This matrix has been listed in equation (1.4) as

$$[+3_z] = \begin{bmatrix} -\frac{1}{2} & \frac{\sqrt{3}}{2} & 0 \\ -\frac{\sqrt{3}}{2} & -\frac{1}{2} & 0 \\ 0 & 0 & 1 \end{bmatrix}$$

The non-zero tensor components are related by sets of equations similar to

$$d_{1111} = \sigma_{11}\sigma_{11}\sigma_{11}\sigma_{11}d_{1111} + \sigma_{11}\sigma_{11}\sigma_{12}\sigma_{12}d_{1122} + \sigma_{11}\sigma_{12}\sigma_{11}\sigma_{12}d_{1212} + \sigma_{11}\sigma_{12}\sigma_{12}\sigma_{11}d_{1221} + \sigma_{12}\sigma_{11}\sigma_{11}\sigma_{12}d_{2112} + \sigma_{12}\sigma_{11}\sigma_{12}\sigma_{11}d_{2121} + \sigma_{12}\sigma_{12}\sigma_{11}\sigma_{11}d_{2211} + \sigma_{12}\sigma_{12}\sigma_{12}\sigma_{12}d_{2222} \quad (3.23)$$

Therefore

$$d_{1111} = \frac{1}{16}d_{1111} + \frac{3}{16}d_{1122} + \frac{3}{16}d_{1212} + \frac{3}{16}d_{1221} + \frac{3}{16}d_{2112} + \frac{3}{16}d_{2121} + \frac{3}{16}d_{2211} + \frac{9}{16}d_{2222}. \quad (3.24)$$

There are no further terms as the elements σ_{13}, σ_{31}, σ_{23} and σ_{32} are zero. The complete set of equations relating the tensor components are given in appendix III. Using the double suffix notation introduced in section 3.2.1., it is possible to represent the 'square law' magnetostriction S_{ijkl} by the tensor S_{AB} and in this case the components are

$S_{11} = S_{22} = S_{12} + 2S_{66}$, $S_{21} = S_{12}$, $S_{13} = S_{23}$, $S_{31} = S_{32}$,

$S_{44} = S_{55}$, $S_{64} = S_{25} = -S_{15}$, $S_{46} = S_{52} = -S_{51}$,

$S_{66} \neq 0$, $S_{33} \neq 0$, and all other terms are zero.

It is convenient to write this tensor in group $\bar{3}m$ in a 6 x 6 matrix form, thus

$$S_{AB} = \begin{bmatrix} S_{12}+2S_{66} & S_{12} & S_{13} & 0 & -S_{25} & 0 \\ S_{12} & S_{12}+2S_{66} & S_{13} & 0 & S_{25} & 0 \\ S_{31} & S_{31} & S_{33} & 0 & 0 & 0 \\ 0 & 0 & 0 & S_{44} & 0 & S_{52} \\ -S_{52} & S_{52} & 0 & 0 & S_{44} & 0 \\ 0 & 0 & 0 & S_{25} & 0 & S_{66} \end{bmatrix} \quad (3.25)$$

Since the defining equation for this effect can be written in dummy suffix notation as

$$E_A = S_{Aij} H_i H_j \qquad (3.26)$$

then the matrix of equation (3.25) produces the following component equations:

$$E_{11} = (S_{12} + 2S_{66}) H_1H_1 + S_{12} H_2H_2 + S_{13} H_3H_3 - 2S_{25} H_1H_3$$
$$E_{22} = S_{12} H_1H_1 + (S_{12} + 2S_{66}) H_2H_2 + S_{13} H_3H_3 + 2S_{25} H_1H_3$$
$$E_{33} = S_{31} H_1H_1 + S_{31} H_2H_2 + S_{33} H_3H_3$$
$$E_{23} = E_{32} = 2S_{44} H_2H_3 + 2S_{52} H_1H_2$$
$$E_{13} = E_{31} = -S_{52} H_1H_1 + S_{52} H_2H_2 + 2S_{44} H_1H_3$$
$$E_{12} = E_{21} = 2S_{25} H_2H_3 + 2S_{66} H_1H_2 \qquad (3.27)$$

These strain equations show that if a magnetic field is applied in any direction in the crystal all longitudinal strain components are present. In addition, if the direction of the applied field does not lie along a principal axis then shear strains are also present. In general it can be said that the strains resulting from 'square law' magnetostriction in hematite are extremely complicated and although the components are mathematically separable it is doubtful whether they could be separated experimentally and the coefficients determined. Linear magnetostriction however, produces a far simpler strain situation as seen from equation (3.20), and without any measurable 'square law' magnetostriction, the linear magnetostriction coefficients can be evaluated from a simple experimental determination. If, in addition, the 'square law' magnetostriction strain is appreciable, it will probably mask the strain

due to the linear term and will produce conditions which make strain analysis virtually impossible.

The possibility of measurement of the linear coefficients therefore depends on the rate of convergence of the terms in the magnetostrictive strain expansion of equation (3.21). If the series converges rapidly, then the linear term predominates and it is possible to determine its coefficients, but if it does not converge very rapidly then the magnetostrictive strain cannot be satisfactorily analysed.

3.2.3. Derivation of Form of 3rd Rank Axial c-tensor in Group 2/m

It has been shown in section 1.5.2. that the high temperature phase of αFe_2O_3 has magnetic symmetry operators 1, $\bar{1}$, 2, $\bar{2}$, so that if the field is applied along a 2-fold symmetry axis it exhibits the symmetry of the group 2/m. The generating matrices for derivation of the form of property tensors in this group are, according to Birss[1], $\left[\bar{1}\right]$ and $\left[2_y\right]$, where the x, y and z axes bear the same relationship to the hematite unit cell as for the low temperature phase of section 3.2.1. This means that the y-axis is parallel to the 2-fold rotation axis. The requirement that the third rank axial property tensor d_{ijk} is invariant under all permissible symmetry operations for the particular symmetry class produces the same equation as previously, i.e.

$$d_{ijk} = |\sigma| \, \sigma_{ip} \, \sigma_{jq} \, \sigma_{kr} \, d_{pqr} \qquad (3.2)$$

The calculation of the form of a 3rd rank axial c-tensor in group 2/m is initially identical to the calculation of the form of

the same tensor in group $\bar{3}m$, for both utilise the generating matrices $[\bar{1}]$ and $[2_y]$. From section 3.2.1. the 13 non-zero coefficients which remain after using the two matrices are d_{121}, d_{211}, d_{231}, d_{321}, d_{112}, d_{132}, d_{222}, d_{312}, d_{332}, d_{123}, d_{213}, d_{233}, d_{323}. Using the double suffix notation introduced previously for the tensor Q_{Ak} it can be seen that its eight non-zero components are Q_{61}, Q_{41}, Q_{12}, Q_{52}, Q_{22}, Q_{32}, Q_{63}, Q_{43}. Hence the linear magnetostriction tensor in group 2/m can be written as

$$Q_{Ak} = \begin{vmatrix} 0 & Q_{12} & 0 \\ 0 & Q_{22} & 0 \\ 0 & Q_{32} & 0 \\ Q_{41} & 0 & Q_{43} \\ 0 & Q_{52} & 0 \\ Q_{61} & 0 & Q_{63} \end{vmatrix} \qquad (3.28)$$

and the component equations can be written as

$$\begin{aligned} E_{11} &= Q_{12} H_2 \\ E_{22} &= Q_{22} H_2 \\ E_{33} &= Q_{32} H_2 \\ E_{23} = E_{32} &= Q_{41} H_1 + Q_{43} H_3 \\ E_{13} = E_{31} &= Q_{52} H_2 \\ E_{12} = E_{21} &= Q_{61} H_1 + Q_{63} H_3 . \end{aligned} \qquad (3.29)$$

From these equations one would expect to observe a longitudinal strain along all three Cartesian axes when a magnetic field is applied parallel to the two-fold axis. ~~In addition all the shear stresses are produced when a magnetic field is applied at any~~

~~orientation to the crystal axes.~~ Finally it must be noted that unlike the case of linear magnetostriction in the $\bar{3}m$ group, strains are produced when the magnetic field is applied parallel to the z-axis of a hematite crystal when in the high temperature phase.

Linear magnetostriction in the 2/m group may have apparently important distinctions from the same tensor in the $\bar{3}m$ group, for in this latter group the spin direction (apart from 180° phase changes) is completely fixed within the lattice. The 2/m group however, being pyromagnetic, allows the direction of the spin pairs to rotate to align with the magnetic field. This means that low field magnetostriction in the 2/m group would be expected to be characteristic of strains occurring during the rotation of the internal magnetisation of a material, and under these strains the effect of linear magnetostriction would probably be masked. Once the rotation of magnetisation is complete, the true linear effect should be exhibited by the material.

This concept of a true linear strain superimposed on the strain resulting from domain reorientations has never previously been considered for a canted spin antiferromagnetic, although the same effect is a well-known phenomenon in ferromagnetics and is known as forced magnetostriction. In nickel which is ferromagnetic, the coefficient of linear increase of strain with applied field at high field values has been found by Kornetzki[62] to be of the order of 10^{-10} oersted^{-1}.

3.2.4. Linear Magnetostriction in Hematite Through the Magnetic Transition

It is of interest to consider the effect of the transition of the magnetic structure of hematite from group $\bar{3}m$ to group 2/m upon the tensor coefficients of linear magnetostriction. In nature, changes are rarely discontinuous, and since the Morin transition occurs as a result of a gradual rotation of spin direction extending over at least 20°, (see Figure 4), it would be reasonable to expect that the tensor components of linear magnetostriction should also be continuous through the transition.

Examination of equations (3.20) and (3.29) would therefore lead one to expect that the value of the components Q_{22} and Q_{41} would be continuous from group $\bar{3}m$ to group 2/m, but that the components Q_{32}, Q_{43} and Q_{63} in group 2/m should rise from zero with increasing temperature from the Morin transition. Similarly close to the transition it should be expected that the components Q_{12} and Q_{61} of the high temperature group would be equal to $-Q_{22}$ of the low temperature group, because the strain components E_{11} and E_{12} would be expected to be continuous. By a similar comparison Q_{52} of the 2/m group should tend, close to the Morin temperature, to the value of $-Q_{41}$ in the $\bar{3}m$ group. From this reasoning it is immediately apparent that for a small temperature range above the Morin transition, magnetostrictive strain along the z-axis of the hematite unit cell must be negligible so as to be continuous with the zero strain below the transition.

3.2.5. Magnetostriction Data from Elastic Constants

In the previous sections, crystal symmetry and magnetic symmetry have been utilised to predict the form of various magnetostriction tensors. This allows one to say that in one crystal linear magnetostriction can exist whilst in another the 'square law' magnetostriction term will predominate, and of course all this is very useful and important. Magnetic symmetry however, cannot give reasons for the existence of these effects, it can only indicate their presence. In this section the reasons for the existence of any form of magnetostriction are considered.

When a magnetic field is applied to a material its thermodynamic free energy is decreased due to the decrease in magnetic energy. Atoms prefer to be situated in positions of minimum energy in the lattice and these minimum energy points change as magnetic energy is impressed upon the material, and for this reason alone atoms move to occupy the bottom of the displaced potential wells. This constitutes magnetostriction. Normally, since magnetic energy is an even function of field, the magnetostriction is also an even function. In some cases, the complicated magnetic structure of a material may cause the internal magnetic energy to be different when the applied field is reversed and it is this difference which constitutes a magnetostriction which is dependent on the odd power of the field.

The formulation of the normal magnetostriction from thermodynamic principles has been performed by Powell[63] in 1931, and

later by Kittel[64]. If E_{ij} is a symmetrical strain tensor, then in the unmagnetised state the stored elastic energy W_o of a crystal is given by

$$W_o = \tfrac{1}{2} c_{ijkl} E_{ij} E_{kl} \qquad (3.30)$$

where the components of c_{ijkl} are the elastic constants. When the crystal is magnetised, the internal energy is increased by the magnetic energy W_m, so that the total energy then becomes

$$W = W_o + W_m. \qquad (3.31)$$

If the absence of linear magnetostriction is assumed, then W_m must be composed of only even terms of intensity of magnetisation I_i in combination with the strain tensor E_{ij}. Then the simplest expansion that can be used is

$$W_m = a_{ij} I_i I_j + b_{ijkl} I_i I_j E_{kl} \qquad (3.32)$$

where the components of a_{ij} are defined as the coefficients of magnetocrystalline anisotropy energy of the crystal, and the components of b_{ijkl} are defined as the magnetoeleastic coupling constants.

It is now known that in certain magnetic crystal classes, linear magnetostriction can exist. In this case the expansion of the magnetic energy W_m can include terms linear in intensity of magnetisation. A suitable expansion that can be used is

$$W_m = d_i I_i + a_{ij} I_i I_j + e_{ijk} I_i E_{jk} + b_{ijkl} I_i I_j E_{kl} \qquad (3.33)$$

where d_i could be called the linear magnetocrystalline anisotropy coefficients and e_{ijk} could be called the linear magnetoelastic coupling constants.

Both in the unmagnetised state and in the magnetised state the internal structure of a material is in a position of zero stress otherwise the stress would cause the ions to move until this position is attained. Stress is the strain differential of energy, so that this equilibrium position can be represented mathematically by the equation

$$\frac{\partial W}{\partial E_{ij}} = 0 \qquad (3.34)$$

where W (from equation (3.31)) is the sum of the strain energy and the magnetic energy. The solution to equation (3.34) gives the magnetostrictive strain corresponding to the particular value of intensity of magnetisation I_i.

In particular examples, crystal symmetry and magnetic symmetry afford considerable simplification of the forms of the various tensor coefficients used in the preceding expressions. The coefficient d_i, which is a first rank axial c-tensor like the pyromagnetic tensor, is known to be zero (from section 1.3.2.) in the $\bar{3}m$ group to which hematite belongs in its low temperature phase. The coefficient a_{ij} is a second rank polar i-tensor and in the group $\bar{3}m$ only even rank axial c-tensors are zero, and the second rank polar i-tensor has the form

$$a_{ij} = \begin{bmatrix} a_{11} & 0 & 0 \\ 0 & a_{11} & 0 \\ 0 & 0 & a_{33} \end{bmatrix} \qquad (3.35)$$

so the particular expression from equation (3.33) becomes

$$a_{ij}I_iI_j = a_{11}(I_1^2 + I_2^2) + a_{33}I_3^2. \qquad (3.36)$$

Similar considerations apply to the forms of the tensors e_{ijk}, b_{ijkl} and c_{ijkl} and from these the equilibrium strain of a material in a magnetic field can be determined.

The form of both linear magnetostriction components in the $\bar{3}m$ group in terms of the elastic constants and the linear magnetoelastic coupling coefficients is derived in appendix IV. The calculation is more of academic interest in relating elasticity to magnetostriction than practical use, for the concept of linear magnetoelastic coupling constants is quite new and values have not yet been determined in actual materials. The calculation shows however, that the predictions of crystal symmetry are self-consistent, for the final form of the strain components agrees completely with the form predicted solely from symmetry considerations (i.e. equation (3.20)).

3.2.6. Spin-lattice Interaction Theory

This section considers the possible atomic mechanism for linear magnetostriction in hematite. Very many antiferromagnetic crystals exist as such because of a superexchange interaction[65] between pairs of magnetic cations via an adjacent anion. This interaction probably takes the form of bonding electrons which are shared between the two magnetic ions and the oxygen ion in the case of hematite. The spatial distribution of these bonding electrons obviously depends radically on the cation-anion-cation separation

and angular direction and in this manner controls the strength of the superexchange interaction. It has been recently postulated[66] that the distribution of bonding electrons depends also on the direction of the spin moment of the magnetic cations, so that if the spin moment is affected by a magnetic field or if the bonding electrons interact with a magnetic field, then the distribution of bonding electrons is altered. Because the bonding electrons of different spin have different wave functions this could lead to a change in bond lengths and/or an induced polarization of the bonds. The former would cause magnetostriction, whilst the latter would cause the magnetoelectric effect.

Whether such effects will occur macroscopically, and if so, whether they will be linear in applied field depends on the atomic symmetry and on the spin distribution around each atomic site. It is this requirement which introduces the need for a classified system of magnetic symmetry such as has been discussed in Chapter I. Conversely, it also explains in atomic terms, the success of magnetic symmetry in predicting the forms of the various physical tensors.

A reversal of antiferromagnetic domains would be expected to occur by this mechanism immediately on reversal of the applied magnetic field, for if in a given magnetic field a certain spin-charge distribution is more favourable, then upon reversal of the field the opposite spin distribution would be preferable. Since this is a co-operative process it would be easily arrested if certain regions throughout the crystal have their domain type pinned as a

result of lattice imperfections and the like. In this case it would require a finite threshold of magnetic field to reverse the spin direction and there could be expected to be a distribution of threshold field values so that except for very high applied fields, there would remain regions of opposite domain type.

3.3. THEORY APPLIED TO THE SPECIMENS USED

3.3.1. Form of Linear Magnetostriction on (110) Plane in Hematite

Equations giving the linear magnetostrictive strain in hematite for all nine components of the tensor have previously been derived. The common natural cleavage plane of hematite crystals is the (110) plane, and so it is necessary to calculate the form of the strain equations on this plane. Suppose an angular position on the plane is defined by the angle θ, where $\theta = 0$ is aligned with the [001] direction. It is intended to measure strain at a certain angle $\theta = \Delta$ on the plane, and so the first step is therefore to transform the strain component equations from the crystallographic axes to a set of axes rotating in the (110) plane. The fixed axes and the rotating axes at $\theta = 0$ are shown in Figure 25. ϕ is the angle between the (110) plane and the [111] axis, and θ is measured as positive in the direction shown.

The strain $\underline{E}$ in a direction having direction cosines $\beta_i\beta_j$ relative to a particular set of axes is given by

$$E = E_{ij}\beta_i\beta_j \qquad (3.37)$$

If the strain gauge were along the [001] direction on the (110)

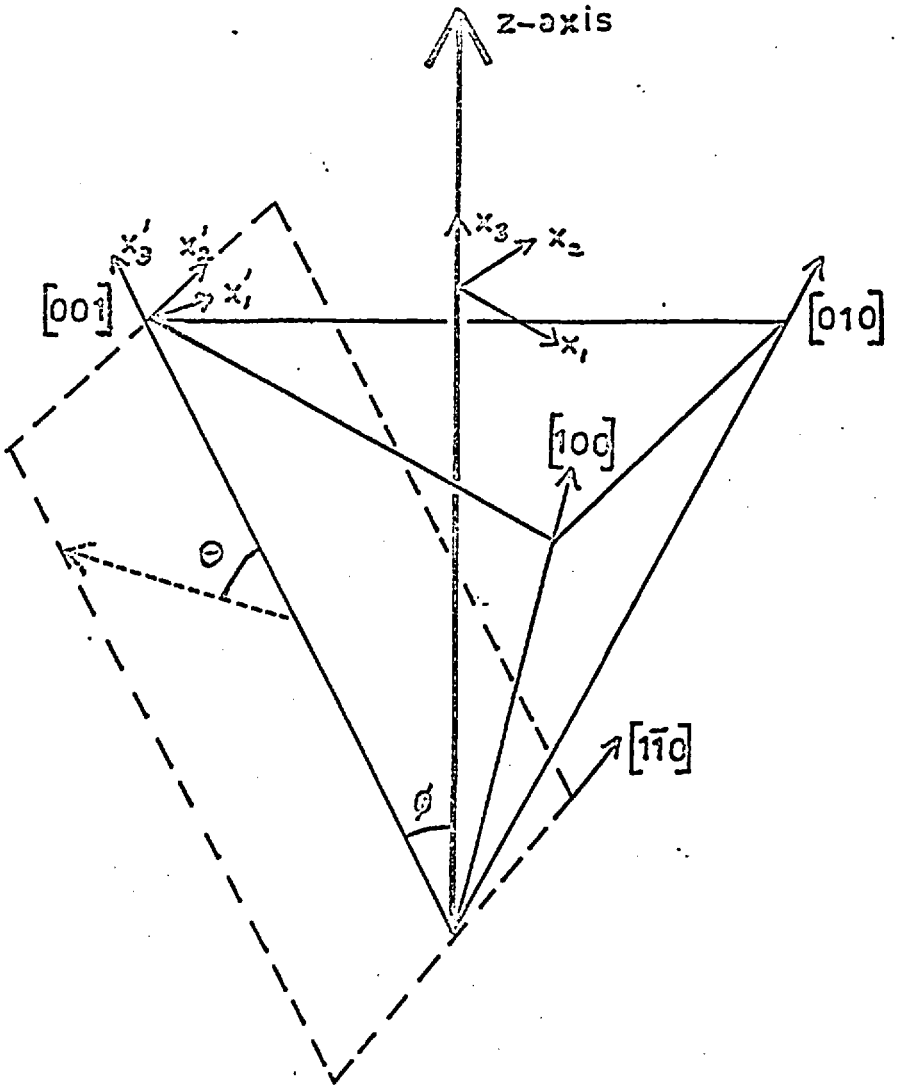


Figure 25. Rotating and fixed axes relative to the (110) plane.

θ is positive in the direction shown.

plane then the cosines would be

$$\beta_1 = -\sin\phi, \quad \beta_2 = 0, \quad \beta_3 = \cos\phi \tag{3.38}$$

However, the gauge is not in this position; it is on the plane at an angle $\theta = \Delta$, and its new direction cosines are given by

$$\beta_i' = \lambda_{ij}\beta_j \tag{3.39}$$

where λ_{ij} is the transformation matrix from crystallographic co-ordinates to co-ordinates on the (110) plane at $\theta = \Delta$. Hence

$$\begin{aligned}\beta_1' &= \lambda_{11}\beta_1 + \lambda_{13}\beta_3 \\ \beta_2' &= \lambda_{21}\beta_1 + \lambda_{23}\beta_3 \\ \beta_3' &= \lambda_{31}\beta_1 + \lambda_{33}\beta_3\end{aligned} \tag{3.40}$$

The transformation matrix must be obtained from geometrical considerations. A general matrix has been derived by Jeffreys and Jeffreys[67] considering successive rotations about one axis, then another and finally a third axis. Adapted to transform to a co-ordinate system rotated through an angle θ about the x_1-axis perpendicular to the (110) plane from crystallographic co-ordinates, it reads

$$\lambda_{ij} = \begin{bmatrix} \cos\theta + \cos^2\phi(1-\cos\theta) & -\sin\phi\sin\theta & \cos\phi\sin\phi(1-\cos\theta) \\ \sin\phi\sin\theta & \cos\theta & -\cos\phi\sin\theta \\ \cos\phi\sin\phi(1-\cos\theta) & \cos\phi\sin\theta & \cos\theta + \sin^2\phi(1-\cos\theta) \end{bmatrix} \tag{3.41}$$

Using this for $\theta = \Delta$ with equation (3.40)

$$\beta_1' = -\left\{\cos\Delta + \cos^2\phi(1-\cos\Delta)\right\}\sin\phi + \cos\phi\sin\phi(1-\cos\Delta)\cos\phi$$

Therefore $\beta_1' = -\cos\Delta \sin\phi$ (3.42)

Likewise $\beta_2' = -\sin\Delta$ (3.43)

and $\beta_3' = \cos\Delta \cos\phi$ (3.44)

In a similar manner the magnetic field components must be transformed from the fixed to the rotating axes. If α_i' are the direction cosines of the field $\underline{H}$ in the rotating co-ordinate system, then these also transform according to

$$\alpha_i' = \lambda_{ij}\beta_j \tag{3.45}$$

giving similar equations to equation (3.40). For each component

$$H_i = H\alpha_i' \tag{3.46}$$

Therefore $H_1 = H(\lambda_{11}\beta_1 + \lambda_{13}\beta_3)$

$$H_2 = H(\lambda_{21}\beta_1 + \lambda_{23}\beta_3)$$

$$H_3 = H(\lambda_{31}\beta_1 + \lambda_{33}\beta_3) \tag{3.47}$$

We can therefore use the same transformations as in equation (3.41) replacing θ for Δ i.e.

$$H_1 = -H\cos\theta\sin\phi$$

$$H_2 = -H\sin\theta$$

$$H_3 = H\cos\theta\cos\phi \tag{3.48}$$

Having transformed both strain measurement and field onto the (110) plane, the resultant strain E along the measurement direction can now be obtained from equation (3.37) since the values of E_{ij} in the $\bar{3}m$ group are known from equation (3.20).

$$E = -Q_{22}H_2(\beta_1')^2 - 2Q_{22}H_1\beta_1'\beta_2' - 2Q_{41}H_2\beta_1'\beta_3' + 2Q_{41}H_1\beta_2'\beta_3' + Q_{22}H_2(\beta_2')^2 \tag{3.49}$$

Replacing for H_1, H_2 and H_3 from equation (3.48) and for β_1', β_2' and β_3' from equations (3.42), (3.43) and (3.44),

$$\frac{E}{H} = Q_{22}(\cos^2\Delta \sin^2\phi - \sin^2\Delta)\sin\theta + 2Q_{22}\cos\Delta\sin\Delta\sin^2\phi\cos\theta - 2Q_{41}\cos^2\Delta\sin\phi\cos\phi\sin\theta + 2Q_{41}\sin\Delta\cos\Delta\cos\phi\sin\phi\cos\theta \qquad (3.50)$$

$$= \left\{Q_{22}(\cos^2\Delta\sin^2\phi - \sin^2\Delta) - (Q_{41}\cos^2\Delta\sin 2\phi)\right\}\sin\theta + \left\{(Q_{22}\sin^2\phi\sin 2\Delta) + (Q_{41}\sin\Delta\cos\Delta\sin 2\phi)\right\}\cos\theta \qquad (3.51)$$

Equation (3.51) gives the total strain E on the (110) plane at an angle Δ to the $[001]$ direction due to linear magnetostriction resulting from a field applied in the plane at an angle θ to the $[001]$ direction. It is therefore possible from this equation to predict the angular dependence of strain, measured at a fixed angle Δ, when the magnetic field is rotated in the (110) plane, and so by measuring this dependence experimentally it is a simple matter to calculate the value of the tensor components.

3.3.2. Optimum Position for Strain Measurement on (110) Plane

For greater strain accuracy, it would be desirable to measure at the particular angle Δ which would be expected to exhibit the maximum strain. For this, a maximum of equation (3.51) at constant θ needs to be determined. Equation (3.51) can be rewritten

$$\frac{E}{H} = \left\{Q_{22}\sin^2\phi\sin\theta - Q_{41}\sin 2\phi\sin\theta\right\}\cos^2\Delta - Q_{22}\sin\theta\sin^2\Delta + \left\{2Q_{22}\sin^2\phi + Q_{41}\sin 2\phi\right\}\cos\theta\sin\Delta\cos\Delta \qquad (3.52)$$

and so by differentiation

$$\frac{\partial(E/H)}{\partial \Delta} = -\left\{Q_{22} \sin^2 \phi \sin\theta - Q_{41} \sin 2\phi \sin\theta\right\} 2\cos\Delta \sin\Delta$$
$$- 2Q_{22} \sin\theta \cos\Delta \sin\Delta$$
$$+ \left\{(2Q_{22} \sin^2 \phi + Q_{41} \sin 2\phi) \cos\theta\right\} (\cos^2\Delta - \sin^2\Delta) \qquad (3.53)$$

$$= -\left\{Q_{22} (\sin^2 \phi + 1) \sin\theta - Q_{41} (\sin 2\phi \sin\theta)\right\} \sin 2\Delta$$
$$+ \left\{(2Q_{22} \sin^2 \phi + Q_{41} \sin 2\phi)\right\} \cos\theta \cos 2\Delta \qquad (3.54)$$

At a maximum or minimum value of Δ, equation (3.54) is zero, which gives the following relationship

$$\frac{\sin 2\Delta}{\cos 2\Delta} = \frac{(2Q_{22} \sin^2\phi + Q_{41} \sin 2\phi) \cos\theta}{\left\{Q_{22} (\sin^2 \phi + 1) - Q_{41} \sin 2\phi\right\} \sin\theta} \qquad (3.55)$$

i.e. $\tan 2\Delta = \text{constant} \times \cot\theta$ (3.56)

Equation (3.56) shows that there is no clearly defined strain maximum, independent of the angle of the applied field. There are however, apparent restrictions on the value of Δ, for if $\cot\theta$ is to have a value between ∞ and zero, then 2Δ must lie between 90° and zero, i.e. Δ must lie between 45° and zero. If $\Delta = 0$, then from equation (3.52) the maximum strain occurs at $\theta = 0$, but since at this angle the strain equation only contains sine terms it is impossible to evaluate both tensor coefficients from the strain angular dependence. The strain gauge can therefore be stuck on the (110) face of the hematite crystal at any angle between 0 and 45° to the [001] axis, although it is preferable not to measure at $\Delta = 0$ so that both tensor coefficients may be evaluated.

3.3.3. Form of Linear Magnetostriction on (111) Plane in Hematite

It may be noticed from section 3.1. that not all of the crystals used for magnetostriction purposes had cleaved (110) faces, for some had (111) faces. The previous calculation determining the form of the strain equation on the (110) plane must be repeated for the (111) plane. Fortunately one of the three Cartesian axes can coincide with the principal crystallographic axis, so that the (111) plane is also the $x_1 x_2$ plane, as shown in Figure 26. θ is the angle on the (111) plane between a particular vector and the x_2 axis, measured positive in the direction shown.

Suppose the measurement of strain is performed on this plane at an angle $\theta = \Delta$, then the direction cosines β_i of the gauge are

$$\beta_1 = \sin \Delta , \qquad \beta_2 = \cos \Delta , \qquad \beta_3 = 0 \tag{3.57}$$

The strain E in this direction is given by

$$E = E_{ij}\, \beta_i \beta_j \tag{3.58}$$

and values of E_{12}, E_{11} and E_{22} can be replaced from equation (3.20) producing

$$E = -2Q_{22}\, H_1\, \beta_1\, \beta_2 - Q_{22}\, H_2\, (\beta_1)^2 + Q_{22}\, H_2\, (\beta_2)^2 . \tag{3.59}$$

The components of the magnetic field applied in the plane are

$$H_1 = H \sin \theta, \qquad H_2 = H \cos \theta, \qquad H_3 = 0 \tag{3.60}$$

so that

$$\frac{E}{H} = Q_{22} \left\{ (\cos^2 \Delta - \sin^2 \Delta) \cos \theta - 2 \sin \Delta \cos \Delta \sin \theta \right\} \tag{3.61}$$

This permits evaluation of only one of the two tensor coeff-

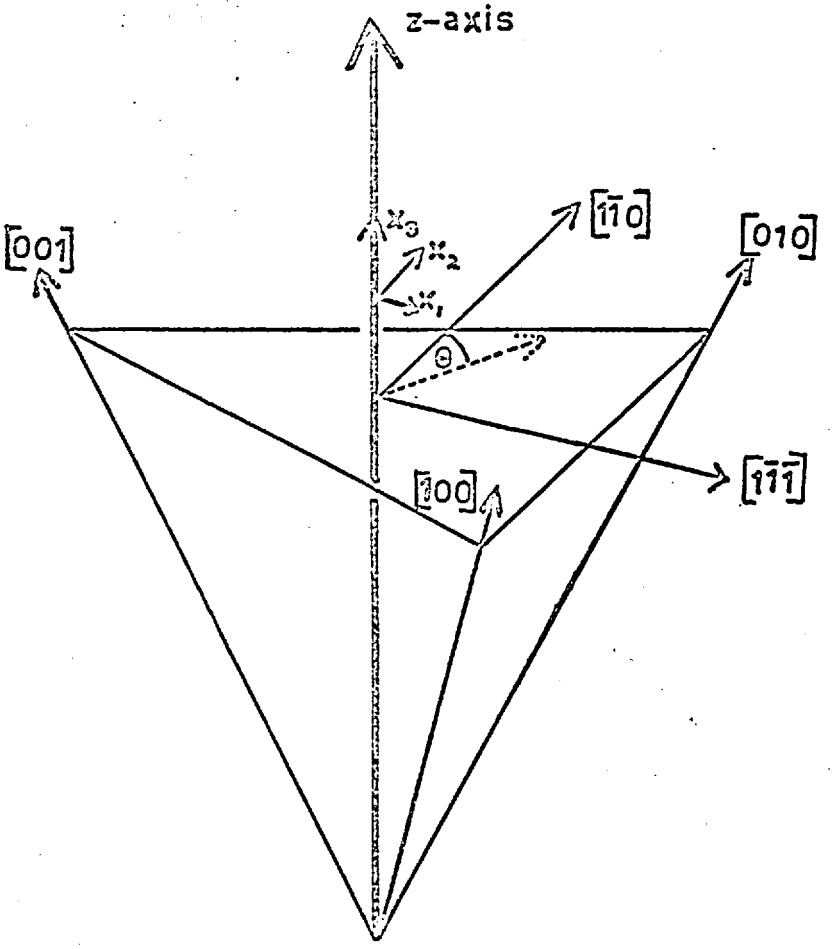


Figure 26. Rotating and fixed axes relative to the (111) plane. θ is positive in the direction shown.

icients from the angular dependence of the magnetostrictive strain on the (111) plane. If $\Delta = 0$ (i.e. the strain gauge lying along the $(1\bar{1}0)$ direction), the strain equation reduces to the very simple form

$$\frac{E}{H} = Q_{22} \cos\theta. \tag{3.62}$$

3.3.4. Optimum Position for Strain Measurement on (111) Plane

It is desirable to know where the strain is a maximum on the (111) plane. Taking equation (3.61) and differentiating it with respect to Δ,

$$\frac{\partial(E/H)}{\partial\Delta} = Q_{22}\left\{(-2\cos\Delta\sin\Delta - 2\cos\Delta\sin\Delta)\cos\theta - 2(-\sin^2\Delta + \cos^2\Delta)\sin\theta\right\} \tag{3.63}$$

$$= -Q_{22}\left\{2\sin 2\Delta\cos\theta + 2\cos 2\Delta\sin\theta\right\} \tag{3.64}$$

The differential is zero at positions of maximum and minimum strain; the angle at which this occurs is given by

$$\frac{\sin 2\Delta}{\cos 2\Delta} = -\frac{\sin\theta}{\cos\theta} \tag{3.65}$$

i.e. $$\tan 2\Delta = -\tan\theta \tag{3.66}$$

In a similar manner to the previous calculation concerning the (110) plane, equation (3.66) shows that there is no clearly defined strain maximum, independent of the angle of the applied field. There are restrictions on the value of Δ for if $\tan\theta$ is to have a value between zero and ∞, then Δ must have a value between zero and 45°. If Δ is taken as 45°, then from equation (3.61) the maximum strain of $-Q_{22}H$ occurs at $\theta = 90^\circ$; but if Δ is taken as zero, then the

maximum strain of Q_{22} H occurs at $\theta = 0$.

3.3.5. Form of 'Square Law' Magnetostriction on (110) Plane

The preceding sections have shown that an excellent way of experimentally determining the values of the linear magnetostriction tensor coefficients is to record the angular dependence of strain and then, by harmonic analysis, extract the coefficients of the sine and cosine terms. All the linear magnetostriction strain is characterised by first order terms in θ, and so it is interesting to see the type of angular dependence produced by the 'square law' magnetostriction.

Firstly both strain and magnetic field direction cosines are referred to the measurement orientation, for it is known from section 3.2.1. that the values of β_i and $H\alpha_i$ when related to axes on the (110) plane with x_3 rotated by angle θ from the $[\bar{0}0\bar{1}]$ axis, are as follows

$$\beta_1 = -\cos\Delta \sin\phi \tag{3.42}$$

$$\beta_2 = -\sin\Delta \tag{3.43}$$

$$\beta_3 = \cos\Delta \cos\phi \tag{3.44}$$

$$H_1 = -H\cos\theta\sin\phi$$

$$H_2 = -H\sin\theta$$

$$H_3 = H\cos\theta\cos\phi \tag{3.47}$$

Also from before, the strain measured by the gauge is given by

$$E = E_{ij}\,\beta_i\beta_j \tag{3.37}$$

Therefore

$$E = E_{11}(\beta_1)^2 + 2E_{12}\beta_1\beta_2 + 2E_{13}\beta_1\beta_3 + 2E_{23}\beta_2\beta_3 + E_{22}(\beta_2)^2 + E_{33}(\beta_3)^2 \qquad (3.67)$$

Replacing for the strain components from equation (3.27)

$$\begin{aligned} E = {} & \{(S_{11} + 2S_{66})\, H_1^2 + S_{12}\, H_2^2 + S_{13}\, H_3^2 - S_{25}\, H_1H_3\}(\beta_1)^2 \\ & + 2\beta_1\beta_2 \{S_{25}\, H_2H_3 + S_{66}\, H_1H_2\} + 2\beta_1\beta_3 \{-S_{52}\, H_1^2 + S_{52}\, H_2^2 \\ & + S_{44}\, H_1H_3\} + 2\beta_2\beta_3 \{S_{44}\, H_2H_3 + S_{52}\, H_1H_2\} \\ & + \{S_{31}\,(H_1^2 + H_2^2) + S_{33}\, H_3^2\}(\beta_3)^2 \\ & + \{S_{12}\, H_1^2 + (S_{12} + 2S_{66})\, H_2^2 + S_{13}\, H_3^2 + S_{25}\, H_1H_3\}(\beta_2)^2 \end{aligned} \qquad (3.68)$$

Equation (3.68) is already long and complicated, and the next step involving replacement of β_1, β_2 and β_3 and H_1, H_2 and H_3 will expand it further.

Fortunately these steps are not necessary to find the form of the angular dependence of the 'square law' magnetostriction if it is noted that every term in equation (3.68) involves the second power of the magnetic field components. From equation (3.47) it can be seen that each component depends on either sin θ or cos θ, so that it is obvious that terms involving the second power of the magnetic field components will depend on either $\sin^2\theta$, sin θ cos θ or $\cos^2\theta$. Applying this to equation (3.68), the 'square law' magnetostriction on the (110) plane must exhibit an angular dependence containing only terms even in θ; i.e. a constant, sin 2θ or cos 2θ.

Hence the harmonic analysis method of determining the linear magnetostriction tensor components also serves to isolate the higher order terms from the linear effect.

3.3.6. Form of 'Square Law' Susceptibility Term on (110) Plane

It has been seen in section 1.5.4. that a term which results in a non-linear antiferromagnetic susceptibility also provides an energy difference between antiferromagnetic domains related to each other by time inversion. The tensor coefficient C_{ijk} has a non-zero value in the group $\bar{3}m$, to which hematite belongs at low temperatures, so it is of use to determine its form in that group, and in particular its form on the (110) plane of hematite.

The non-linear susceptibility coefficient is a third rank axial c-tensor and so would appear to be represented by the same matrix as linear magnetostriction. Intrinsic symmetry arising as a result of the independence of the order of the magnetic field components in the energy expression $C_{ijk}H_iH_jH_k$ causes the following equality,

$$C_{ijk} = C_{jki} = C_{kji} \quad \text{etc.} \tag{3.69}$$

Considering the two tensor components Q_{22} and Q_{41}, of equation (3.18) we have, replacing C_{ijk} for Q_{ijk},

$$C_{41} = C_{231} = C_{321} = C_{123} = C_{63} \tag{3.70}$$

and $C_{63} = 0$, hence for this particular intrinsic symmetry situation $C_{41} = 0$, and the $\bar{3}m$ non-linear susceptibility matrix becomes

$$C_{ijk} = \begin{bmatrix} 0 & 0 & 0 & 0 & 0 & -C_{22} \\ -C_{22} & C_{22} & 0 & 0 & 0 & 0 \\ 0 & 0 & 0 & 0 & 0 & 0 \end{bmatrix} \qquad (3.71)$$

so that the free energy resulting from this term is

$$F = C_{ijk} H_i H_j H_k$$

$$= -3C_{22} H_1 H_1 H_2 + C_{22} H_2 H_2 H_2 \qquad (3.72)$$

If the magnetic field components are referred to the field H rotating through an angle θ about an axis perpendicular to the (110) plane, then the components are the same as those used in section 3.3.1. i.e.

$$H_1 = -H \cos\theta \sin\phi$$

$$H_2 = -H \sin\theta$$

$$H_3 = H \cos\theta \sin\phi \qquad (3.47)$$

The free energy arising from the non-linear susceptibility term on the (110) plane is therefore

$$F = 3C_{22} H^3 \cos^2\theta \sin\theta \sin^2\phi - C_{22} H^3 \sin^3\theta. \qquad (3.73)$$

Equation (3.73) obviously has the value of zero at $\theta = 0$ and the value $-C_{22} H^3$ at $\theta = 90^\circ$. This energy arises from a time anti-symmetric effect and so reverses sign between 180° antiferromagnetic domain types. The maximum energy difference between opposite anti-ferromagnetic domains is thus $2C_{22} H^3$ at $\theta = 90^\circ$.

CHAPTER IV

DISCUSSION OF RESULTS

4.1. MAGNETOSTRICTION AT HIGH TEMPERATURES

4.1.1. Synthetic Crystal

The magnetostriction of an initially demagnetised synthetic crystal of hematite was measured at room temperature as a function of applied magnetic field. Figure 27(a) shows the field dependence at four separate field orientations on the (110) plane; the 0^{o} curve corresponds to the field applied along the $[00\bar{1}]$ direction. On this and the following curves, expansive strain is shown as positive. The strain is typically that exhibited by a parasitic ferromagnetic material, for it shows no difference between positive and negative magnetic field directions. This would be expected, because the antiferromagnetic domains should rotate with the ferromagnetic domains to follow the applied field direction as discussed in section 1.5.5.

In low fields the strain varies rapidly with field as a result of rotation of ferromagnetic domains from the crystallographic easy direction, but after this process is completed a saturation of strain occurs. This is evident at a field of about 3500 oersteds along the $[00\bar{1}]$ axis and at about 2300 oersteds perpendicular to it. This latter direction lies within the (111) basal plane of the unit cell and so it would be expected that at room temperature,

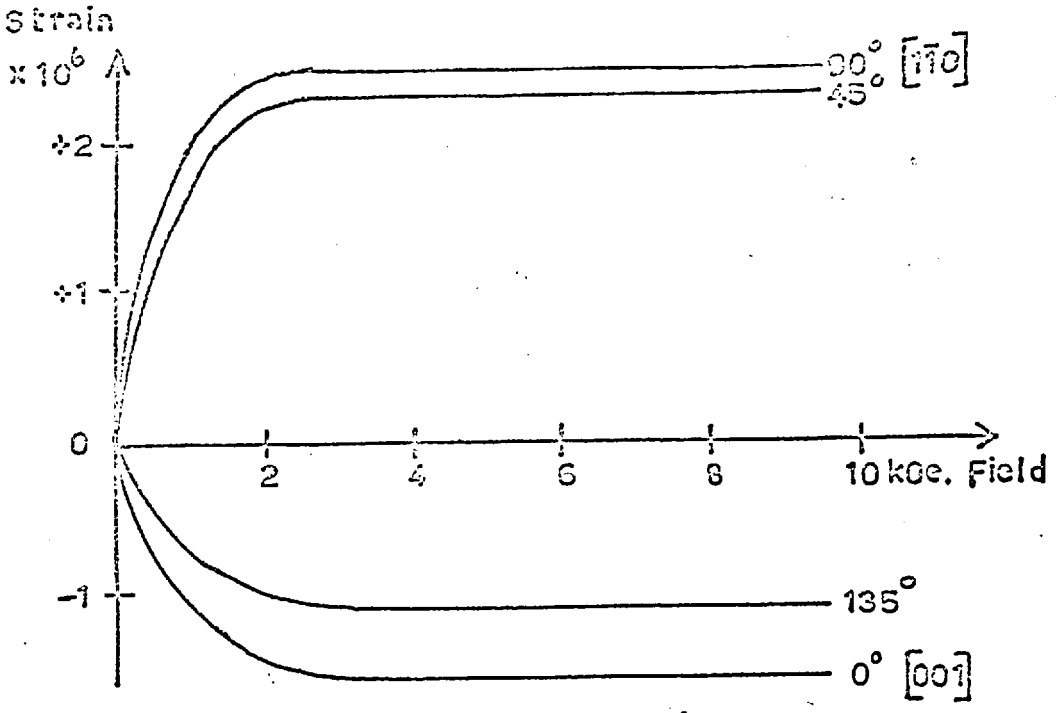


Figure 27(a). Strain in the synthetic crystal produced by a field applied at various angles to the [001] direction.

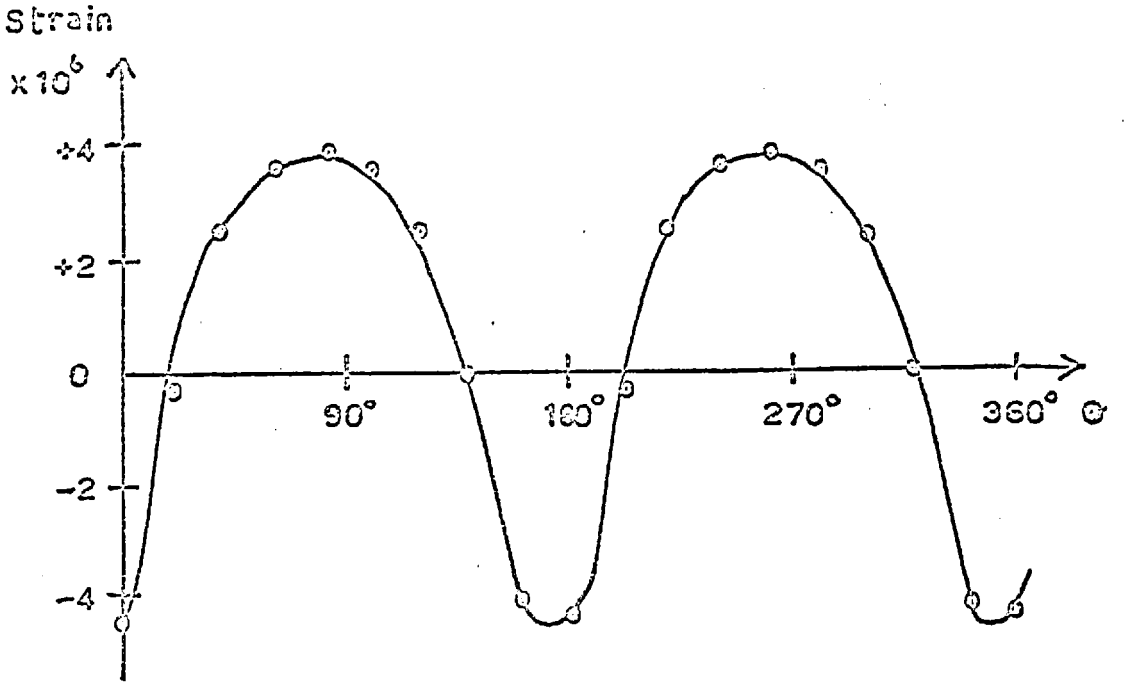


Figure 27(b). Strain in the synthetic crystal produced by a field of 4500 oersteds rotating on the (110) plane. Curve corresponds to equation (4.1).

where the spins lie in this plane, saturation would occur at a lower field than at any other angle to the plane. The high field saturation strain is only very slightly dependent on the magnitude of the applied field, which would indicate that in this crystal the true linear magnetostriction strain ~~in the 2/m group~~ which is exhibited as a forced magnetostriction, has a value less than 0.5×10^{-7} at 7000 oersteds.

The strain along the gauge direction caused by a field of 4500 oersteds rotating in the (110) plane is shown in Figure 27(b), the zero of angle corresponding to the [001] direction. Although the maxima and minima of strain occur for fields at 0° and 90° respectively, corresponding to the crystallographic directions [001] and [1$\bar{1}$0], the curve is by no means a simple 2θ function. Harmonic analysis of the experimental points showed them to be best represented by the function

$$\frac{\delta l}{l} = + 0.86 \times 10^{-6} - 3.91 \times 10^{-6} \cos (2\theta + 18^{\circ}) - 1.35 \times 10^{-6} \cos (4\theta + 57^{\circ}\ 12') \qquad (4.1)$$

counting expansive strain as positive. Equation (4.1) is unfortunately not of fundamental significance as total strain is plotted in Figure 27(b), and this is composed of components due to both ferromagnetic domain rotation and a linear effect in a reversible domain system.

4.1.2. Annealed Synthetic Crystal

After a complete set of high and low temperature measurements

were made on the synthetic crystal, it was removed from the experimental apparatus and thermally annealed in oxygen to remove strains and lattice dislocations, and possibly to improve the stoichiometry. After the magnetic remanence had been measured and the crystal returned to the apparatus with the strain gauge repositioned exactly, the room temperature magnetostriction was measured.

The resultant field dependences for four field directions on the (110) plane are shown in Figure 28(a) with expansive strain shown as positive. It is very interesting to compare Figure 28(a) with Figure 27(a), which is the corresponding diagram for the unannealed crystal. It is immediately obvious that the magnitudes of most of the saturation strains have increased radically. The strain due to a field along the $[001]$ axis has increased to 1.7 times its previous value, the strain due to a field along the $[1\bar{1}0]$ axis has increased to 1.9 times the previous value, whilst with the field at 45° to the $[001]$ axis, a 1.55 times increase in strain is evident. In addition the high field linear magnetostriction coefficients ~~in the 2/m group~~ must have increased appreciably so as to produce a measurable linear term. The value of this term along the $[001]$ axis is -4.6×10^{-11} per oersted, and its value at both directions at $\pm 45^{\circ}$ to the $[001]$ axis is $+6.3 \times 10^{-11}$ per oersted. Along the $[1\bar{1}0]$ axis the value of the linear term is much smaller and is certainly less than 1×10^{-11} per oersted.

It is of interest to note that in the synthetic crystal before

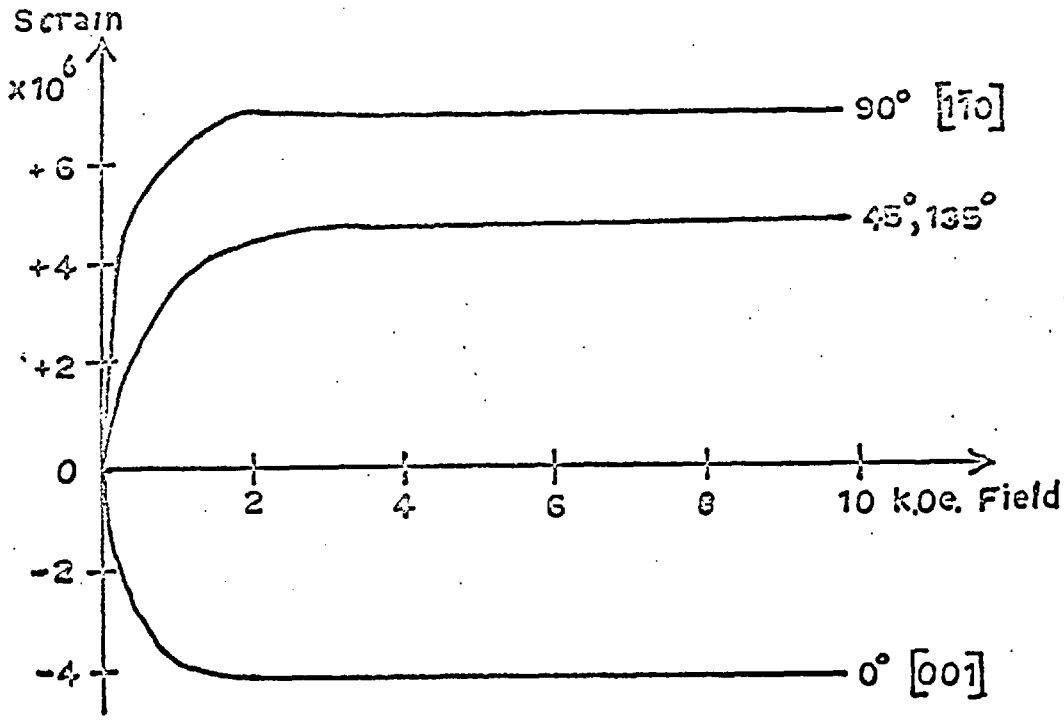


Figure 28(a). Strain in the annealed synthetic crystal produced by a field applied at various angles to the [001] direction.

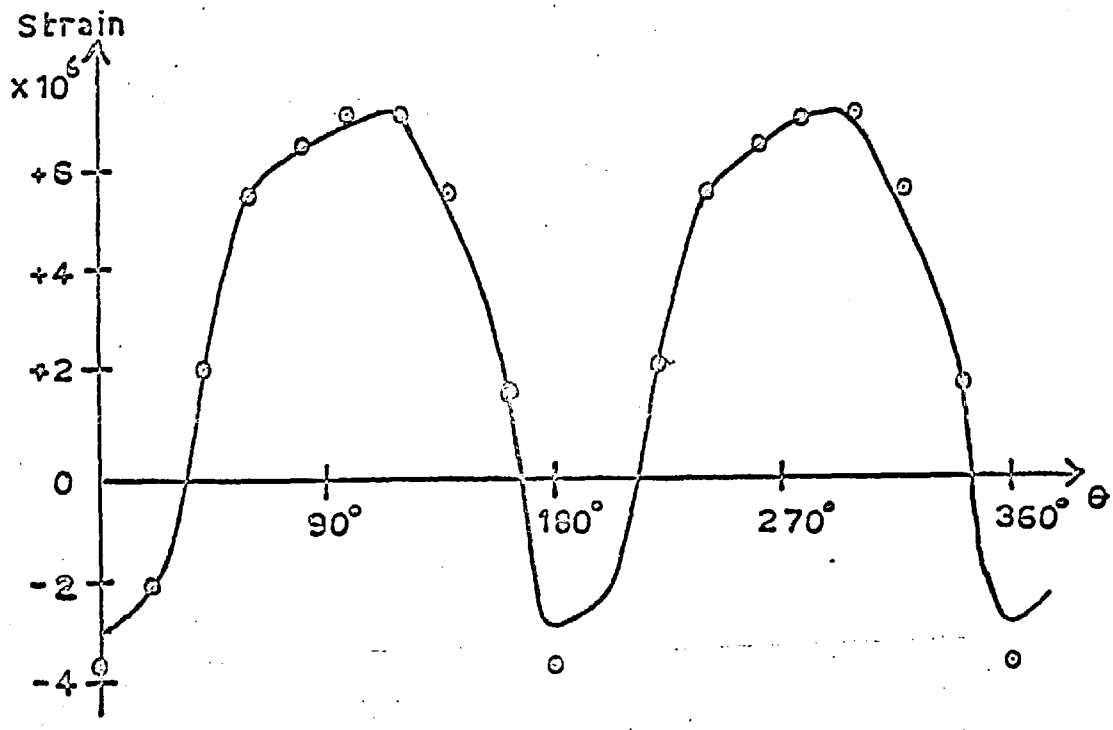


Figure 28(b). Strain in the annealed synthetic crystal produced by a field of 4500 oersteds rotating on the (110) plane. Curve corresponds to equation (4.2).

annealing, a magnetic field applied at 135° to the [001] direction produced a contraction, but after annealing the same field produced an expansion. This is seen by reference to Figure 28(b) which shows the strain along the gauge direction resulting from a field of 4500 oersteds rotating in the (110) plane. The curve has a slightly different shape from that of Figure 27(b), for the peak of contractive strain is sharper and that of expansive strain is broader, and as a result of this relatively slight change in shape of the angular dependence curve, the previous contraction at the 135° position has become an expansion. This change in shape is probably caused by a change in the magnetocrystalline anisotropy energy resulting from the removal of inbuilt strains.

The total amplitude of the strain variation has only increased from 8.3×10^{-6} before annealing to 11×10^{-6} after annealing (i.e. about 1.3 times the former value), and so the larger increase in strain observable from the field dependence curves must be attributable to the change in shape of the angular variation curve. Harmonic analysis of the experimental points of Figure 28(b) showed it to be best represented by the function

$$\frac{\delta l}{l} = + 3.35 \times 10^{-6} - 5.1 \times 10^{-6} \cos (2\theta + 2^{\circ}\ 30') + 1.63 \times 10^{-6} \cos (4\theta + 18^{\circ}) \qquad (4.2)$$

which is not very similar to equation (4.1) even though the actual curves are almost identical in shape.

4.1.3. Elba Crystal

In this specimen, the most pure natural crystal investigated, the magnetostrictive strain was measured on the (110) face along the $[\bar{1}11]$ direction, which makes an angle of 135° with the [001] direction. The observed strain would be expected to show some similarities to the strain existing at 10° to the [001] axis, although not being identical to it.

The strain resulting from magnetic fields applied at various orientations in the (110) plane are shown in Figure 29(a). None of these curves show complete saturation of strain, so it must be assumed that domain rotation in a room temperature Elba crystal still proceeds in fields up to 9000 oersteds. This is quite remarkable since domain saturation was shown by previous measurements of the synthetic crystal to be completed in fields less than 3000 oersteds applied at any orientation in the same plane. In the ferromagnetic state it would be expected that domain rotation would be impeded by all of the many defects and dislocations which are exhibited by most natural crystals. The actual values of the magnetostrictive strains are considerably less than those produced in the synthetic crystal, but this could possibly be solely due to the strain gauge at 135° to the [001] axis only experiencing a small resolved component of the strains. There is considerable difficulty in calculating the value of this resolved component due to the presence of eight non-zero tensor components representing linear magnetostriction in the

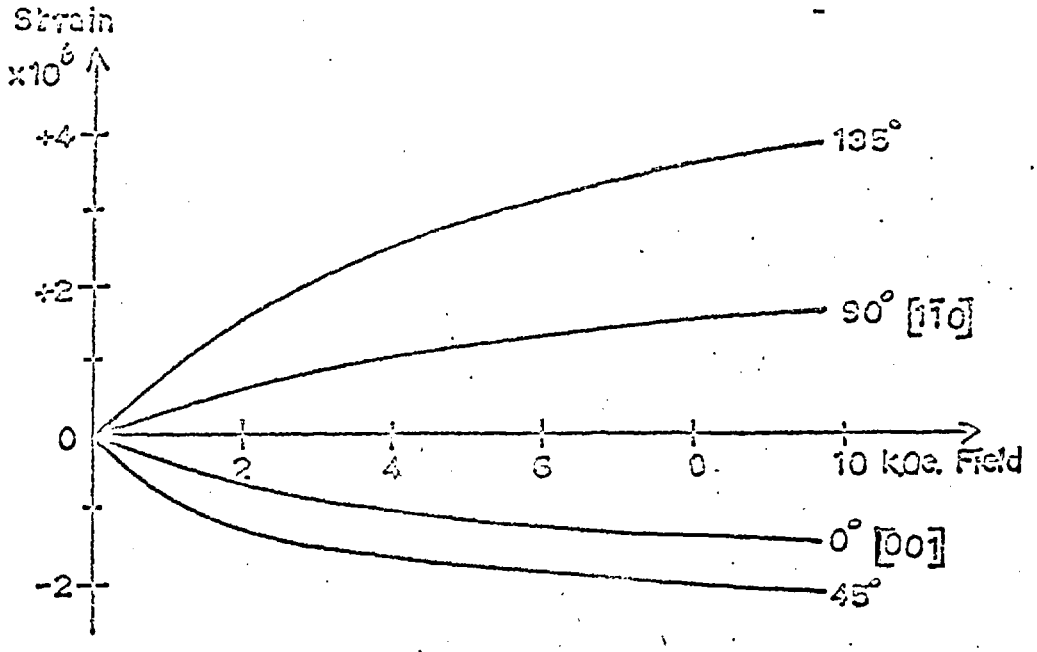


Figure 29(a). Strain in the Elba crystal produced by a field applied at various angles to the [001] direction.

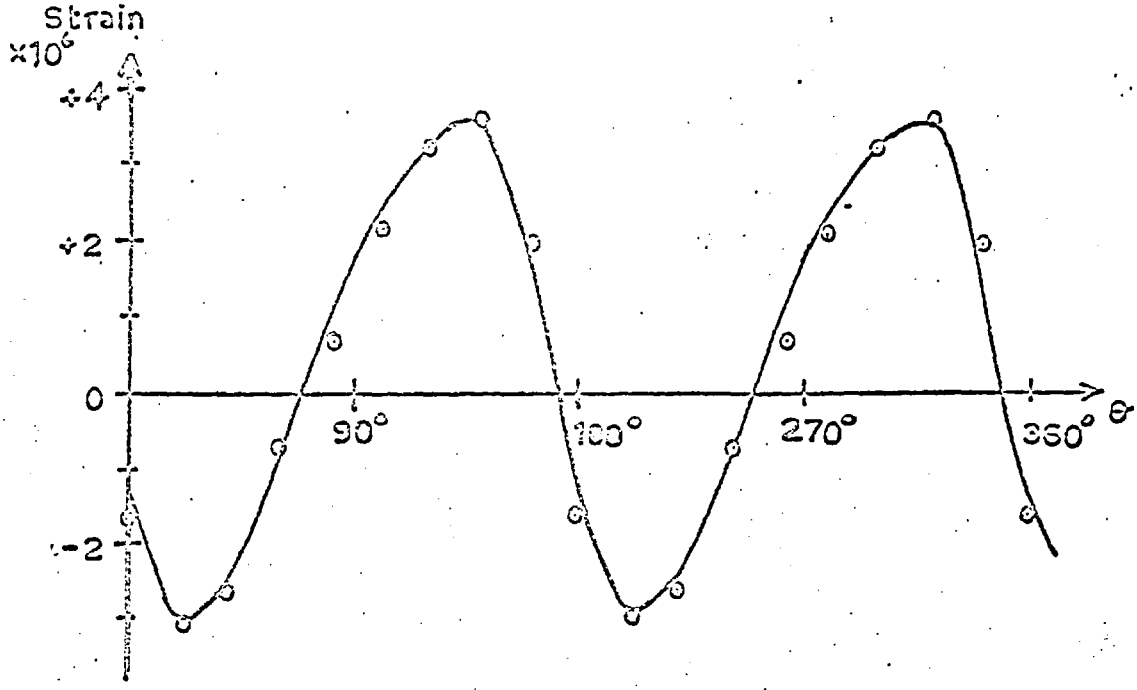


Figure 29(b). Strain in the Elba crystal produced by a field of 7500 oersteds rotating on the (110) plane. Curve corresponds to equation (4.3).

2/m magnetic group.

The strain existing at 135° to the [001] axis when a magnetic field of 7500 oersteds was rotated in the (110) plane is shown in Figure 29(b). The dependence upon angle appears quite different from that of the synthetic crystal, for increased rotational hysteresis of the internal ferromagnetic domain structure of the material causes the curve to take on the appearance of a saw-tooth function. In addition the maxima and minima of strain occur for fields at angles of 20°, 140° and 200° to the [001] axis, which is not in accordance with theory because the separation of the first pair of peaks is 120° and the separation of the second pair is 60°, whereas according to the perpendicular 2-fold symmetry axes on the (110) plane, all peaks should be 90° apart. This behaviour has previously been met in measurements of room temperature magnetostriction in hematite by Urquhart and Goldman[35], and is also associated with a large rotational hysteresis which is superimposed on the four-fold symmetry of the (110) plane.

A harmonic analysis of the curve shows it to be represented by the equation

$$\frac{\delta l}{l} = -0.46 \times 10^{-6} + 3.05 \times 10^{-6} \cos(2\theta - 67^\circ\ 20') + 0.67 \times 10^{-6} \cos(4\theta - 53^\circ\ 30') + 0.15 \times 10^{-6} \cos(6\theta - 38^\circ\ 10') \qquad (4.3)$$

which is closer to a true 2θ variation than in previously investigated crystals. This is probably only fortuitous and does not reflect the quality of the crystal, since as mentioned in section

4.1.1., the total strain is composed of components resulting from both ferromagnetic domain rotation and a linear effect in a reversible domain system (i.e. forced magnetostriction).

4.1.4. Arizona Crystal

Strain in this crystal was measured in the $[1\bar{1}0]$ direction lying in the (111) basal plane of the unit cell. This is a convenient axis to use for it is the only direction which is common to both the (111) and (110) planes. The strains (with expansion shown positively) resulting from magnetic fields applied at various orientations to the $[1\bar{1}0]$ axis (and also at the same angle to the strain gauge) are shown in Figure 30(a). These curves for the basal plane are quite different from those considered previously, for although both of them show a saturation effect, a low field peak of strain is in evidence in these (111) plane measurements. This bears a resemblance to the peak existing in the low field magnetostriction of ferromagnetic materials and this is explicable[47] in terms of the strains incurred by domain wall displacements and rotations. The reason that the shape of the strain curve resulting from these processes is different on the (111) plane from (110) plane is that on the latter only strains of one sign are caused by domain reorientation, whereas on the (111) plane strains of both signs are produced at different field strengths.

Saturation of strain occurs at approximately 5000 oersteds

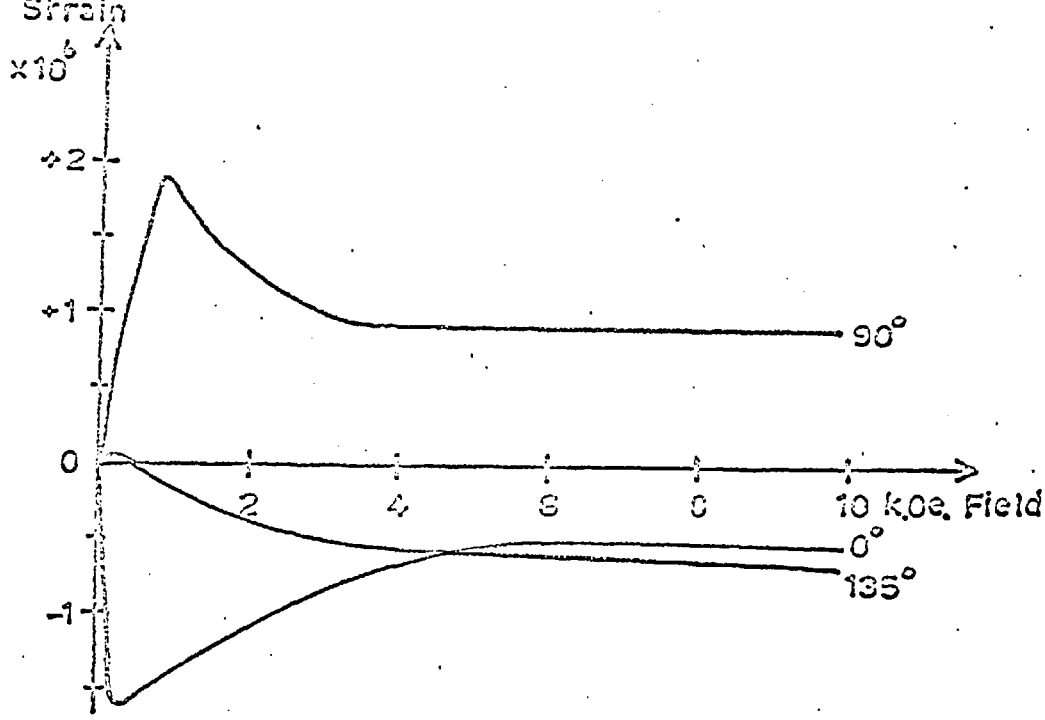


Figure 30(a). Strain in the Arizona crystal produced by a field applied at various angles to the $[1\bar{1}0]$ direction.

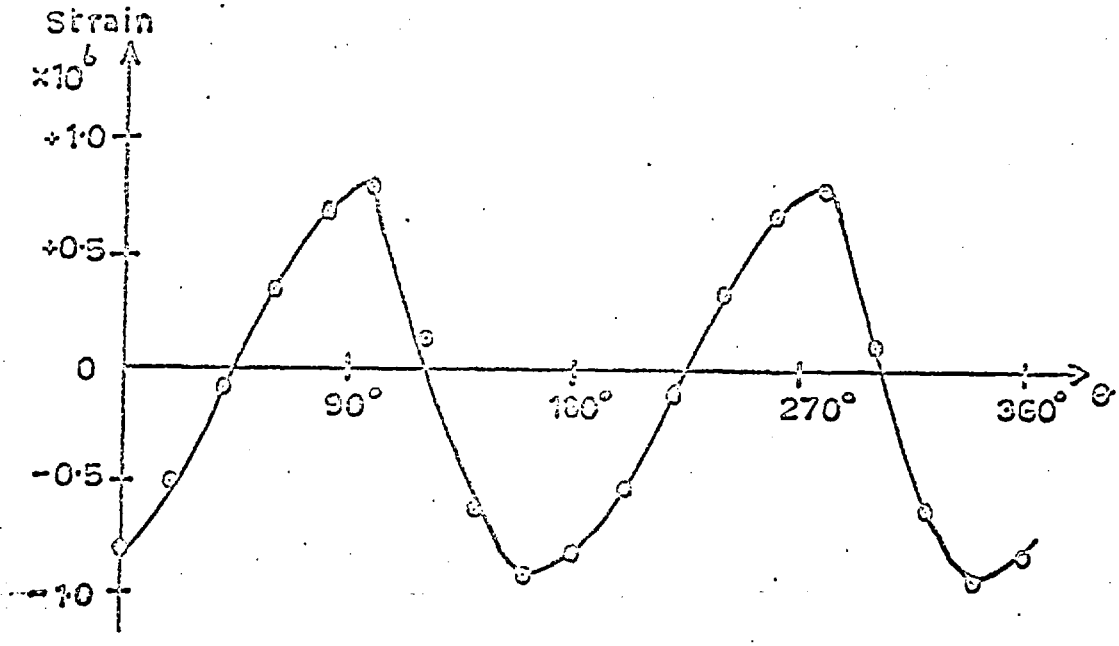


Figure 30(b). Strain in the Arizona crystal produced by a field of 4500 oersteds rotating on the (111) plane. Curve corresponds to equation (4.4).

with the field applied at any angle, but the process is quite gradual particularly when field and gauge are parallel. The saturation effect is seen to combine with a relatively large linear magnetostriction strain. The value of the linear term with gauge and field parallel is $+ 4.5 \times 10^{-11}$ oersted^{-1} and when the field is applied at 135° to the gauge the linear term is $- 2.2 \times 10^{-11}$ per oersted, and at the remaining two angles it is too small to measure with any accuracy.

The strain existing along the $[1\bar{1}0]$ axis when a magnetic field of 4500 oersteds was rotated in the (111) plane is shown in Figure 30(b). A 6θ component is not immediately visible, for even though the basal plane has a six-fold anisotropy it is very weak and would certainly be completely saturated by a field of 4500 oersteds applied at any orientation in this plane. In this relatively high field the (111) plane behaves isotropically and so the predominate shape of Figure 30(b) is a 2θ variation. A harmonic analysis of the curve produces the strain equation

$$\frac{\delta l}{l} = + 10^{-7} + 8.5 \times 10^{-7} \cos (2\theta + 15^{\circ}) - 1.6 \times 10^{-7} \cos (4\theta - 34^{\circ}\ 36') \qquad (4.4)$$

which shows that there is principally a $\cos 2\theta$ variation. The strain amplitude of the angular dependence of field curve is very considerably smaller for the same field than for any other crystal examined so far.

4.1.5. St. Gothard Crystal

The strain existing on the (111) plane of this crystal was measured parallel to the $[1\bar{1}1]$ axis, which is perpendicular to the strain measurement direction in the Arizona crystal. The strains resulting from magnetic fields applied at various orientations to this axis (and also at the same angle to the strain gauge) are shown in Figure 31(a). This is quite different from Figure 30(a) which shows basal plane curves for a material of much higher chemical and magnetic purity. The sign of the strain resulting from a field is the same as the previous crystal, but the St. Gothard curves rise gradually to saturation and do not show a strain peak at low fields. At room temperature these crystals are highly ferromagnetic and this could possibly be the reason for complete suppression of the high initial strains. The ferromagnetic properties appear to predominate, for there is no evidence of any linear magnetostriction resulting from the field applied at any orientation in the (111) plane.

The strain existing along the $[1\bar{1}1]$ axis when a magnetic field of 7500 oersteds was rotated in the (111) plane, which is shown in Figure 31(b), provided further evidence as to the ferromagnetic nature of this crystal. The curve is almost exactly represented by the equation

$$\frac{\delta l}{l} = -1.75 \times 10^{-6} \cos 2\theta \qquad (4.5)$$

which is the form theoretically expected from a purely ferro-

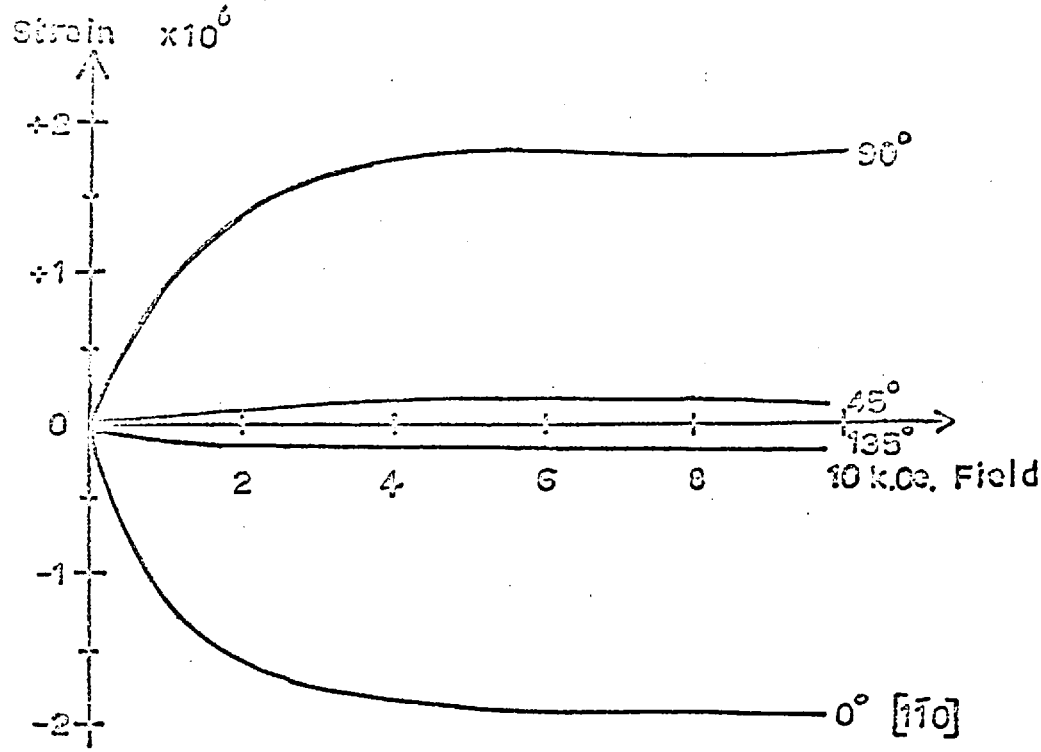


Figure 31(a). Strain in the St. Gothard crystal produced by a field applied at various angles to the [1$\bar{1}$0] direction.

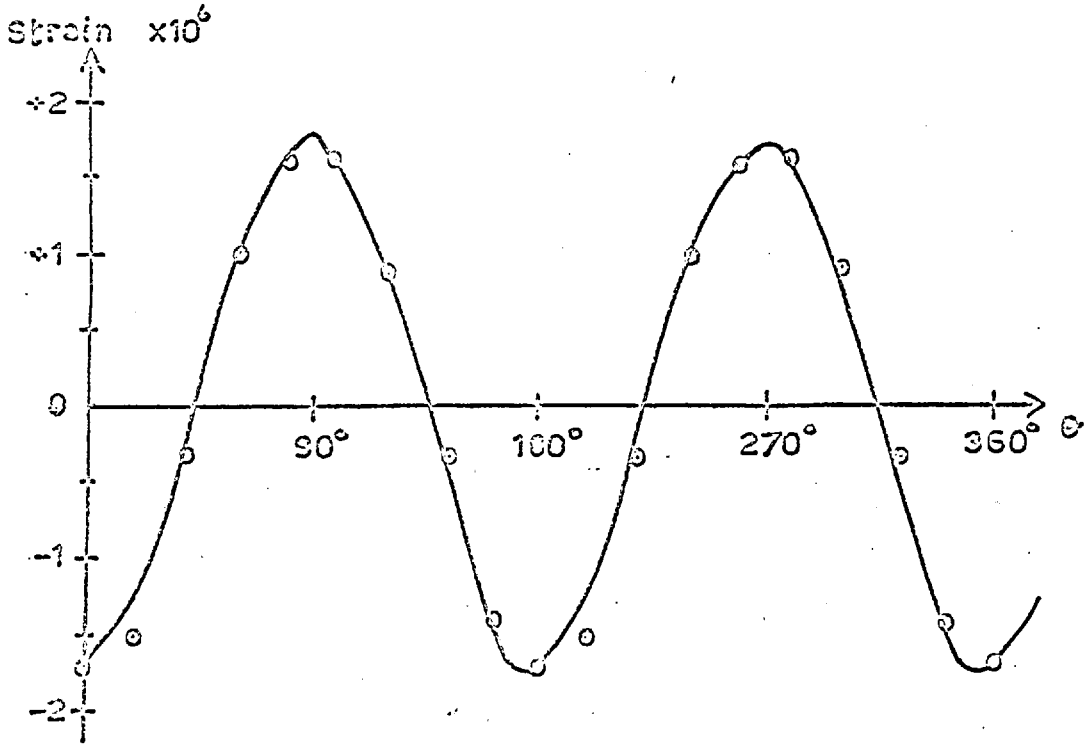


Figure 31(b). Strain in the St. Gothard crystal produced by a field of 7500 oersteds rotating on the (111) plane. Curve corresponds to equation (4.5).

magnetic type of 'square law' magnetostriction. There is no constant term in equation (4.5) which means that the strain resulting from a field applied perpendicular to the strain gauge is of the same magnitude but opposite in sign to the strain existing when field and gauge are parallel.

4.1.6. Polycrystalline Specimens

The magnetostrictive strain in pressed powder samples composed of both commercial grade and high purity powder was measured parallel to the applied field direction. Both curves showed a typical ferromagnetic saturation effect (see Figure 32(a)). The strain amplitude is considerably less than any single crystal value but this is obviously a result of absorption of a greater part of the strain by the epoxy resin binding material. Saturation of magnetostriction occurs at about 4 kilo-oersteds in the commercial grade powder, but at about 7 kilo-oersteds in the high purity material. The latter is rather a high field but Chevallier and Mathieus[34] have shown that particles below 10 microns in diameter do not have identical magnetic properties to bulk hematite, and it is probable that the particle size of the high purity material was less than this value. Magnetisation of particles of this size is always difficult because of the absence of domain walls. In both polycrystalline specimens no linear effect occurring either with or without domain reversal was observable.

Nothing could be gained in the experimental results by obtaining

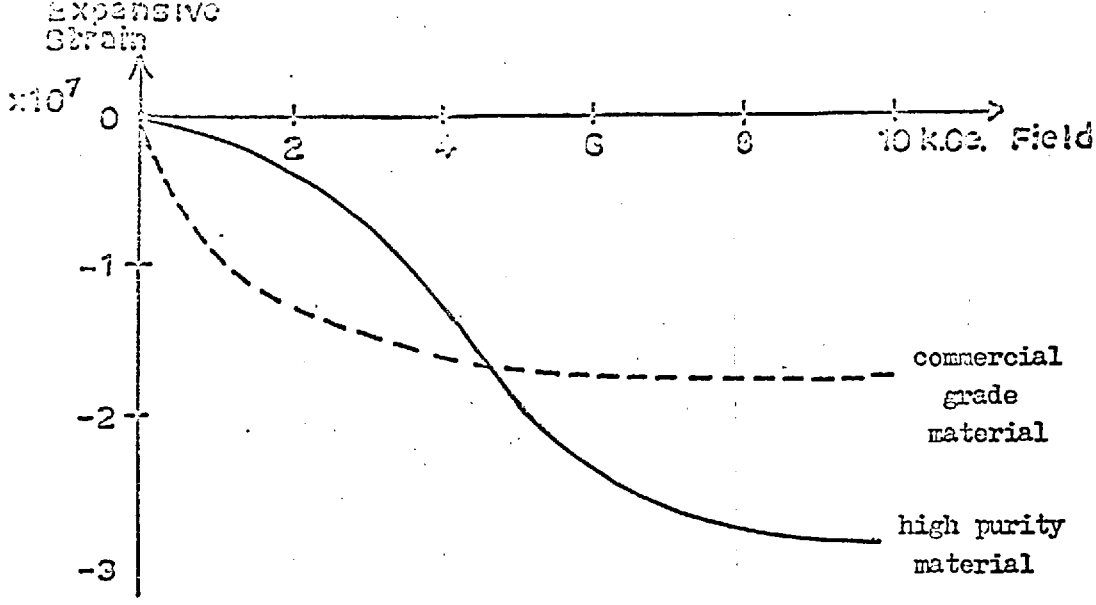


Figure 32(a). Strain in the polycrystalline samples at +23°C. produced by a field applied parallel to the gauge.

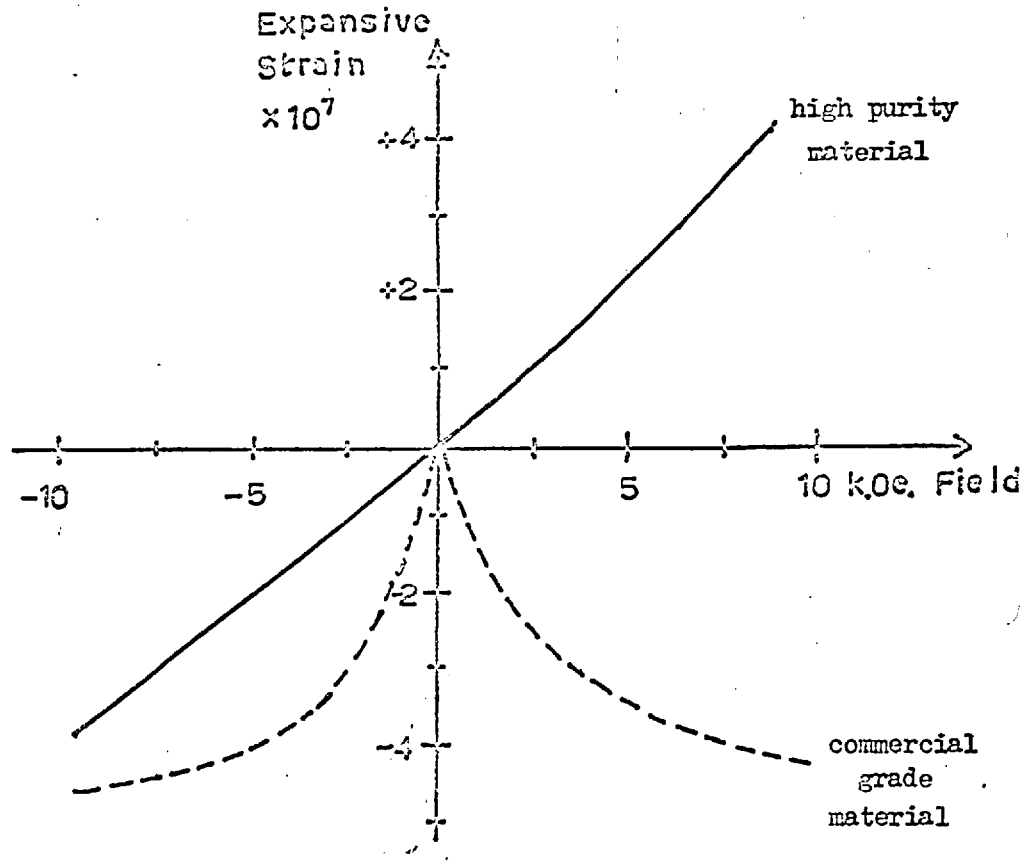


Figure 32(b). Strain in the polycrystalline samples at -196°C. produced by a field applied parallel to the gauge.

the field dependence at other angles or the strain resulting from a rotating field, since the polycrystalline material is also isotropic and the angular variation would result solely from the geometrical dependence of the components of strain.

4.2. MAGNETOSTRICTION AT LOW TEMPERATURES

4.2.1. Synthetic Crystal

The field dependence of magnetostrictive strain resulting from fields applied along the [001] and [1$\bar{1}$0] directions was determined in the synthetic crystal before and after the annealing process. The strains along the [1$\bar{1}$0] direction at -78° C and at -196° C in the unannealed crystal are shown in Figure 33. The measurements were performed after the crystal had been subjected to optimum magnetic annealing conditions (which will be discussed later). It is important to note that the annealing was in the positive field direction, and in this field direction the strain was almost completely linear and temperature independent. This part of the curve exhibits linear magnetostriction in a single domain crystal, the domain previously being located favourably to the measurement field by means of the annealing field. The linear coefficient at both temperatures was approximately 11 x 10^{-11} per oersted.

When the measurement field was applied in the opposite direction to the annealing field it produced an unexpected effect. At very low fields a contraction took place as expected, but when a

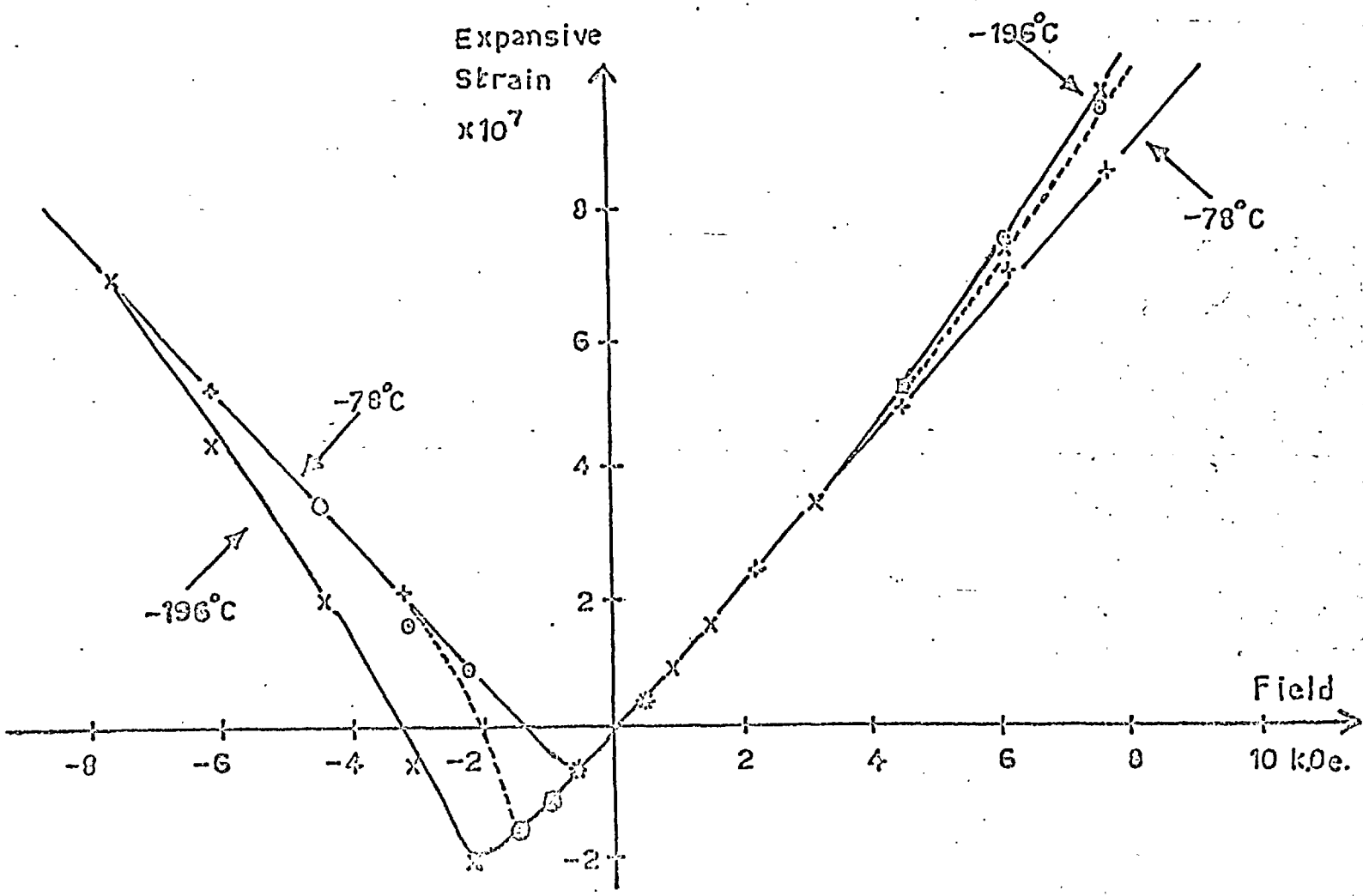


Figure 33. Magnetostrictive strain along the [1$\bar{1}$0] direction plotted against field in the synthetic crystal at -196° C (shown as x) and -78° C (shown as +) before annealing, and at -196° C (shown as o and broken curve) after annealing.

certain negative field value was exceeded, the contraction no longer increased and immediately started to decrease. High negative fields produced a roughly linear strain increase, but the linear magnetostriction coefficient appeared to have reversed.

These observations are explicable if it is assumed that the measuring field in the opposite direction to the annealing field caused a reversal of the antiferromagnetic domain direction. This process came about gradually as various crystallographic impurities and imperfections impeded the reversal and as a result the strain reversal showed this process as smoothly dependent upon magnetic field. In this direction the high field strain did not manifest itself as an exactly linear function until all of the material had reversed its domain state. For example, at -196° C and 3200 oersteds the strains due to each linear term from the opposite domains were equal, so that there was no resultant strain at that field. The onset of domain reversal can be seen from Figure 33 to be temperature dependent, since at -78° C it occurred at 800 oersteds but at -196° C it required 2200 oersteds to effect a reversal.

The magnetostrictive strain parallel to the $[00\bar{1}]$ axis, being perpendicular to the previously considered direction, was very small, for although it varied linearly with field it only rose to a value of 1.5×10^{-7} in a field of 7 kilo-oersteds. The strain did not show any evidence of domain reversal with the field applied in this direction.

4.2.2. Annealed Synthetic Crystal

The strain existing at 10° to the [001] axis of this crystal at liquid nitrogen temperature with the magnetic field applied along the [1$\bar{1}$0] axis, is shown as the broken curve of Figure 33. It will be noticed that after thermal annealing the domain reversal is more acute and occurs over a much smaller range of fields than in the natural state. The domain reversal threshold field, i.e. the field required to first start the domain moving, is now 1600 oersteds which is considerably less than the field of 2300 oersteds needed before annealing, so a very rough estimate gives a threshold field reduction of 30% resulting from annealing. Annealing has also caused the reversal to be substantially complete at about 2000 oersteds instead of at least 3000 oersteds as previously.

All of these facts are indicative of the thermal annealing, which it is already known reduces the thermal remanence, also reducing the number of antiferromagnetic domain pinning centres and also reducing the energy of each centre. This effect, which results in the easier passage of a domain reversal wall through the material, is probably caused by a reduction in the lattice imperfections and internal strains, all of which would constitute an impedence to the progression of a spin reversal wave.

The overall shape of the broken curve of Figure 33 for the annealed specimen is really just the same as the solid curves for the unannealed material. The linear portion, which corresponds to

measurements performed in a favourable direction of domain orientation, has a gradient of 11.5×10^{-11} per oersted for the annealed crystal.

When looking for the true 'square law' magnetostriction it is necessary to examine the field dependence measured in the same direction as the annealing field so as to eliminate domain reversal effects. Within experimental error, which is $\pm 0.1 \times 10^{-7}$ on each strain point, there was no low temperature 'square law' magnetostriction at -78° C in the unannealed crystal. The annealed crystal at -196° C exhibited a non-linear strain of $+ 1.2 \times 10^{-7}$ at 8000 oersteds, which would correspond to a 'square law' coefficient of approximately 2×10^{-15} per $(\text{oersted})^2$.

4.2.3. Elba Crystal

The maximum strain as measured along the gauge direction on the (110) plane of the Elba crystal at liquid nitrogen temperature was produced by a field applied perpendicular to the gauge. With annealing in the same direction as previously, the field dependence curve, which is reproduced in Figure 34, is not vastly different from that shown in Figure 33 for a crystal of higher purity. Domain reversal is still in evidence but its onset is not visible until at least 3000 oersteds have been applied in the direction necessary to reverse the domain. Associated with this higher threshold field, there is a marked reluctance of the unfavourably oriented domain to

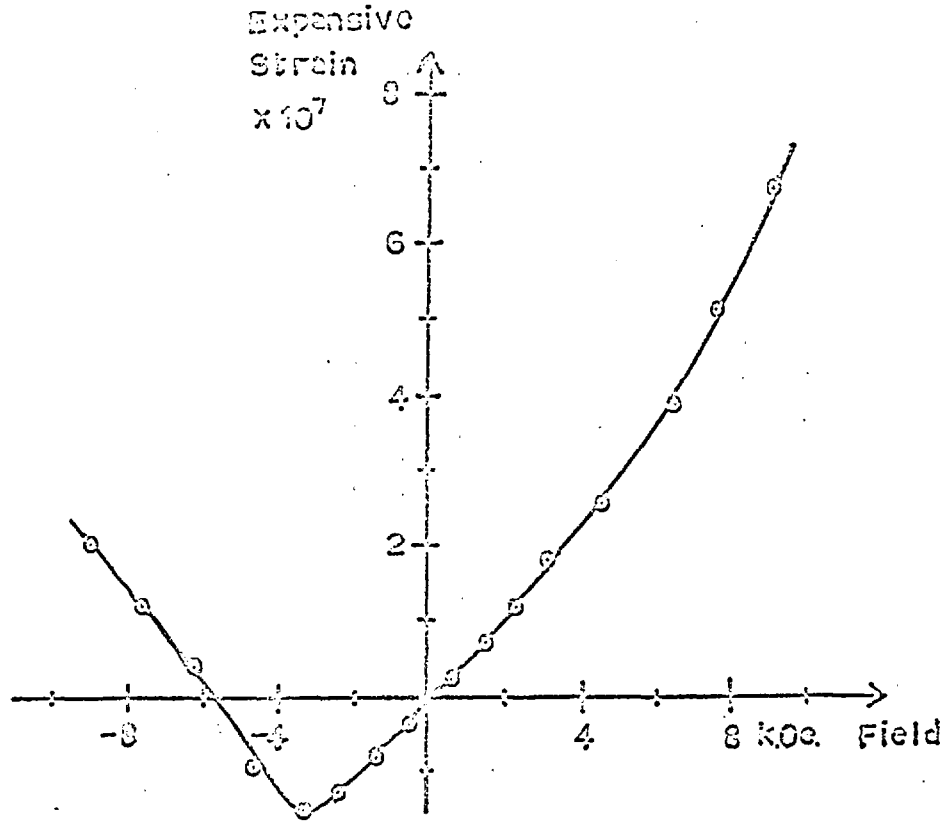


Figure 34. Strain in the Elba crystal produced by a field applied along the $[1\bar{1}0]$ direction at -196°C.

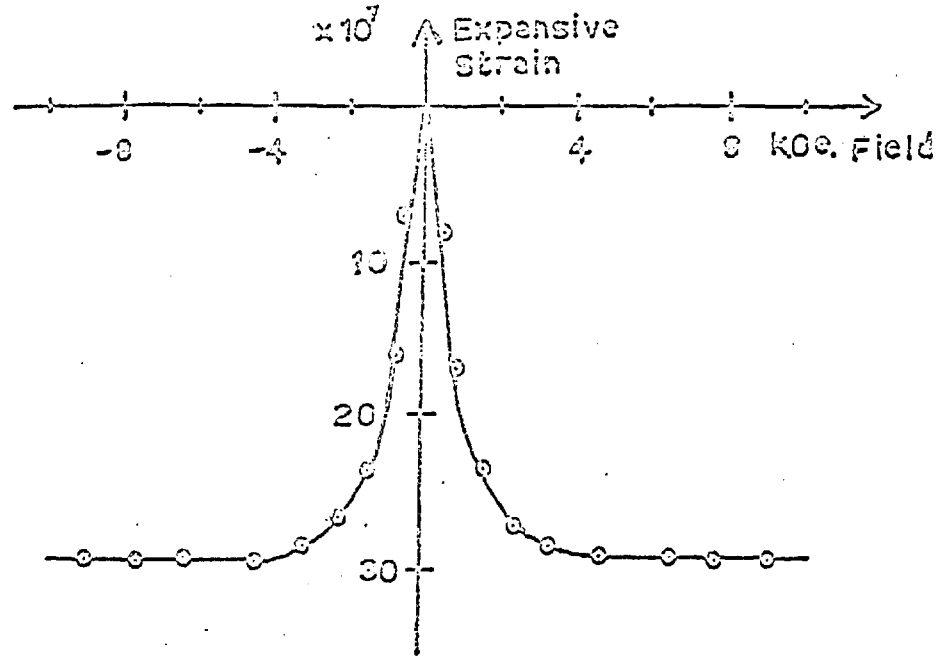


Figure 35. Strain in the St. Gothard crystal produced by a field applied along the $[1\bar{1}0]$ direction at -196°C.

rotate into the favourable direction after the threshold field has been surpassed. At 9 kilo-oersteds, which was the highest field applied to this crystal, 30% of the specimen remained in the unfavourable domain state. Although it is to be expected that in a less pure material the passage of a domain wall would require more energy, there is another effect to be taken into consideration. In section 4.5.1. where domain switching energies are considered more closely, it is seen that only the field component along the $[1\bar{1}0]$ axis on the (110) plane has any effect on the antiferromagnetic domains. If this is the case, then only 0.707 of the applied field was available in this crystal to cause domain movement.

The linear term in the strain expansion appropriate to the Elba crystal had a maximum value of 5.5×10^{-11} per oersted. Figure 34 shows that in addition to the linear strain, a 'square law' strain was visible at higher fields, and estimating that it accounted for a strain of 1.9×10^{-7} in a field of 9000 oersteds, the corresponding coefficient in the strain expansion would have an approximate value of 2.4×10^{-15} per $(\text{oersted})^2$.

4.2.4. Arizona Crystal

The maximum low temperature magnetostriction on the (111) plane in the Arizona crystal showed no essential differences from that existing on the (110) plane. The field dependence along the $|1\bar{1}0|$ direction, which was very similar to the curve of Figure 34,

indicated domain reversal occurring in a threshold field of approximately 1800 oersteds. Fields of 6 kilo-oersteds produced substantially complete (>90%) reversal of the unfavourably oriented domain state. The linear coefficient for a field applied along the [1$\bar{1}$0] crystallographic axis with strain measured parallel to this direction is 8.75×10^{-11} per oersted. Like previous natural crystals, the strain showed a 'square law' component which amounted to a value of 10^{-7} in a field of 9 kilo-oersteds, so that the appropriate coefficient had the value 1.2×10^{-15} per (oersted)^2.

4.2.5. St. Gothard Crystal

In section 3.1.6. it was seen that the titanium impurity concentration in St. Gothard crystals is greater than 2%, and it appears from magnetic domain observations[60] that as a result there is no transition to the purely antiferromagnetic state in this material. There remains the possibility however, that due to the presence of a large number of $FeTiO_3$ ferrimagnetic impurity regions dispersed throughout the crystal, excessive internal magnetisation may remain to exhibit a domain pattern even though a greater part of the material is a pure antiferromagnetic. This question cannot be completely resolved by magnetostriction measurements because of the necessity to measure overall strain, which if the crystal is ferromagnetic in any part, will be predominately of a ferromagnetic nature.

The strain on the (111) plane along the $[\bar{1}\bar{1}\bar{1}]$ axis with the field applied at liquid nitrogen temperature parallel to the same direction is shown in Figure 35. There is no measurable difference in strain when the magnetic field is applied in one direction or in the reverse direction. Although the shape of the curve is very similar to that obtained at room temperature (Figure 31(a)), the saturation strain at the particular orientation is increased by 66% above the room temperature value.

This comparison of size of the saturation strain at high and low temperatures can give some indication of the magnetic state of the material at liquid nitrogen temperature, for if a magnetic transition takes place the ferromagnetic strain component should be considerably reduced. Experimentally the reverse is the case and so it is probable that no Morin transition occurs over an appreciable volume of the crystal even down to -200° C. The evidence points to this absence being attributable to some form of pinning of the antiferromagnetic spins in a canted state rather than being solely due to the external magnetic effects of an impurity material.

4.2.6. Polycrystalline Specimens

The magnetostrictive strain in pressed powder samples composed of both commercial grade and high purity powder was measured parallel to the applied field direction at liquid nitrogen temperature. The field dependence of both materials is shown in

Figure 32(b), and it is immediately obvious that the commercial grade powder shows a ferromagnetic saturation whilst the high purity material exhibits typical antiferromagnetic characteristics. The former has probably such a high impurity concentration that it does not exhibit a magnetic transition at all, and in this case the saturation strain would be expected to be much larger at low temperatures due to the very considerable hardening of the epoxy resin binding material. A comparison of Figures 32(a) and 32(b) shows there to be more than a three-fold increase in saturation strain upon cooling.

The high purity material shows a linear strain effect with a coefficient of approximately 5×10^{-11} per oersted, which is very large for this type of polycrystal and is almost 50% of a good single crystal value.

4.3. ANTIFERROMAGNETIC DOMAIN ANNEALING

In section 1.5.5. the possibility of annealing a single antiferromagnetic domain state into the lattice at low temperatures by means of a magnetic field alone was found to be feasible. Experimentally, the production of single antiferromagnetic domain crystals was performed by cooling the material through the Morin transition in the presence of a static magnetic field. The proportion of the crystal which became single domain was assessed from the magnitude and sign of the linear magnetostriction coefficients in the low

temperature $\bar{3}m$ magnetic group; 100% single domain was taken to correspond to the largest value that could be obtained for the linear coefficients.

4.3.1. Angular Dependence

The direction of maximum strain on the (110) plane was always along the $[1\bar{1}0]$ direction, independent of the annealing conditions, but the magnitude of the strain in this direction depended critically on the magnitude and direction of the annealing field. The strain measured under favourable domain conditions was approximately 10% greater at high fields when annealed and measured along the $[1\bar{1}0]$ direction than when measured in this direction after annealing perpendicular to it (i.e. along the [001] direction).

A reversal of annealing along the $[1\bar{1}0]$ axis caused no change in the maximum strain conditions, but referring to Figure 33, the positive and negative field parts of the curve were interchanged. This means that the linear coefficients changed their sign but remained constant in magnitude when annealing conditions were reversed which is indicative of a reversal of the domain state of the crystal. Reversal of the strain direction at a certain field value as also shown in Figure 33, was evidenced in measurements both at -196° C and -78° C after annealing parallel to the $[1\bar{1}0]$ axis with either a positive or negative magnetic field. The field required to cause reversal was exactly opposite under opposite annealing

conditions.

After annealing in a field of 9 kilo-oersteds applied on the (110) plane along the $[00\bar{1}]$ axis and measuring along the $[1\bar{1}0]$ direction, the strain produced was virtually independent of the sense of the measurement field (in a similar manner to Figure 36). This means that no preferred domain direction was given to the crystal, and as a result statistically equal regions of opposite domain type were produced. Small measurement fields caused an effectively single domain state in one direction or in the other and so no discontinuous domain reversal effects were visible. Thus the application of an annealing field parallel to the strain gauge produced no effect, and rather like demagnetisation, left the crystal in an unannealed condition.

It has been shown experimentally that the annealing effect is the greatest along the $[1\bar{1}0]$ direction on the (110) plane, and it is important to note that this is the only crystallographic direction which also lies in the (111) basal plane. This supports the suggestion that annealing is caused by alignment of the ferromagnetic component of the high temperature domains in hematite, for this component always lies in the basal plane and so therefore a magnetic field acting upon the moment would cause the most effective alignment when applied here. There is also a rapid saturation of strain meaning easy domain alignment shown in the room temperature magnetostriction curve of this direction, as in Figure 27(a).

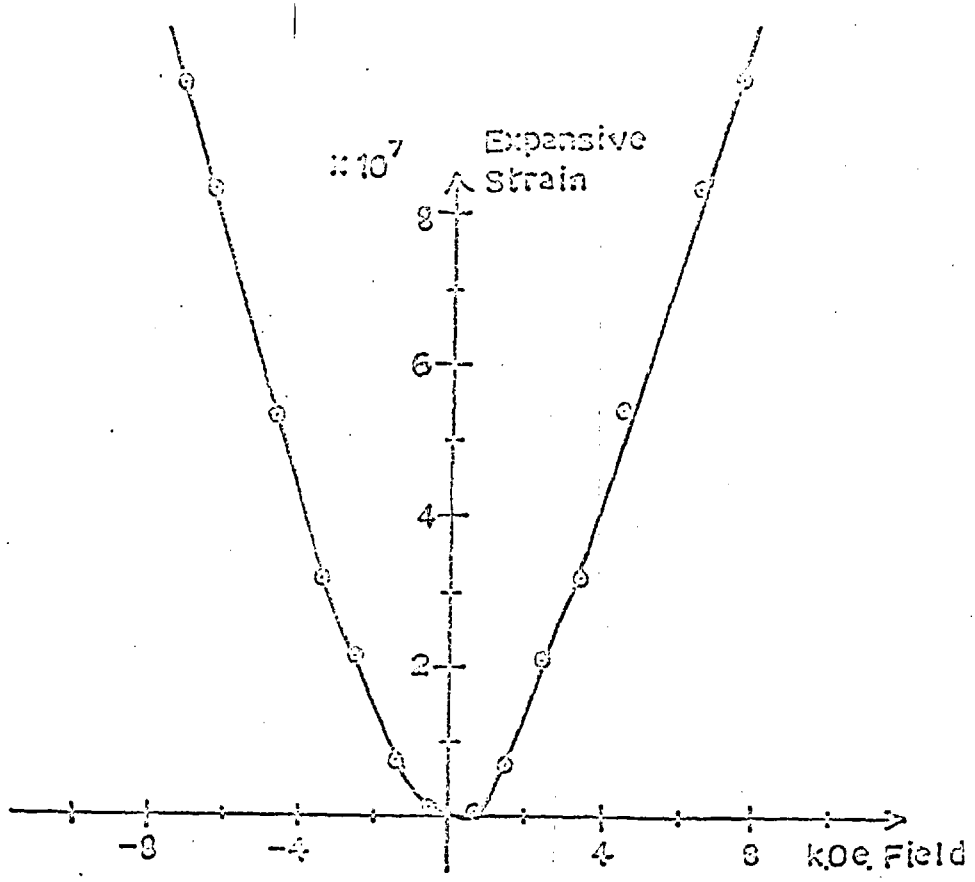


Figure 36. Field dependence of strain along the [1$\bar{1}$0] direction in the annealed synthetic crystal after demagnetised quenching.

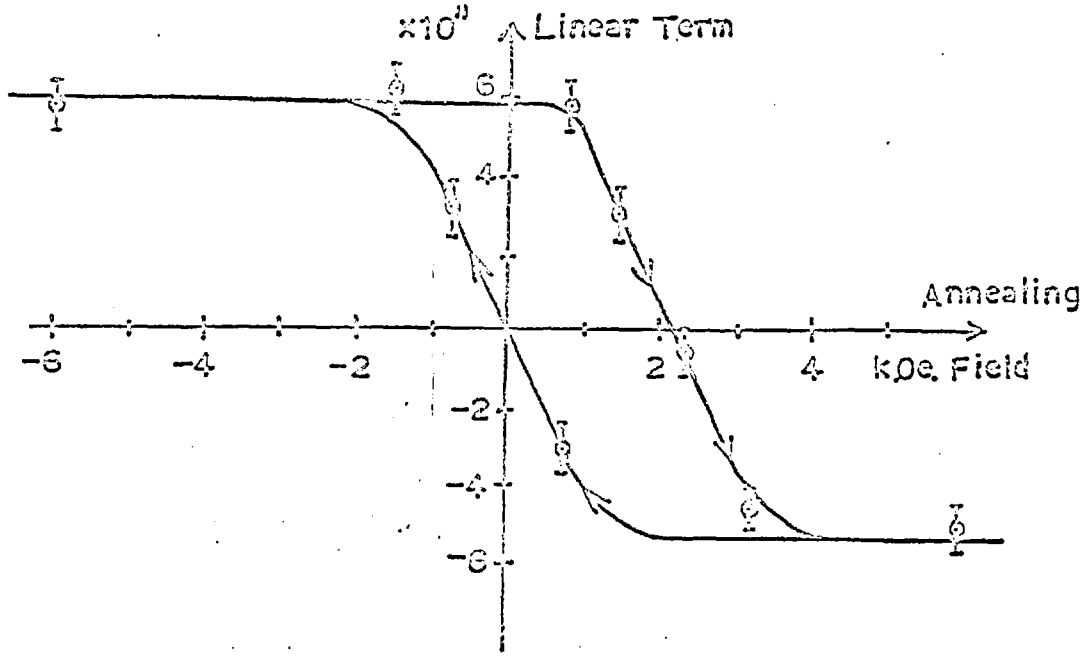


Figure 37. Dependence of the linear term on the annealing field in the Elba crystal.

In the basal plane the six-fold anisotropy is small[68] and so the annealing resulting from a field applied in the (111) plane should be virtually independent of orientation, and this also is supported experimentally.

4.3.2. Demagnetisation

Demagnetisation of the crystal before annealing, or annealing in an a.c. magnetic field produced a measured strain along the $[1\bar{1}0]$ direction which had a field dependence as shown in Figure 36. The tangent to the curve near the origin is almost horizontal showing virtually zero overall linear magnetostriction which would indicate the presence of roughly equal volumes of oppositely oriented antiferromagnetic domains.

It would appear from the curve that the crystal was made into an effectively single domain state by small measurement fields. It is therefore reasonable to assume that it requires only relatively low fields in the low temperature magnetic phase to produce a single domain state, and only slightly larger fields are needed to reverse domains. As a result there is no clearly observable 'reversal field' and this process can occur almost spontaneously, so that a non-saturated antiferromagnetic domain state in hematite is quite possibly a condition of unstable equilibrium.

4.3.3. Rate of Cooling

A short investigation was conducted to determine whether the effect of the annealing field was dependent on the rate of cooling of the material. Normal cooling to -196° C was effected by slowly adding liquid nitrogen to the dewar flask in which the experimental specimens were situated, and the rate could be changed by varying the quantity and frequency of addition of the liquid gas. No difference in annealing effect was observed whether cooling through the 200 deg C. took place in one minute or in thirty minutes.

4.3.4. Field Dependence

The relation between the size of the annealing field and the amount of antiferromagnetic annealing it produced was experimentally determined in both the annealed synthetic and a natural crystal. In both cases the field was applied along the $[1\bar{1}0]$ direction on the (110) plane. In the annealed synthetic crystal the linear magnetostriction coefficient was measured for annealing fields of 250 oersteds and 100 oersteds and for zero applied field. These values were chosen with reference to the 90° curve of Figure 28(a), for they are the fields required to produce 50% and 25% respectively of the saturation magnetostriction strain at room temperature.

The initial linear coefficients resulting from these annealings were $(6 \pm 0.5) \times 10^{-11}$ per oersted and $(2.8 \pm 0.3) \times 10^{-11}$ per oersted respectively, and the coefficient exhibited after cooling

in zero field was $(1.0 \pm 0.5) \times 10^{-11}$ per oersted. When compared with a coefficient of 12×10^{-11} per oersted after saturation annealing it is seen that the effect of annealing in a certain field is proportional, within experimental error, to the amount of magnetostrictive strain saturation produced at room temperature by the same field.

In section 4.1.1. it was seen that a large initial increase in room temperature strain for low fields was due to domain reorientation and that when strain saturation occured the material consisted of a single canted spin domain. From this and the experimental observations it would seem probable that the success of magnetic annealing in the low temperature phase is proportional to the degree of domain saturation in the high temperature phase.

Further confirmatory evidence was afforded by measurements of the hysteresis of domain annealing of the Elba crystal, since it is easy to observe hysteresis in this crystal because of its relatively high room temperature remanence. The various annealing fields were applied in turn along the $[1\bar{1}0]$ direction on the (110) plane at room temperature without previously demagnetising the crystal, and the corresponding antiferromagnetic domain state was obtained each time from measurements of the linear strain term at liquid nitrogen temperature. The dependence of the linear term on the annealing field is shown in Figure 37.

The loop which was traversed experimentally starting from the

negative saturation part, is completely non-symmetrical about the origin. This is a little surprising since the annealing should follow the distribution of canted spin domains and this should be symmetrical in the applied field. A possible cause is that the hysteresis loop is displaced by some form of fixed internal field of approximately -1000 oersteds at room temperature in this particular crystal, so that any positively applied annealing field is decreased and any negatively applied annealing field is increased. The mechanism for the existence of this internal field is completely unknown although it has been found to be only slightly affected by any external field, for an annealing field of +7500 oersteds does not materially affect it. The inbuilt preference for negative annealing may have been caused by many previous annealings in a negative saturation field.

Whatever the reason for this remanent field, the existence of the hysteresis loop of Figure 37 further underlines the relationship between success of annealing and the degree of domain saturation which in this case is evidenced by the relative magnetostriction at room temperature.

4.3.5. Memory of Annealing

This is a property of the material closely linked with the previous annealing hysteresis. It is virtually certain that annealing results from a change in the high temperature domain pattern,

but it is not known how stable is this pattern through a cooling-warming cycle.

In order to determine this point the synthetic crystal was annealed once in a field of +7500 oersteds. When cooled, the gradient of linear strain was measured, the last measurement field always being in the direction of the original annealing, and then the crystal was warmed to room temperature and then cooled in the unannealed condition and the linear gradient measured again. This process was repeated four times and the linear magnetostriction coefficients were found to remain constant to better than $\pm 5\%$ throughout the cycling. This showed that providing the antiferromagnetic domain state was not reversed at low temperatures, the domain pattern remained constant when cycling through the transition.

Blackman and Gustard[69] obtained a cine-film of the weak ferromagnetic domain pattern, using a magnetic colloid, when a crystal of hematite was cycled through the transition temperature. Upon cooling, the domain pattern disappeared but subsequent warming caused an identical pattern to be formed again, thus showing that high temperature domain nucleating points must be memorized in the antiferromagnetic phase. If the assumption is taken that magnetic annealing depends on the high temperature domain state of the material, then the present observation of memory of annealing through the transition is to be expected from the similar memory of the domain pattern.

4.4. LINEAR MAGNETOSTRICTION COEFFICIENTS

The field dependence of magnetostriction at a particular angle will produce the linear term for that orientation of field and gauge, but in general this term will consist of two tensor components. In order to evaluate the components separately it is necessary to observe the field dependence of magnetostriction along a fixed direction resulting from at least two different orientations of the applied magnetic field.

4.4.1. Synthetic Crystal

The method actually used consisted of obtaining the linear term from the strain (v) field curves measured by the fixed strain gauge, and with the magnetic field applied firstly along the $[00\bar{1}]$ direction, then at 20° to it, then at 40° to it, etc., rotating in the (110) plane. The antiferromagnetic domain state of the crystal was kept in a known saturated condition by adopting a standardized annealing field of +7500 oersteds along the $[1\bar{1}0]$ direction (i.e. $\theta = 90^\circ$).

The nine field dependence curves are shown in Figure 38, and from each was extracted the linear term near the origin. The resulting angular dependence of the linear term (E/H) is shown in Figure 39. A harmonic analysis for the first order component of these experimental points produced the strain equation

$$E/H = 1.83 \times 10^{-11} \cos\theta + 8.4 \times 10^{-11} \sin\theta \qquad (4.6)$$

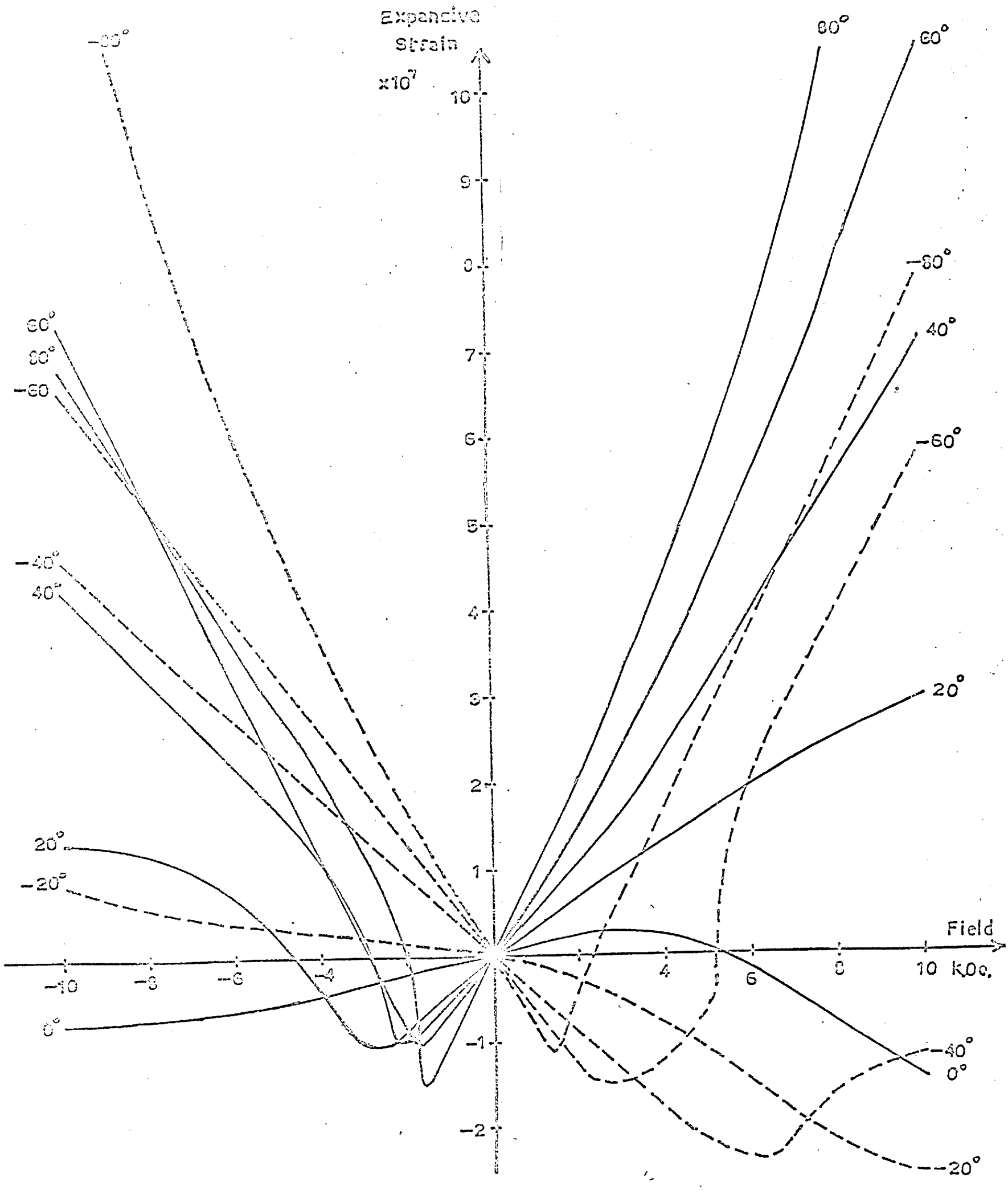


Figure 38. Strain in the synthetic crystal produced by a field applied at 20° angular intervals on the (110) plane, zeroed on the [100] axis.

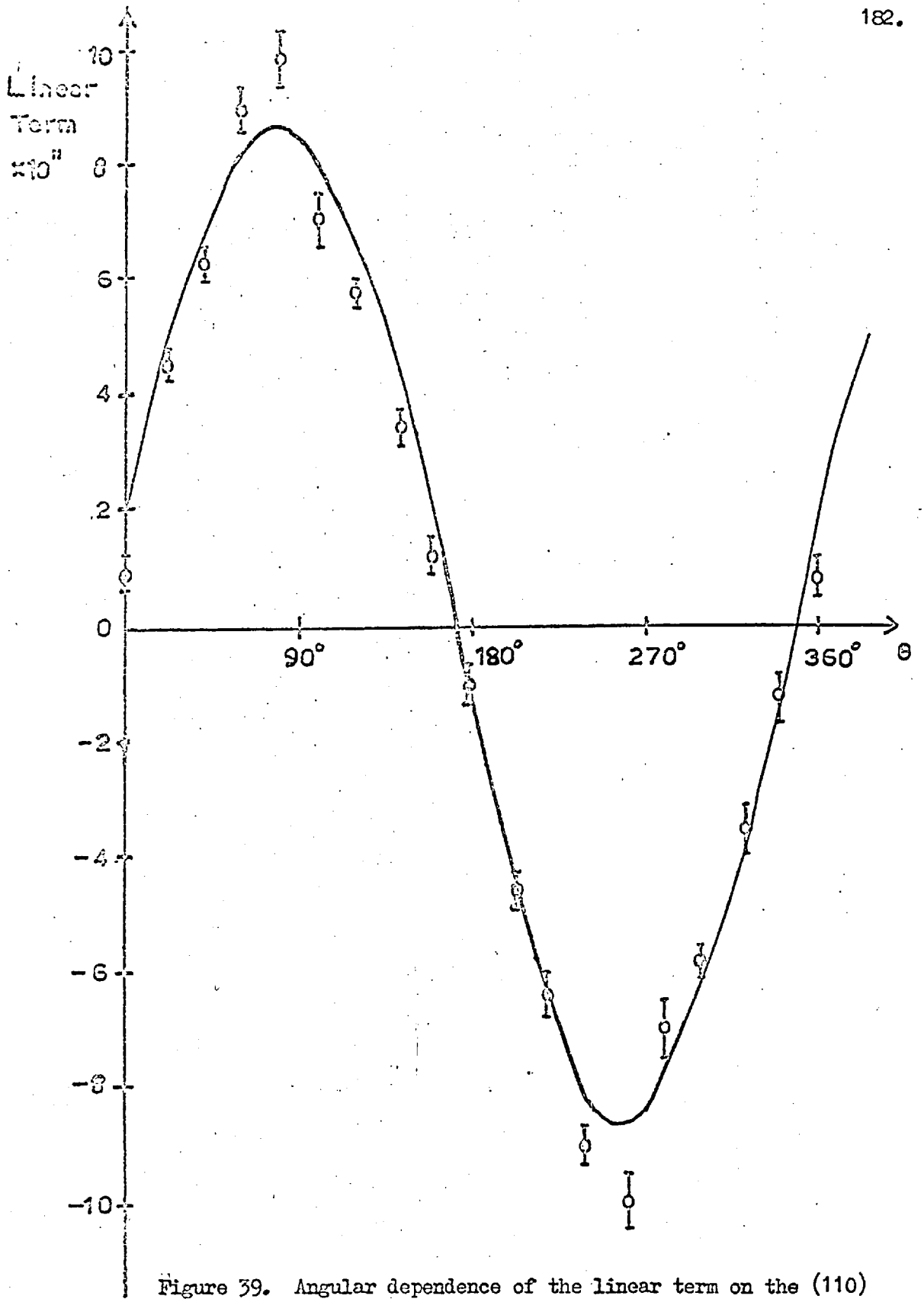


Figure 39. Angular dependence of the linear term on the (110) plane of the synthetic crystal.

where θ is the angle between the field and the $[\bar{0}01]$ direction. A curve of this function is shown in Figure 39 and the deviation of the experimental points from this curve, which may be represented by terms of higher order than θ, is probably caused by various angular and strain measurement errors. The magnitude of these overall errors in the synthetic crystal may be judged from the ratio of the coefficients of the 3θ and θ terms, which is 0.09.

It was seen in section 3.3.1. that the magnetostrictive strain on the (110) plane measured at an angle Δ to the $[001]$ direction and resulting from a rotating field, was given by equation (3.51). For $\Delta = 10^{\circ}$ and ϕ, the angle between the (110) plane and the $[111]$ axis equal to 36°, equation (3.51) reduces to the form

$$E/H = \sin\theta\left\{0.305\ Q_{22} - 0.922\ Q_{41}\right\} + \cos\theta\left\{0.118\ Q_{22} + 0.163\ Q_{41}\right\} \qquad (4.7)$$

Comparing with the experimental values of equation (4.6), it can immediately be seen that Q_{22} and Q_{41} are related by two simultaneous equations

$$0.305\ Q_{22} - 0.922\ Q_{41} = 8.39 \times 10^{-11} \qquad (4.8)$$

$$0.118\ Q_{22} + 0.163\ Q_{41} = 1.83 \times 10^{-11} \qquad (4.9)$$

Solving these, the tensor coefficients become

$$Q_{22} = 19.3 \times 10^{-11} \text{ per oersted}$$

and $$Q_{41} = -2.9 \times 10^{-11} \text{ per oersted} \qquad (4.10)$$

There is a certain ambiguity about the sign of these coefficients as they obviously change sign with domain reversal. It is

certain however, that Q_{22} and Q_{41} have opposite signs, and the values derived above are based on the domain type formed when the annealing field is in the direction $\theta = +90^{o}$.

4.4.2. Annealed Synthetic Crystal

After the thermal annealing process the linear magnetostriction coefficients of the synthetic crystal were re-measured in an identical manner to the preceding section. The field dependence of magnetostrictive strain resulting from fields applied at 20^{o} intervals around the (110) plane is shown in Figure 40. The variations are very similar to Figure 38 except that the amplitude of all the curves has been increased due to the annealing process.

The angular dependence of the linear term (E/H), which is the gradient of the curves at the origin, is plotted in Figure 41. A harmonic analysis of the experimental values produced the strain equation having first order terms thus

$$E/H = 1.9 \times 10^{-11} \cos\theta + 12.0 \times 10^{-11} \sin\theta \qquad (4.11)$$

where, as before, θ is the angle between the field and the [001] direction. This function is shown in Figure 41 together with the experimental points so that the deviation between them may be examined. The mathematical curve of equation (4.11) shows very good agreement with the experimental points and some estimate of the overall errors may be obtained from the ratio of the coefficients of the 3θ and θ terms, which is 0.045.

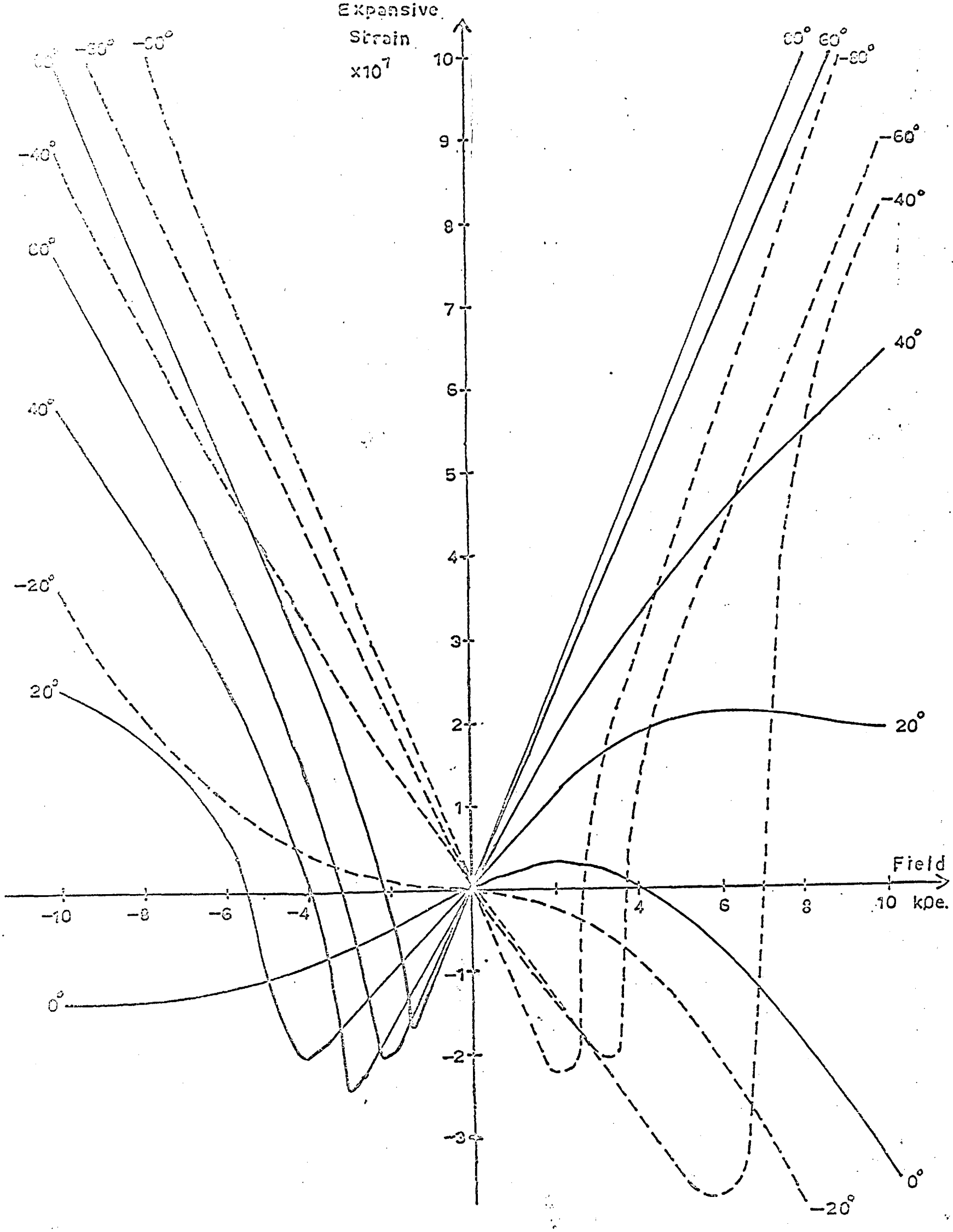


Figure 40. Strain in the annealed synthetic crystal produced by a field applied at 20° angular intervals on the (110) plane, zeroed on the [100] axis.

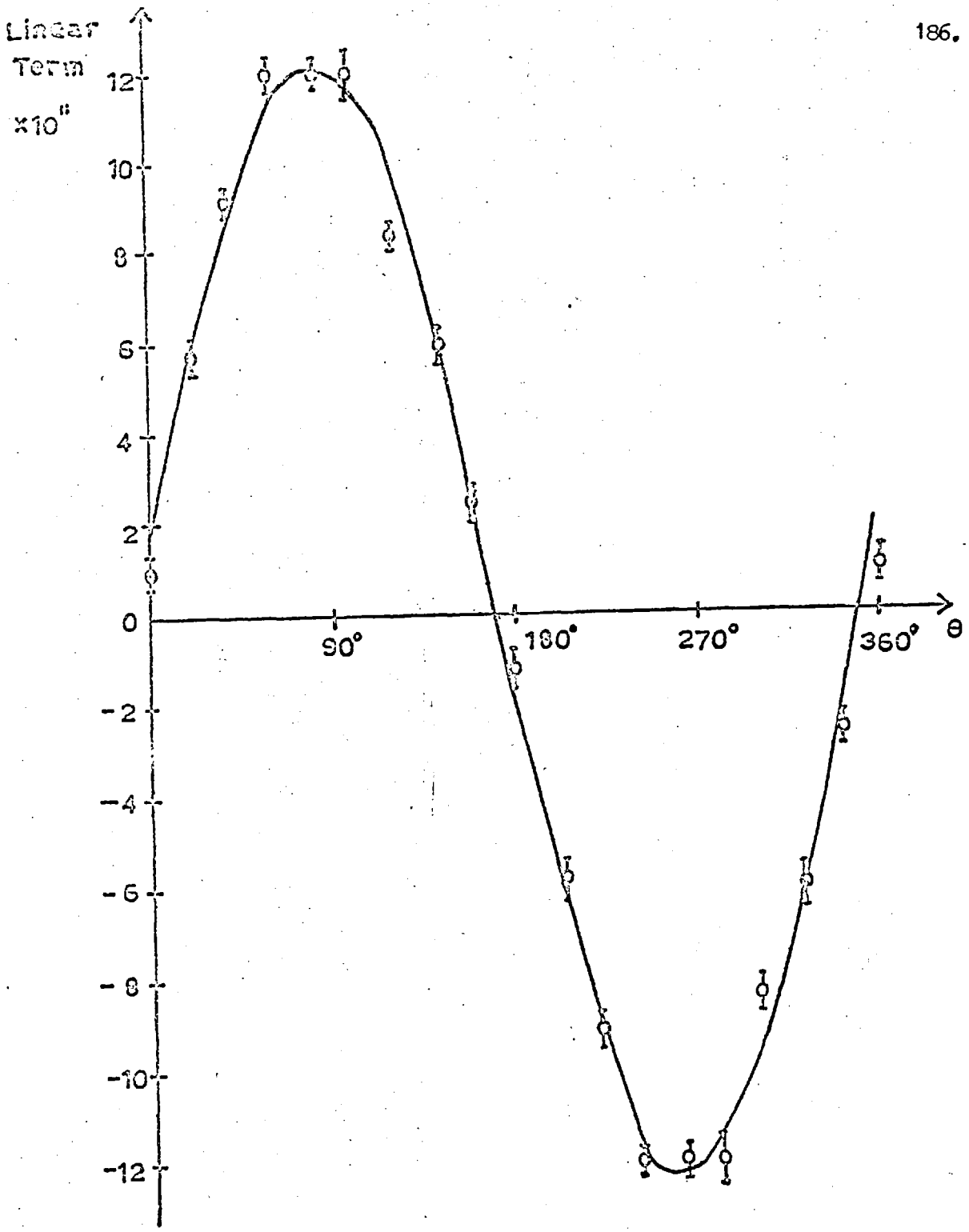


Figure 41. Angular dependence of the linear term on the (110) plane of the annealed synthetic crystal.

The experimental conditions are the same as in the preceding section, so that the same theoretical expression of equation (4.7) may be used. Comparing this with the experimental values of equation (4.11), it can immediately be seen that Q_{22} and Q_{41} are related by two simultaneous equations

$$0.305\ Q_{22} - 0.922\ Q_{41} = 12.0 \times 10^{-11} \qquad (4.12)$$

$$0.118\ Q_{22} + 0.163\ Q_{41} = 1.9 \times 10^{-11} \qquad (4.13)$$

Solving these the tensor coefficients become

$$Q_{22} = 23.4 \times 10^{-11} \text{ per oersted}$$

and $$Q_{41} = -5.3 \times 10^{-11} \text{ per oersted} \qquad (4.14)$$

The sign of the coefficients being determined under the same annealing conditions as in the previous section.

Comparing equations (4.10) and (4.14) for the same crystal before and after the thermal annealing process, it can be seen that both coefficients are increased. Q_{22} has increased by 21% and Q_{41} has increased by 45%, and since the former coefficient is by far the larger and therefore more accurately known from the harmonic analysis, the proportional increase in Q_{22} can be taken as resulting solely from the thermal annealing techniques. The increase in Q_{41} is quite possibly due not only to the annealing but also to the improved accuracy of the orientation and measurement.

4.4.3. Elba Crystal

The linear magnetostriction coefficients in the Elba crystal

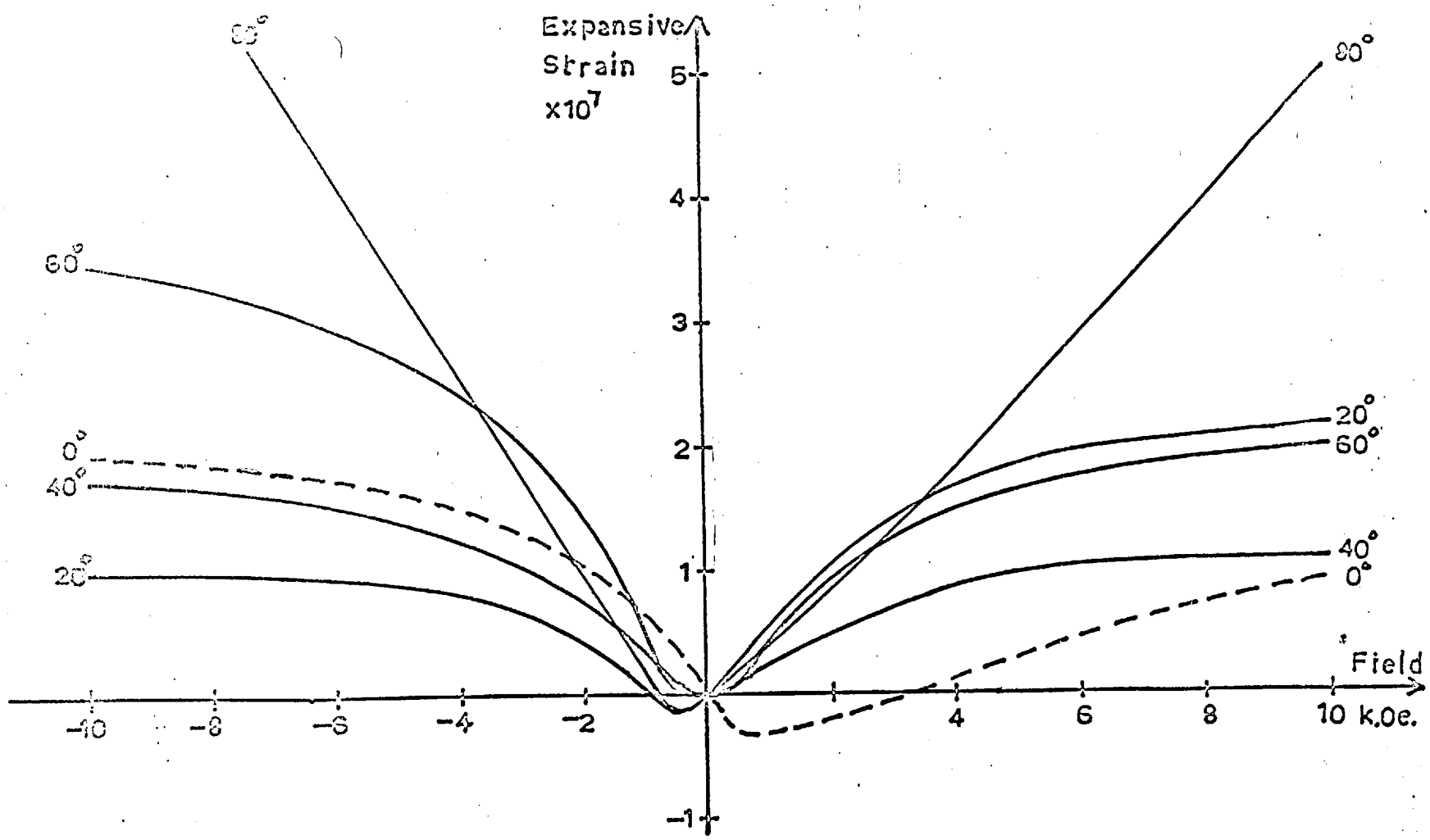
were determined in an analogous but not identical manner to those in the synthetic crystal. The strain was measured on the (110) plane along a line making an angle of 135° with the $[00\bar{1}]$ direction and the magnetic field was applied firstly along the $[00\bar{1}]$ direction, then at 20° to it, then at 40° to it, etc., rotating in the (110) plane. The domain state of the material was kept in the same condition as in the synthetic crystal by application of the same annealing field of +7500 oersteds along the $[1\bar{1}0]$ direction.

The field dependence curves at 20° intervals are reproduced in Figure 42, and are somewhat similar to those of the synthetic crystal although domain reversal is shown to be a far more continuous process. It should be expected that there are differences between the curves of synthetic and Elba crystals, because the position of strain measurement on the (110) plane is rotated through 55°.

The angular dependence of the linear term (E/H) is shown in Figure 43, and a harmonic analysis of the measured value gives the first order terms as

$$E/H = -2.2 \times 10^{-11} \cos\theta + 3.5 \times 10^{-11} \sin\theta \qquad (4.15)$$

θ being as in the previous crystal. This function is plotted in Figure 43 and the deviation of the experimental points from it is seen to be far greater than for the corresponding measurements on the synthetic crystal. This is probably attributable to the decreased size of the measured strains and so the experimental error forms a higher proportion of the total recorded value. The ratio of the



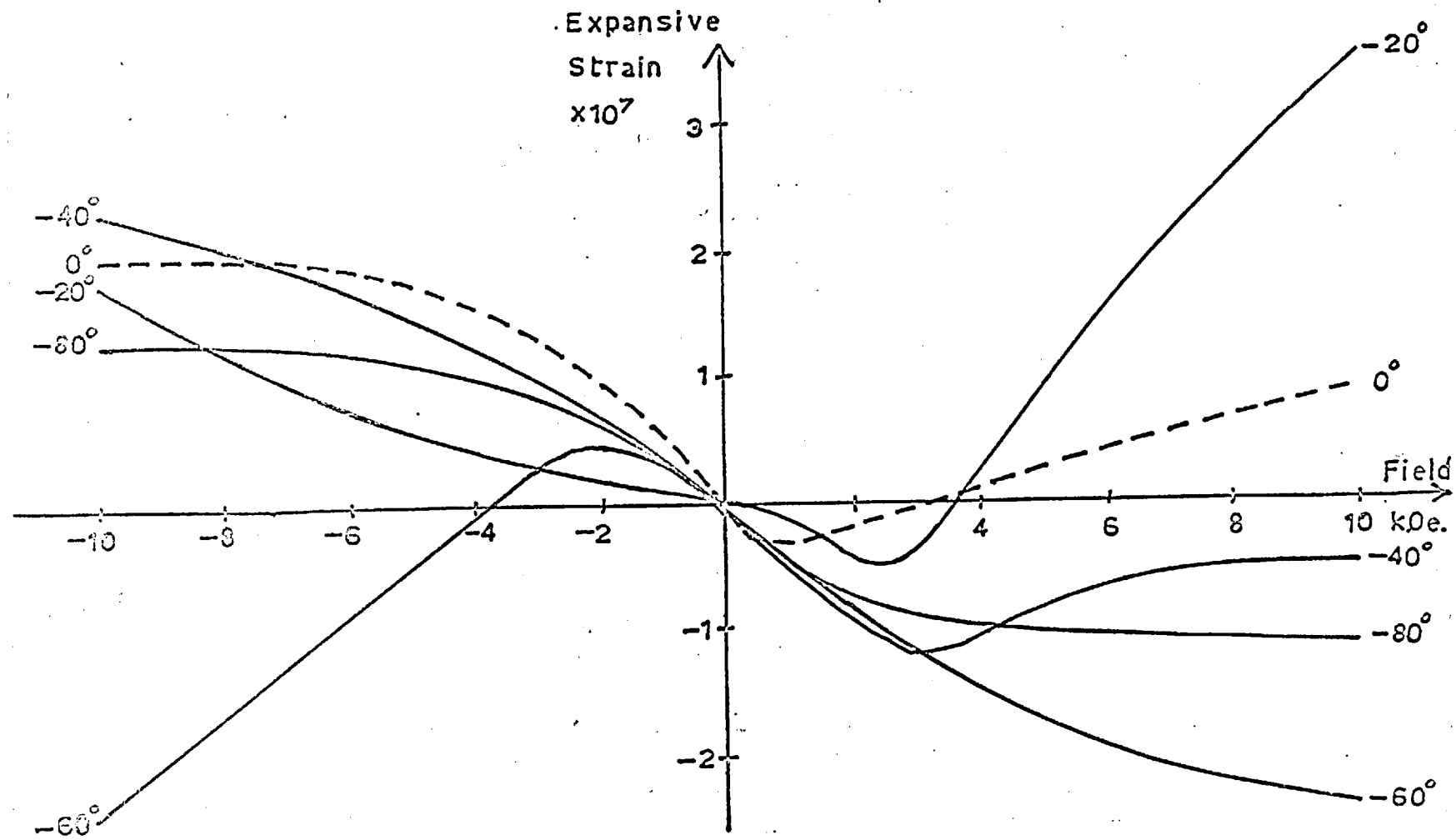


Figure 42. Strain in the Elba crystal produced by a field applied at 20° angular intervals on the (110) plane, zeroed on the [100] axis.

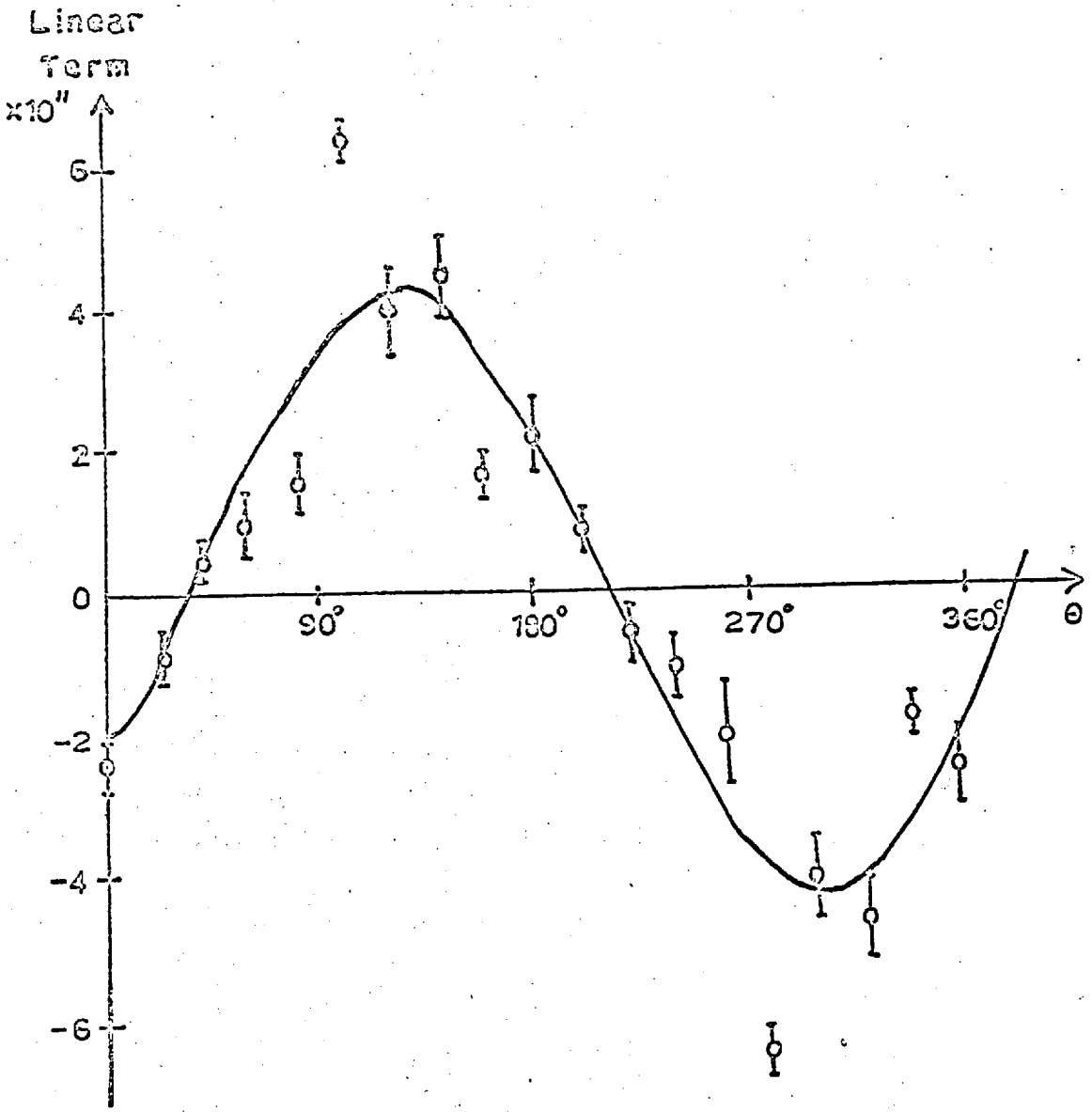


Figure 43. Angular dependence of the linear term on the (110) plane of the Elba crystal.

coefficients of the 3θ and θ terms, which has been taken previously as some estimate of the overall errors, is 0.22.

Equation (3.51) from section 3.3.1. gives the strain on the (110) plane at an angle Δ to the [001] axis resulting from a rotating field. For $\Delta = 135^{\circ}$ and the crystallographic angle ø equal to 36° as previously, this equation reduces to

$$E/H = \left\{0.327Q_{22} - 0.475Q_{41}\right\} \sin\theta - \left\{0.346Q_{22} + 0.475Q_{41}\right\} \cos\theta \qquad (4.16)$$

so that Q_{22} and Q_{41} can be obtained in a simultaneous equation form by comparing equations (4.16) and (4.15). The relationships are

$$0.327Q_{22} - 0.475Q_{41} = + 3.5 \times 10^{-11} \qquad (4.17)$$

$$0.346Q_{22} + 0.475Q_{41} = + 2.2 \times 10^{-11} \qquad (4.18)$$

Solving these, the tensor coefficients are found to be

$$Q_{22} = + 8.5 \times 10^{-11} \text{ per oersted}$$

and $$Q_{41} = - 1.5 \times 10^{-11} \text{ per oersted} \qquad (4.19)$$

These coefficients are respectively 36% and 28% of the coefficients of the annealed synthetic crystal, and so because of this, errors of constant magnitude are proportionally three times more important when investigating the Elba crystal.

4.4.4. Arizona Crystal

Magnetostriction measurements were performed on this crystal on the (111) plane, and as a result it was impossible to determine the tensor coefficient Q_{41} because the strain equation on this plane

only includes the term Q_{22}. Strain was measured along the $[1\bar{1}0]$ direction and the magnetic field applied successively along this direction, then at 20° to it, then at 40° to it, etc., rotating in the (111) plane. These curves are shown in Figure 44.

The domain state of the crystal was kept in the same condition as all the previous crystals by annealing in a field of +7500 oersteds along the $[1\bar{1}0]$ axis. ~~This field may just possibly have not been enough to saturate the domain state, for the 0° curve of Figure 30(a) shows that saturation of strain did not occur completely at 7500 oersteds.~~

The angular dependence of the linear term (E/H) on the (111) plane is plotted in Figure 45, and a harmonic analysis of these points gives the first order terms as

$$E/H = 5.9 \times 10^{-11} \cos\theta + 1.4 \times 10^{-11} \sin\theta \qquad (4.20)$$

$$= 6.06 \times 10^{-11} \cos(\theta - 13^{\circ}\,20') \qquad (4.21)$$

where θ is measured from the $[1\bar{1}0]$ axis. In section 3.3.3. a theoretical equation for the strain existing along the $[1\bar{1}0]$ axis caused by a magnetic field rotating in the (111) plane was derived and it was found to contain only a cos θ component, viz.

$$E/H = Q_{22} \cos\theta \qquad (3.62)$$

Hence $Q_{22} = 6.0 \times 10^{-11}$ per oersted, (4.22)

and the sin θ term of equation (4.20) must be considered as some measure of the total error of the experimental points.

The discrepancy between these points and equation (3.62) which

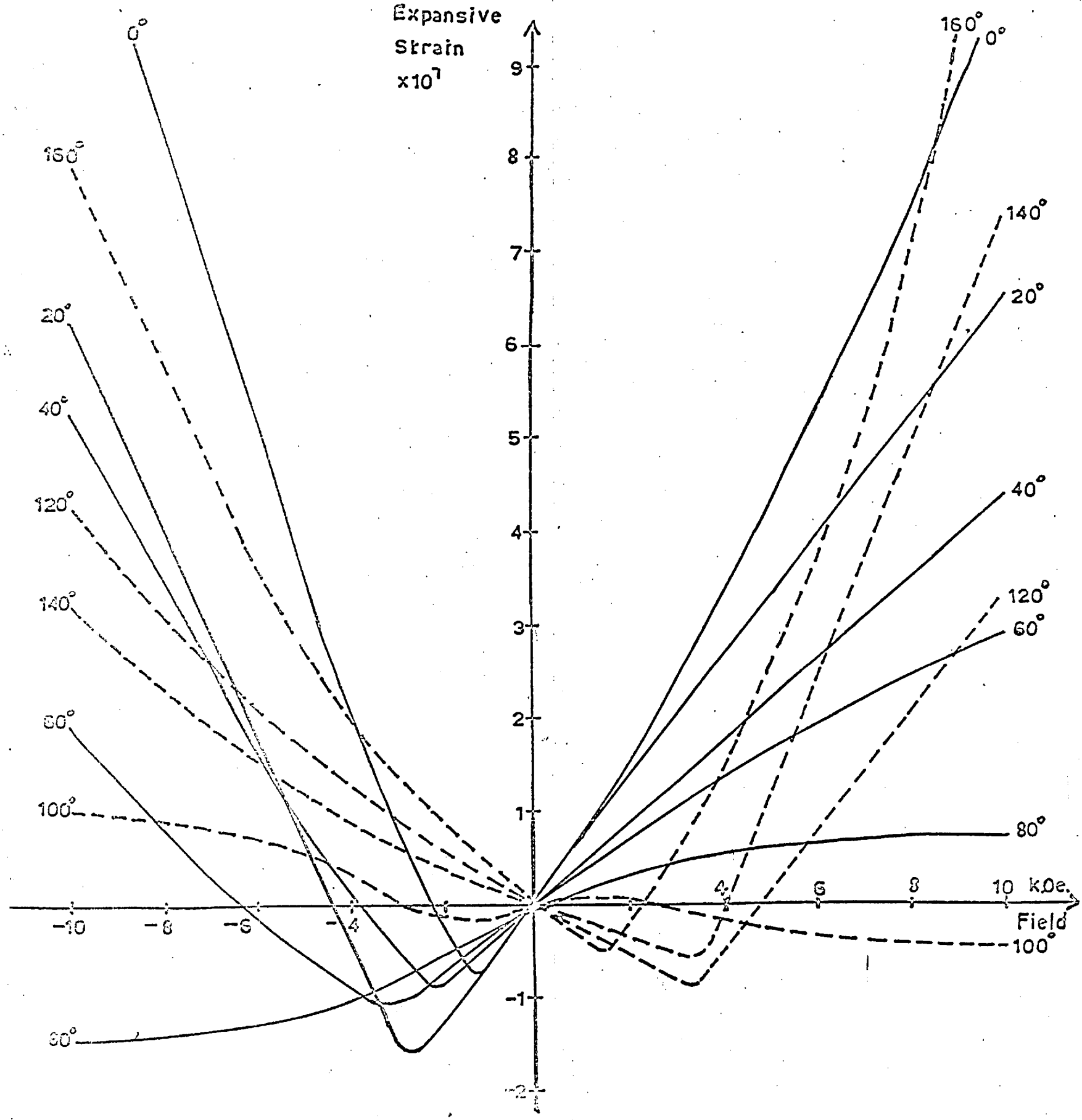


Figure 44. Strain in the Arizona crystal produced by a field applied at 20° angular intervals on the (111) plane, zeroed on the [1T0] axis.

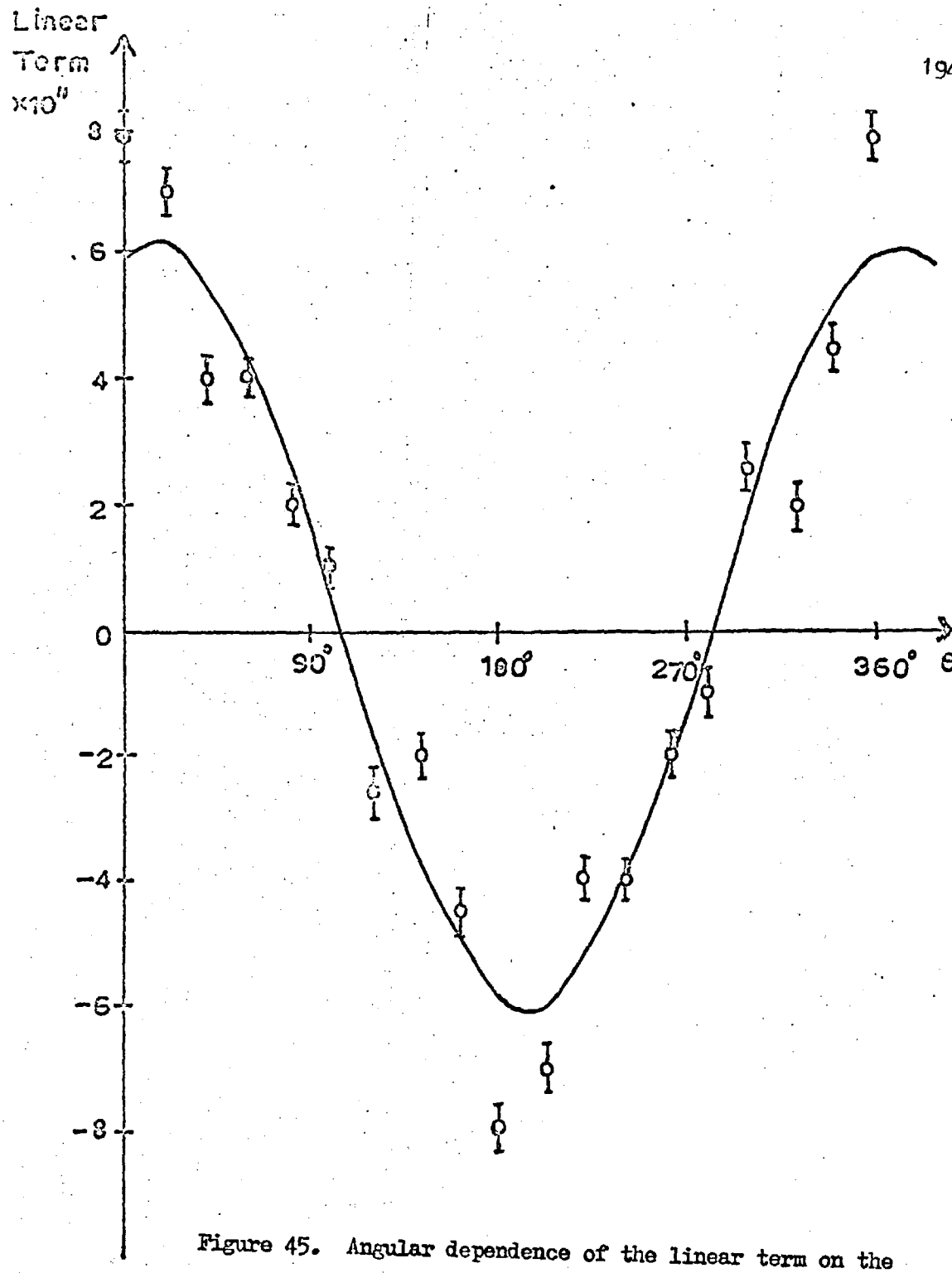


Figure 45. Angular dependence of the linear term on the (111) plane of the Arizona crystal.

is also plotted in Figure 45 is not as large as the corresponding discrepancy for the Elba crystal even though the coefficient Q_{22} is only 70% of the Elba value. The reason for this is two-fold; firstly the Q_{22} values result from different equations since measurements are performed on different planes and actually the linear gradient is approximately 50% larger on the (111) plane in the Arizona crystal than on the (110) plane in the Elba crystal. Secondly, equation (4.21) plotted in Figure 45 has a shifted origin from the theoretical equation and so gives a false impression of greater agreement between theory and practice.

4.5. ANTIFERROMAGNETIC DOMAIN SWITCHING

It was seen in section 4.2. that reversal or switching occurs at low temperatures under field conditions favourable to the effect. In this section the experimental evidence for the nature and speed of switching is presented together with the facts about domain wall motion derived from other authors.

The existence of antiferromagnetic domains is now generally accepted, principally from the evidence of polarized neutron diffraction. The first domains to be 'seen' in this way[79] were in MnF_2 and the actual domain distribution was found to be determined by the magnetic field applied to the crystal as it was cooled through the Neel point. A given cooling field produced a certain fixed domain configuration and reversing the biasing field switched the

domain types without changing the distribution. One large antiferromagnetic domain was seen to be at least 2 mm. across.

When attention was turned to low temperature hematite crystals, domains related by time inversion were observed by Pickart et al[38,42] although no estimate of their physical dimensions was attempted. It was reported, in agreement with the present work, that the degree of single domainness could be increased by cooling from a more nearly single domain state above the transition. In addition, Pickart et al found that the low temperature domain state could not be altered by an external field. This last result is at variance with those of Borovik-Romanov[30] on cobalt and manganese fluorides who reported observing the results of domain reversal below the Neel point in piezomagnetic measurements under fields of approximately one kilo-oersted.

A final piece of confirmatory evidence for the existence of antiferromagnetic domain switching in hematite below the transition is the reversal of the direction of change of strain in Figures 33 and 34 when the magnetic field was applied in the opposite direction to the annealing field.

4.5.1. Angular Dependence of Switching Field

Experimental investigation of the variables of domain switching was initiated by obtaining the angular dependence of the field required for switching as derived from the field vs. strain curves.

In the annealed synthetic crystal, which showed switching most clearly, the critical field at which the strain suddenly departed from linearity was found at 20° angular intervals from Figure 40. This angular dependence of the switching field is shown in Figure 46 together with the more approximate values of the critical field obtained from measurements on the synthetic crystal before annealing.

Both curves closely resemble the shape of an inverse sinusoidal function and so a harmonic analysis was performed on the reciprocal of each field value. The equation for the switching field H_s is experimentally

$$1/H_s = 4.8 \times 10^{-4} \sin\theta - 0.88 \times 10^{-4} \sin(3\theta + 32^{\circ}\ 48') \qquad (4.23)$$

so that to better than $\pm$ 5%, the switching field in oersteds on the (110) plane is given by

$$H_s = 2.1 \times 10^{3} \operatorname{cosec}\theta, \text{ oersteds} \qquad (4.24)$$

with θ zeroed on the $[001]$ axis.

This is in agreement with the hypothesis that the energy required for domain switching is a constant and is only derived from a field along the $[1\bar{1}0]$ direction (i.e. lying within the basal plane). The switching field is then just simply the field required to give a large enough component along the $[1\bar{1}0]$ direction to provide the switching energy.

So that switching energy $\propto H_s \sin\theta$

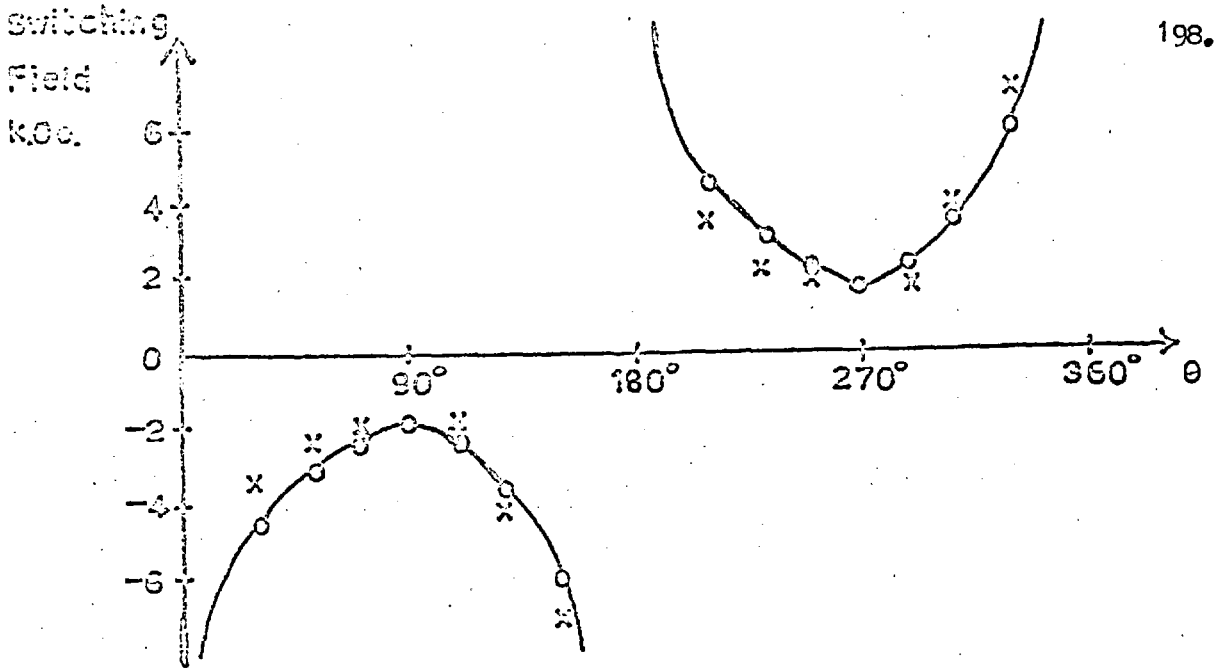


Figure 46. Angular dependence of field needed for antiferromagnetic domain switching on the (110) plane at -196°C. Shown as x before annealing, o after annealing the synthetic crystal.

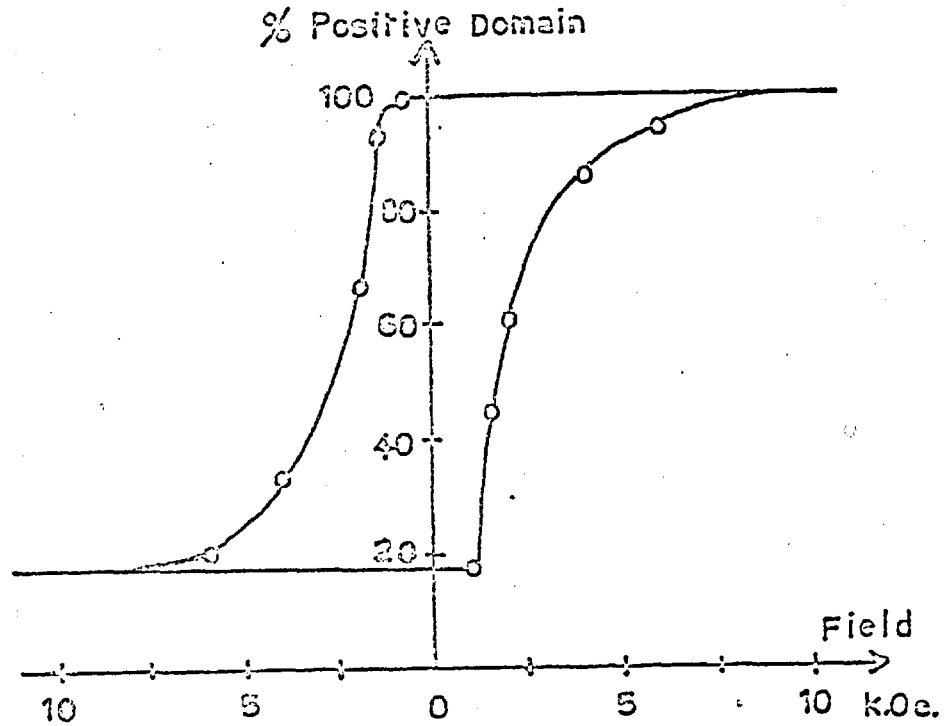


Figure 48. Hysteresis of field dependence of strain on the (110) plane in the annealed synthetic crystal at -196°C.

i.e. switching energy $\propto 2.1 \times 10^3$ (4.25)

and the right hand side of equation (4.25) is a constant, so that as expected, the switching energy in the crystal is independent of the angle of observation.

4.5.2. Hysteresis of Domain Switching

In all ferromagnetics, domain reversal and even domain rotation always exhibit some form of hysteresis, that is to say that a certain non-zero magnetic field is always required to be applied before domain movement can proceed whether in one direction or in the other. Magnetically soft materials such as 3.8% Si-Fe only require fields of the order of 0.2 oersted along the $[\bar{1}00]$ axis in order to initiate reversal, whereas very hard materials such as the permanent magnet Alnico 5 require fields as high as 600 oersteds[70]. The reason that a definite field is needed to change the domain pattern is that this usually occurs by movement of domain walls and the passage of these is always obstructed by lattice imperfections and magnetic anomalies. There is therefore the tendency for the domain pattern to preserve the status quo unless the applied energy is enough to cause the walls to surmount the particular energy barrier.

The most probable mechanism for the switching of the antiferromagnetic domain state is by domain wall movement, since the domains themselves have zero resultant magnetic moment, and this in turn would lead one to expect a switching hysteresis. To detect this

effect, the thermally annealed synthetic crystal was magnetically annealed in a field of 7500 oersteds and cooled to liquid nitrogen temperature. The magnetostriction was then measured as the strain difference between zero field and measurement field conditions, but the procedure differed from usual in that the highest positive field was used first. The field was decreased to zero in the usual measurement steps and then increased negatively in stages, and at a certain negative field, domain switching took place.

After a maximum field of -9000 oersteds was reached the field was progressively reduced in the usual measurement steps and of course no switching took place. It required a certain positive threshold field to switch back to the initial domain pattern. The strain hysteresis loop resulting from a field along the $[\bar{1}10]$ direction, which is shown as the 'butterfly loop' of Figure 47, could be traversed from positive field to negative field and back many times.

This loop provides an excellent method of determining how the overall domain state of the crystal varies with applied field, for the measured strain at any field point is dependent on the domain configuration at that point. This of course ignores the presence of any higher order magnetostrictive strains but these are known to be negligible in the synthetic crystal. The calculation is based on the proven assumption of section 4.3.4. that annealing in a field of +7500 oersteds produces 100% positive domains in the crystal.

If the linear term in a certain direction is A, then the strain

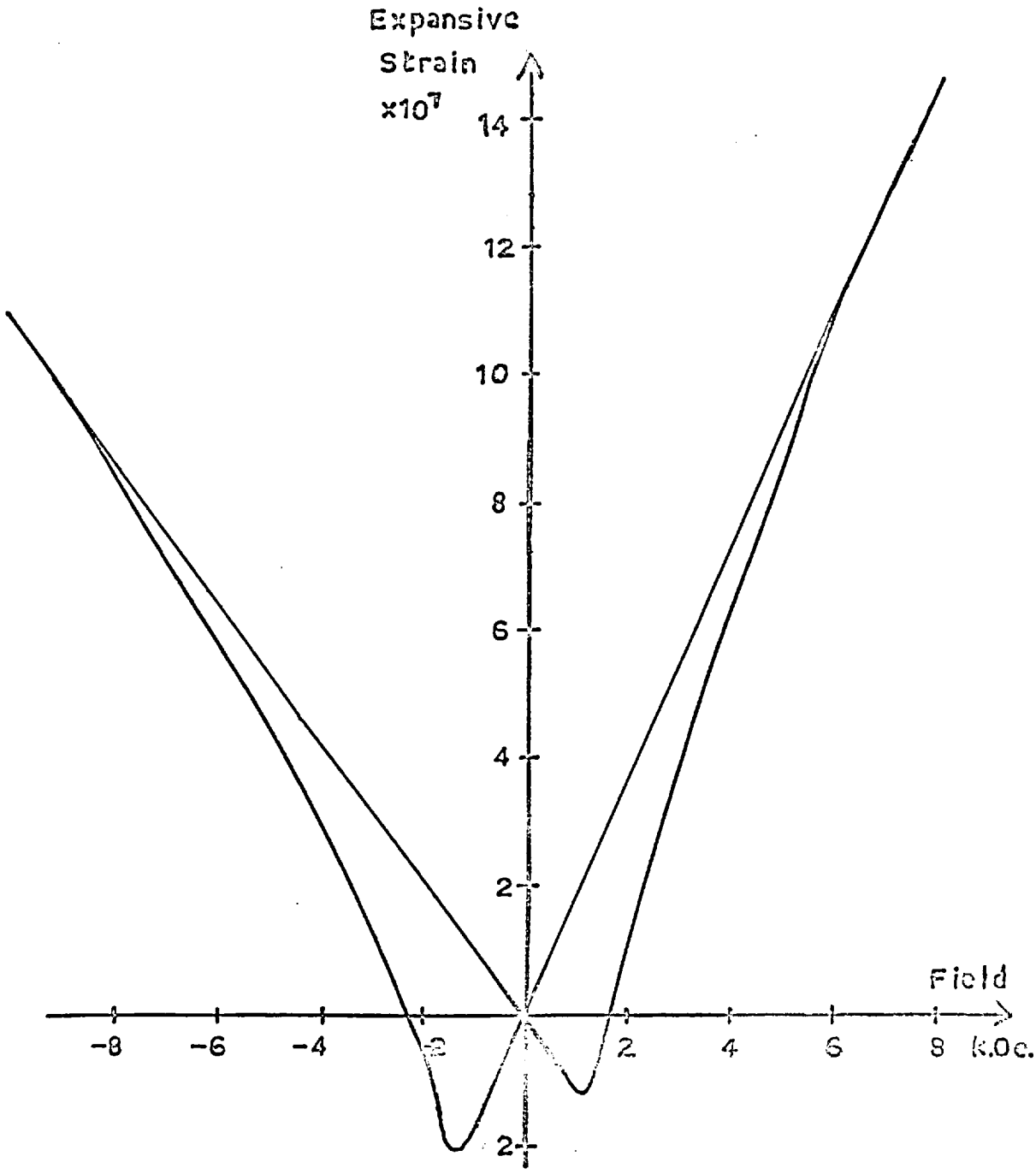


Figure 47. Hysteresis of field dependence of strain on the (110) plane of the annealed synthetic crystal at -196°C.

in a field +H is just +AH. If in a field of the same value applied negatively, x% of the crystal has changed to a negative domain state with linear coefficient -A, then the observed strain E is given by

$$E = \frac{A(100 - x)H}{100} - \frac{AxH}{100} \qquad (4.26)$$

so that $$x = \frac{100(AH - E)}{2AH} \qquad (4.27)$$

This enables one to calculate the overall domain state of the crystal at any particular field value whether positive or negative and whether increasing or decreasing. Plotting proportion of initial domain that still exists against applied field, a usual type of hysteresis loop is produced as shown in Figure 48.

It is worthwhile to consider this loop a little further - firstly, the initial switching field region is almost symmetrical about the zero field line and this symmetry is extended more approximately to higher field values. Secondly, only approximately 80% of the crystal switches its domain state in fields up to 9 kilo-oersteds, and there is no evidence to show that fields only slightly in excess of this value will change the situation at all. It would appear therefore that roughly 20% of the crystal has its domain state pinned during annealing such that fields of 9 kilo-oersteds cannot switch it.

If the previous assumption that domain switching occurs as a result of wall movement is used, then hysteresis can be explained in terms of the energy needed to overcome wall obstacles when sweeping through the crystal. The failure to switch 20% of the

crystal can then be attributed to various regions of positive domain which cannot be swept out by the domain wall as they are firmly pinned to the lattice. There are many forms that the pinning can take and the most likely is a discontinuity in the spin repetition caused by a dislocation or vacancy defect, although other pinning centres such as ferrimagnetic impurities could possibly be important.

If a large enough negative measurement field could be applied to the material, there is the likelihood that the remaining 20% of the crystal would switch and if this occurs, then when the field is reduced the domain state contains 0% positive domains until (with reference to Figure 48) +1000 oersteds is applied and the hysteresis loop is commenced. At +9 kilo-oersteds the crystal would contain only 80% positive domains and final switching to the 100% state would require the previous much larger field.

4.5.3. Rate of Domain Switching

In this section, the rate of domain switching is taken to mean the rate at which switching occurs in a field close to the threshold for reversal. If it is assumed that this process occurs as a result of the passage of a domain wall through the material then the wall has a certain statistical probability of overcoming any energy barrier in its path. If the energy applied to the wall is far in excess of the pinning energy of any obstruction, then the wall will progress through the material at the same rate as any thermal wave or shock

wave. If, however, the energy applied to the wall is just less than that of a certain energy barrier, then it is known from Boltzman statistics applied to the thermal energy of the magnetic ion that there is still a finite probability that the barrier may be surmounted after a long period of time. An experiment utilising time intervals of minutes and even hours could conveniently be performed with the apparatus described previously.

It is first necessary accurately to determine the critical switching field at liquid nitrogen temperature. Strain measurements were made at 300 oersted intervals close to the switching field and the resulting variation is reproduced in Figure 49. It can be seen that the strain reversal is completed within a maximum of 200 oersteds about a value of 2500 oersteds, which agrees well with the hypothesis that once the annealed domain is 'unpinned', very little extra field is needed to achieve a substantially reversed domain crystal.

Experimentally the crystal was returned to its positive annealed state by the application of a field of +9000 oersteds at liquid nitrogen temperature. A negative field of 70% of the switching threshold (i.e. -1700 oersteds) was applied to the crystal for three hours whilst the magnetostrictive strain was monitored at frequent time intervals by recording the final galvanometer deflection in zero field, -1700 oersteds, zero, +1700 oersteds and zero field again in quick succession. The strain plotted against a logarithmic

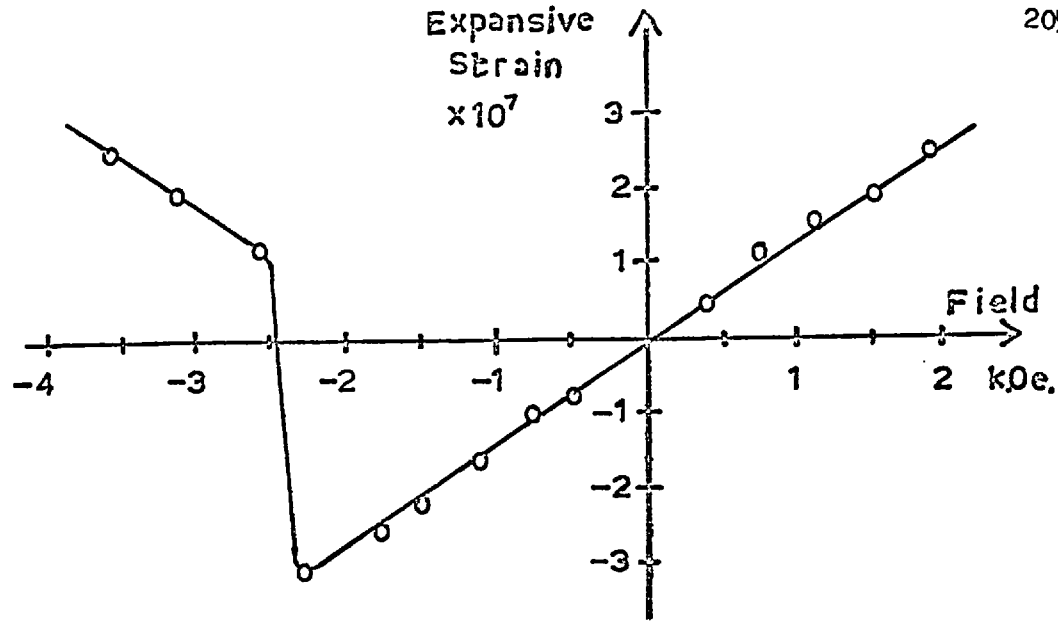


Figure 49. Magnetostrictive strain in the annealed synthetic crystal for accurate determination of switching field along the [1$\bar{1}$0] axis.

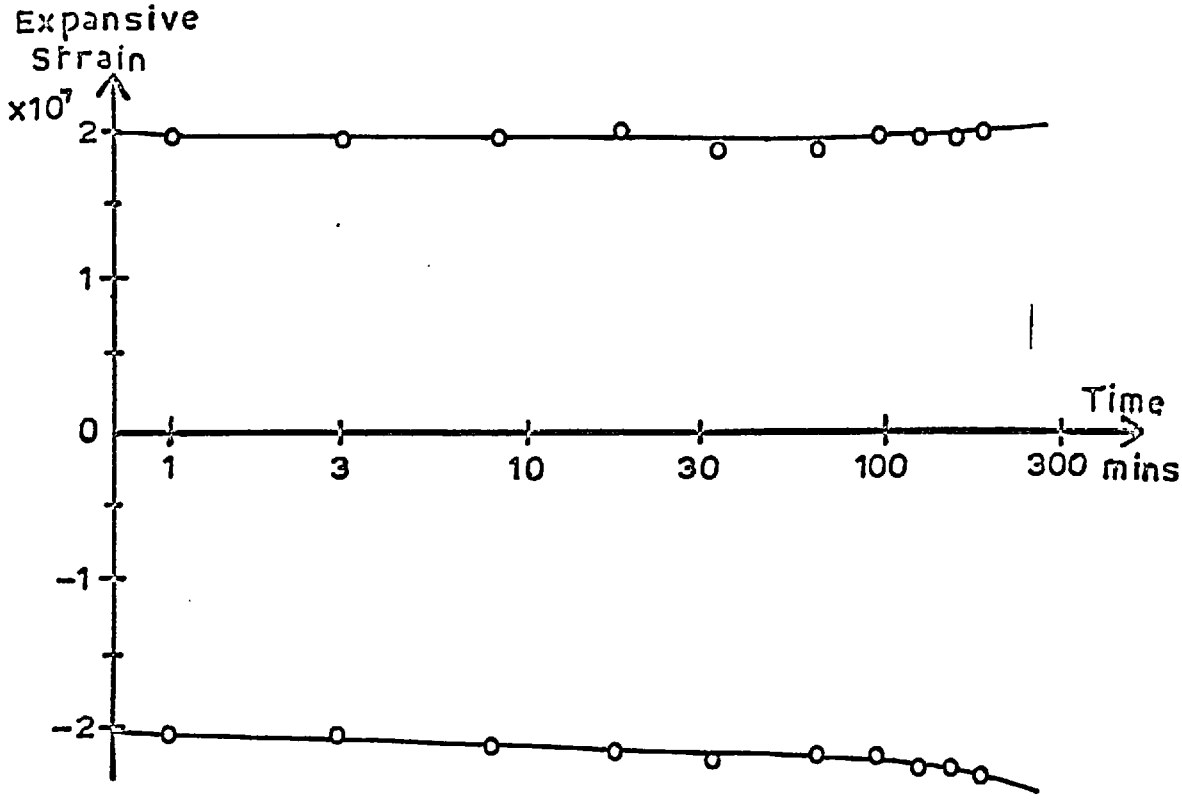


Figure 50. Magnetostrictive strain in the annealed synthetic crystal caused by a field of 70% of the switching threshold.

time scale is shown in Figure 50, and is virtually constant over all the time. No switching is visible and the slight departure from linearity after 100 minutes, which results in the strain increasing when measured in either field direction is almost certainly due to the magnetostrictive strain causing a slight permanent deformation of the crystal.

4.5.4. Possible Mechanism for Antiferromagnetic Domain Switching

Before proposing a reason for the switching of domains it is desirable to consider firstly the theories of reversal of magnetisation in ferromagnetics in the light of the preceding experimental evidence for an antiferromagnetic material.

In ferromagnetics reversal occurs by nucleation and growth of reversed domains and by propagation of domain walls through the crystal[64], and only when this process is completed do the domains rotate to follow the magnetising field. The former is the most probable mechanism in hematite, since actual rotation of the domains would have to take place against the anisotropy field of approximately 10 kilo-oersteds[71] which acts along the c-axis. From this one would expect that there would be a threshold field below which it will be energetically unfavourable for reversed domains to grow. This is supported by the evidence of a clearly defined switching threshold of 2500 $\pm$ 100 oersteds along the $[1\bar{1}0]$ direction in the particular crystal investigated. The step is clearly defined since

it was found that 70% of the critical field when applied for three hours failed to produce any switching.

There is no reason to expect a preferred direction for the switching threshold except as resulting from the magnetic annealing process and so it follows that a hysteresis of switching (which has been found experimentally) should be expected. On the domain wall model it is unreasonable to suppose that all the crystal would switch in one step since there is the probability of more than one type of pinning centre acting on each domain wall. It was found in practice that approximately 80% of the crystal switched in the first step and presumably the remainder would switch in one or more additional steps. This behaviour has been observed by Martin[72] in antiferromagnetic domain switching in Cr_2O_3 when investigated using the magnetoelectric effect.

Up to the present time the width of an antiferromagnetic domain wall has not been measured experimentally, but a theoretical consideration by Li[73] gives a value of 10^{-3} cms. which is the same order of magnitude as the ferromagnetic wall thickness. This is far smaller than the dimensions of any crystal used in the present work.

All the observed phenomena are explicable in terms of domain switching, but it is necessary to postulate a mechanism by which a purely antiferromagnetic domain without any external magnetisation can be affected by a magnetic field. An immediate possibility is the reversible domain energy arising from the non-linear suscept-

ibility term $C_{ijk}H_iH_jH_k$ which was discussed in section 1.3.6. An estimate of the maximum value of C_{ijk} may be made from the susceptibility values of Lin[43]. In his published work there is no visible deviation from linearity in the magnetisation vs. field curve, and this puts an upper limit of 5×10^{-11} e.m.u./grm. on C_{ijk}. Calculating from this the maximum value of the non-linear susceptibility energy at the switching field, it is found to be 0.08 erg/cc., which is very considerably less than the lowest switching energy of approximately 25 ergs/cc. that has been observed as a threshold in Cr_2O_3 by Martin[72].

An alternative suggestion to account for the interaction of the magnetic field with the antiferromagnetic domains is an extension of Lin's explanation[43] of the remanent moment which was discussed in section 1.5.6. Since the remanent moment followed the annealing field direction it was suggested that it could be due to slightly unequal sublattice moments which were aligned by the external field. This theory fitted all the facts of remanence but to account for the linking between field and domain direction it is necessary to extend the theory to suppose that the small inequality of sublattice moments has only one direction in each domain and by measurement of this, the domain direction is defined.

On this basis, annealing in a positive field aligns all the moments in some general positive direction and then a negative applied field attempts to rotate the internal magnetisation of the

material, and this in turn is intimately linked with its domain direction. This situation then allows the natural introduction of the concept of domain reversal occurring as a result of the passage of a domain wall, for the unequal sublattice moments are very similar in behaviour to a ferromagnetic spin array.

Looking at this theory from the quantative point of view, a typical remanent moment of 10^{-3} e.m.u./grm. would give the crystal an energy in the reversal field of approximately 2 ergs/grm. or approximately 15 ergs/cc. If this theory is correct, and at the moment it fits all the experimental facts of switching and remanence, then the reversible domain energy derived from the non-linear susceptibility term is negligible as compared with this unequal sublattice moment energy.

4.6. TEMPERATURE DEPENDENCE OF MAGNETOSTRICTION

The temperature dependence of magnetostrictive strain was obtained in the annealed synthetic crystal by recording the field dependence of strain at various fixed temperatures from -200° C. up to room temperature. The reasons for using constant temperature baths have been discussed in section 2.6., and the liquids actually used are listed in Table III of that section.

4.6.1. High Temperature Phase

The field dependence of strain at room temperature (+23° C.)

with the gauge at 10° to the [001] axis has already been seen in section 4.1.2. and the curves reproduced in Figure 28(a). When measurements were performed at the temperature of melting ice, the field dependency curves, shown in Figure 51, were almost identical in shape to the room temperature curves.

The direction of field giving maximum saturation strain has changed from the [1$\bar{1}$0] axis to the [001] axis, because the strain caused by a field applied parallel to the [001] direction has increased by 70% whilst the strain caused by a field parallel to the [1$\bar{1}$0] direction has decreased by 20%. At 45° and 135° to the [001] axis the saturation strain has decreased by 25% and 38% respectively. The reason for these changes in strain is linked with the temperature variation of the magnetostriction constants along each of the principal directions, and since hematite is highly anisotropic it should not be expected that the various coefficients would have the same temperature dependence. The linear coefficients in the reversible domain system at 0° C. are so small as to be unmeasurable at any angle of the applied field.

4.6.2. Low Temperature Phase.

The field dependence of strain at low temperatures provides a much more interesting and informative picture. Measurements of field dependence were performed in the low temperature phase of hematite at 77° K, 113° K, 195° K, 229° K and 250° K, and curves

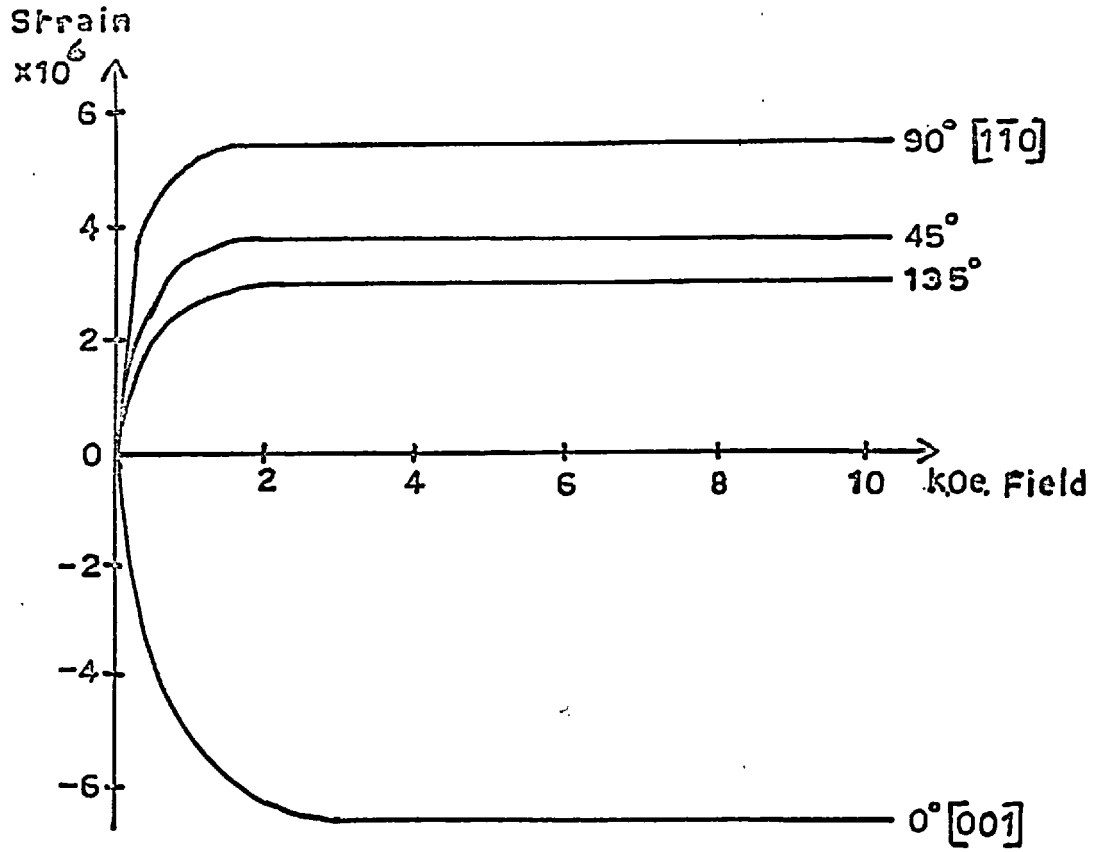


Figure 51. Strain in the annealed synthetic crystal at 0°C. produced by fields applied at various orientations on the (110) plane.

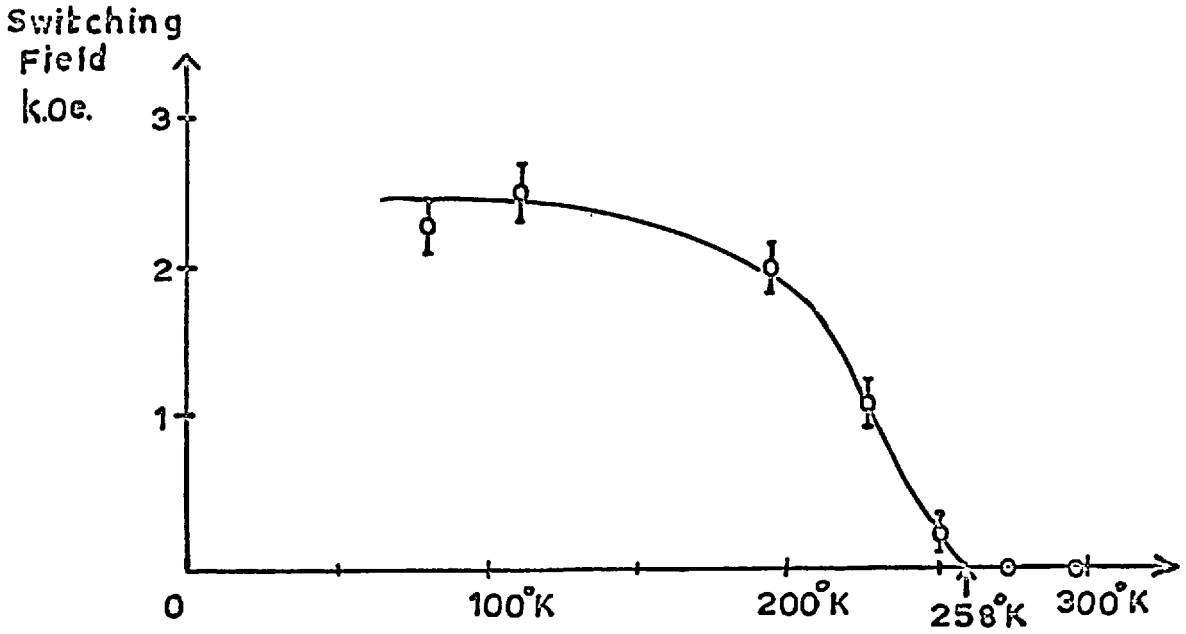


Figure 53. Temperature dependence of the antiferromagnetic domain switching field along the [1̄10] direction.

were obtained as shown in Figure 52. Immediately it can be seen that at 77° K, 113° K and 195° K the linear coefficient in the truly antiferromagnetic state is absolutely constant at 11 x 10^{-11} per oersted and is independent of field and temperature. At 229° K, after an initial very low field region where it appears that domain movement takes place because annealing has not had its full effect, the linear coefficient has increased to 13 x 10^{-11} per oersted.

At 250° K, which is almost exactly on the transition temperature in high purity hematite, the linear term at low fields appears to have increased considerably to a value of 57 x 10^{-11} per oersted. However, this obvious conclusion is almost certainly incorrect, for examination of the whole of the field dependence curve corresponding to measurements at this temperature reveals that there is a very considerable strain component due to 'square law' magnetostriction. This is typical of a canted spin antiferromagnetic, and would imply that at 250° K a substantial portion of this particular crystal is in the process of spin rotation to the high temperature phase. This in turn would lead one to expect to observe a large low field strain due to canted spin domain reorientation, and it is probably this which gives a false impression of a very large initial term.

Figures 23(a) and 51 which are field dependency curves in the high temperature phase show a saturation of the domain reorientation strain. The reason that this is not visible at 250° K lies in the very low moment resulting from the extremely small spin canting just

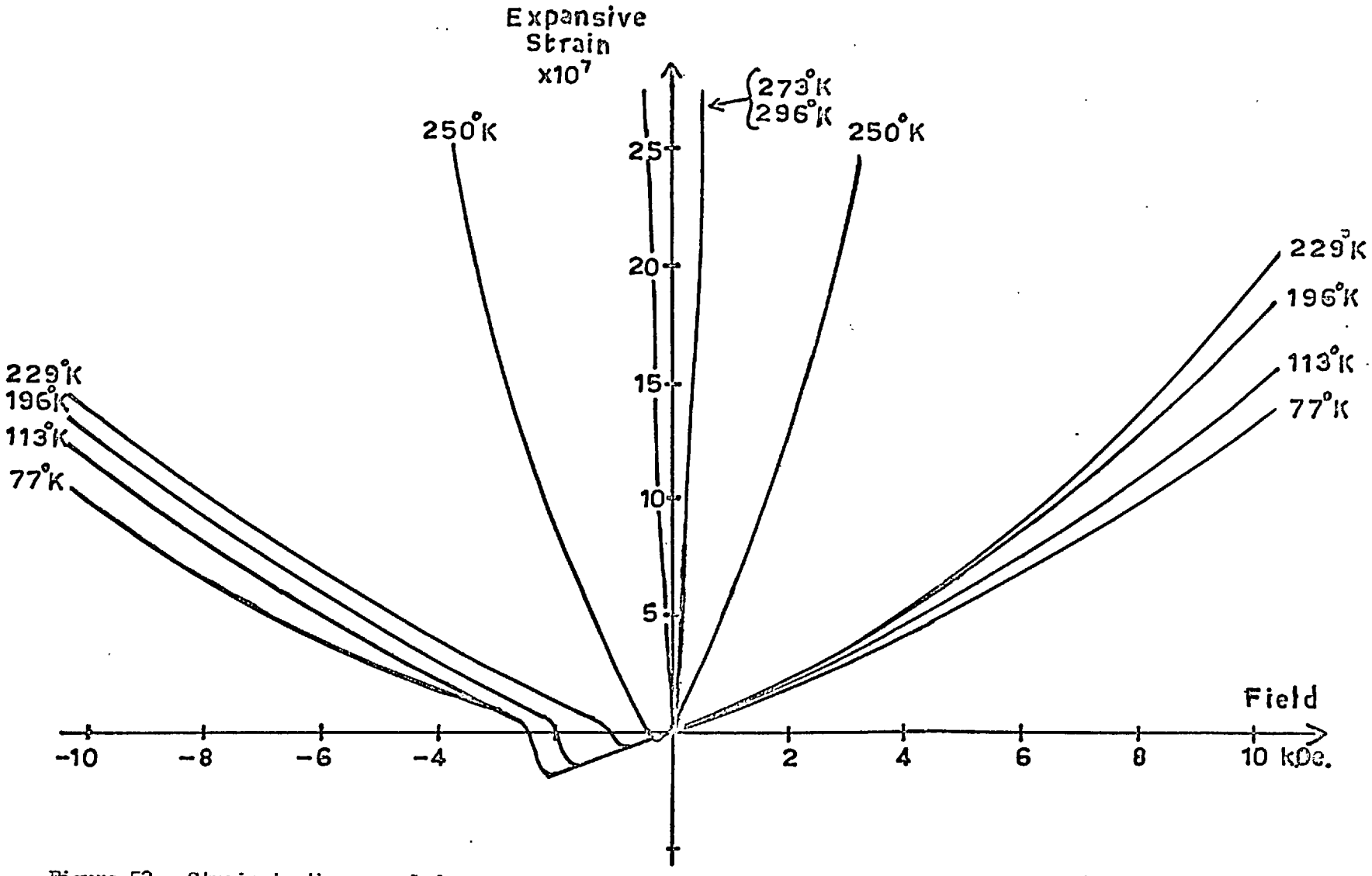


Figure 52. Strain in the annealed synthetic crystal caused by fields applied along the [1T0] direction at 77°K, 113°K, 195°K, 229°K, 250°K, 273°K and 296°K.

at the transition temperature, and because of this weak linkage between moment and applied field, saturation would occur in fields far higher than those available. Similarly if the 0° C and room temperature curves from zero to one kilo-oersted (mentioned previously) could be expanded ten times along the field axis they would probably look like the 250° field dependence curve.

It can be seen from the curves of Figure 52 that the threshold field for domain switching is quite highly temperature dependent. Switching occurs at approximately 2300 oersteds at 77° K and at approximately 2500 oersteds at 113° K. At the higher temperature of 195° K, switching still occurs in a field of approximately 2 kilo-oersteds. As the transition region is approached the threshold field decreases rapidly so that switching occurs in a field of approximately one kilo-oersted at 229° K and in only 250 oersteds at 250° K. Above this temperature, when the material is predominately in the high temperature phase the magnetostrictive strain reverses easily and the threshold field for domain switching is effectively zero.

Figure 53 shows the temperature dependence of the threshold switching field. Within experimental error this forms a smooth curve in which the field decreases more rapidly the higher the temperature is raised until it reaches zero at the generally accepted transition temperature of 252° K. This shape is to be expected for the thermal agitation energy of the magnetic ions adds to the

magnetic energy when attempting to rotate pinned spins against the anisotropy field of the pinning centres. At low temperatures the thermal energy is small so that the magnetic energy must be correspondingly larger to compensate for this. At higher temperatures, not only does the thermal energy increase but the overall magnetocrystalline anisotropy field decreases[71] so the field required for switching drops rapidly. Above the transition temperature the spin pinning energy is so small as to make the switching field undetectable on the scale of measurement used.

4.6.3. Field Dependence of Transition Temperature

When comparing magnetostrictive strains in both high and low temperature phases, it has been seen that comparison of the apparent linear coefficients is really quite false. In Figure 54 is plotted the actual measured strain in the annealing direction at fixed field values as a function of temperature. At 1, 3, and 5 kilo-oersteds the strain is temperature independent at low temperatures, but at 8 kilo-oersteds the strain increases by 30% over the temperature range from 77° K to 229° K.

At the transition temperature there is a rapid increase of strain in all fields after which the strain attains a uniform temperature dependence with the same slope for all fields above 3 kilo-oersteds but for lower fields the slope is less. There are two very important characteristics shown in Figure 54 which need explaining further.

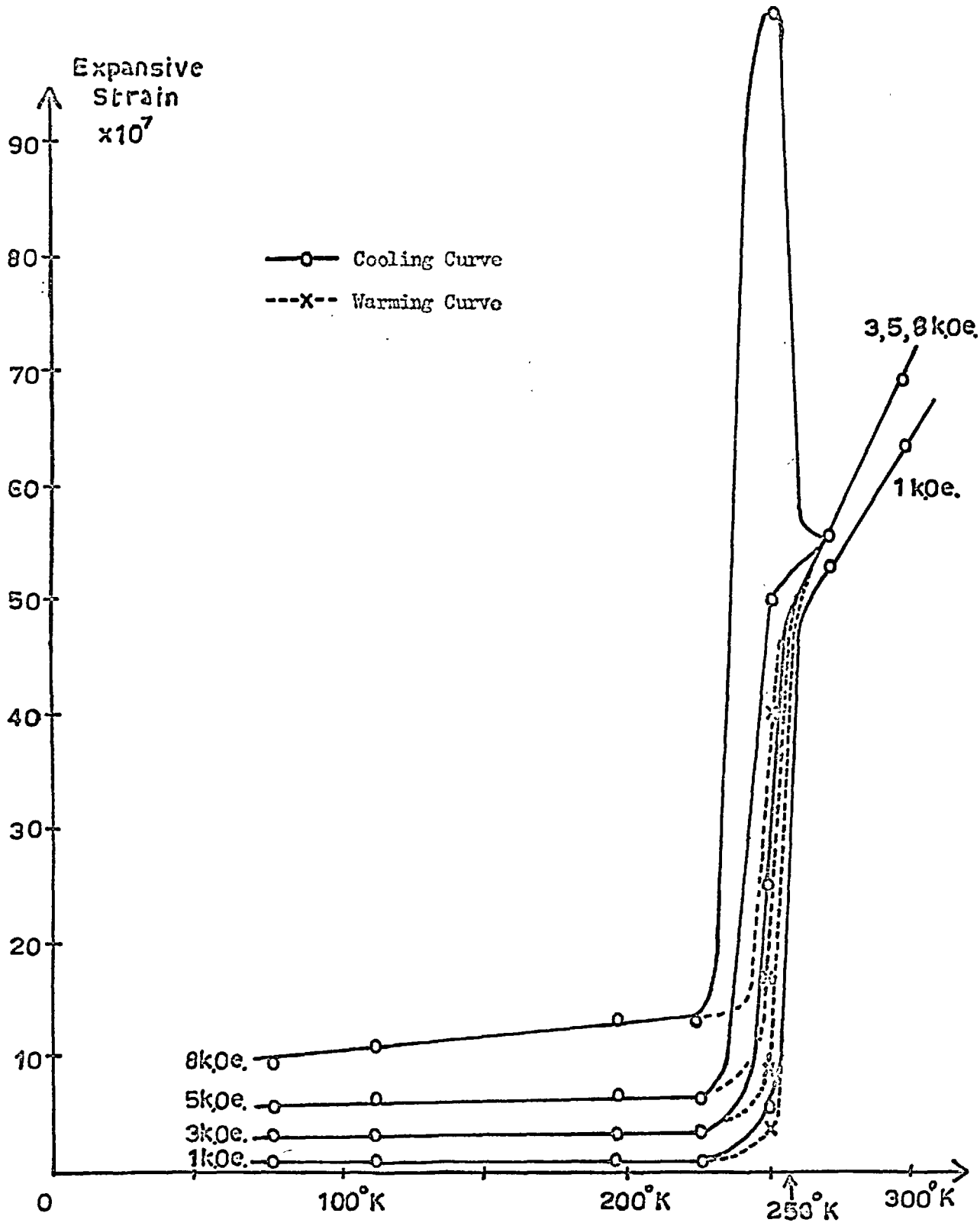


Figure 54. Temperature dependence of strain in the annealed synthetic crystal resulting from fields of 1, 3, 5 and 8 k.Oe. applied along the $[1\bar{1}0]$ axis.

Firstly, if the transition temperature is taken as the temperature at which a sudden increase in strain occurs then this temperature is seen to be field dependent. This variation can be understood in terms of the weak ferromagnetism existing above the transition temperature, for the application of a field will cause the weak moment to align itself with the field consequently lowering the energy of this phase. It is intuitively obvious that of two phases, a material exists in the one in which it has the lower internal energy and this is supported mathematically by Landau's Phase transition theory[6]. Because of the reduction of the energy of the ferromagnetic phase by the magnetic field, the low temperature phase can only give the material a lower internal energy at a temperature lower than the usual zero field transition point. Since the transition occurs when the energies of the two phases are equal, this will occur at a lower temperature as the energy of the canted spin phase is further reduced by the application of a larger field, so that the transition temperature will be field dependent.

If a field is applied to a crystal of hematite at a temperature just below the transition, the material exists in the antiferromagnetic phase until the field is large enough to reduce the energy of the canted spin phase to such an extent that it is equal to the energy of the existing phase whereupon a transition occurs to the weak ferromagnetic state. If the field is removed and the temperature reduced slightly, the internal energy of the purely anti-

ferromagnetic phase is also reduced and it therefore requires a higher field to bring about the transition to the weak ferromagnetic state. This means in general, that the phase transition can be made to occur at a reduced temperature by the application of a magnetic field of a suitable size.

Landau's theory suggests that the reduction in energy of the low temperature phase just below the transition is proportional to the temperature difference measured from the zero-field transition. This decrease in energy due to the reduction of the temperature is equal in the transition to the decrease in energy caused by the field in the weak ferromagnetic phase, and the latter is proportional to field. This would then indicate that the depression of the transition temperature is directly proportional to the applied field.

The field induced antiferromagnetic to weak ferromagnetic transition is very similar to the effect known as 'spin flopping', occurring at temperatures well below the transition. This is often illustrated physically by considering that the applied field in the basal plane forcibly rotates the spins of the low temperature phase away from the trigonal axis and into the field direction thus creating a ferromagnetic configuration. This effect has recently been reported by Besser and Morrish[74] and by Hirone[75], and has been found to occur in fields of approximately 70 kilo-oersteds below 100° K. Observation of the magnetoelectric effect in Cr_2O_3 through a cycle of spin flopping[76] showed that the overall anti-

ferromagnetic domain distribution remained fixed, and hence it is probable that similar domains in αFe_2O_3 are also fixed under the same conditions.

The depression of the transition temperature in comparatively low fields has been found in the present investigation to be completely linearly dependent on the magnitude of the field applied along the $[1\bar{1}0]$ direction which lies in the basal plane. This is shown in Figure 55. In addition, the antiferromagnetic domain annealing was found to be retained by the crystal, when cycled through the phase transition by means of a field applied at constant temperature.

A very similar increase in magnetostrictive strain at a certain field which is temperature dependent has previously been reported by Urquhart and Goldman[35], and the straight line pertaining to this work and relating the change in transition temperature to the applied field is also shown in Figure 55. The antiferromagnetic to weak ferromagnetic transition close to the usual Morin temperature has recently been detected by Kaczér and Shalnikova[77] using torque measurements and by Flanders and Shtrikman[78] using magnetisation measurements. The field dependence of the depression of the transition temperature obtained from these authors results is also shown in Figure 55 for comparison.

There is good agreement between all three reported field dependencies and the present results taken with the specimen temperature

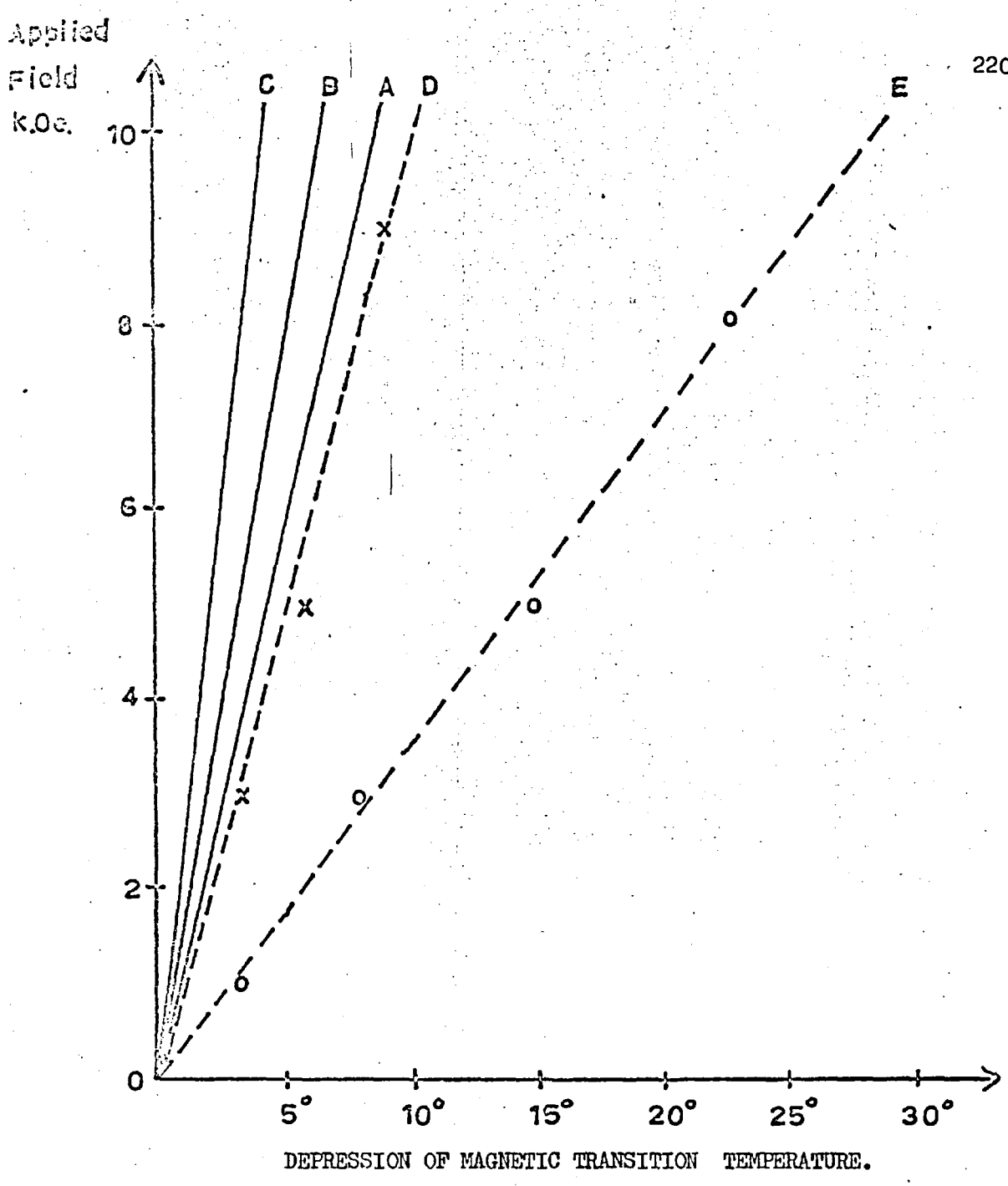


Figure 55. Field dependence of the depression of the magnetic transition temperature along the $[1\bar{1}0]$ axis in a synthetic crystal.

Curve A. from reference 78. Curve B. from reference 77.

Curve C. from reference 35.

Curve D. present investigation, measuring under increasing temperature.

Curve E. Present investigation, measuring under decreasing temperature.

increasing. However, the depression of the transition temperature measured when cooling is far larger than when warming. This means that the strain at a certain field when the temperature is reduced from above the transition value is not identical with that measured after the temperature has increased from below the transition point, even though measurements are performed at the same temperature as read by a thermocouple.

This can be understood by consideration of the energies each side of the phase transition, for if the field is applied above the transition temperature, the crystal is a single domain and the magnetic energy has the same sign throughout the crystal. As the specimen warms from the antiferromagnetic phase below the transition, the weak ferromagnetic domains have to nucleate and grow in order that the field-induced depression of the transition temperature may operate. Thus it is to be expected that the zero field transition temperature must be more nearly approached before nucleation and growth can become significant.

4.6.4. Anomalous Strains at the Transition Temperature

The second important point shown in Figure 54 which needs explaining is the anomalously high magnetostriction observable in high fields close to the transition. This effect has also been reported by Urquhart and Goldman[35] although an explanation was not offered. Dilatometric measurements[36] in zero fields have shown that at the transition temperature there is a measurable volume change, so that

the thermal expansion coefficient takes on a very sharp peak at the Morin temperature. Under an externally applied magnetic field which would amplify any effect of the transition, this volume change would be expected to be much larger.

Figure 55 shows that at a fixed temperature just below the zero field transition, the application of a certain field will bring about the transition and with it of course the appropriate volume change. This is obviously what happens at 250° K with a field of 8 kilo-oersteds, and since the crystal presumably comprises a mixture of the two phases which is field dependent, the strain resulting from the transition adds itself gradually to the magnetostrictive strain and so it is difficult to isolate either component from the resulting combination.

CHAPTER V

FINAL CONCLUSIONS

The original intention at the commencement of work on this project was to measure and investigate linear magnetostriction; the converse effect of piezomagnetism. This was fulfilled by measurement of linear magnetostriction in hematite in four effectively different crystals and the subsequent calculation of the relevant tensor components Q_{22} and Q_{41} in the low temperature phase. The angular dependence of measured strain was in complete agreement with the prediction of magnetic symmetry. The values of the tensor components for each crystal together with values of magnetic thermal remanence are listed in Table IV.

Table IV

Material	Q_{22} Oe^{-1}	Q_{41} Oe^{-1}	T_r e.m.u./grm.
annealed synthetic crystal	$+23.4 \times 10^{-11}$	-5.3×10^{-11}	2.5×10^{-4}
synthetic crystal	$+19.3 \times 10^{-11}$	-2.9×10^{-11}	1.5×10^{-3}
Elba crystal	$+8.5 \times 10^{-11}$	-1.5×10^{-11}	3.0×10^{-2}
Arizona crystal	$+6.0 \times 10^{-11}$	---	1.0×10^{-1}

It is generally accepted that the size of the low temperature remanence in hematite is a reliable guide to the magnetic purity of the material, and it is also probable that the linear magnetostriction coefficients are dependent on magnetic purity, for, since the effect is

an external manifestation of interatomic forces, these would be modified by any internal magnetisation. The values of remanence quoted in Table IV for both natural crystals are only typical of each particular type of crystal.

Experimentally, the equation

$$Q_{22} = - 7 \times 10^{-11} \log_{10} T_r \qquad (5.1)$$

was found to give an accurate prediction of each crystal's characteristics. Unfortunately it has not been possible to base equation (5.1) on any theoretical reasoning, mainly because so very little is known about either the low temperature remanence in hematite or about the additional remanence introduced by impurities.

Above the transition temperature the magnetostriction was of the type expected from the weak ferromagnetism existing in this phase. Small applied fields produced high internal strains which resulted from ferromagnetic domain reorientation. A small linear effect was exhibited at saturation in high fields ($\sim$ 2000 oersteds) corresponding to forced magnetostriction in ferromagnetics.

Linear magnetostriction being a 'forbidden' effect is sensitive to the antiferromagnetic domain direction of the material, and as a consequence magnetic annealing of each crystal before cooling to the low temperature phase was very important. All the experimental evidence pointed to the cause of annealing being the alignment of the canted spin domains by an external field at room temperature, and then this order was carried through the transition point to the

low temperature phase by the linkage of ferromagnetic and antiferromagnetic domain walls.

The degree of saturation of room temperature magnetostrictive strain was dependent on the ferromagnetic domain state, so that the success of annealing a single domain state into the low temperature phase by means of a certain field was estimated from the ratio of strain produced by the same field to the saturation strain. Since the high temperature atomic spin direction lies within the basal plane of the unit cell, a field lying in this plane was most effective for annealing.

The measured field dependences of strain invariably exhibited a reversal of the antiferromagnetic domain state of the crystal by the measurement field, applied in the opposite direction to the annealing, when it exceeded a certain switching threshold value. Domain switching from the annealed state took place by an increase in size of the opposite domain and a decrease in size of the 'annealed in' domain type as the measurement field exceeded the energy required to release the domain walls from their pinned locations. This process must occur by the passage of the walls through the crystal and these would be impeded by the crystallographic and magnetic defects of the lattice so requiring a definite field to overcome each obstacle. Switching from one domain type to another and back again showed a hysteresis effect, with 80% of the annealed synthetic crystal switching in one step at 2300 $\pm$ 100 oersteds applied along the $[\bar{1}10]$ direction.

The mechanism of interaction of the field with the purely antiferromagnetic domains is a matter of some speculation, but Lin's postulate of hematite having slightly unequal sublattice magnetisations in the low temperature phase appears to fit the experimental results of remanent magnetisation. If this is extended a little further to imply that the antiferromagnetic domain direction is specified by the direction of the very small resultant moment, then both qualitatively and quantatively this explains the field interaction with the antiferromagnetic domains. From this the energy required to switch domains in the particular crystal investigated was found to be 15 ergs/cc.

Finally from the temperature dependence of the magnetostrictive strains it was shown that the linear coefficients were virtually independent of temperature in the range 77° K to 220° K. Above this temperature the strain increased rapidly at the onset of the ferromagnetic properties.

Magnetostriction also revealed a field induced reduction of the Morin transition temperature, this being related to the relative thermodynamic potentials of the two phases. This reduction explains the unusually large measured strains close to the transition in terms of the volume changes resulting from the magnetic transition superimposed on the usual magnetostriction. Separation of these two strains was not attempted because of its extreme difficulty, and as a result it was not possible to determine the temperature variation of the linear coefficients from 220° K to the transition point of 258°K.

A P P E N D I X I

Classification of antiferromagnetics showing forbidden effects:- PZ piezomagnetic, PY pyromagnetic, ME magnetoelectric, L linear magnetostrictive.

Material	Neel Temperature	Spin Reference	Group	Properties
$CoCO_3$		1	$\bar{1}$	PY,PZ
CoF_2	35°K	2	4/mmm	PZ,L
CoO	280°K	3,4	mmm	PY,PZ
Cr_2O_3	300°K	4,5	$\bar{3}$m	ME
CrS		6	assumed 6/mmm	PZ,L
CrSb	670°K	6,7	6/mmm	PZ,L
$FeCO_3$	35°K	1,6	$\bar{3}$m	PZ,L
FeF_2	80°K	2	4/mmm	PZ,L
$FeGe_2$		8	assumed 222	PY,ME,PZ
FeO	190°K	3,4	$\bar{3}$	PY,PZ
αFe_2O_3	below 250°K	4,5	$\bar{3}$m	PZ,L
αFe_2O_3	above 250°K	4,5	2/m	PY,PZ
FeS	410°K-430°K	6,9,10	6/mmm	PZ,L
$FeSn_2$	384°K	8	222	PY,ME,PZ
FeTe		6	assumed 6/mmm	PZ,L
$GaFeO_3$	350°K	11	mm2	PY,ME,PZ
MnAs	400°K	6	assumed 6/mmm	PZ,L
MnBi	600°K	6	assumed 6/mmm	PZ,L
$MnCO_3$		1	2/m	PY,PZ

Material	Neel Temperature	Spin Reference	Group	Properties
MnF_2	70°K	2	4/mmm	PZ,L
MnO	120°K	3,4	mmm	PY,PZ
MnS	150°K	3,4	mmm	PY,PZ
MnSe	250°K	3,4	mmm	PY,PZ
$MnSn_2$		8	assumed 222	PY,ME,PZ
MnTe	320°K	6	assumed 6/mmm	PZ,L
$MnTiO_3$	60°K	12	$\bar{3}$	ME
NiAs		6	assumed 6/mmm	PZ,L
$NiCO_3$	25°K	1	$\bar{1}$	PY,PZ
NiF_2	75°K	2	mmm	PY,PZ
NiO	523°K	3,4	mmm	PY,PZ
Ti_2O_3	260°K	13		ME

Spin Structure References

1. ALIKHANOV, R. A., J. Phys. Soc. Japan 17, B-III, 58 (1962)

2. ERICSON, R. A. and SHULL, C. G., Phys. Rev. 83, 208 (1951)

3. SHULL, C. G. and SMART, J. S., Phys. Rev. 76, 1256 (1949)

4. SHULL, C. G., STRAUSER, W. A. and WOOLAN, E. Q., Phys. Rev. 83, 333 (1951)

5. BROCKHOUSE, B.N., J. Chem. Phys. 21, 961 (1953)

6. LE CORRE, Y., J. Phys. et Rad. 19, 750 (1958)

7. SNOW, I., Phys. Rev. 85, 365 (1952)

8. IYENGAR, P. Y., DASANNACHARYA, B. A., VIJAYARAGHAVAN, P. R. and ROY, A. P., J. Phys. Soc. Japan 17, B-III, 41 (1962)

9. MURAKAMI, M., J. Phys. Soc. Japan 16, 187 (1961)

10. SPARKS, J. T., MEAD, W., KIRSCHBAUM, A. J. and MARSHALL, W., J. Appl. Phys. 31, 356S (1960)

11. RADO, G. T., Phys. Rev. Letters 13, 335 (1964)

12. SHIRANE, G., PICKART, S. J. and ISHIKAWA, I., J. Phys. Soc. Japan 14, 1352 (1959)

13. AL'SHIN, B. I. and ASTROV, D. N., Zh. Eksper. Teor. Fiz. 44, 1195 (1963) (Soviet Physics - J.E.T.P. 17, 809)

APPENDIX II

Relationships between tensor components of a 3rd rank axial tensor in group $\bar{3}m$:-

The matrix

$$[+3_z] = \begin{bmatrix} -\frac{1}{2} & \frac{\sqrt{3}}{2} & 0 \\ -\frac{\sqrt{3}}{2} & -\frac{1}{2} & 0 \\ 0 & 0 & +1 \end{bmatrix}$$

can be used to provide relationships between the 13 non-zero tensor components of section 3.2.1. These are

$$d_{121} = \sigma_{11}\,\sigma_{22}\,\sigma_{11}\,d_{121} + \sigma_{12}\,\sigma_{21}\,\sigma_{11}\,d_{211} + \sigma_{11}\,\sigma_{21}\,\sigma_{12}\,d_{112} + \sigma_{12}\,\sigma_{22}\,\sigma_{12}\,d_{222} \qquad (A.1)$$

$$\therefore\ d_{121} = -\tfrac{1}{8}d_{121} + \tfrac{3}{8}d_{211} + \tfrac{3}{8}d_{112} - \tfrac{3}{8}d_{222} \qquad (A.2)$$

$$\text{and } d_{211} = \sigma_{21}\,\sigma_{12}\,\sigma_{11}\,d_{121} + \sigma_{22}\,\sigma_{11}\,\sigma_{11}\,d_{211} + \sigma_{21}\,\sigma_{11}\,\sigma_{12}\,d_{112} + \sigma_{22}\,\sigma_{12}\,\sigma_{12}\,d_{222} \qquad (A.3)$$

$$\therefore\ d_{211} = \tfrac{3}{8}d_{121} - \tfrac{1}{8}d_{211} + \tfrac{3}{8}d_{112} - \tfrac{3}{8}d_{222} \qquad (A.4)$$

$$\text{and } d_{112} = \sigma_{11}\,\sigma_{12}\,\sigma_{21}\,d_{121} + \sigma_{12}\,\sigma_{11}\,\sigma_{21}\,d_{211} + \sigma_{11}\,\sigma_{11}\,\sigma_{22}\,d_{112} + \sigma_{12}\,\sigma_{12}\,\sigma_{22}\,d_{222} \qquad (A.5)$$

$$\therefore\ d_{112} = \tfrac{3}{8}d_{121} + \tfrac{3}{8}d_{211} - \tfrac{1}{8}d_{112} - \tfrac{3}{8}d_{222} \qquad (A.6)$$

and $d_{222} = \sigma_{21}\,\sigma_{22}\,\sigma_{21}\,d_{121} + \sigma_{22}\,\sigma_{21}\,\sigma_{21}\,d_{211} + \sigma_{21}\,\sigma_{21}\,\sigma_{22}\,d_{112}$

$$+ \sigma_{22}\,\sigma_{22}\,\sigma_{22}\,d_{222} \qquad (A.7)$$

$$\therefore\ d_{222} = -\tfrac{3}{8}d_{121} - \tfrac{3}{8}d_{211} - \tfrac{3}{8}d_{112} - \tfrac{1}{8}d_{222} \qquad (A.8)$$

Equations (A.2), (A.4), (A.6) and (A.8) can respectively be re-written as

$$9d_{121} = 3d_{211} + 3d_{112} - 3d_{222} \qquad (A.9)$$

$$9d_{211} = 3d_{121} + 3d_{112} - 3d_{222} \qquad (A.10)$$

$$9d_{112} = 3d_{121} + 3d_{211} - 3d_{222} \qquad (A.11)$$

$$9d_{222} = -3d_{121} - 3d_{211} - 3d_{112} \qquad (A.12)$$

Subtracting equation (A.10) from equation (A.9) gives

$$9d_{121} - 9d_{211} = 3d_{211} - 3d_{121}$$

Therefore $$d_{121} = d_{211} \qquad (A.13)$$

Similarly subtracting equation (A.11) from equation (A.9) gives

$$9d_{121} - 9d_{112} = 3d_{112} - 3d_{121}$$

Therefore $$d_{112} = d_{121} \qquad (A.14)$$

Adding equations (A.9) and (A.10) gives

$$9d_{121} + 9d_{211} = 3d_{211} + 3d_{121} + 6d_{112} - 6d_{222}$$

Therefore $$d_{222} = -d_{121} \qquad (A.15)$$

Thus $$d_{121} = d_{211} = d_{112} = -d_{222} \qquad (A.16)$$

The matrix of $\left[+3_z\right]$ also provides another set of equations relating the remaining components

$$d_{231} = \sigma_{21}\,\sigma_{33}\,\sigma_{12}\,d_{132} + \sigma_{22}\,\sigma_{33}\,\sigma_{11}\,d_{231} \qquad (A.17)$$

Therefore $$d_{231} = -\tfrac{3}{4}d_{132} + \tfrac{1}{4}d_{231} \qquad (A.18)$$

and $$d_{312} = \sigma_{33}\,\sigma_{12}\,\sigma_{21}\,d_{321} + \sigma_{33}\,\sigma_{11}\,\sigma_{22}\,d_{312} \qquad (A.19)$$

Therefore $$d_{312} = -\tfrac{3}{4}d_{321} + \tfrac{1}{4}d_{312} \qquad (A.20)$$

and $$d_{123} = \sigma_{12}\,\sigma_{21}\,\sigma_{33}\,d_{213} + \sigma_{11}\,\sigma_{22}\,\sigma_{33}\,d_{123} \qquad (A.21)$$

Therefore $$d_{123} = -\tfrac{3}{4}\,d_{213} + \tfrac{1}{4}\,d_{123} \qquad (A.22)$$

and $$d_{332} = d_{233} = d_{323} = 0 \qquad (A.23)$$

because $\sigma_{23} = 0$.

The solutions of equations (A.18), (A.20) and (A.22) are respectively

$$d_{231} = -\,d_{132}, \quad d_{312} = -\,d_{321}, \quad d_{123} = -\,d_{213} \qquad (A.24)$$

All the remaining tensor components are therefore related or equated to zero by equations (A.16), (A.23) and (A.24).

APPENDIX III

Relationships between tensor components of a 4th rank polar tensor in group $\bar{3}m$:-

The matrix $\left[\begin{matrix}+3_z\end{matrix}\right]$ can be used to provide relationships between the 41 non-zero tensor components of section 3.2.2. These are

$$\begin{aligned} d_{1111} = {} & \sigma_{11}\,\sigma_{11}\,\sigma_{11}\,\sigma_{11}\,d_{1111} + \sigma_{11}\,\sigma_{11}\,\sigma_{12}\,\sigma_{12}\,d_{1122} \\ & + \sigma_{11}\,\sigma_{12}\,\sigma_{11}\,\sigma_{12}\,d_{1212} + \sigma_{11}\,\sigma_{12}\,\sigma_{12}\,\sigma_{11}\,d_{1221} \\ & + \sigma_{12}\,\sigma_{11}\,\sigma_{11}\,\sigma_{12}\,d_{2112} + \sigma_{12}\,\sigma_{11}\,\sigma_{12}\,\sigma_{11}\,d_{2121} \\ & + \sigma_{12}\,\sigma_{12}\,\sigma_{11}\,\sigma_{11}\,d_{2211} + \sigma_{12}\,\sigma_{12}\,\sigma_{12}\,\sigma_{12}\,d_{2222} \end{aligned} \qquad (A.25)$$

$$\therefore\ d_{1111} = \tfrac{1}{16}\,d_{1111} + \tfrac{3}{16}\,d_{1122} + \tfrac{3}{16}\,d_{1212} + \tfrac{3}{16}\,d_{1221} + \tfrac{3}{16}\,d_{2112} + \tfrac{3}{16}\,d_{2121} + \tfrac{3}{16}\,d_{2211} + \tfrac{9}{16}\,d_{2222} \qquad (A.26)$$

Similarly

$$d_{1122} = \tfrac{3}{16}\,d_{1111} + \tfrac{1}{16}\,d_{1122} - \tfrac{3}{16}\,d_{1212} - \tfrac{3}{16}\,d_{1221} - \tfrac{3}{16}\,d_{2112} - \tfrac{3}{16}\,d_{2121} + \tfrac{9}{16}\,d_{2211} + \tfrac{3}{16}\,d_{2222} \qquad (A.27)$$

$$d_{1212} = \frac{3}{16} d_{1111} - \frac{3}{16} d_{1122} + \frac{1}{16} d_{1212} - \frac{3}{16} d_{1221} - \frac{3}{16} d_{2112} + \frac{9}{16} d_{2121} - \frac{3}{16} d_{2211} + \frac{3}{16} d_{2222} \quad (A.28)$$

etc. for d_{1221}, d_{2121}, d_{2211}, d_{2112} and d_{2222}.

The group of eight equations can be rearranged to form a set of eight simultaneous equations relating the eight unknowns.

$$15d_{1111} = 3d_{1122} + 3d_{1212} + 3d_{1221} + 3d_{2112} + 3d_{2121} + 3d_{2211} + 9d_{2222} \quad (A.29)$$

$$15d_{1122} = 3d_{1111} - 3d_{1212} - 3d_{1221} - 3d_{2112} - 3d_{2121} + 9d_{2211} + 3d_{2222} \quad (A.30)$$

$$15d_{1212} = 3d_{1111} - 3d_{1122} - 3d_{1221} - 3d_{2112} + 9d_{2121} - 3d_{2211} + 3d_{2222} \quad (A.31)$$

$$15d_{1221} = 3d_{1111} - 3d_{1122} - 3d_{1212} + 9d_{2112} - 3d_{2121} - 3d_{2211} + 3d_{2222} \quad (A.32)$$

$$15d_{2112} = 3d_{1111} - 3d_{1122} - 3d_{1212} + 9d_{1221} - 3d_{2121} - 3d_{2211} + 3d_{2222} \quad (A.33)$$

$$15d_{2121} = 3d_{1111} - 3d_{1122} + 9d_{1212} - 3d_{1221} - 3d_{2112} - 3d_{2211} + 3d_{2222} \quad (A.34)$$

$$15d_{2211} = 3d_{1111} + 9d_{1122} - 3d_{1212} - 3d_{1221} - 3d_{2112} - 3d_{2121} + 3d_{2222} \quad (A.35)$$

$$15d_{2222} = 9d_{1111} + 3d_{1122} + 3d_{1212} + 3d_{1221} + 3d_{2112} + 3d_{2121} + 3d_{2211} \quad (A.36)$$

Subtracting equation (A.36) from (A.29) gives immediately

$$d_{1111} = d_{2222} \quad (A.37)$$

Subtracting equation (A.35) from (A.30) gives

$$d_{2211} = d_{1122} \qquad (A.38)$$

Subtracting equation (A.34) from (A.31) gives

$$d_{2121} = d_{1212} \qquad (A.39)$$

Subtracting equation (A.33) from (A.32) gives

$$d_{1221} = d_{2112} \qquad (A.40)$$

Replacing equations (A.37), (A.38), (A.39) and (A.40) into equation (A.29) we get

$$15d_{1111} = 6d_{1122} + 6d_{1212} + 6d_{1221} + 9d_{1111} \qquad (A.41)$$

Therefore $d_{1111} = d_{1122} + d_{1212} + d_{1221}$ (A.42)

No further information may be obtained from equations (A.29) to (A.36), and so further sets of equations are sought which will give relations between the other tensor components.

For example:-

$$d_{1113} = \sigma_{11}\sigma_{11}\sigma_{11}\sigma_{33}d_{1113} + \sigma_{11}\sigma_{12}\sigma_{12}\sigma_{33}d_{1223} + \sigma_{12}\sigma_{11}\sigma_{12}\sigma_{33}d_{2123} + \sigma_{12}\sigma_{12}\sigma_{11}\sigma_{33}d_{2213} \qquad (A.43)$$

Therefore $d_{1113} = -\frac{1}{8}d_{1133} - \frac{3}{8}d_{1223} - \frac{3}{8}d_{2123} - \frac{3}{8}d_{2213}$ (A.44)

In a similar manner

$$d_{1223} = -\frac{3}{8}d_{1113} - \frac{1}{8}d_{1223} + \frac{3}{8}d_{2123} + \frac{3}{8}d_{2213} \qquad (A.45)$$

$$d_{2123} = -\frac{3}{8}d_{1113} + \frac{3}{8}d_{1223} - \frac{1}{8}d_{2123} + \frac{3}{8}d_{2213} \qquad (A.46)$$

$$d_{2213} = -\frac{3}{8}d_{1113} + \frac{3}{8}d_{1223} + \frac{3}{8}d_{2123} - \frac{1}{8}d_{2213} \qquad (A.47)$$

Equations (A.44) to (A.47) inclusive can be rearranged to form four simultaneous equations relating the four unknowns. Thus:-

$$9d_{1113} = -3d_{1223} - 3d_{2123} - 3d_{2213} \qquad (A.48)$$

$$9d_{1223} = -3d_{1113} + 3d_{2123} + 3d_{2213} \qquad (A.49)$$

$$9d_{2123} = -3d_{1113} + 3d_{1223} + 3d_{2213} \qquad (A.50)$$

$$9d_{2213} = -3d_{1113} + 3d_{1223} + 3d_{2123} \qquad (A.51)$$

and the solution to these is

$$d_{1223} = d_{2123} = d_{2213} = -d_{1113} \qquad (A.52)$$

Yet another set of equations is

$$d_{1131} = \sigma_{11}\,\sigma_{11}\,\sigma_{33}\,\sigma_{11}\,d_{1131} + \sigma_{11}\,\sigma_{12}\,\sigma_{33}\,\sigma_{12}\,d_{1232} + \sigma_{12}\,\sigma_{11}\,\sigma_{33}\,\sigma_{12}\,d_{2132} + \sigma_{12}\,\sigma_{12}\,\sigma_{33}\,\sigma_{11}\,d_{2231} \qquad (A.53)$$

Therefore $d_{1131} = -\frac{1}{8}d_{1131} - \frac{3}{8}d_{1232} - \frac{3}{8}d_{2132} - \frac{3}{8}d_{2231}$ (A.54)

etc.

This set gives four equations

$$9d_{1131} = -3d_{1232} - 3d_{2132} - 3d_{2231} \qquad (A.55)$$

$$9d_{1232} = -3d_{1131} + 3d_{2132} + 3d_{2231} \qquad (A.56)$$

$$9d_{2132} = -3d_{1131} + 3d_{1232} + 3d_{2231} \qquad (A.57)$$

$$9d_{2231} = -3d_{1131} + 3d_{1232} + 3d_{2132} \qquad (A.58)$$

and the solution to these is

$$d_{1232} = d_{2132} = d_{2231} = -d_{1131} \qquad (A.59)$$

There are two more similar sets of four equations which give solutions of the same type as equations (A.52) and (A.59). These other solutions giving a relation between components of the tensor d_{ijkl} are

$$d_{3122} = d_{3212} = d_{3221} = -d_{3111} \qquad (A.60)$$

and

$$d_{1322} = d_{2312} = d_{2321} = -d_{1311} \qquad (A.61)$$

There are now only 15 tensor components that have not been re-

lated to each other or to zero. A usable equation is

$$d_{1133} = \sigma_{11}\,\sigma_{11}\,\sigma_{33}\,\sigma_{33}\,d_{1133} + \sigma_{12}\,\sigma_{12}\,\sigma_{33}\,\sigma_{33}\,d_{2233} \quad (A.62)$$

i.e. $d_{1133} = \frac{1}{4}\,d_{1133} + \frac{3}{4}\,d_{2233}$ (A.63)

$\therefore \quad d_{1133} = d_{2233}$ (A.64)

Very similar equations give as solutions

$$d_{1331} = d_{2332} \quad (A.65)$$

$$d_{1313} = d_{2323} \quad (A.66)$$

$$d_{3113} = d_{3223} \quad (A.67)$$

$$d_{3131} = d_{3232} \quad (A.68)$$

$$d_{3311} = d_{3322} \quad (A.69)$$

Other simple equations give

$$d_{1333} = d_{3133} = d_{3313} = d_{3331} = 0 \quad (A.70)$$

and $d_{3333} = d_{3333}$ (A.71)

All of the components of the tensor d_{ijkl} have now been identified and their values calculated. There remains a further important simplification, being due to the intrinsic symmetry of the property tensor, for the stress tensor is symmetrical in its components and the positions of the magnetic field vectors in the equation (3.21) are also symmetrical. This means

$$d_{ijkl} = d_{jikl} = d_{ijlk} = d_{jilk} \quad (A.72)$$

So, using the double suffix notation introduced in section 3.2.1. we get for example

$$d_{1111} = S_{11}, \quad d_{2311} = S_{41}, \quad d_{1231} = S_{65} \quad \text{etc.} \quad (A.73)$$

Thus, using the derived relationships between components of d_{ijkl}

of equations (A.37) to (A.40), (A.42), (A.52), (A.59) to (A.61), and (A.64) to (A.71) it is possible to obtain the following simple equations relating the components of the 4th rank tensor S_{AB}.

$$S_{11} = S_{22} = S_{12} + 2S_{66}, \quad S_{21} = S_{12}, \quad S_{13} = S_{23}, \quad S_{31} = S_{32},$$
$$S_{44} = S_{55}, \quad S_{64} = S_{25} = -S_{15}, \quad S_{46} = S_{52} = -S_{51},$$
$$S_{53} = S_{35} = 0, \quad S_{66} \neq 0, \quad S_{33} \neq 0, \text{ all other terms zero.} \qquad (A.74)$$

All the tensor components are therefore related or equated to zero by equation (A.74).

A P P E N D I X I V

Derivation of the linear magnetostriction coefficients from elastic and magnetoelastic constants in group $\bar{3}m$:-

Since only terms linear in magnetic field are being considered, the simplified expansion

$$W = \tfrac{1}{2} c_{ijkl} E_{ij} E_{kl} + e_{ijk} I_i E_{jk} \qquad (A.75)$$

can be used. E_{ij} is the strain resulting from an intensity of magnetisation I_i. The third rank axial c-tensor e_{ijk} in group $\bar{3}m$ should be derived from components identical to those of the linear magnetostriction tensor of section 3.2.1., except that where $Q_{ijk} = Q_{jik}$ the intrinsic symmetry is now changed to $e_{ijk} = e_{ikj}$. This completely changes some equations relating tensors when the double suffix e_{iA} instead of Q_{Ak} is used, and in particular it is to be noted that $e_{16} = -2e_{22}$, i.e. twice as large as the linear magnetostriction component. The appropriate matrix is therefore

$$e_{iA} = \begin{bmatrix} 0 & 0 & 0 & e_{14} & 0 & -2e_{22} \\ -e_{22} & e_{22} & 0 & 0 & -e_{14} & 0 \\ 0 & 0 & 0 & 0 & 0 & 0 \end{bmatrix} \qquad (A.76)$$

and the particular expression from equation (A.75) expands to

$$e_{ijk}\, I_i\, E_{jk} = e_{14}\, I_1\, E_4 - 2e_{22}\, I_1\, E_6 + e_{22}\, I_2(E_2 - E_1) - e_{14}\, I_2\, E_5 \qquad (A.77)$$

The only other coefficient to be considered is the 4th rank polar i-tensor c_{ijkl}. The form of this tensor may be derived from that of the 'square law' magnetostriction tensor of equation (3.25) but with the additional simplification afforded by the intrinsic symmetry of the two already symmetrical strain tensors of equation (A.75). Thus

$$c_{ijkl} = c_{jikl} = c_{ijlk} = c_{jilk} = c_{klij} = c_{lkij} \text{ etc.} \qquad (A.78)$$

so that from equation (3.25)

$$c_{AB} = \begin{bmatrix} c_{12}+2c_{66} & c_{12} & c_{13} & 0 & -c_{25} & 0 \\ c_{12} & c_{12}+2c_{66} & c_{13} & 0 & c_{25} & 0 \\ c_{13} & c_{13} & c_{33} & 0 & 0 & 0 \\ 0 & 0 & 0 & c_{44} & 0 & c_{25} \\ -c_{25} & c_{25} & 0 & 0 & c_{44} & 0 \\ 0 & 0 & 0 & c_{25} & 0 & c_{66} \end{bmatrix} \qquad (A.79)$$

so that

$$\begin{aligned} 2W_o &= c_{ijkl}\, E_{ij}\, E_{kl} \\ &= (c_{12}+2c_{66})\, E_1^2 + (c_{12}+2c_{66})\, E_2^2 + 2c_{12}\, E_1\, E_2 + 2c_{13}(E_1E_3+E_2E_3) \\ &\quad + c_{33}\, E_3^2 + 2c_{25}(-E_1E_5 + E_2E_5 + E_4E_6) + c_{44}(E_4^2 + E_5^2) + c_{66}\, E_6^2 \end{aligned} \qquad (A.80)$$

The next step in deriving the linear magnetostrictive strain is to add equations (A.77) and (A.80) to produce equation (A.75) expanded into its components. The magnetic ions are in equilibrium in the presence of a field when $\frac{\partial W}{\partial E_{ij}} = 0$ and so to perform this calculation it is necessary to differentiate the component equations for W with respect to E_1, E_2 ..... E_6 in turn, thus:-

$$\frac{\partial W}{\partial E_1} = (c_{12} + 2c_{66})\, E_1 + c_{12}\, E_2 + c_{13}\, E_3 - c_{25}\, E_5 - e_{22}\, I_2 = 0 \qquad (A.81)$$

$$\frac{\partial W}{\partial E_2} = (c_{12} + 2c_{66})\, E_2 + c_{12}\, E_1 + c_{13}\, E_3 + c_{25}\, E_5 + e_{22}\, I_2 = 0 \qquad (A.82)$$

$$\frac{\partial W}{\partial E_3} = c_{13}\,(E_1 + E_2) + c_{33}\, E_3 = 0 \qquad (A.83)$$

$$\frac{\partial W}{\partial E_4} = c_{25}\, E_6 + c_{44}\, E_4 + e_{14}\, I_1 = 0 \qquad (A.84)$$

$$\frac{\partial W}{\partial E_5} = c_{25}\,(-E_1 + E_2) + c_{44}\, E_5 - e_{14}\, I_2 = 0 \qquad (A.85)$$

$$\frac{\partial W}{\partial E_6} = c_{25}\, E_4 + c_{66}\, E_6 - 2e_{22}\, I_1 = 0 \qquad (A.86)$$

The solution of these equations is accomplished as follows:-

Adding equations (A.81) and (A.82) we get

$$2c_{12}\,(E_1 + E_2) + 2c_{66}\,(E_1 + E_2) + 2c_{13}\, E_3 = 0 \qquad (A.87)$$

but from equation (A.83)

$$(E_1 + E_2) = -\,(c_{33}/c_{13})\, E_3 \qquad (A.88)$$

Hence from equation (A.87) we get

$$\left\{ \frac{c_{13}^{\,2} - c_{33}\,(c_{12} + c_{66})}{c_{13}} \right\} E_3 = 0 \qquad (A.89)$$

so that either $E_3 = 0$ or $c_{13}^{\,2} = c_{33}\,(c_{12} + c_{66})$.

Taking the solution $E_3 = 0$ as most probable, since it is in agreement with the crystal symmetry predictions of the form of the tensor (section 3.2.1.), then from equation (A.83)

$$E_1 = - E_2. \tag{A.90}$$

From this, equation (A.81) becomes

$$2c_{66} E_1 - c_{25} E_5 - e_{22} I_2 = 0 \tag{A.91}$$

and equation (A.85) becomes

$$- 2c_{25} E_1 + c_{44} E_5 - e_{14} I_2 = 0. \tag{A.92}$$

Multiplying equation (A.91) by c_{44} and equation (A.92) by c_{25} and adding we get

$$(2c_{66} c_{44} - 2c_{25}^2) E_1 = (e_{22} c_{44} + e_{14} c_{25}) I_2 \tag{A.93}$$

Therefore

$$E_1 = \left\{ \frac{e_{22}c_{44} + e_{14}c_{25}}{2c_{66}c_{44} - 2c_{25}^2} \right\} I_2 \tag{A.94}$$

but from equation (3.20) derived from the linear magnetostriction matrix

$$E_1 = - Q_{22} H_2 = - Q_{22} I_2 / \chi_\perp \tag{A.95}$$

hence

$$Q_{22} = \chi_\perp \left\{ \frac{e_{22}c_{44} + e_{14}c_{25}}{2c_{25}^2 - 2c_{66}c_{44}} \right\}. \tag{A.96}$$

The matrix of equation (3.35) for a 2nd rank polar i-tensor in group $\bar{3}m$ indicates that $\chi_{11} = \chi_{22} = \chi_\perp$ and that all cross-terms are zero.

It is quite simple to find the other coefficient Q_{41} in terms of the elastic constants. Replace for E_1 from equation (A.94) into equation (A.92),

$$- \left\{ \frac{e_{22}c_{25}c_{44} + c_{66}e_{14}c_{44}}{c_{66}c_{44} - c_{25}^{2}} \right\} I_2 + c_{44}E_5 = 0 \qquad (A.97)$$

Therefore

$$(c_{66}c_{44} - c_{25}^{2})\, E_5 = (e_{22}c_{25} + c_{66}e_{14})\, I_2 \qquad (A.98)$$

It is known from the matrix form of the linear magnetostriction tensor that

$$E_5 = - Q_{41}\, H_2 = - \frac{Q_{41} I_2}{\chi_{\perp}} \qquad (A.99)$$

Hence

$$Q_{41} = \chi_{\perp} \left\{ \frac{e_{22}c_{25} + c_{66}e_{14}}{c_{25}^{2} - c_{66}c_{44}} \right\} \qquad (A.100)$$

BIBLIOGRAPHY

1. BIRSS, R. R. Symmetry and Magnetism (Amsterdam: North Holland Publishing Company) 1964

2. TAVGER, B. A. and ZAITSEV, V. M. Zh. Eksper. Teor. Fiz. 30, 564 (1956) (Soviet Physics - J E.T.P. 3, 430)

3. ZOCHER, W. and TÖRÖK, H. Proc. Nat. Acad. Sci., U.S.A. 39, 681 (1953)

4. BIRSS, R. R. Proc. Phys. Soc. 79, 946 (1962)

5. NEEL, L. and PAUTHENET, R. Compt. Rend. 234, 2172 (1952)

6. DZYALOSHINSKII, I. E. Zh. Eksper. Teor. Fiz. 32, 1547 (1957) (Soviet Physics - J E.T.P. 5, 1259)

7. TAVGER, B.A. Kristallografiya (Soviet Physics - Crystallography) 3, 341 (1958)

8. NAGATA, T., YAMA-AI, M and AKIMOTO, S. Nature 190, 620 (1961)

9. TASAKI, A. and IIDA, S. J. Phys. Soc. Japan 19, 1091 (1964)

10. ALIKHANOV, R. A. J. Phys. Soc. Japan 17 Suppl B-III, 58 (1962)

11. BOROVIK-ROMANOV, A. S. and ORLOVA, M. P. Zh. Eksper. Teor. Fiz. 31, 579 (1956) (Soviet Physics - J E.T.P. 4, 531)

12. ERICSON, R. A. Phys. Rev. 90, 779 (1953)

13. ROTH, W. L. Phys. Rev. 110, 1333 (1958)

14. ROZORTH, R. M. and JOENK, R. J. Proc. Int. Conf. Magnetism, Nottingham (1964) p.493.

15. DZYALOSHINSKII, I. E. Zh. Eksper. Teor. Fiz. 37, 881 (1959) (Soviet Physics - J. E.T.P. 10, 628)

16. ASTROV, D. N. Zh. Eksper. Teor. Fiz. 38, 984 (1960) (Soviet Physics - J.E.T.P. 11, 708)

17. FOLEN, V. J., RADO, G. T. and STALDER, E. W. Phys. Rev. Letters 6, 607 (1961)

18. RADO, G. T. and FOLEN, V. J. J. App. Phys. (Suppl.) 33S, 1126 (1962)

19. AL'SHIN, B. I. and ASTROV, D. N. Zh. Eksper. Teor. Fiz. 44, 1195 (1963) (Soviet Physics - J.E.T.P. 17, 809)

20. RADO, G. T. Phys. Rev. Letters 13, 335 (1964)

21. BOROVIK-ROMANOV, A. S. Zh. Eksper. Teor. Fiz. 36, 1954 (1959) (Soviet Physics - J.E.T.P. 9, 1390)

22. BOROVIK-ROMANOV, A. S., ALEKSANJAN, G. G. and RUDASHEVSKII, E.G. Int. Conf. on Magnetism and Crystallography, Kyoto, Japan (1962) Paper 155.

23. BIRSS, R. R. and ANDERSON, J. C. Proc. Phys. Soc. 81, 1139 (1963)

24. SHTRIKMAN, S and TREVES, D. Proc. Int. Conf. Magnetism, Nottingham (1964) p.485.

25. GORODETZKY, G. and TREVES, D. Phys. Rev. (in press)

26. VOIGT, W. Lehrbuch der Kristallphysik, p.938 (Leipzig: Teubner) 1928.

27. DZYALOSHINSKII, I. E. Zh. Eksper. Teor. Fiz. 33, 807 (1957) (Soviet Physics - J.E.T.P. 6, 621)

28. LE CORRE, Y. J. Phys. et Rad. 19, 750 (1958)

29. MORIYA, T. J. Phys. Chem. Solids 11, 73 (1959)

30. BOROVIK-ROMANOV, A. S. Zh. Eksper. Teor. Fiz. 38, 1088 (1960) (Soviet Physics - J.E.T.P. 11, 786)

31. PAULING, L. and HENDRICKS, S. B J. Am. Chem. Soc. 47, 781 (1925)

32. SHULL, C. G., STRAUSER, W. A. and WOLLAN, E. O. Phys. Rev. 83, 333 (1951)

33. MORIN, F. J. Phys. Rev. 78, 819 (1950)

34. CHEVALLIER, M R. and MATHIEUS, S. Ann. de Phys. [11] 18, 258 (1943)

35. URQUHART, H. M A. and GOLDMAN, J. E. Phys. Rev. 101, 1443 (1956)

36. ISERENTANT, C. M., ROBBRECHT, G. G. and DOCLO, R. J. Physics Letters 11, 14 (1964)

37. MORIN, F. J. Phys. Rev. 83, 1005 (1951)

38. PICKART, S. J., NATHANS, R., BROWN, P. J. and ALPERIN, H. A. J App. Phys. 34, 1200 (1963)

39. BLACKMAN, M., HAIGH, G. and LISGARTEN, N. D. Nature 179, 1288 (1957)

40. WILLIAMS, H. J., SHERWOOD, R. C. and REMEIKA, J. P. J. App. Phys. 29, 1772 (1958)

41. BLACKMAN, M. and GUSTARD, B. Nature 193, 360 (1962)

42. NATHANS, R., PICKART, S. J., ALPERIN, H. A. and BROWN, P. J. Phys. Rev. 136, A1641 (1964)

43. LIN, S. T. J. Phys. Soc. Japan 17 Suppl B-I, 226 (1962)

44. IWATA, M., IWATA, T. and YAMAMOTO, M. J. Phys. Soc. Japan 17 Suppl B-I, 231 (1962)

45. TASAKI, A. and IIDA, S. J. Phys. Soc. Japan 18, 1148 (1963)

46. TASAKI, A. and IIDA, S. J. Phys. Soc. Japan 19, 1091 (1964)

47. LEE, E. W. Science Progress No. 161, p.58 (1953)

48. BELOV, K. P. and LEVITIN, R. Z. Zh. Eksper. Teor. Fiz. 37, 565 (1959) (Soviet Physics - J E.T.P. 10, 400)

49. ALBERTS, L. and LEE, E. W. Proc. Phys. Soc. (G.B.) 78, 728 (1961)

50. NAKAMICHI, T. and YAMAMOTO, M J.Phys. Soc. Japan 17 B-I, 214 (1962)

51. MC GUIRE, T. R. and CRAPO, W. A. J. App. Phys. 33S, 1291 (1962)

52. CALLEN, E. R., CLARK, A. E., DE SAVAGE, B., COLEMAN, W. and CALLEN, H. B. Phys. Rev. 130, 1735 (1963)

53. GOLDMAN, J. E. Phys. Rev. 72, 529 (1947)

54. GOLDMAN, J. E. J. Phys. et Rad. 12, 471 (1951)

55. BIRSS, R. R. and LEE, E. W. J. Sci. Instr. 37, 225 (1960)

56. ROBBRECHT, G. G. and DOCLO, R. J. Physics Letters 3, 85 (1962)

57. CORNER, W. D. and HUNT, G. H. Proc. Phys. Soc. (G.B.) A68, 133 (1955)

58. DAY, E. E. and SEVAND, A. H. Proc. Soc. Exptl. Stress Anal. 8, 133 (1950)

59. MC CLINTOCK, R. M. Rev. Sci. Instr. 30, 715 (1959)

60. KAYE, G. Ph.D. Thesis, London (1960)

61. ISHIKAWA, Y. and AKIMOTO, S. J. Phys. Soc. Japan 13, 1298 (1958)

62. KORNETZKI, M. Z. Phys. 97, 662 (1935)

63. POWELL, F. C. Proc. Camb. Phil. Soc. 27, 561 (1931)

64. KITTEL, C. Rev. Mod. Phys. 21, 541 (1949)

65. ANDERSON, P W. Phys. Rev. 79, 350 (1950)

66. HALPERN, V. to be published

67. JEFFREYS, H. and JEFFREYS, B. S. Methods of Mathematical Physics, 2nd ed., p.122 (Cambridge: University Press) 1950

68. IIDA, S. and TASAKI, A. Proc. Int. Conf. Magnetism, Nottingham (1964) p.583.

69. BLACKMAN, M. and GUSTARD, B. Proc. Int. Conf. Magnetism, Nottingham (1964) p.600.

70. BOZORTH, R. M. Ferromagnetism (New York: Van Nostrand) 1951.

71. ARTMAN, J. O., MURPHY, J. C. and FONER, S. Phys. Rev. 138, A912 (1965)

72. MARTIN, T. J. Private communication.

73. LI, Y. Y. Phys. Rev. 101, 1450 (1956)

74. BESSER, P. J and MORRISH, A. H. Physics Letters 13, 289 (1964)

75. HIRONE, T. J. App. Phys. 36, 988 (1965)

76. FONER, S. and HANABUSA, M. J. App. Phys. 34, 1246 (1963)

77. KACZÉR, J. and SHALNIKOVA, T. Proc. Int. Conf. Magnetism, Nottingham (1964) p.589.

78. FLANDERS, P. J. and SHTRIKMAN, S. Mullard Research Labs., Report No. 540 (1965)

79. ALPERIN, H.A., BROWN. P.J, NATHANS, R, and PICKART, S.J Phys Rev Letters 8 237 (1962)

Reprinted from

PROCEEDINGS of the INTERNATIONAL CONFERENCE ON MAGNETISM

Nottingham

7th-11th September 1964

Linear magnetostriction in hematite

J. C. ANDERSON*, R. R. BIRSS† and R. A. M. SCOTT*

*Imperial College of Science and Technology, London S. W. 7, England
†University of Sussex, Falmer, Brighton, Sussex, England

ABSTRACT. A single crystal of hematite (α-Fe_2O_3) has been found to exhibit linear magnetostriction at low temperatures. At −196°C the coefficients characterizing this effect are given by $P_{22} \simeq \pm 19 \times 10^{-11}$ Oe^{-1} and $P_{14} \simeq \mp 3 \times 10^{-11}$ Oe^{-1}, the choice of sign being dictated by the direction in which a magnetic field is applied to the specimen as it is cooled down through the transition temperature. Such fields need only be as large as 100 Oe to produce domain saturation; the application of an a.c. field destroys the linear magnetostriction, presumably due to the formation of antiparallel antiferromagnetic domains.

1. Introduction

An antiferromagnetic crystal is said to exhibit linear magnetostriction when the application of a magnetic field **H** is accompanied by a deformation of the crystal characterized by a (symmetrical) strain tensor E_{ij} that depends linearly on the components of **H**. Such an effect is the inverse of the piezo-magnetic effect, the existence of which was demonstrated in certain fluorides by Borovik-Romanov (1959, 1960). The magnetic crystal classes in which linear magnetostriction can occur have been listed by Birss and Anderson (1963).

Hematite (α-Fe_2O_3) is a rhombohedral antiferromagnetic crystal having two different spin structures. Below the magnetic transition temperature at about −15°C the antiferromagnetic spins are aligned along the rhombohedral c axis and the crystal belongs to the magnetic crystal class $\bar{3}$m, which can exhibit linear magnetostriction. Above −15°C the spins are arrayed in planes perpendicular to the c axis. The crystal then belongs to the magnetic crystal class 2′/m, and although it does not show linear magnetostriction, it does exhibit 'pyromagnetism' or parasitic ferromagnetism. This is caused by the spins being able to incline slightly away from their antiferromagnetic position without changing the symmetry of the crystal. In effect this gives hematite weak ferromagnetic properties at room temperature. In this paper measurements on hematite are reported in which linear magnetostriction has been observed.

For an antiferromagnetic crystal of the magnetic crystal class $\bar{3}$m, an applied magnetic field **H** gives rise to linear magnetostriction characterized by a (symmetrical) strain tensor $E_{ij} = P_{ijk}H_k$ with components

$$E_{11} = -P_{22}H_2, \quad E_{22} = P_{22}H_2, \quad E_{33} = 0,$$

$$E_{23} = E_{32} = P_{14}H_1, \quad E_{31} = E_{13} = -P_{14}H_2,$$

$$E_{12} = E_{21} = -P_{22}H_1,$$

where P_{22} and P_{14} are coefficients that may be determined by experiment. The suffixes 1, 2, 3 refer to rectangular cartesian coordinate axes orientated so that the x_2 and x_3 axes are parallel respectively to a twofold and the threefold crystallographic axes. The strain in a direction with direction cosines $\beta_1, \beta_2, \beta_3$ is

$$\lambda = \sum_{i=1}^{3}\sum_{j=1}^{3} E_{ij}\beta_i\beta_j$$

$$= P_{22}(\beta_2^2 - \beta_1^2)H_2 + 2P_{14}(\beta_2 H_1 - \beta_1 H_2)\beta_3 - 2P_{22}\beta_1\beta_2 H_1. \qquad (1)$$

If the measuring direction coincides with a [001] direction and a field is applied in the (110) plane so as to make an angle θ with this [001] direction, then equation (1) reduces to

$$\frac{\lambda}{H} = (\sin^2\varphi\ P_{22} - \sin 2\varphi\, P_{14}) \sin\theta,$$

where φ is the angle (36°) that the [111] direction makes with the [001] direction. Thus

$$\frac{\lambda}{H} = (0.345\ P_{22} - 0.951\ P_{14}) \sin\theta,$$

and this particular experimental configuration does not permit the separate determination of P_{22} and P_{14}.

If, however, the measuring direction makes an angle Δ with the [001] direction, then

$$\frac{\lambda}{H} = \sin\theta\,[(\sin^2\varphi\cos^2\Delta - \sin^2\Delta)P_{22} - (\sin 2\varphi\cos^2\Delta)P_{14}] + \cos\theta\,[(\sin^2\varphi\sin 2\Delta)P_{22} + (\sin 2\varphi\sin\Delta\cos\Delta)P_{14}]. \qquad (2)$$

In this case, if Δ is known, P_{22} and P_{14} can be evaluated from the two experimental values for the coefficients of $\sin\theta$ and $\cos\theta$. This will be done by plotting strain against θ and applying Fourier analysis to obtain the coefficients of the sine and cosine terms. These then give two equations for the two unknowns.

2. Experimental procedure

An artificial hematite crystal was used after orientation by the Laue technique. It was found that all its natural cleavage planes were of the (110) type which do not contain a [111] axis (c axis) in the rhombohedral cell. The measurements were made by mounting a strain gauge on such a (110) face of the crystal at an angle $\Delta = 10°$ to the [001] direction. (Because of the

geometry of the specimen it was not convenient to increase Δ much above this value.)

Measurement of ferromagnetic magnetostriction in a natural α-Fe_2O_3 crystal by Urquhart and Goldman (1956) indicated strains of the order of 2×10^{-8} below −25°C in a field of 9000 oersteds. The sensitivity aimed at in the present apparatus was such as to permit measurements of strains down to one part in 10^8. Since the coefficient of thermal expansion in hematite at these temperatures is of the order of 10^{-5} degC^{-1} it is necessary to compensate for thermal expansion of the specimen. This was done by mounting an identical strain gauge on a piece of soda glass, of closely similar expansion coefficient to hematite, placed near the crystal. The overall coefficient of thermal expansion of the combination was found to be 5×10^{-7} deg C^{-1}, so that a temperature stability of 1 50 deg C was required during measurements. The gauges formed two arms of a balanced Wheatstone bridge provided with a stabilized current supply, and high sensitivity in measuring the out-of-balance current was achieved by using a split photocell amplifier. The strain gauges had a nominal resistance of 100 Ω and active length of 0.5 cm.

Initial measurements were made at room temperature, where hematite exhibits weak ferromagnetism. A magnetostrictive contraction, having a saturation value of $(3.65 \pm 0.10) \times 10^{-6}$, in a minimum field of 1500 Oe was obtained: Urquhart and Goldman obtained about 8×10^{-6} but they made measurements on a natural crystal and along the c axis.

For measurements at low temperatures, where hematite is nominally antiferromagnetic, the crystal was subjected to a steady magnetic field of 7500 Oe perpendicular to the direction of strain measurement as the specimen was cooled down through the transition temperature. At −196°C the magnetostriction revealed no indication of saturation in fields of up to 9000 Oe. For all directions of the applied magnetic field, the magnetostrictive strain may be expressed as the sum of two functions, respectively odd and even in the magnetic field. An analysis of the experimental data reveals that, for fields up to 1500 Oe, the odd function may be satisfactorily represented by just one term of the form PH, where P is a constant factor depending only on the field direction. The magnitude of P is determined by the domain state of the specimen. After being taken through the transition temperature with an a.c. field applied, the coefficient P for perpendicular fields is generally small and of random sign, indicating the formation of antiparallel domains. If, however, a steady field is applied as the specimen is cooled through the transition temperature the linear term is constant in value and has the same sign as the applied field. This indicates that the presence of the field causes the antiferromagnetic domains to nucleate and grow all with the same orientation. Fields as small as 100 Oe are sufficient to switch domains in the ferromagnetic state at room temperature, and this field is sufficient to give domain saturation in the antiferromagnetic state, as is evidenced by the reproducibility of the coefficient P.

The value of the factor P may be obtained immediately from the slope at the origin of the curves of magnetostrictive strain plotted against field. Figure 1 shows the angular dependence of these curves and the corresponding values of the factor P are plotted, as a function of the angle θ, in figure 2.

Fourier analysis of the data shown in figure 2 reveals that P is sinusoidal with period π, since the coefficients of the higher harmonics are well within the limits of experimental error. The fundamental is given by

$$P = \frac{\lambda}{H} = (8.4 \sin\theta + 1.8 \cos\theta) \times 10^{-11}\ \mathrm{Oe}^{-1}. \qquad (3)$$

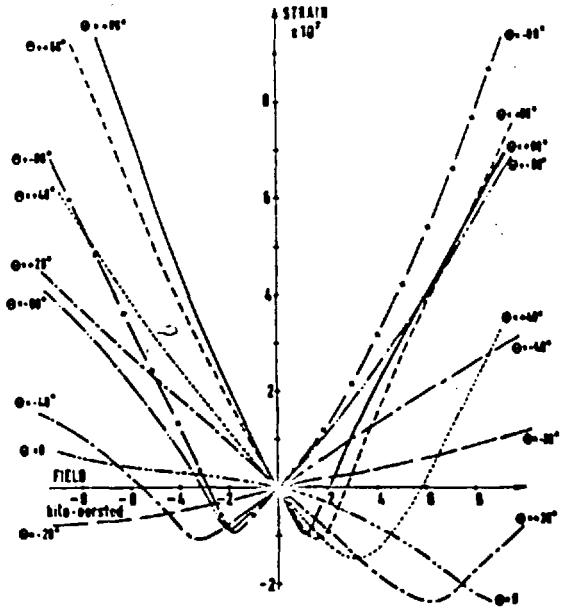


Figure 1. Variation of magnetostrictive strain with the magnetic field applied in various directions at −196°C.

The result (3) is in excellent agreement with the equation derived from (2) when Δ = 10°, namely

$$\frac{\lambda}{H} = \sin\theta\ (0.305\ P_{22} - 0.922\ P_{14}) + \cos\theta\ (0.118\ P_{22} + 0.163\ P_{14}).$$

from which it may be deduced that $P_{22} \simeq 19 \times 10^{-11}$ Oe^{-1} and $P_{14} \simeq -3 \times 10^{-11}$ Oe^{-1}. With a reverse annealing field the sign of both these coefficients is changed.

3. Discussion

The even component of the magnetostriction at low temperatures cannot be represented (for a fixed value of θ) solely by a term proportional to H^2. It can, of course, be analysed into a power series in H^2, and the coefficient of the leading term is gratifyingly small compared with the coefficient of the odd component ($2 \cdot 10^{-14}$, cf. 8.6×10^{-11} for perpendicular magnetization); but the higher terms do not exhibit a similar convergence and the field dependence of the even component is rather reminiscent of that of a ferromagnetic material below saturation. It is not suggested that the crystal is ferromagnetic in the normal sense, but merely that the magnetostrictive behaviour could be

fairly represented as a superposition of the linear magnetostriction of a normal antiferromagnetic with the even magnetostriction of a ferromagnetic suitably reduced by a volume weighting factor. This feature is

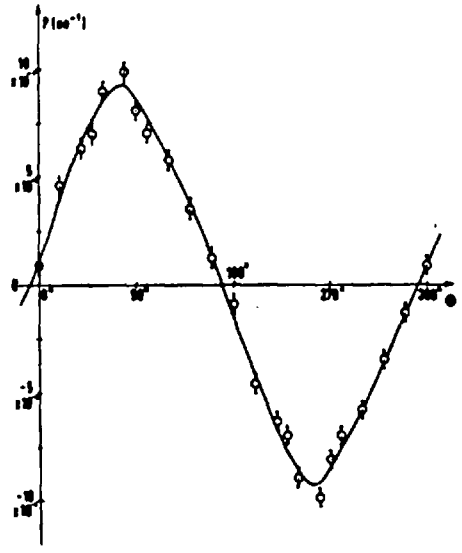


Figure 2. Angular variation of the coefficient P characterizing linear magnetostriction in small fields.

also reflected in the behaviour of the (thermal) remanent magnetization of the crystal, the temperature dependence of which is shown in figure 3. It will be seen that there is a constant remanent moment of about 10^{-3} e.m.u. g^{-1} below the transition point. The deviation in the region of −10°C is believed to be associated with the formation of domains. This curve agrees well with the results reported by Iwata et al. (1962).

The coefficient of sin θ in the odd component of the magnetostriction is of the same order of magnitude as the coefficient of forced magnetostriction in a ferromagnetic material. In this effect the magnetostrictive strain is found to increase linearly with applied field, at high field values the slope of this linear increase is of the order of 10^{-10} in nickel (Kornetzki 1935). Although the ferromagnetic effect reverses with field it is, in reality, a linear effect. The reversal arises because reversing a large field reverses all the spins and it is not possible (as it is in the antiferromagnetic case) to preserve the same spin direction—and hence the same magnetic crystal class—in the presence of a large opposing field.

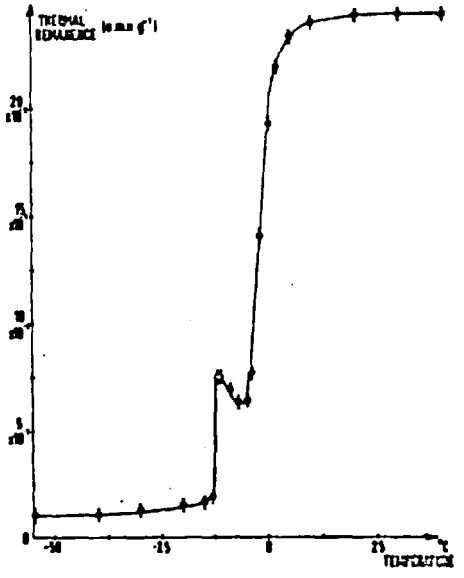


Figure 3. Variation of thermal remanence with temperature (heating curve).

Acknowledgments

The authors wish to thank Mr. T. E. Gallon for providing the data shown in figure 3 and Professor M. Blackman for the load of the specimen. One of us (R.A.M.S.) is indebted to the Department of Scientific and Industrial Research for the provision of a maintenance grant.

References

Birss, R. R., and Anderson, J. C., 1963, Proc. Phys. Soc., **81**, 1139.

Borovik-Romanov, A. S., 1959, Zh. Eksp. Teor. Fiz., **36**, 1954 (translation: Soviet Physics J E T P, **9**, 1390).

—, 1960, Zh. Eksp. Teor. Fiz., **38**, 1088 (translation: Soviet Physics J E T P, **11**, 786).

Iwata, M., Iwata, T., and Yamamoto, M., 1962, J. Phys. Soc. Japan, **17**, Suppl. B-1, 31.

Kornetzki, M., 1935, Z. Phys., **97**, 662.

Urquhart, H. M. A., and Goldman, J. E., 1956, Phys. Rev., **101**, 1443.